Synthesis and Characterisation of a Radioligand for Positron Emission Tomography Imaging of the 5-HT $_{1A}$ Receptor

Caroline McCardle

Submitted in fulfilment of the requirements for the degree of Doctor of Philosophy

Institute of Neuroscience – Newcastle University

July 2014

Abstract

Dysfunction of the central 5-HT system has been implicated in affective disorders such as anxiety and depression. However, one factor which has restricted the progress of investigations into possible changes in brain levels of 5-HT in affective disorders is the limited tools available to estimate *in vivo* 5-HT levels in the human brain. The *in vivo* imaging technique Positron Emission Tomography (PET) could address this issue.

This thesis describes the chemical synthesis and biological characterisation of the 5-HT_{1A} receptor PET ligand 4-(2'-methoxy-)phenyl-1-[2'-(*N*-2"-pyridinyl-)*4*-[^{18}F]fluorobenzamido-]ethyl piperazine (4-[^{18}F]MPPF), with the aim of determining whether this might be a suitable ligand to estimate *in vivo* 5-HT levels in the brain.

Development of a routine radiosynthesis starting with low activity was performed. Successful 4-[^{18}F]MPPF production was achieved using a combination of the Eckert and Zielgler ModularLab and a microwave reactor *via* a fluorodenitration reaction of 4-(2'-methoxy-)phenyl-1-[2'-(*N*-2"-pyridinyl-)*4*-nitrobenzamido-]ethyl piperazine (4-$MPPNO_2$) with fluorine-18. A radiochemical yield of 33.5% was achieved with a total synthesis time of 60 minutes.

PET and autoradiography studies in rats revealed 4-[^{18}F]MPPF specifically bound in areas rich in 5-HT_{1A} receptors and binding could be blocked by pre-treatment with cold 4-MPPF.

The ability of the 5-HT releasing agent fenfluramine to increase the concentration of endogenous 5-HT in the brain and displace radioligands from the 5-HT_{1A} receptor was examined in parallel with PET, *in vitro* and *ex vivo* autoradiography, and microdialysis studies. The microdialysis studies revealed that fenfluramine (3 mg/kg) increased 5-HT levels to approximately 400% of basal levels, reaching a maximum concentration of 1 x 10^{-8} M 5-HT (in hippocampus). PET and autoradiography studies indicated that 4-[^{18}F]MPPF was not displaced using this dose of fenfluramine.

These studies demonstrate that the Eckert and Zielgler ModularLab is an effective radiosynthesis platform for the synthesis of 4-[^{18}F]MPPF for use in PET and 4-[^{18}F]MPPF is a suitable PET ligand for the examination of the distribution of 5-HT_{1A} receptors in the rat brain. However, this study suggests that 4-[^{18}F]MPPF may not be suitable for use in examining possible changes in 5-HT in the brain in affective disorders.

Acknowledgements

Firstly I would like to express my great thanks to my supervisors, Dr. Sasha Gartside, Dr. Richard McQuade and Dr. Michael Carroll, for their time, expertise, advice and most of all their patience.

Many thanks to the EPSRC for sponsoring my project and the Professional Aids Council for providing me with a grant.

A special thanks goes to Dr. Stephen Hobson, Ian Wilson and Dr. David Cousins for their guidance and sharing their expertise, without which this project would not have been finished.

To the members of the MAC group; Sam Bhatt, Michael Charlton, Dr. Luke Dixon, Dr. Stephen Hobson, Dr. Guillaume Launay, Dr. David Molyneux, Chris Reed and their partners; thank you for sharing my experience, your friendship and making my PhD a very special time.

Lastly, a huge thank you to Chris Hannah for all his support and encouragement throughout my time at Newcastle University, and for funding me in my last year!

Table of Contents

List of Figures

List of Tables

List of Schemes

List of Abbreviations

5-HT; 5-hydroxytryptamine

5HIAA; 5-Hydroxyindoleacetic acid

4-MPPF; 4-(2'-methoxy-)phenyl-1-[2'-(*N*-2"-pyridinyl-)*4*-fluorobenzamido-]ethyl piperazine

4-MPPNO$_2$; 4-(2'-methoxy-)phenyl-1-[2'-(*N*-2"-pyridinyl-)*4*-nitrobenzamido-]ethyl piperazine

4-MPPI; 4-(2'-Methoxyphenyl)-1-[2'-[N-(2''-pyridinyl)- p-iodobenzamido] ethyl]piperazine

(±)-8-OH-DPAT; (±) 8-hydroxy-2(di-n-propylamino)tetralin hydrobromide

aCSF; Artificial cerebrospinal fluid

ANOVA; Analysis of variance

CNS; Central nervous system

CT; (X-ray) computed tomography

DMF; Dimethylformamide

DMSO; Dimethyl sulfoxide

DOPAC; 3,4-Dihydroxyphenylacetic acid

DRN; Dorsal raphe nucleus

EtOH; Ethanol

FCWAY; *N*-{2-[4-(2-methoxyphenyl)piperazino]}-*N*-(2-pyridinyl)*trans*-4-fluorocyclohexanecarboxamide

FDG; Fluorodeoxyglucose

FWHM; Full width at half maximum

HPLC; High-performance liquid chromatography

MeOH; Methanol

MRI; Magnetic resonance imaging

MRN; Median raphe nucleus

NaOAc; Sodium acetate

NMR; Nuclear magnetic resonance

PET; Positron emission tomography

PFC; Pre-frontal cortex

RCY; Radiochemical yield

ROI; Region of interest

SA; Specific activity

SERT: Serotonin transporter

SPECT; Single-photon emission computed tomography

SUV; Standard uptake value

TAC; Time-activity curve

THF; Tetrahydrofuran

TLC; Thin layer chromatography

UV; Ultraviolet

VOI; Volume of interest

WAY100635; *N*-[2-[4-(2-methoxyphenyl)-1-piperazinyl]ethyl]- *N*-(2-pyridyl)cyclohexanecarboxamide

Chapter 1. Introduction

The development of non invasive *in vivo* 3-D imaging techniques such as PET (positron emission tomography) and MRI (magnetic resonance imaging) has provided the ability to examine the biological basis for many diseases including diseases of the central nervous system (CNS). Such imaging techniques are used to diagnose and study the progression of disease in addition to quantifying the efficacy of pharmacological treatments. Such techniques are used in both pre-clinical animal research as well as clinically in human studies and diagnostics (Garcia-Alloza and Bacskai, 2004).

In vivo brain imaging techniques should ideally have high temporal and spatial resolution (Garcia-Alloza and Bacskai, 2004). These criteria are especially important when applied to small animal research, as the smaller brain size makes examining sub cellular structures and mechanisms a greater challenge. MRI has both high spatial and temporal resolution. However, although PET has lower spatial and temporal resolution compared to MRI, it has the ability to provide quantitative metabolic data such as the kinetics of neurotransmission and specific receptor densities, both of which can be altered in CNS diseases. In addition, the high sensitivity of PET means it can detect low concentrations relevant for many molecules studied in neuropsychiatric disorders, in the range of 10^{-9} to 10^{-12} M (Fumita and Innis, 2002, Levin and Zaidi, 2007). Small animal models of disease therefore commonly employ PET to study the pathology of CNS diseases as well as pharmacological treatments of these diseases (Garcia-Alloza and Bacskai, 2004).

1.1 The 5-HT system

It has been known since 1868 that blood contained a vasoconstrictive substance, and in 1937 Vittorio Erspamer isolated 5-HT in the gut, naming it enteramine (Erspamer, 1986). However, it was the work of Irvine Page, Arda Green and the post-doctoral student Maurice Rapport, between 1946 and 1949, which finally isolated the substance and named it serotonin (Green, 2006). Serotonin was further identified as 5-hydroxytryptamine (5-HT) by Maurice Rapport in 1949 (Rapport, 1949). Since then over 90,000 papers have been published on the subject of 5-HT (Green, 2006).

5-HT is a neurotransmitter and neuromodulator of the central nervous system. Initially it contributes to the neurodevelopmental process and in the adult regulates a wide variety of functions and behaviours, including emotion and cognition (Aznavour and Zimmer, 2007, Whitaker-Azmitia et al., 1996).

5-HT neurones originate in the dorsal and median raphe nucleus (DRN and MRN). Approximately a third of the neurones in the DRN, a number of around 11,000, are 5-HT . However, few axon terminals are found here and most of the 5-HT release in the DRN is pre-synaptic (somatodendritic) in origin (Aznavour and Zimmer, 2007).

A wide distribution of brain areas receive input from the raphe nuclei, such as the hippocampus, frontal cortex, septum, amygdala and hypothalamus and these areas are rich in post synaptic 5-HT receptors (Sharp et al., 2007, Lesch and Gutknecht, 2004).

Fourteen different subtypes of 5-HT receptors have been identified, all (except the 5-HT $_3$ family) belonging to the G-protein-coupled receptor family. They are divided into seven families, with subtypes within each family denoted by a letter (Savitz et al., 2009). The 5-HT $_{1A}$ receptors are the best characterised of all the 5-HT receptor subtypes in terms of distribution, structure and electrophysiological properties.

The 5-HT $_{1A}$ receptors found on the soma-dendrites of 5-HT neurones in the raphe nucleus act as autoreceptors, controlling the firing rate of 5-HT neurones, quantity of 5-HT released in an action potential and the synthesis of 5-HT . Therefore it can be inferred that these autoreceptors have a powerful control of 5-HT transmission in the projection areas (Savitz et al., 2009).

5-HT $_{1A}$ receptors have been implicated in a variety of processes including regulation of body temperature, sleep and mood states, and neurogenesis (Aznavour and Zimmer, 2007) making them an important biological target in both the research and treatment of CNS disease.

1.1.1 5-HT $_{1A}$ receptors in disease

Dysfunction of the 5-HT $_{1A}$ receptor has been implicated in affective disorders such as anxiety and depression. Studies have examined 5-HT $_{1A}$ knockout mice or transgenic mice over expressing 5-HT $_{1A}$ receptors. Such animals displayed anxiety like behaviours supporting the role of 5-HT $_{1A}$ receptors in mood disorders (Heisler et al., 1998, Kusserow et al., 2004, Parks et al., 1998, Ramboz et al., 1998).

The evidence that 5-HT $_{1A}$ receptor dysfunction plays a role in depression comes from four sources; Firstly, pharmacological challenges, where increased extracellular 5-HT and post synaptic 5-HT $_{1A}$ receptor function/transmission is altered, gives rise to an antidepressant effect (Detke et al., 1995, Haddjeri et al., 1998, Savitz et al., 2009). Secondly, post mortem studies have revealed changes in 5-HT $_{1A}$ ligand binding in the brains of patients with depression vs. healthy controls (Arango et al., 1995, Boldrini et al., 2008, Matsubara et al., 1991, Stockmeier et al., 1998, Savitz et al., 2009). Thirdly, neuroreceptor imaging, such as PET, has reported reduced 5-HT $_{1A}$ ligand binding in 5-HT $_{1A}$ receptor rich areas, such as the hippocampus and raphe nucleus, in patients with depression (Didelot et al., 2008, Drevets et al., 2000, Hirvonen et al., 2008, Sargent et al., 2000, Shively et al., 2006, Savitz et al., 2009). Lastly, genetic analysis has revealed characteristic and abnormal allele phenotypes for the 5-HT $_{1A}$ receptor gene in depressed patients vs. healthy controls (Savitz et al., 2009, Neff et al., 2009, Szewczyk et al., 2009, Zhang et al., 2009).

5-HT $_{1A}$ dysfunction is also implicated in disorders such as schizophrenia, where 5-HT $_{1A}$ receptor density has been found to be high in the frontal cortices of patients, as well as panic disorders, where antidepressant drugs that alter 5-HT $_{1A}$ receptor function alleviate symptoms. In addition, 5-HT $_{1A}$ receptor modulation, using agonists such as (±)-8-OH-DPAT, has been shown to have a

therapeutic role in Parkinson's disease by improving symptoms caused by degeneration of dopamine neurones (Jones and Blackburn, 2002, Ohno, 2011).

1.1.2 Altered 5-HT levels in disease

Whilst it has long been proposed that affective disorders are associated with decreased 5-HT levels in the brain, direct evidence for this is limited. There are some reports of a decrease in the CSF levels of the 5-HT metabolite, 5-hydroxyindolacetic acid (5-HIAA) in depressed patients (Asberg et al., 1976, Traskman-Bendz et al., 1984). However, not all studies have reported similar results. Furthermore, it is debatable whether 5-HIAA levels are a good indicator of the levels of 5-HT itself. In the main, the evidence for altered 5-HT levels contributing toward the neuropathology of affective disorders is indirect and comes from studies where manipulations of brain 5-HT levels have been shown to have effects on mood. Thus, the classic tryptophan depletion challenge (described below), which causes an acute decrease in brain 5-HT levels, results in lowering of mood in euthymic depressed patient and individuals at risk of depression (Ruhé et al., 2007). One factor which has restricted the progress of research into possible changes in brain levels of 5-HT in affective disorders is the limited tools available to estimate 5-HT levels in the human brain *in vivo.*

1.1.3 Pharmacological interventions to alter 5-HT levels in the brain

Endogenous 5-HT can be manipulated by pharmacological intervention. A number of drugs can either increase or reduce the amount of extracellular 5-HT , giving a route to characterise radioligands in the presence of changing levels of endogenous 5-HT . Drugs such as fenfluramine, a 5-HT releasing agent, fluoxetine and citalopram, which are selective serotonin reuptake inhibitors (SSRI) can increase the amount of extracellular 5-HT . In addition, loading with 5-HT precursors tryptophan or 5-hydroxytryptophan can increase 5-HT synthesis and release.

It is also possible to reduce 5-HT synthesis and 5-HT release by using *p*-ethynylphenylalanine or *p*-chlorophenylalanine, inhibitors of tryptophan hydroxylase (Stokes et al., 2000, Gál et al., 1970) or by introducing a low tryptophan diet for 24 hours, followed by a tryptophan free amino acid drink

prior to the start of an experiment (tryptophan depletion challenge) (Udo De Haes et al., 2002a).

1.1.4 The opportunity for investigating the 5-HT system using PET imaging

Investigation of neurochemical changes involving the 5-HT system provides a vital opportunity to characterise the pathology of the diseases discussed above, as well as developing and assessing the efficacy of novel therapies. PET imaging provides the functionality and sensitivity to study such neurochemical systems and is a proven tool in the research of neurotransmitter changes, both clinically and pre-clinically.

It has previously been demonstrated that some radioligands are sensitive to changes in levels of extracellular neurotransmitter, whereas others are not (Laruelle, 2000). Where a radioligand is sensitive to changes in extracellular neurotransmitter levels, the radioligand could be used to examine any possible changes in extracellular neurotransmitter levels. Thus, the extent of binding of the 'displaceable' radioligand would depend on the existing concentration of the extracellular neurotransmitter and would therefore be an indicator of endogenous neurotransmitter levels. However, where a radioligand is not sensitive to changes in levels of extracellular neurotransmitter, the radioligand may only be used to examine receptor number and distribution (Udo De Haes et al., 2002a).

A number of displaceable radioligands are already available for clinical PET imaging studies examining dopaminergic function, such as the D2 receptor ligand [^{11}C]raclopride, the D2/D3 receptor ligand [^{18}F]fallypride and the dopamine antagonist [^{123}I]iodobenzamide (Slifstein et al., 2010, Breier et al., 1997, Laruelle et al., 1999). In one study in healthy patients, an amphetamine induced release of dopamine resulted in reduced binding of [^{18}F]fallypride, suggesting the radioligand is sensitive to changes in endogenous dopamine release (Slifstein et al., 2010). In another study investigating the reduction in binding of [^{11}C]raclopride after an amphetamine induced release of dopamine, patients with schizophrenia had significantly greater reductions in ligand binding vs. healthy controls. From this it was inferred that the schizophrenic patients

had enhanced pre-synaptic dopamine function (Breier et al., 1997). This and other imaging studies have concluded that the dopamine dysfunction characteristic in schizophrenia, is possibly due to a dysregulation of the pre-synaptic neurone, rather than changes in post synaptic receptor sensitivity (Laruelle et al., 1999).

Currently the 5-HT $_{1A}$ antagonist [*carbonyl*-^{11}C]WAY100635 is a suitable PET ligand for the quantification and brain distribution of 5-HT $_{1A}$ receptors. However, this ligand is not displaceable by endogenous 5-HT , so there is a need to develop displaceable 5-HT $_{1A}$ PET ligands to examine pre-synaptic 5-HT function (Zimmer and Le Bars, 2013).

The 5-HT $_{1A}$ antagonist PET ligand 4-[^{18}F]MPPF (4-(2'-methoxy-)phenyl-1-[2'-(*N*-2"-pyridinyl-)4-[^{18}F]fluorobenzamido-]ethyl piperazine) has been studied and shows promise as a suitable PET ligand to study pre-synaptic 5-HT function, as a number of studies report this ligand is displaced by endogenous 5-HT, (Zimmer et al., 2002b, Zimmer et al., 2002a, Zimmer et al., 2003, Aznavour et al., 2006, Rbah et al., 2003, Riad et al., 2004, Udo de Haes, 2005). However, others report 4-[^{18}F]MPPF binding is not affected by changes in endogenous 5-HT , or that it is only detectable in certain 5-HT $_{1A}$ receptor rich areas but not others (Aznavour et al., 2006, Ginovart et al., 2000, Moulin-Sallanon et al., 2009, Riad et al., 2004, Riad, 2008, Udo De Haes et al., 2006).

1.2 Positron emission tomogrophy

PET is a non invasive *in vivo* imaging technique which detects molecules labelled with a positron emitting radioisotope to give metabolic information about the biological structure of interest. Some positron emitting radionuclides such as ^{11}C, ^{13}N and ^{15}O (Table 1) are isotopes of elements found naturally in bio-molecules and it is therefore possible to label such molecules without altering their biological activity (Miller et al., 2008). In addition to those shown in Table 1 gallium-68 (half-life 68 min, ^{68}Ge : ^{68}Ga by β^+ decay) is another well known radionuclide.

Positron emission is a type of beta radioactive decay, indicated by the symbol β^+. A proton rich and therefore unstable nucleus converts a proton to a neutron

by emission of a positron (the antimatter equivalent of an electron) and a neutrino.

Once a molecule of biological interest is identified it can be labelled with a positron emitter and administered to the test subject. The PET radionuclide decays by positron (β^+) emission in the body which travels a short distance (0.5-2.0 cm depending on the kinetics of the particular isotope) before colliding with an electron within the nearby tissue. The collision of matter with antimatter causes mutual annihilation producing two gamma (γ) ray photons of 511 keV, that travel 180° from each other. The PET scanner, which consists of a series of detectors in a ring around the test subject, detects the pair of γ rays which allows the approximate determination of the location of the radiolabelled molecule (Figure 1). Used in combination with an anatomical imaging method such as X-ray computed tomography (CT), where the PET image is overlaid on the CT image, the anatomical location of the radiolabelled molecule can be determined (Miller et al., 2008).

PET is a quantitative imaging method which can monitor the distribution and concentration of radiolabelled molecules over time, giving invaluable evidence of physiological and pathological events (Miller et al., 2008).

Radionuclide	Half-life, $t_{1/2}$ (min)	Nuclear reaction	Target	Product	Decay product
^{11}C	20.4	$^{14}N(p,\alpha)^{11}C$	$N_2(+O_2)$ $N_2(+H_2)$	$[^{11}C]CO_2$ $[^{11}C]CH_4$	^{11}B
^{13}N	9.97	$^{16}O(p,\alpha)^{13}N$	H_2O $H_2O + EtOH$	$[^{13}N]NO_x$ $[^{13}N]NH_3$	^{13}C
^{15}O	2.04	$^{15}N(p,n)^{15}O$	$N_2(+O_2)$	$[^{15}O]O_2$	^{15}N
^{18}F	110	$^{20}Ne(d,\alpha)^{18}F$ $^{18}O(p,n)^{18}F$	$Ne(+F_2)$ $[^{18}O]H_2O$	$[^{18}F]F_2$ $^{18}F^-$	^{18}O

Table 1: The most commonly used short-lived radionuclides in PET, their half-lives, method of production, target products, and decay products (Miller et al., 2008).

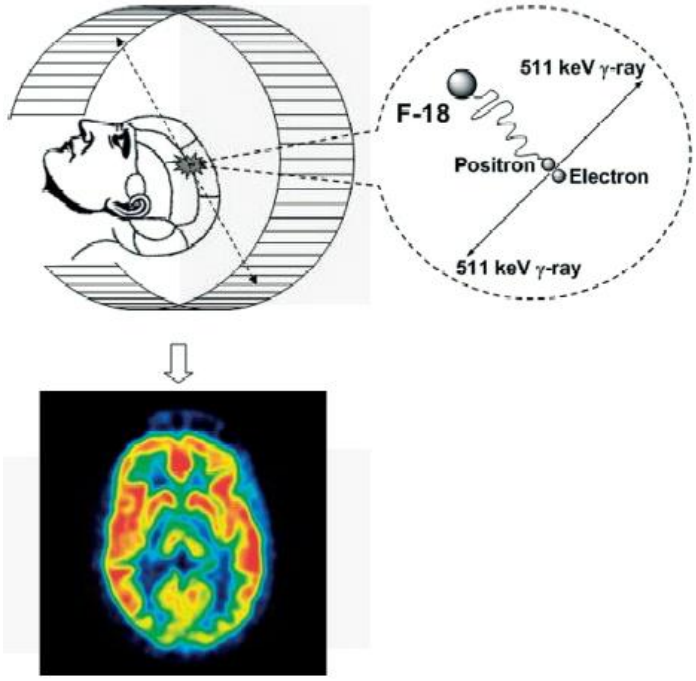

Figure 1: Positron decay and an example of a PET image in the human brain (Cai et al., 2008)

1.2.1 Small animal PET scanners

In biomedical research the use of animal models to study disease is of great importance, not only for examining the pathology of disease, but also for assessing the efficacy and safety of new treatments. In the last two decades the availability of small animal PET, among other imaging techniques, has contributed to our ability to study these animal models *in vivo (Yao et al., 2012)*.

However, there are a number of factors unique to small animal PET that need to be addressed. Firstly, there is a need for a dedicated small animal PET scanner, rather than using scanners designed for human use in preclinical studies. The spatial resolution, defined as the minimum distance between two points in an image that a scanner can differentiate (Saha, 2010), must be optimised in these machines to accommodate the smaller size of research animals. To obtain the same structural detail as a human PET scanner, the spatial resolution of a small animal PET scanner needs to be around 1 mm for the rat and 0.4 mm for the mouse (Yao et al., 2012). Indeed, the system

sensitivity, defined as the number of counts per unit time detected for each unit of activity present (Saha, 2010), is approximately three times greater in small animal PET scanners compared to human PET scanners. There is also the need for dedicated small animal scanners that can be located separately from human scanners, which may be necessary for regulatory purposes as well as being more conveniently placed near animal housing and laboratories (Myers and Hume, 2002).

Small animal PET also suffers from a number of practical problems. Firstly there is the need to anaesthetize the animal, not only to prevent movement which would spoil images, but also to reduce stress on the animal. A consideration of the pharmacological effects of the anaesthetic must therefore be taken into consideration when investigating neurotransmitter systems (Myers and Hume, 2002, Yao et al., 2012, Alstrup and Smith, 2013, McCardle and Gartside, 2012). Secondly, there is a need for a stereotaxic frame to firmLy fix the animal in the correct orientation and prevent movement which may arise from breathing and other movements under anaesthesia (Myers and Hume, 2002). Thirdly, rodents are susceptible to heat loss during scanning and therefore a heating source must be used to maintain body temperature (Yao et al., 2012). This is important not only to ensure the animal is kept in peak physical state and able to recover, but also to provide reproducible and reliable results when physiological parameters, such as blood flow, affect outcome measurements. Lastly, there are limits to the mass and volume of ligand that can be injected into an animal. Therefore ligand radioactivity and specific activity must be sufficient to allow detection at small doses (Yao et al., 2012).

Small animal PET must be used in conjunction with an anatomical imaging modality such as X-ray CT or MRI. As PET imaging is primarily functional, the image quality is often too poor to identify the region of interest which can be overcome when used in combination with an anatomical imager (Myers and Hume, 2002, Ritman, 2002, Yao et al., 2012). There are a number of multimodality scanners that can perform PET and CT or MRI in tandem. However, it is also possible to perform these imaging techniques separately and co-register the images at a later stage.

A number of small animal PET scanners are now commercially available including the Mediso NanoScan PET/CT which has a very high spatial

resolution of 0.7 mm (Mediso) and the SofieBiosciences G4 PET/X-ray which has a spatial resolution of 1.4 mm but boasts a sensitivity of 14%, 2 – 4 times that of competitors (SofieBiosciences). A number of commercially available small animal PET scanners are compared in Table 2. In this thesis the Phillips Mosaic HP small animal PET scanner is used, with a spatial resolution of 1.9 – 2.7 mm and a sensitivity of 1.1 - 3.6% (Surti et al., 2005, Yao et al., 2012, Huisman et al., 2007).

Manufacturer	Model	FOV (mm)		At CFOV...			Reference
		Transaxial	Axial	FWHM spatial resolution (mm)	Sensitivity (%)	Energy window (keV)	
Bioscan/Mediso	NanoPET	45–123	94	1.2	8.3	250–750	(69)
Carestream	Albira	80	40–148	<1.3	3–9	Not available	(70)
Gamma Medica/GE Healthcare	LabPET	110	38–113	1.3	1.1–5.4	250–650	(15)
Philips	Mosaic HP	128	120	2.7	1.1	410–665	(71)
Raytest Isotopenmessgeräte GmbH	ClearPET	94	110	1.5	1.9	250–750	(72)
Sedecal, S.A.	rPET-1	68	47	1.5	0.5	250–650	(72)
Siemens Preclinical Solutions	microPET Focus 120	100	76	1.3	7.1	250–750	(73)
	microPET Focus 220	190	76	1.3	3.4	250–750	(74)
	microPET Inveon DPET	100	127	1.4	9.3	250–625	(32)

CFOV = center field of view.

Table 2: Comparison of the specifications of commercially available small animal PET scanners (Yao et al., 2012).

1.2.2 Radioligands

A radioligand is composed of two elements; the molecular compound, which in the case of imaging neuroreceptors is a specific receptor ligand, and the positron emitting radionuclide. The ligand is responsible for the biological characteristics and defines how the molecule will interact both chemically and biologically *in vivo*. The radionuclide provides a signal which is detectable by the PET scanner (Wadsak and Mitterhauser, 2010). Addition of a radionuclide onto a ligand, rather than exchange of an existing atom with its radioactive isotope, can both positively and negatively affect the bio-characteristics of the molecule as a whole. This must be assessed during development to ensure the new characteristics still provide the necessary requirements for a radioligand, as detailed below.

1.2.3 Requirements for a radioligand for brain imaging

i. High selectivity and affinity for the receptor
ii. None, or relatively small amounts of, metabolites
iii. Relatively slow clearance matched with the half-life of the radionuclide
iv. Moderate lipophilicity for brain imaging agents
v. Low molecular weight for brain imaging agents

A molecular mass of around 400-600 daltons and high lipophilicity are required for a molecule to pass the lipid bilayer of the blood-brain-barrier. However, once within the brain, low lipophilicity and high affinity and selectivity for the target receptor is required to ensure high specific binding. High lipophilicity can increase binding to plasma proteins increasing non-specific binding resulting in poor differentiation between the target receptor and the surrounding tissue, known as the signal to noise ratio. It can be seen therefore that the lipophilicity must be balanced to accommodate these two opposing needs (Fumita and Innis, 2002).

The data from the PET scan is used to produce a ligand time-activity curve in the volume of interest, which characterizes the uptake and washout periods. The lipophilicity and affinity of the radioligand must be balanced so that uptake and washout in the brain is in a time scale suitable for measurements to be taken. In addition, washout must be aligned to the half-life of the radionuclide. It must not be so slow that washout phase measurements cannot be made before the specific radioactivity of the radioligand is too low for detection (Fumita and Innis, 2002).

Lastly, it is necessary to ensure radioligands do not produce unwanted metabolites which can interfere with measurements. Even if not biologically active, those that can pass through the blood-brain-barrier can still interfere with measurements by increasing non-specific binding (Fumita and Innis, 2002).

It can be seen therefore that, with such specific requirements, the development of suitable radioligands is the major bottleneck to the progression of PET imaging.

1.3 Synthesis of Radioligands

1.3.1 Radiosynthesis of radioligands

Development of rapid synthetic methods for labelling ligands with radioisotopes continues to be a challenge in radiochemistry. Due to the short half-lives of the radioisotopes (Table 1) radioligands must be synthesised, purified and analysed within an extremely short time frame to ensure there is enough radio-emitting nuclide to be detectable during PET imaging (Miller et al., 2008). As a guideline, synthesis should take no more than approximately three isotope half-lives (Miller et al., 2008). Therefore, it is advantageous to have a cyclotron or generator for the production of radioisotopes and radiosynthesis and PET facilities in immediate vicinity to each other to facilitate speedy production and imaging of PET ligands (Miller et al., 2008).

Two important factors that must be taken into consideration when radiolabelling a ligand are the radiochemical yield (RCY) and the specific activity (SA) of the final radiolabelled compound. The RCY is dependent on the chemical yield and the half-life of the radioisotope used in labelling and is expressed as a percentage of the radioactivity originally present (Miller et al., 2008). This value can be calculated as either decay or non-decay corrected, where decay corrected takes into account the time elapsed producing the radiolabelled ligand. The SA gives the amount of radioactivity per unit mass of radiolabelled ligand with typical activities for PET ligands in the range of 50-500 GBq μmol^{-1} (Miller et al., 2008). Low specific activity can occur due to dilution with the stable isotope of the element.

1.3.2 Fluorine-18 in PET imaging

Fluorine-18 is the most widely used radionuclide in PET imaging (Miller et al., 2008). Its benefits over other radionuclides are summarised below:

- Due to the production method it is obtained as “no carrier added”; a high ratio of [^{18}F]fluoride ion radioactivity vs. the total mass of carrier or fluoride ion leads to a high specific activity. High specific activity allows for the administration of low volumes of radiolabelled ligands. This is

essential for small animal imaging where body size restricts the volume of PET ligand which can be administered. It is also an advantage in human patients where low volume injections ensures low toxicity (Cai et al., 2008).

- Fluorine-18 has a half-life of 109.7 min which allows sufficient time for transportation of the isotope to the radiochemist, a multistep synthesis of the radiolabelled ligand and subsequent transportation to the PET facilities for administration and imaging of the subject (Cai et al., 2008, Miller et al., 2008).
- Fluorine-18 emits a low energy positron (max 0.635 MeV) which travels only a short distance *in vivo* before annihilation with an electron. The distance the positron travels is related to the spatial resolution of the PET image. The short path taken by positrons emitted from fluorine-18 gives the best quality PET images compared to other radioisotopes (Cai et al., 2008, Miller et al., 2008, Rowland et al., 2002).
- Fluorine-18 decays to give the harmLess ^{18}O decay product (Cai et al., 2008).

1.3.3 Fluorine-18 production and preparation

The most common method of production of fluorine-18 is the proton irradiation of ^{18}O-enriched water. This nuclear reaction $^{18}O(p,n)^{18}F$ is performed in a cyclotron (Cai et al., 2008). This produces [^{18}F]fluoride ions in [^{18}O]water which reduces its reactivity due to its high strength and degree of hydration. To achieve the necessary nucleophilicity required for most reactions, the majority of the water must be removed and the subsequent [^{18}F]fluoride ion must be dissolved in an organic solvent to perform chemical reactions (Cai et al., 2008).

The most common method for preparing the [^{18}F]fluoride ion is detailed below (Figure 2) though variations on this procedure can be made, such as alternative base (hydrogen carbonate, oxalate), kryptand and counterion (Rb^+, Cs^+). Firstly, to recover the ^{18}O water, the [^{18}F]fluoride ion is absorbed onto ion exchange resin and then eluted using a weak aqueous base such as potassium carbonate (K_2CO_3). This is followed by several cycles of azeotropic evaporation with acetonitrile which removes the water from the solution. Use of a kryptand

in this step, such as aminopolyether (K_{222}), allows the counter ion to coordinate with [^{18}F]fluoride ion. At this stage the cation is physically separated from the [^{18}F]fluoride anion making the anion more available for further reaction. Finally the product is dried under nitrogen in a small vessel. As the [^{18}F]fluoride ion can absorb onto the vessel wall during drying, only certain materials can be used which reduce the possibility of absorption. Of these, platinum is the best vessel material. Truly dry [^{18}F]fluoride ions are never obtained as each water molecule of hydration becomes successively more difficult to remove, therefore some will remain hydrated by trace amounts of residual water. As the nucleophilicity increases with each reduction in hydration a well dried product is needed for more difficult reactions such as aromatic nucleophilic substitution (Cai et al., 2008).

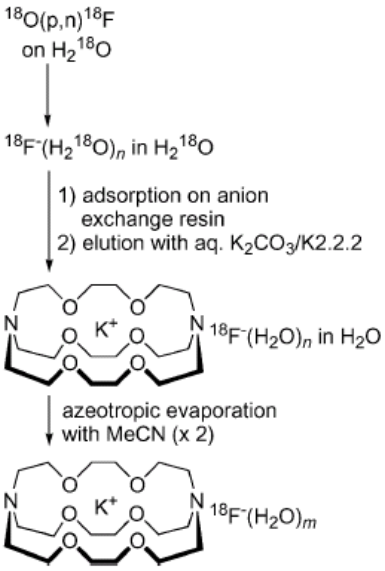

Figure 2: [^{18}F]fluoride ion preparation flow chart showing [^{18}F]fluoride ion-K_{222}-K^+ complex (Cai et al., 2008)

1.3.4 Labelling with fluorine-18

There are a large variety of methods to radiolabel bio-molecules of interest for PET imaging. However, this review will concentrate on two methods that are within the scope of this project.

Aromatic nucleophilic substitution

Direct aromatic nucleophilic substitution is the most successful method to introduce fluorine-18 onto aryl carbons. The reaction requires a good leaving group on the aryl ring in addition to an electron withdrawing group in the 2- or 4-position. Usual leaving groups in order of increasing reactivity are I < Br < Cl < F < NO_2 ≤ N^+Me_3 and usual electron-withdrawing groups in order of increasing withdrawing properties are 3-NO_2 < 4-Ac < 4-CHO < 4-CN ≤ 4-CF < 4-NO_2. Harsh reaction conditions are required, such as 120-180°C in DMSO in the presence of a kryptand and a base, such as K_2CO_3 (Cai et al., 2008).

This reaction was employed by Bars *et al.* to synthesise 4-[^{18}F]MPPF. Substitution of the nitro leaving group in the precursor MPPNO_2 (4-(2'-methoxy-)phenyl-1-[2'-(*N*-2"-pyridinyl-)4-nitrobenzamido-]ethyl piperazine) with [^{18}F]fluoride ion (Scheme 1) gave a radiochemical yield (RCY) of 25% (Bars et al., 1998).

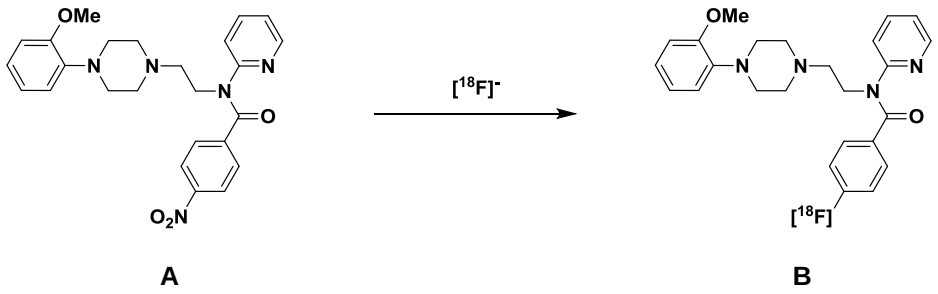

A **B**

Scheme 1: Radiosynthesis of 4-[^{18}F]MPPF (B) by aromatic nucleophilic substitution of 4-MPPNO_2 (A)

^{19}F/[^{18}F] isotopic exchange

Element (X)	van der Waals radius [Å]	Electronegativity (Pauling scale)	Bond length of C–X [Å]
H	1.20	2.20	1.09
O	1.52	3.44	1.43
F	1.47	3.98	1.35

Table 3: Van der Waals radii, electronegativity and bond lengths to carbon of various atoms (Cai et al., 2008)

A fluorine atom may substitute for a hydrogen atom resulting in similar biological activity. However a fluorine atom is more sterically similar to oxygen and has a comparable bond length to carbon, so may also substitute for a hydroxyl group (Table 3) (Cai et al., 2008). The replacement of a hydrogen or hydroxyl group with a fluorine atom affects pharmacokinetics and pharmacodynamics and is therefore often used in drug development (Blom et al., 2009). For this reason it is common to have fluorinated drug molecules, including 4-MPPF, that contain one or more fluorine-19 (Scheme 2). However isotope exchange is prone to producing low specific activity (SA) due to an equilibrium being formed between the [^{18}F] and ^{19}F fluorinated materials.

Blom *et al.* report heating 4-MPPF (17.5 mM) with no carrier added fluorine-18 (approx. 0.5 GBq) in DMF (200 µL) at 150 °C for 15 minutes. This resulted in a radiochemical yield of 8 ± 1% and specific activity of 0.01 GBq/µmol (Blom et al., 2009).

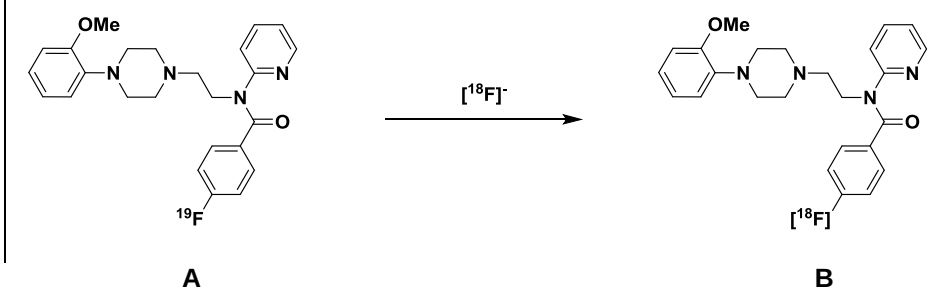

A **B**

Scheme 2: Isotopic exchange of 4-[^{19}F]MPPF (A) to 4-[^{18}F]MPPF (B)

1.3.5 Microwave and microfluidic techniques

Microwave reactors

In comparison to traditional thermal heating the use of microwave reactors (Figure 3) in radiosynthesis can decrease reaction time, thereby increasing RCY and also decreasing the quantity of precursor required to perform the reaction, all of which have popularised the use of this technique. In addition, certain reactions which are difficult to achieve under normal thermal conditions can be achieved using a microwave reactor as well as producing cleaner reaction mixtures through decreased sample decomposition (Cai et al., 2008, Stone-Elander and Elander, 2002).

Figure 3: Typical laboratory microwave reaction cavity and infrared thermometer containing a 5 mL reaction vial (Resonance Instruments Inc., 2011)

Microfluidic reactors

Microfluidic reactors, such as the commercially available Advion Nanotek (Figure 4) allow reactions to take place on a miniaturised scale and can provide a high degree of reproducibility. In addition they can be controlled remotely from behind shielding, which is an especially important safety consideration when dealing with radioisotopes. They consist of micron-sized channels (in the range of 100-300 µm), filters, separation columns and reaction loops. The

internal volume of the reaction loops is in the range of 30 µL for a 4 m length with a diameter of 100 µm. Reaction mixtures that enter the reaction loops mix under laminar flow and equilibrate to the reactor set temperature. The reaction time is set by the flow rate and is essentially the residence time within the reactor. Microfluidic system reactions can be performed rapidly under precisely controlled conditions of time, temperature and reaction stoichiometry. In addition the temperature can be set above the boiling point of most organic solvents due to containment of the increased pressure in the system. Another valuable feature of this technique is that only milligram quantities of precursors are required which is especially important when using expensive or difficult to obtain compounds (Chun et al., 2010, Cai et al., 2008).

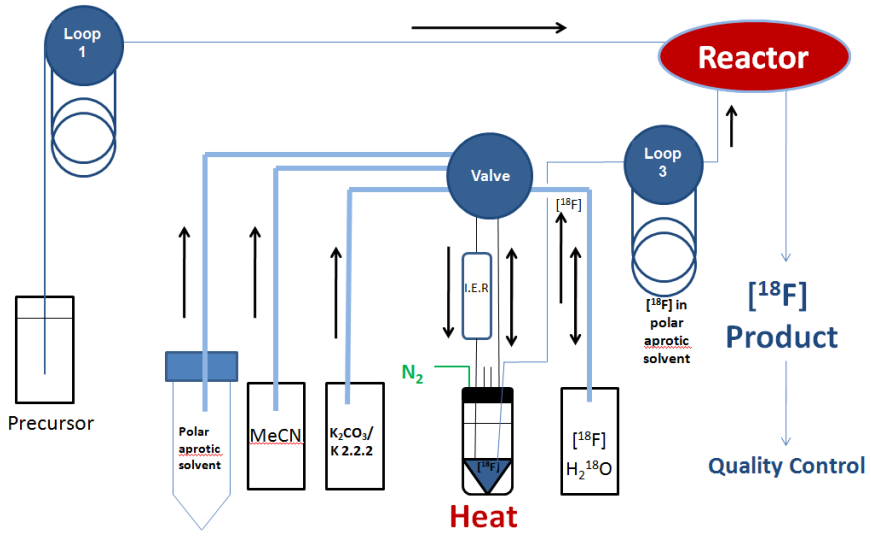

Figure 4: Schematic diagram showing a possible set up for the Advion Nanotek microfluidic system. The [^{18}F]fluoride ion is separated from $H_2{}^{18}O$ by absorption onto an ion exchange resin (I.E.R), eluted into the vessel below using K_2CO_3/K_{222}, then azeotropically dried using acetonitrile followed by further drying under N_2 and heat. The kryptand coordinated [^{18}F]fluoride ion is then dissolved in a polar aprotic solvent, such as dimethylformamide and is sent to the reactor in tandem with the precursor for the reaction to take place. Original image created by C. Reed.

1.4 Development of 5-HT $_{1A}$ ligands for PET

1.4.1 5-HT PET ligands

There is still a great need to develop new PET ligands to examine the 5-HT system as, to date, only five 5-HT receptors and the serotonin transporter have PET ligands available to examine their function. These include 5-HT_{1A}, 5-HT_{1B}, 5-HT_{2A}, 5-HT_4 and 5-HT_6, as well as the serotonin transporter (SERT) (Zimmer and Le Bars, 2013, Paterson et al., 2013). Out of those available, table 4 summarises the 5-HT PET ligands currently of most interest.

Target	Radioligand	Pre-clinical studies
5-HT_{1A}	[^{11}C]WAY-100635	10
	[^{18}F]MPPF	27
	[^{18}F]FCWAY	7
5-HT_{2A}	[^{18}F]setoperone	3
	[^{18}F]altanserin	6
	[^{11}C]MDL100907	5
SERT	[^{11}C]DASB	17
	[^{11}C]MADAM	1

Table 4; Summary of the current leading 5-HT PET ligands (Paterson et al., 2013)

Table 5 summarises the 5-HT_{1A} ligands that have been studied for PET and SPECT. As can be seen, some of these ligands have already failed to meet the requirements for a PET or SPECT ligand, and most have known problems. This highlights the ongoing need for the development of new 5-HT_{1A} PET ligands with superior characteristics.

Target	Type	Radioligand	Rodent	Nonhuman primate	Human	Ongoing studies	Reason for failure	Known problems
5-HT$_{1A}$	SPECT	[^{123}I]p-MPPI	✓	✓	×	–	No specific 5-HT$_{1A}$ binding Rapid metabolism Possible brain exclusion via efflux transporter	–
	PET	[^{11}C]WAY-100635	✓	✓	✓	✓	–	Fast systemic metabolism; difficult kinetic modelling with arterial input function, reference tissue models complicated by radiometabolites in plasma
		[^{11}C]CPC-222	✓	ND	✓	ND		Lower signal-to-background ratio than [^{11}C]WAY-100635
		[^{11}C](R)-RWAY	×	✓	×	–	Possible influx of lipophilic radiometabolite	P-gp substrate in rodent
		[^{11}C]DWAY	✓	✓	✓	ND		Unreliable radiolabelling technique; low radioactive yield
		[^{18}F]6FPWAY	ND	✓	×	–	Moderate uptake	–
		[^{18}F]MPPF	✓	✓	✓	✓	–	P-gp substrate; fast brain clearance and low uptake
		[^{18}F]FCWAY	✓	✓	✓	✓	–	Defluorination of parent compound; sub-optimal imaging
		[^{18}F]MefWAY	ND	✓	ND	–		
		[^{11}C]NAD-299	ND	✓	ND	–		
		[^{11}C]CUMI-101	✓	✓	✓		–	Partial, not full agonist

Table 5: PET and SPECT radioligands studied for the 5-HT$_{1A}$ receptor; showing both failed ligands and those with ongoing studies (Paterson et al., 2013).

Although the need to find displaceable 5-HT ligands is of great interest, not all studies are set up to examine this characteristic and instead focus on other factors such as biodistribution, specificity for receptor type and metabolite studies. For instance, 4[^{18}F]MPPF has been examined in twenty-seven pre-clinical studies, but only twelve of these attempted to establish whether it is displaceable by endogenous 5-HT (Aznavour et al., 2006, Ginovart et al., 2000, Millet et al., 2008, Moulin-Sallanon et al., 2009, Rbah et al., 2003, Riad, 2008, Riad et al., 2004, Udo de Haes, 2005, Udo De Haes et al., 2006, Zimmer et al., 2002a, Zimmer et al., 2002b, Zimmer et al., 2003). This trend continues for other 5-HT ligands. For example the 5-HT$_{2A}$ PET ligand [^{18}F]altanserin has been examined in six pre-clinical studies, but only one examines whether it is displaceable by endogenous 5-HT (Staley et al., 2001).

This paucity of studies examining the displacable nature of 5-HT PET ligands highlights the need for further studies focused on displacability by endogenous 5-HT starting at the pre-clinical level.

1.4.2 5-HT $_{1A}$ PET ligands

5-HT $_{1A}$ receptor PET ligands generally fall into one of two classes; (i) those which are structurally similar to the 5-HT $_{1A}$ antagonist WAY-100635 or (ii) derivatives of the 5-HT $_{1A}$ agonist (±)-8-OH-DPAT (Scheme 3)

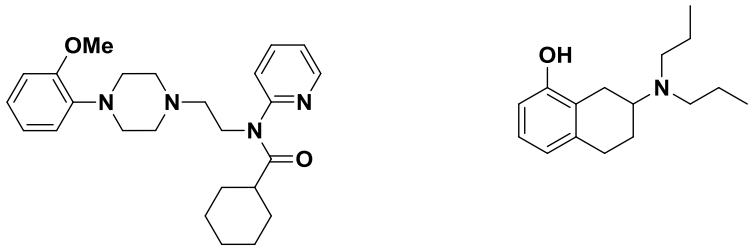

A **B**

Scheme 3: WAY100635 (A) and (±)-8-OH-DPAT (B)

To date all PET radioligands used in clinical studies are antagonists, although efforts continue in the development of 5-HT$_{1A}$ agonist ligands (Kumar and Mann, 2007, Lemoine et al., 2010, Zimmer and Le Bars, 2013).

WAY100635 is a potent 5-HT $_{1A}$ receptor antagonist and was the first fully selective 5-HT $_{1A}$ antagonist to be discovered. The first radiolabelled version [*O-methyl*-^{11}C]WAY100635 was found to have a radiolabelled metabolite with the ability to pass through the blood-brain-barrier, which interfered with PET measurements by increasing non-specific binding. This was overcome by incorporating the radiolabel at the *amide carbonyl* position, resulting in [*carbonyl*-^{11}C]WAY-100635 (Scheme 4). This analogue maintained a high affinity for 5-HT $_{1A}$ receptors (K_D = 0.2 nM) in addition to having no interfering metabolites. These features now make [*carbonyl*-^{11}C]WAY-100635 a commonly used 5-HT $_{1A}$ PET radioligand (Kumar and Mann, 2007, Cliffe, 2000, Lang et al., 1999).

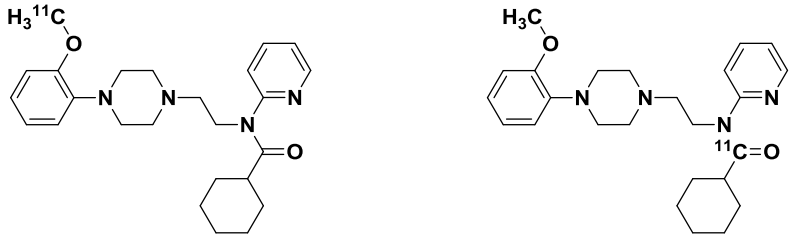

Scheme 4: [O-methyl-^{11}C]WAY-100635 (A) and [carbonyl-^{11}C]WAY-100635 (B)

However, [*carbonyl*-^{11}C]WAY100635 has a fast metabolism and is rapidly cleared from the brain. In addition, the short half-life of carbon-11 results in low radioactivity in plasma samples making it unsuitable for kinetic quantification of the radioligand in the brain (McCarron et al., 2004). Therefore compounds labelled with the isotope fluorine-18 are more desirable as its longer half-life ($t_{1/2}$ = 109.7 min vs. 20.3 min for ^{11}C, Table 1) allows for both longer radiosynthetic methods and increased PET imaging time.

One analogue of WAY100635, FCWAY (Scheme 5), was developed and successfully radiolabelled with fluorine-18. [^{18}F]FCWAY showed some pharmacokinetic improvements over [*carbonyl*-^{11}C]WAY100635 but has the major disadvantage of fluorine-18 defluorination *in vivo* (Cliffe, 2000, Kumar and Mann, 2007). In addition one study suggests it is not sensitive to changes in endogenous 5-HT (Jagoda et al., 2006).

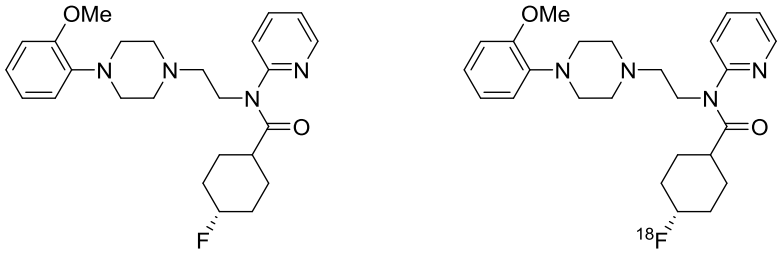

Scheme 5: FCWAY (A) and [^{18}F]FCWAY (B)

The aromatic version of FCWAY is 4-MPPF, which has also been successfully labelled with fluorine-18 and shows many promising attributes needed for a 5-HT $_{1A}$ antagonist radioligand. One feature is its lower affinity towards 5-HT $_{1A}$ receptors compared to WAY100635. 4-MPPF binding to 5-HT $_{1A}$ receptors has been shown to be reversible and could therefore potentially be displaced by endogenous 5-HT (Kumar and Mann, 2007). This feature is of particular interest in the scope of this project as displacement by endogenous 5-HT could reveal possible changes in neurotransmitter levels associated with affective disorders.

1.4.3 Towards MPPF as a 5-HT PET ligand

A series of 4-(2'-methoxyphenyl)-1-[2'(*N*-2"-pyridinyl)halobenzamido] ethyl]piperazines were prepared by Zhuang *et al.* to develop new radiolabelled antagonists of the 5-HT $_{1A}$ receptor. Among these was a fluorinated version, with the fluorine in the 4- position, 4-MPPF and three iodinated versions, 2-, 3- and 4-MPPI (Figure 5) (Zhuang et al., 1994).

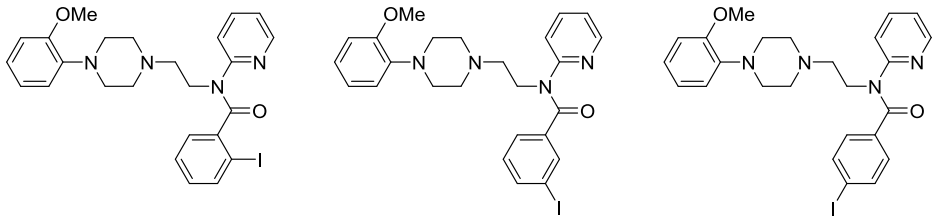

Figure 5: 2-MPPI (A), 3-MPPI (B) and 4-MPPI (C)

The brain distribution of 4-MPPI radiolabelled with iodine-123 or iodine-125 was examined in the rat brain. 4-MPPI displayed good initial uptake in the brain (1.22% dose/organ 2 minutes after i.v injection) and demonstrated high selectivity for the 5-HT $_{1A}$ receptor. This was shown by the high uptake in the hippocampus, where 5-HT $_{1A}$ receptor density is high, and low uptake in the cerebellum, which is almost devoid of 5-HT $_{1A}$ receptors (Pazos et al., 1987).

The selectivity was further demonstrated with blocking studies which pre-treated with the selective 5-HT $_{1A}$ antagonist WAY100635 or the 5-HT $_{1A}$ agonist (±)-8-OH-DPAT. This had the effect of a dramatic reduction of hippocampal uptake, with the hippocampus : cerebellum uptake ratio reducing from 3.69 to 1.21 for (±)-8-OH-DPAT and 1.07 for WAY100635. This reduction is explained by binding competition at the receptor with the agonist or antagonist therefore suggesting 4-MPPI is selective for the 5-HT $_{1A}$ receptor (Kung et al., 1996a, Zhuang et al., 1994).

However an *in vivo* study in non-human primates revealed 4-MPPI produces iodinated metabolites which dramatically reduced the binding to 5-HT $_{1A}$ receptors (Kung et al., 1996a, Aznavour and Zimmer, 2007).

Therefore, other studies were focusing on 4-MPPF as a possible new 5-HT $_{1A}$ antagonist. The distribution of 4-[^{18}F]MPPF binding in the rat brain was confirmed to match that of 5-HT $_{1A}$ receptors by autoradiography, which was in line with immunocytochemistry using specific antibodies against 5-HT $_{1A}$ (Aznavour and Zimmer, 2007). 4-MPPF has been shown to be a selective antagonist of the 5-HT $_{1A}$ pre-synaptic autoreceptors and postsynaptic heteroreceptors (Thielen and Frazer, 1995, Thielen, 1996, Zhuang et al., 1994). The brain uptake is low (0.055% whole brain, 0.066% DRN, 0.018% cerebellum injected dose/g after 30 min in rats) (Plenevaux et al., 2000, Zimmer et al., 2002b). However, this uptake has been shown in subsequent studies to be sufficient for PET detection. 4-MPPF demonstrated high selectivity for the 5-HT $_{1A}$ receptor (Kung et al., 1996c) and has a comparable affinity (Inhibition constant K_i=3.3nM ± 0.8) (Zhuang et al., 1994), compared to the endogenous neurotransmitter 5-HT (K_i=4.17nM) (Van Wijngaarden et al., 1990), where Ki is the inhibition constant of compounds on the binding of (±)-8-OH-DPAT). Therefore it can be inferred that endogenous 5-HT could displace 4-MPPF from the 5-HT $_{1A}$ receptor, giving a measure of changes in the endogenous 5-HT levels. In addition 4-[^{18}F]MPPF has been found to have no unwanted radioactive metabolites (Plenevaux et al., 2000).

In summary, 4-[^{18}F]MPPF has been shown to fit many of the criteria for a good PET tracer. It has the ability to cross the blood-brain-barrier followed by washout indicating adequate lipophilicity, has high selectivity and affinity for the 5-HT $_{1A}$ receptor, binds reversibly to the 5-HT $_{1A}$ receptor and has a washout

time in the scale suitable for PET imaging, in addition to producing no unwanted metabolites.

1.4.4 Synthesis and purification of 4-[^{18}F]MPPF

Initially 4-MPPF was radiolabelled with iodine-123 or iodine-125 (Zhuang et al., 1994) and tritium (Kung et al., 1996b) but later was successfully radiolabelled with fluorine-18 by Shiue *et al.* (Shiue et al., 1997). An optimised synthesis of the regio-isomers of both MPPF and $MPPNO_2$ to produce cold standards (Scheme 6) and a general procedure for [^{18}F]fluorination *via* a nucleophilic substitution of the nitro precursor, $MPPNO_2$, (Scheme 1) was published by Bars *et al.* (Bars et al., 1998). The radiosynthesis, performed on a Liege robotic system, gave methods for both standard (150 ºC, 20 min, aluminium block) and microwave heating (3 min, 500 W), resulting in a 25% radiochemical yield, 37 – 185 GBq/µmol specific activity in 70 min and was the general protocol followed by subsequent papers. It has since been shown that radiosynthesis of 4-[^{18}F]MPPF *via* a fluorodenitration reaction can be fully automated on a Tracer Lab FX_{FN} (Shao et al., 2011) and a NIRS synthesis module (Hayashi et al., 2012).

Chromatographic and spectrographic techniques were assessed by Koivula *et al.* in relation to the notoriously difficult to separate 4-[^{18}F]MPPF from the precursor $MPPNO_2$. (Koivula et al., 2010). Optimised separation methods using HPLC (C_{18} semi preparative column, THF/MeOH : 0.05 M NaOAc (18:27:55 v/v) pH 5, 2 mL/min. Retention times; 4-[^{18}F]MPPF 15 min, $MPPNO_2$ 22 min) and TLC (60 F_{254} silica gel plates, CH_3CN : H_2O 90:10% mobile phase) were described.

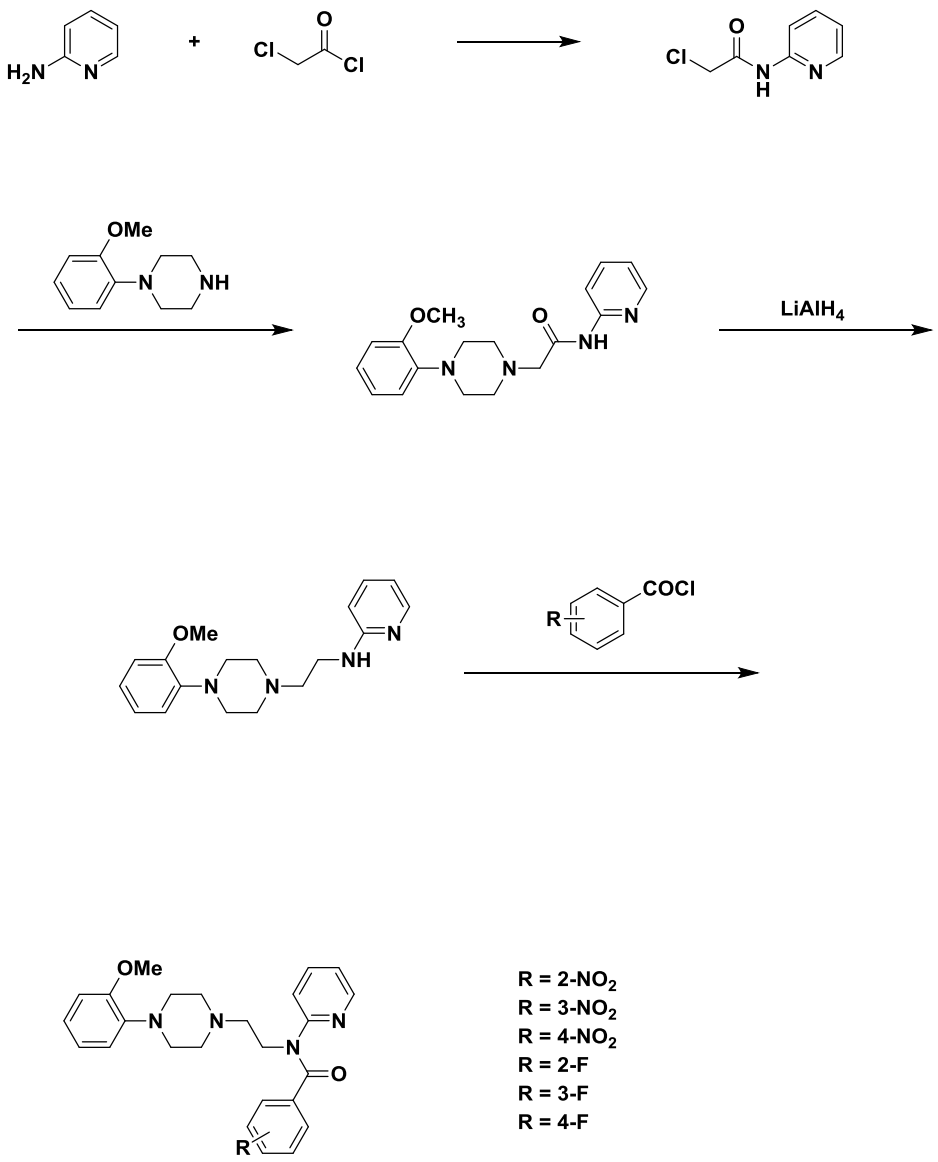

Scheme 6: General synthesis of 2-, 3- and 4- regioisomers of MPPF and MPPNO$_2$ as performed by Bars et al. (Bars et al., 1998)

1.5 Aims of thesis

The aims of this thesis are to:

- Optimise the synthesise the 4-[^{18}F]MPPF precursors, 4-MPPF and 4-MPPNO_2, for analytical method & reaction development.
- Develop a routine radiosynthetic method for the production of 4-[^{18}F]MPPF suitable for low radioisotope activity.
- Use parallel standardised protocols in *in vivo* microdialysis, autoradiography and PET imaging to characterise the binding distribution and displacability of 4-[^{18}F]MPPF in the rat brain.

The thesis is organised into two main research areas. Chapters 2 and 3 describe the development of the chemistry and radiochemistry for the synthesis of 4-[^{18}F]MPPF and its precursors. Chapters 4 and 5 describe the characterisation of the 4-[^{18}F]MPPF in the rat brain.

Chapter 2. Synthesis of 4-MPPF and 4-MPPNO$_2$

2.1 Introduction

It is the aim of this thesis to characterise the PET ligand 4-[^{18}F]MPPF using PET imaging and autoradiography. As the radioisotope fluoride-18 has a short half-life, the radioligand must be produced on the day of use. Therefore precursors to 4-[^{18}F]MPPF must first be obtained. This study requires relatively large quantities of precursors to complete extensive analytical and radiosynthesis development and *in vivo* studies. Therefore it was necessary to synthesise the precursors as part of the present study in order to obtain sufficient quantities for the project. These precursors are used in Chapter 3 to radiosynthesise 4-[^{18}F]MPPF.

As discussed in the Chapter 1 (Section 1.3.4), two possible radiosynthesis reaction routes are being considered in this study; ^{19}F/[^{18}F] isotopic exchange and aromatic nucleophilic substitution, in the form of a fluorodenitration reaction. Each reaction route requires a precursor; 4-MPPF and 4-MPPNO$_2$ respectively and therefore the synthesis of these materials will be described in this chapter.

Therefore, the aims of this chapter are to;

- Synthesise the ^{19}F standard, 4-MPPF
- Synthesise the nitro precursor, 4-MPPNO$_2$.
- To evaluate alternative synthesis routes.

.

2.2 Results and Discussion

It was an aim of this project to synthesise 4-MPPF and 4-MPPNO$_2$ for use in later studies. The 2-, 3- and 4- regioisomers of MPPF and MPPNO$_2$ have previously been synthesised by Bars *et al.* (Bars et al., 1998) (Scheme 6) using a four step synthesis. Therefore synthesis was undertaken following the general procedure as reported by Bars et al. (Bars et al., 1998). A small scale synthesis was first undertaken to ensure the published procedure could be replicated, with some work up procedures modified as required. Of the small scale crude products, 4-MPPF was purified and characterised by ^{1}H, ^{13}C and ^{19}F NMR. The successful small scale synthesis was followed by large scale synthesis of both 4-MPPF and 4-MPPNO$_2$. 4-MPPF was obtained in a yield of 61% (2.85 g) and the structure was confirmed using ^{1}H, ^{13}C, ^{19}F NMR and elemental analysis. Crystals suitable for x-ray crystallography analysis were grown from dissolving 4-MPPF in ethyl acetate (60 ºC to RT), followed by addition of petrol. (Figure 6, Appendix A). 4-MPPNO$_2$ gave a yield of 40% (0.83 g) and the structure was confirmed using ^{1}H,^{13}C NMR and elemental analysis.

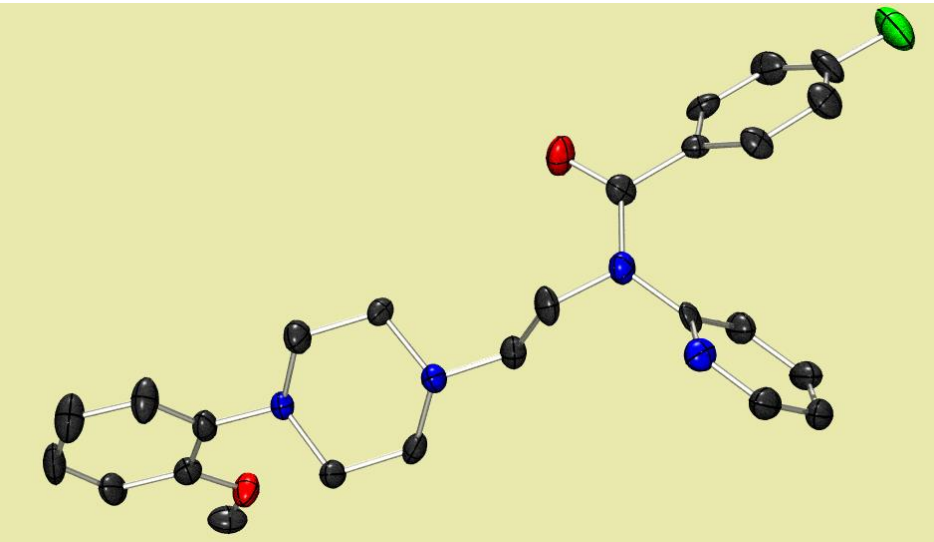

Figure 6: Solid state structure of 4-MPPF, as determined by x-ray crystallography. Atomic key: black: carbon, red: oxygen, blue: nitrogen, green: fluorine.

In addition, alternative synthesis routes were evaluated with the aim of removing a step from the published synthesis and therefore reducing synthesis time. The third step of the synthesis is a reduction step, which could be avoided if an alkyl group was introduced directly rather than *via* the intermediate acetyl group. Therefore, four alternative syntheses were attempted (Scheme 7) with the proposed full synthesis shown in Scheme 8 and 9. In each case TLC and ^{1}H NMR revealed only starting materials at the end of the reaction, confirming no reaction took place.

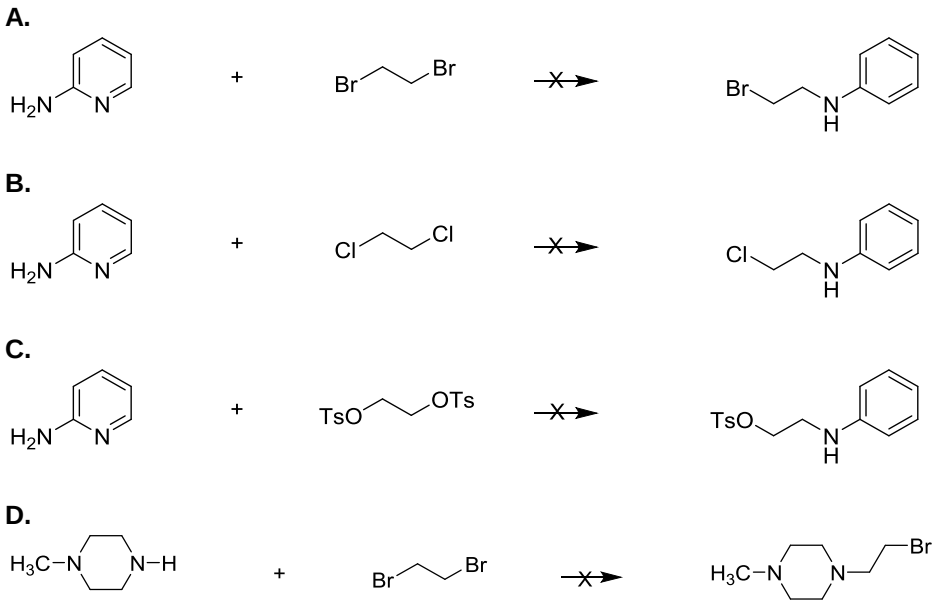

Scheme 7: Four alternative first step reactions attempted for the synthesis of MPPF. Reaction conditions; ***A1****. Tetrahydrofuran (THF), NaH, RT, 12 hr.* ***A2****. THF, NaH, reflux, 12 hr.* ***B1.*** *THF, NaH, reflux, 12 hr.* ***B2****. 1, 2-dichloroethane, NaH, relux,12 hr.* ***B3.*** *THF, NaH, reflux, 72 hr.* ***C.*** *THF, NaH, reflux, 12 hr.* ***D.*** *CH_3CN, K_2CO_3, reflux, 4 hr.*

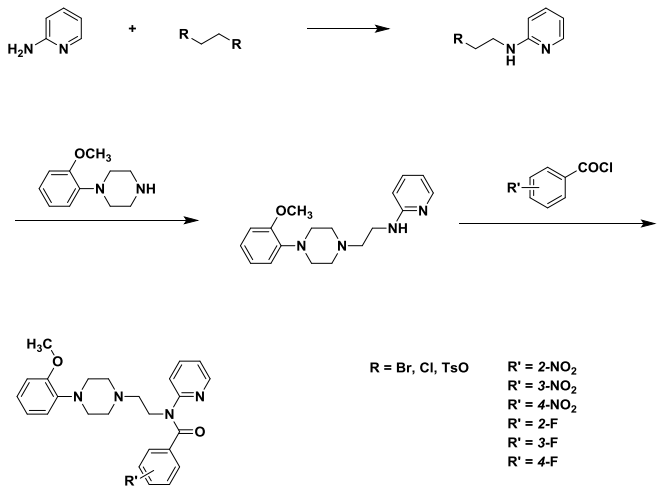

Scheme 8: Proposed synthesis scheme using alternative reaction steps A, B or C (Scheme 7)

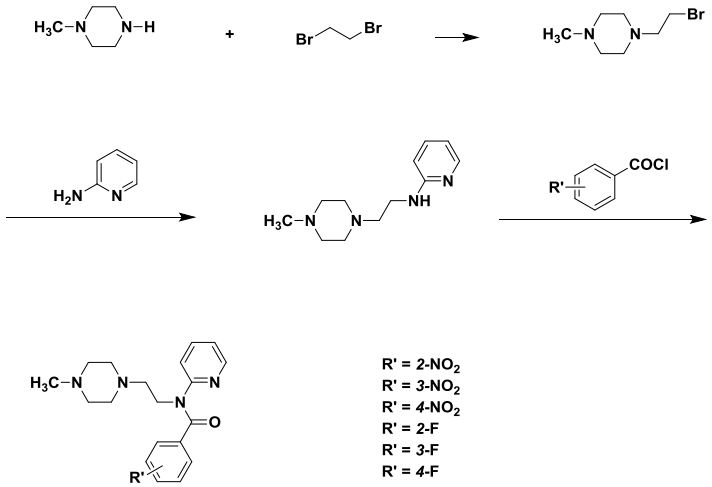

Scheme 9: Proposed synthesis scheme using alternative reaction step D starting with a model compound (Scheme 7).

2.3 Summary

In this chapter 4-MPPF and 4-MPPNO$_2$ were synthesised with suitable purity and in sufficient volume to be used in Chapter 3 as the 4-[^{18}F]MPPF precursors to develop a radiosynthesis method and then routinely radiosynthesise 4-[^{18}F]MPPF for PET and autoradiography experiments.

It was also shown a number of alternative synthesis routes did not produce product at the given conditions. It should also be noted that although a reaction step was removed in the alternative synthesis routes, the new proposed reaction step is likely to react more slowly than in the reaction step in the original synthesis, therefore may not have an overall benefit.

2.4 Experimental

Reactions requiring anhydrous conditions were performed with glassware dried with heat under vacuum and reactions conducted under a positive pressure of nitrogen. Anhydrous solvents were prepared using standard protocols or by storage over molecular sieves (4Å). Flash chromatography was performed on a Varian 971-FP Flash purification system. Thin layer chromatography was performed using Kieselgel 60F$_{254}$, 0.2 mm silica gel plates with aluminium backing and visualised using short (254µm) and long (356µm) UV light and $KMnO_4$ solution. ^{1}H and ^{13}C NMR spectra were carried out on a JeolECS 400 MHz spectrometer with residual protic solvent as the reference. ^{19}F NMR spectra were recorded on a Jeol ECS 400MHz spectrometer using $CFCl_3$ as an external reference. Melting points were determined using a Gallenkamp MF-370 melting point apparatus and are uncorrected. Elemental analysis were performed by London Metropolitan University Elemental Analysis Service and are reported as the average of two runs. X-ray crystal structures was performed by the Newcastle University X-ray crystallography department.. Analytical HPLC was performed on the Agilent Technologies 1200 series with a Phenomenex polystyrene divinylbenzene, 50 x 4 mm, 5 micron column.

2.4.1 Synthesis of 2-, 3- and 4-MPPF, 3- and 4-MPPNO2

2-chloro-N-2-pyridinyl acetamide, 1 (Bars et al., 1998)

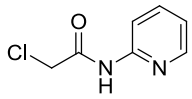

2-Aminopyridine (0.95 g, 10 mmol) was added to CH_2Cl_2 (20 mL) and Et_3N (1.68 mL, 0.012 mol) and stirred in an ice bath. Chloroacetyl chloride (0.97 mL, 12 mmol) was then added and allowed to stir in an ice bath for 85 min. After confirmation by TLC that the 2-aminopyridine had been consumed, water (10 mL) was added. The organic layer was separated and the aqueous layer was extracted with CH_2Cl_2 (x3). The combined organic layers were dried ($MgSO_4$), filtered and concentrated *in vacuo* to give the crude product as grey-brown solid. The product was used in the next step without further purification.

Small scale

Grey-brown solid (1.59 g, 9.32 mmol). (R_f = 0.65 (1:3 petrol : ethyl acetate, 2 developments); ^{1}H NMR($CDCl_3$, 400 MHz): signals selected from crude; δ (ppm) 8.84 (br, 1H), 8.31 (m, 1H), 8.18 (d, *J*=8.4 Hz, 1H), 7.72 (ddd, *J*=8.4, 7.5, 1.9 Hz, 1H), 7.09 (ddd, *J*=7.4, 4.9, 1.0 Hz, 1H), 4.18 (s, 2H); ^{13}C NMR($CDCl_3$, 101 MHz): δ (ppm) 164.5, 150.4, 148.2 and 148.1, 138.7 and 138.5, 120.9 and 120.6, 114.1 and 113.9, 42.9.

Large Scale

With 2-aminopyridine (50 g, 530 mmol). Grey-brown solid (94.46 g, 550 mmol, 104%). R_f = 0.56 (1:1 petrol : ethyl acetate). NMR data matches above.

4-(2'-Methoxy-)phenyl-1-(2'-pyridinylaminocarbonyl-)methyl piperazine, 2 (Bars et al., 1998)

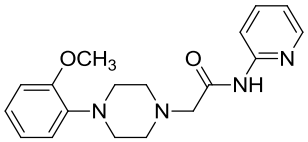

The crude 2-chloro-N-2-pyridinyl acetamide **(1)** (1.32 g, 7.76 mmol) was added to DMF (12 mL) followed by K_2CO_3 (3.25 g, 23.3 mmol) and stirred vigorously for 5 min. 1-(2'-methoxyphenyl)piperazine (2.01 g, 8.54 mmol) was added to the mixture and stirred vigorously at room temperature for 18 h. After confirmation by TLC that 1-(2"-Methoxyphenly) piperazine had been consumed, water (20 mL) was added. The mixture was extracted with CH_2Cl_2 and the organic layer was dried ($MgSO_4$), filtered and concentrated *in vacuo.* Purification using column chromatography (SiO_2, ethyl acetate : petrol 40-60, 30 : 70) gave the product as a pale yellow solid.

Formatted: Font: Not Bold

Small scale

Pale yellow solid (1.47 g, 4.52 mmol, 58%). Mp 84 -85 °C (lit.(Park et al., 2005) 84 ºC) from acetone, R_f = 0.68 (1:4 petrol : ethyl acetate, 2 developments); ^{1}H NMR($CDCl_3$, 400 MHz): δ (ppm) 9.66 (s, 1H), 8.32 – 8.27 (m, 1H), 8.24 (d, J=8.3 Hz, 1H), 7.69 (t, J=7.9 Hz, 1H), 7.05 – 6.89 (m, 4H), 6.85 (d, J=8.0 Hz, 1H), 3.85 (s, 3H), 3.25 (s, 2H), 3.18 (br, 4H), 2.84 (t, 4H); ^{13}C NMR($CDCl_3$, 101 MHz): δ (ppm) 152.3, 151.1, 148.1, 140.9, 138.4, 123.4, 121.1, 120.0, 118.5, 114.0, 111.3, 62.3, 55.5, 53.9, 50.6.

Large scale

With 2-chloro-N-2-pyridinyl acetamide(**1**) (58 g, 340 mmol). Final purification was performed by recrystallisation (x2) with acetone and petrol 40-60 to give a pale yellow solid.

Pale yellow solid (37.17 g, 111 mmol, 34%).Mp 85 - 86°C (lit.(Park et al., 2005) 84 ^{0}C) from acetone; R_f = 0.47 (1 : 1 petrol : ethyl acetate); NMR data matches above.

4-(2'-Methoxyphenyl)-1-[2'-(2''-pyridinyl-)amino]ethyl piperazine, 3 (Bars et al., 1998)

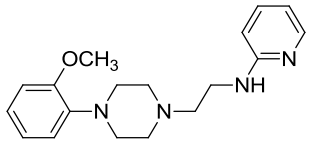

4-(2'-methoxy-)phenyl-1-(2'-pyridinylaminocarbonyl-)methyl piperazine (**2**) (510 mg, 1.56 mmol) in THF (10 mL) was added dropwise at room temperature to a slurry of $LiAlH_4$ (190 mg, 5.01 mmol) also in THF (10 mL). The mixture was heated at reflux (75 °C for1 hr) then cooled to room temperature. After confirmation by TLC that (**2**) had been consumed, the mixture was diluted with diethyl ether (20 mL) then cooled to 0 °C in an ice bath. Water (0.2 mL), NaOH (15% aqueous solution, 0.2 mL) and water (0.6 mL) were added successively dropwise and the mixture was allowed to warm to room temperature. $MgSO_4$ (~1 g) was added and the solution allowed to stir for 15 min. The solution was vacuum filtered and concentrated *in vacuo* to give the crude product as an orange oil. The product was used in the next step without further purification.

Small scale

Orange oil (0.33 g, 0.99 mmol, 64%). R_f = 0.22 (1:4 petrol : ethyl acetate, 2 developments); ^{1}H NMR($CDCl_3$, 400 MHz): δ (ppm) 8.07 (dd, *J*=5.0, 1.4 Hz, 1H), 7.43 – 7.36 (m, 1H), 7.02 – 6.81 (m, 4H), 6.55 (ddd, *J*=7.2, 5.1, 0.7 Hz, 1H), 6.42 (d, *J*=8.3 Hz, 1H), 5.25 (s, 1H), 3.84 (s, 3H), 3.41 (dd, *J*=11.2, 5.4 Hz, 2H), 3.11 (s, 4H), 2.79 – 2.67 (m, 6H); ^{13}C NMR($CDCl_3$, 101 MHz): δ (ppm) 158.8, 152.3, 148.1, 141.2, 137.4, 123.1, 121.1, 118.3, 112.8, 111.2, 107.4, 56.9, 55.4, 53.2, 50.5, 38.4.

Large scale

With 4-(2'-methoxy-)phenyl-1-(2'-pyridinylaminocarbonyl-)methyl piperazine (**2**) (14.88 g, 46 mmol). The product was purified by recrystallisation (ethyl acetate and petrol) to give a white crystalline solid.

White crystalline solid (4.93 g, 0.016 mol, 34%). Mp 96 - 97 °C (lit.(Park et al., 2005) 63- 64 ^{0}C)from ethyl acetate; R_f= 0.24 (1:4 petrol : ethyl acetate); NMR data matches above.

4-(2'-Methoxy-)phenyl-1-[2'-(*N*-2"-pyridinyl-)*4-fluorobenzamido*-]ethyl piperazine (4-MPPF), 4 (Bars et al., 1998)

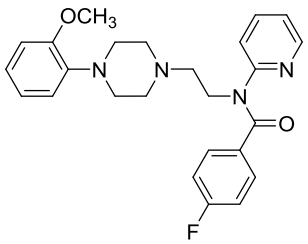

4-(2'-,methoxy-)phenyl-1-[2'-(2"-pyridinyl-)amino]ethyl piperazine (**3**) (0.21 g, 0.71 mmol) and Et_3N (0.24 mL, 0.17 mol) were added to CH_2Cl_2 (5 mL) and the solution allowed to cool to 0 °C in an ice bath. 4-Fluorobenzoyl chloride (0.1 mL, 0.85 mol) in CH_2Cl_2 (5 mL) was added dropwise at 0 °C and the mixture allowed to stir for a further hour at room temperature. After confirmation by TLC that (**3**) had been consumed, water (2 mL) was added and the mixture extracted with CH_2Cl_2 (x3). The combined organic layers were dried ($MgSO_4$), filtered and concentrated *in vacuo.* Purification using column chromatography (SiO_2, ethyl acetate : petroleum ether 40-60 °C % 50 : 50) gave a white solid.

Small scale

White solid (0.07 g, 0.17 mmol, 24%).R_f= 0.37 (1:4 petrol : ethyl acetate, 2 developments); ^{1}H NMR($CDCl_3$, 400 MHz): δ (ppm) 8.41 – 8.39 (m, 1H), 7.42 – 7.37 (m, 1H), 7.34 – 7.28 (m, 2H), 7.01 (ddd, *J*=7.3, 4.9, 0.8 Hz, 1H), 6.98 –

6.80 (m, 6H), 6.74 (d, *J*=8.1 Hz, 1H), 4.28 (t, *J*=6.7 Hz, 2H), 3.81 (s, 3H), 2.93 (s, 4H), 2.76 (t, *J*=6.5 Hz, 2H), 2.66 (s, 4H); ^{13}C NMR($CDCl_3$, 101 MHz): δ (ppm) 169.7, 164.9, 162.4, 156.5, 152.3, 148.8, 141.3, 137.3, 132.3, 131.2 and 131.1, 122.9, 121.1 and 121.0, 118.2, 115.3and 115.1, 111.2, 56.4, 55.4, 53.4, 50.5, 45.5.; ^{19}F NMR($CDCl_3$, 376 MHz): δ (ppm) -109.2.

Large scale

With 4-(2'-methoxy-)phenyl-1-[2'-(2"-pyridinyl-)amino]ethyl piperazine (**3**) (3.2 g, 10.8 mmol). Purified by column chromatography (SiO_2,ethyl acetate 100%) and recrystallisation (diethyl ether and petrol) to give a white crystalline solid.

White crystalline solid (2.85 g, 6.56 mmol, 61%).Mp 82 – 83 ^{0}C (lit. (Bars et al., 1998) 81.8 ^{0}C); R_f = 0.59 (1:4 petrol : ethyl acetate); NMR data matches above.

4-(2'-Methoxy-)phenyl-1-[2'-(*N*-2"-pyridinyl-)*4*-nitrobenzamido-]ethyl piperazine (4-MPPNO$_2$), 5, (Bars et al., 1998)

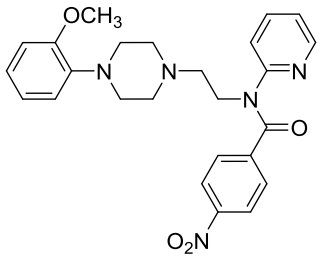

4-(2'-methoxy-)phenyl-1-[2'-(2"-pyridinyl-)amino]ethyl piperazine (**3**) (1.56 g, 5 mmol) and Et_3N (0.17 mL, 6 mmol) were added to CH_2Cl_2 (20 mL) and the solution allowed to cool to 0 °C in an ice bath. 4-Nitrobenzoyl chloride (0.93 g, 5 mmol) in CH_2Cl_2 (20 mL) was added dropwise at 0 °C and the mixture allowed to stir for a further hour at room temperature. After confirmation by TLC that (**3**) had been consumed, water was added (10 mL) and the mixture extracted with CH_2Cl_2 (x3). The combined organic layers were dried ($MgSO_4$), filtered and concentrated *in vacuo.* Purification using column chromatography (SiO_2.100%

ethyl acetate) and recrystallisation (ethyl acetate and petrol) gave a yellow crystalline solid.

Yellow crystalline solid (0.83 g, 2 mmol, 40%). Mp 153 - 156 °C (lit. (Bars et al., 1998) 166 ºC); R_f = 0.28 (1:4 petrol : ethyl acetate); ^{1}H NMR($CDCl_3$, 400 MHz): δ (ppm) 8.40 – 8.34 (m, 1H), 8.06 – 7.99 (m, 2H), 7.49 – 7.40 (m, 3H), 7.08 – 7.02 (m, 1H), 6.99 – 6.92 (m, 1H), 6.91 – 6.79 (m, 4H), 4.26 (t, J=6.6 Hz, 2H), 3.81 (d, J=6.7 Hz, 3H), 2.91 (s, 4H), 2.73 (t, J=6.6 Hz, 2H), 2.62 (s, 4H); ^{13}C NMR($CDCl_3$, 101 MHz): δ (ppm) 168.5, 155.7, 152.3, 149.1, 148.3, 142.5, 141.3, 137.7, 129.6, 123.3, 122.9, 122.5, 121.7, 121.0, 118.1, 111.3, 56.3, 55.4, 53.4, 50.7, 45.8. Anal. Calcd for $C_{25}H_{27}N_5O_4$: C, 65.06; H, 5.90; N, 15.17; Found: C, 64.89; H, 4.92; N, 15.33. *m/z* (ESI) 462 ($M+H^+$, 100%), 163 (4). Found: M+ 462.2130. $C_{25}H_{28}O_4N_5$ requires 462.2136.

4-(2'-Methoxy-)phenyl-1-[2'-(*N*-2"-pyridinyl-)*2*-fluorobenzamido-]ethyl piperazine (*2*-MPPF),6, (Bars et al., 1998)

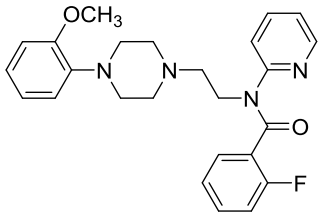

4-(2'-methoxy-)phenyl-1-[2'-(2"-pyridinyl-)amino]ethyl piperazine (**3**) (1.56 g, 5 mmol) and Et_3N (0.17 mL, 6 mmol) were added to CH_2Cl_2 (20 mL) and the solution allowed to cool to 0 °C in an ice bath. 2-Fluorobenzoyl chloride (0.59 g, 5 mmol) in CH_2Cl_2 (20 mL) was added dropwise at 0 °C and the mixture allowed to stir for a further hour at room temperature. After confirmation by TLC that (**3**) had been consumed, water was added (10 mL) and the mixture extracted with CH_2Cl_2 (x3). The combined organic layers were dried ($MgSO_4$), filtered and concentrated *in vacuo* to give an orange solid.

Orange solid (1.19 g, 2.7 mmol, 55%). R_f= 0.39 (1:4 petrol : ethyl acetate); ^{1}H NMR($CDCl_3$, 400 MHz): δ (ppm) 8.32 (m, 1H), 7.85 – 7.86 (m, 1H), 7.24 – 7.25 (m, 1H), 6.94 – 6.98 (m, 1H), 6.84 – 6.89 (m, 8H), 4.39 (t, J=6.4 Hz, 2H), 3.82 (s, 3H), 3.12 (br, 4H), 3.01 (t, J = 6.4 Hz, 2H), 2.97 (br,4H)

4-(2'-Methoxy-)phenyl-1-[2'-(*N*-2"-pyridinyl-)*3*-fluorobenzamido-]ethyl piperazine (*3*-MPPF), 7 (Bars et al., 1998)

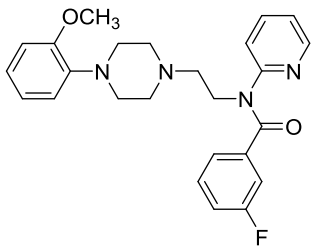

4-(2'-methoxy-)phenyl-1-[2'-(2"-pyridinyl-)amino]ethyl piperazine (**3**) (1.56 g, 5 mmol) and Et_3N (0.17 mL, 6 mmol) were added to CH_2Cl_2 (20 mL) and the solution allowed to cool to 0 °C in an ice bath. 3-Fluorobenzoyl chloride (0.60 g, 5 mmol) in CH_2Cl_2 (20 mL) was added dropwise at 0 °C and the mixture allowed to stir for a further hour at room temperature. After confirmation by TLC that (**3**) had been consumed, water was added (10 mL) and the mixture extracted with CH_2Cl_2 (x3). The combined organic layers were dried ($MgSO_4$), filtered and concentrated *in vacuo* to give a brown oil.

Brown oil (0.056 g, 0.12 mmol, 3%), R_f= 0.38 (1:4 petrol : ethyl acetate); ^{1}H NMR($CDCl_3$, 400 MHz): δ (ppm) 8.34 – 8.35 (m, 1H), 7.77 – 7.79 (m, 1H), 6.86 – 7.03 (m, 10H), 4.33 (t, J=6.6 Hz, 2H), 3.82 (s, 3H), 3.04 (br, 4H), 2.90 (t, J = 6.6 Hz, 2H), 2.84 (br,4H)

4-(2'-Methoxy-)phenyl-1-[2'-(*N*-2"-pyridinyl-)*3*-nitrobenzamido-]ethyl piperazine (*3*-MPPNO$_2$),8 (Bars et al., 1998)

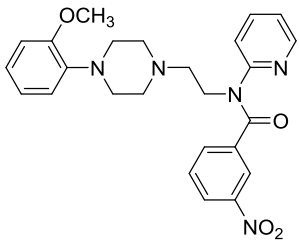

4-(2'-methoxy-)phenyl-1-[2'-(2"-pyridinyl-)amino]ethyl piperazine (**3**) (1.56 g, 5 mmol) and Et_3N (0.17 mL, 6 mmol) were added to CH_2Cl_2 (20 mL) and the solution allowed to cool to 0 °C in an ice bath. 3-Nitrobenzoyl chloride (0.93 g, 5 mmol) in CH_2Cl_2 (20 mL) was added dropwise at 0 °C and the mixture allowed to stir for a further hour at room temperature. After confirmation by TLC that (**3**) had been consumed, water was added (10 mL) and the mixture extracted with CH_2Cl_2 (x3). The combined organic layers were dried ($MgSO_4$), filtered and concentrated *in vacuo* to give a dark brown oil (0.80 g, 1.7 mmol, 35%).

Dark brown oil (0.80 g, 1.7 mmol, 35%), R_f= 0.54 (1:4 petrol : ethyl acetate); ^{1}H NMR($CDCl_3$, 400 MHz): δ (ppm) 8.37 (m, 1H), 8.14 – 8.15 (m, 2H), 7.63 – 7.64 (m, 2H), 7.47-7.48 (m, 1H), 6.89 – 6.92 (m, 6H), 4.26 (t, J=6.6 Hz, 2H), 3.82 (s, 3H), 2.75 (br, 4H), 2.73 (t, J = 6.6 Hz, 2H), 2.64 (br,4H)

Chapter 3. Radiochemistry

3.1 Introduction

As discussed in the main introduction fluorine-18 is the radioisotope of choice for producing a PET ligand. However the short half-life means a rapid on-site synthesis of the PET ligand is required in order to perform subsequent PET and autoradiography studies (Reed et al., 2012, Pascalia et al., 2010). In addition, a high level of automation is preferable to reduce exposer of the operator to radiation.

Due to the limitations of fluoride delivery from external suppliers and the design of the in house ABT cyclotron, the [^{18}F]fluoride available for this study had a relatively low activity (approx. 1 – 3 GBq).

Therefore, the development of a fast and reliable radiosynthesis method, starting with low activity, to produce 4-[^{18}F]MPPF was essential for this study.

The aims of this chapter are;

- To investigate two different production methods;
    - The Advion NanoTek, a microfluidic reactor capable of rapid and repeated synthesis.
    - The Eckert and Zielger ModularLab, a batch reaction platform.

- To investigate two reaction routes to synthesise 4-[^{18}F]MPPF;
    - ^{19}F/[^{18}F] isotopic exchange using the precursor 4-MPPF
    - Fluorodenitration reaction using the precursor 4-MPPNO$_2$

The purpose of the project was to produce 4-[^{18}F]MPPF which was suitable for PET and *ex vivo* autoradiography experiments rather than to fully optimise the radiochemical reaction. Therefore only preliminary optimisation was performed in order to assess feasibility of the synthesis route for PET ligand production.

3.2 Methods

3.2.1 Materials and general methods

All solvents were commercially available HPLC grade (Fisher Scientific, UK) and used without any further purification unless otherwise stated. DMSO was passed through an Al_2O_3 SPE cartridge (Waters Sep-Pak Light Accell Plus, Waters, Ireland) dried on molecular sieves (24 h 4 Å molecular sieves, 24 h 3 Å molecular sieves) and kept under positive nitrogen flow. Fluorine-18 in $[^{18}O]H_2O$ was purchased from Erigal (Preston, UK), Petnet Solutions (Nottingham, UK) or produced on the in house ABT Cyclotron ($^{18}O(p,n)^{18}F$ reaction, 7.5 MeV, 4 µV, 310 µL ^{18}O-water, 30-60 min). 4-MPPF and 4-MPPNO$_2$, were passed through an Al_2O_3 SPE cartridge (Waters Sep-Pak Light Accell Plus, Waters, Ireland). Tetraethylammonium hydrogen carbonate ($(CH_3CH_2)_4N.HCO_3$) and potassium carbonate (K_2CO_3) were purchased from Sigma Aldrich (UK). QMA anion exchange resign cartridges were used to trap $[^{18}F]$fluoride ions (QMA: Waters Sep-Pak Light Accell Plus, Waters, Ireland.) Pre-condition method A: 500 mM K_2CO_3 (10 mL) followed by H_2O (20 mL) then air (20 mL)) then with 5 mL solution of $(CH_3CH_2)_4N.HCO_3$ ($(CH_3CH_2)_4N.HCO_3$ (39.73 mM) in 4.5 mL CH_3CN and 0.5 mL H_2O. Method B: 50 mM NaOH (5 mL) followed by H_2O (10 mL) then air (2 x 20 mL)). $[^{18}F]$fluoride ions were eluted with a solution of $(CH_3CH_2)_4N.HCO_3$ (131 mM in 0.8 mL CH_3CN and 50 µL H_2O)). Radioactivity was measured using a Capintec (CRC-25PET, Southern Scientific Ltd, England).

The identity and radiochemical yield (RCY) of crude product was determined using radio/UV high performance liquid chromatography (HPLC). This was performed using an Agilent 1200 (fitted with a vacuum degasser G1379B, binary pump G1312A, auto-sampler G1329A, column oven G1316A, variable wavelength detector (λ_{max} 276 nm) G1314B in series with a radio-detector B-FC-4100, LabLogic, Germany and a 500 µL injection loop) with Laura software (LabLogic v. 4.1.3.50). A manual switch box allowed the exit bolus to be directed to waste or a collection vial. All radioactivities are quoted as uncorrected values.

3.2.2 Initial HPLC Method

Before radiosynthesis could commence, an HPLC method had to be developed. A solvent system suitable for *in vivo* injection was required, therefore aqueous ethanol was chosen. 4-MPPF and 4-MPPNO$_2$ (2.3 mM in DMF) were injected (10 µL) on to the HPLC fitted with an analytical column (Phenomenex Polymer X (G013-4326-D0), Ace 5 C18 (ACE-121-1546) or an ACE 5 phenyl column (ACE-125-1546), 4.6 x 100 mm) at RT. An isocratic or gradient elution was used with ethanol (20 – 80%) and water (0.1% formic acid, 20 – 80%) at a flow rate of 0.5 – 2.5 mL/min. The optimal separation was found using an ACE 5 phenyl column (4.6 x 100 mm, ACE, UK) at RT eluting with ethanol : water (0.1% formic acid) (30:70% isocratic) at 1 mL/min. The retention time for 4-MPPF was 14 min and 17.5 min for 4-MPPNO$_2$.

This method was used for radiosynthesis experiments performed on the Advion NanoTek. However, changes were made for radiosynthesis performed on the Eckert and Ziegler ModularLab, as described later.

3.2.3 Advion NanoTek methods

Apparatus of the Advion NanoTek Microfluidic System

Drying of [^{18}F]fluoride and radiosynthesis was conducted on an Advion NanoTek Microfluidic system (Advion, USA), which consists of a concentrator module (CM), base module (BM) and a reactor module (RM) controlled by the Advion NanoTek 1.4 software. The CM is comprised of a low pressure six-way valve, reagent cartridge and vessel chamber (5 mL vial). This module is used to prepare dry [^{18}F]fluoride *via* several azeotropic distillations with acetonitrile using a combination of reduced pressure and positive nitrogen gas flow. The BM consists of two reagent cartridges (P1 and P2), which comprise a high-pressure syringe pump connected to an eight way bridge valve with a looped-reservoir from which measured quantities of reagents are dispensed to the microreactor. The RM comprises the isotope reagent cartridge (P3) connected to an eight-way distribution valve (DV) and has slots for up to four microreactor cartridges. P3 receives [^{18}F]Et$_4$NF from the concentrator module (CM) and the distribution valve (DV) is used to route the reaction bolus to the desired location

(Figure 7). The electronic injection valve (Smartline Valve Drive, Knauer, Germany) injects the reaction mixture into the HPLC (Reed et al., 2012).

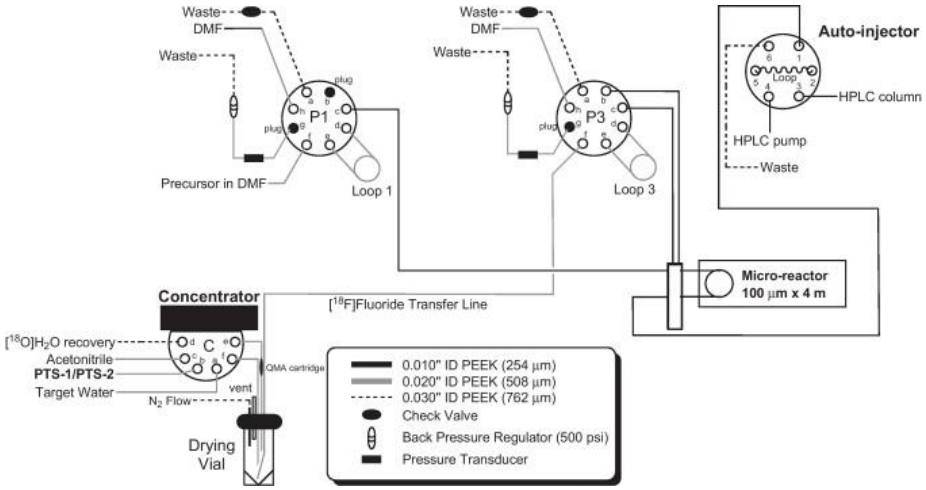

Figure 7: Advion Nano Tek Microfluidic System set-up (Reed et al., 2012).

Production of no-carrier added [^{18}F]fluoride using the Advion NanoTek

No carrier added [^{18}F]fluoride in [^{18}O]H_2O (5 mL, 2.19 – 4.23 GBq) was absorbed on to a QMA cartridge (Pre-condition method A) into a V-Vial,(2 mL, Wheaton)). The solution was dried by two successive azeotropic evaporations with CH_3CN (450 µL, 100^0C) under a positive nitrogen flow. The dry [^{18}F]$(CH_3CH_2)_4N.F$ was dissolved in DMSO (1 mL) and loaded on to the Advion NanoTek storage loop (P3) (Reed et al., 2012).

Radiofluorination of 4-MPPF and 4-MPPNO_2 using the Advion Nanotek

Several reaction runs were performed to prime the system and check all equipment was functioning prior to performing experimental runs. Dry [^{18}F]Et_4NF (2.19 – 4.23 GBq, 1 mL DMSO, from P3) and precursor solutions (4-MPPF 22.56 – 58.04 mM in DMSO or 4-MPPNO_2), 20.82 – 23.43 mM in

DMSO, from P1) were loaded on to storage loops 3 and 1 respectively and capillary lines, running from pumps 1 & 3 to the microreactor, were primed with reagent. A range of volumes of dry [^{18}F]fluoride (10 - 180 µL) and precursor (10 – 180 µL) were simultaneously injected into the pre-heated microreactor (4 or 8 m, 110 – 200 ºC) at a range of flow rates (5 – 50 µL/min). After passage through the reactor the crude reaction mixture was swept into the electronic injection valve for injection onto a radio/UV HPLC (10 µL). Identity of the product was confirmed by comparing the elution time of the UV HPLC peak to a known standard. The RCY was calculated by integration of the product associated radio HPLC peak and taken as a percentage of the total integrated area under the radio-curve. The base module (BM), reactor module (RM), microreactor and transfer lines were flushed with DMSO and the concentrator module (CM) with acetonitrile at the start and end of each experiment series.

The Advion Nanotek has a maximum temperature setting of 200 ^{0}C so all reactions were carried out at or below this temperature.

3.2.4 Eckert and Ziegler ModularLab methods

Apparatus of Eckert and Ziegler ModularLab and microwave reactor

Drying of [^{18}F]fluoride and radiosynthesis was conducted on an Eckert and Ziegler Modular Lab (Eurotope GmbH, Germany), which consists of four solenoid valve modules (SVM), a stopcock manifold module (SMM), activity detectors, a Peltier-reactor module (PRM, temperature range -40 ^{0}C – 150 ^{0}C)) with camera (Vrmagic USB camera development kit 3.9a msi) and pneumatic lift (0-58 mm), heat exchanger (HE-006, temperature range -10 ^{0}C – 40 ^{0}C) and electrical cabinet (EC-0084), controlled by the Modular-Lab4 software (Rev. 04\02.2007, Eurotope GmbH). The apparatus were connected for the production of no-carrier added [^{18}F]Et_4NF (Figure 9) with the dry [^{18}F]Et_4NF in DMSO passing into a microwave reactor (Resonance Instruments Inc., USA, Model 521-I with IR thermometer, 39667-10, Cole Parmer. The apparatus was also connected for C-18 Sep-Pak SPE cartridge formulation (Waters, Ireland, pre-conditioned with 10 mL water followed by 5 mL ethanol) (Figure 9)

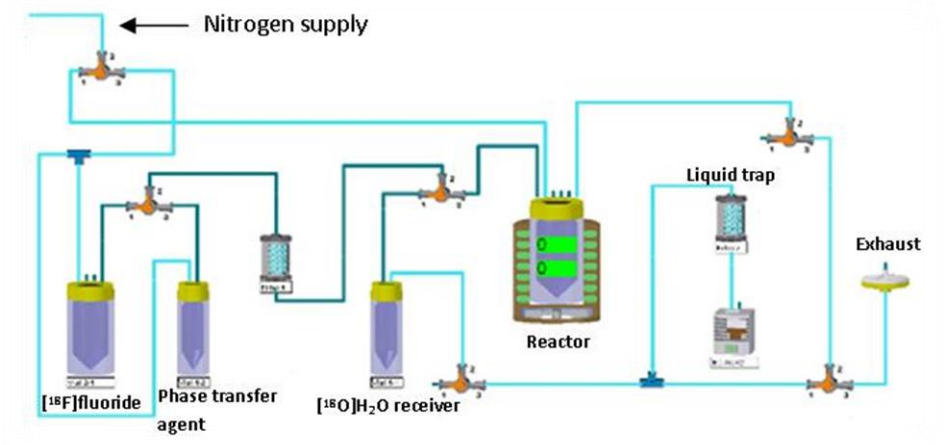

Figure 8: Eckert and Ziegler Modular Lab set-up for [^{18}F]fluoride drying and radiosynthesis.

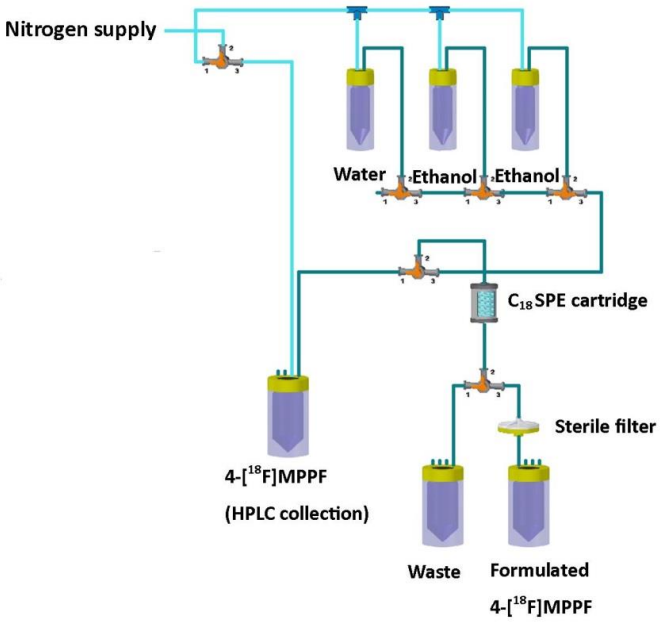

Figure 9: Eckert and Ziegler Modular Lab set-up for C-18 Sep-Pak SPE cartridge formulation

Production of no-carrier added [^{18}F]fluoride using the Eckert and Ziegler Modular Lab

No carrier added [^{18}F]fluoride in [^{18}O]H_2O (0.3-5 mL, 1.48 – 5.61 MBq) was absorbed on to a QMA cartridge (precondition: method B) into a V-Vial (5 mL) in the RM. The resulting solution of [^{18}F]$(CH_3CH_2)_4N.F$ was dried by azeotropic evaporations (110^{0}C and 90^{0}C) under reduced pressure and positive nitrogen gas flow.

Radiofluorination of 4-[^{18}F]MPPNO$_2$ using the Eckert and Ziegler Modular Lab and microwave reactor

To improve reaction yields, the following parameters were varied; reaction solvent (DMF and DMSO, 0.45 – 1.0 mL), microwave settings (time (100 – 200 s), power (50 – 100 W), temperature (120 – 180 ^{0}C)) and repeat microwave heating (2 – 6 repeats). In addition free fluoride ions were extracted from the precursor by passing through an Al_2O_3 SPE cartridge. This resulted in the following method; DMSO (0.45 mL) was added to the dry [^{18}F]$(CH_3CH_2)_4N.F$ in the Peltier-reactor module, stirred, then transferred to a vented reaction vial (5 mL, Wheaton) containing the precursor (4-MPPNO$_2$, 4.5 - 7.2 mg) in the microwave reactor. The solution was heated (2 x 100 s/100 W/ 175^{0}C, 2 x 100 s/70 W/ 175^{0}C) under stirring, then manually injected onto the radio/UV HPLC.

3.2.5 UV/radio-HPLC alternative method for scaled up reaction

A change in the HPLC method was required for the production of 4-[^{18}F]MPPF on the Eckert and Ziegler ModularLab as the experiment was scaled up in order to produce sufficient radioactivity for *in vivo* work. A change in solvent system improved separation of the precursor from the product.

UV/radio HPLC was used to separate the radiolabelled product from the crude reaction mixture and to measure RCY. The HPLC used an ACE 5 phenyl column (4.6 x 100 mm, ACE, UK) at RT and eluted with (THF/MeOH (40:60)) : 0.05M NaOAC (aq.) 45:55) (Koivula et al., 2010), at 4 mL/min. The retention time for 4-[^{18}F]MPPF was 11 min and 13.5 min for 4-MPPNO$_2$.

3.2.6 C-18 Sep-Pak SPE cartridge formulation

The Eckert and Ziegler ModularLab (Eurotope GmbH, Germany) was set-up for product formulation (Figure 9) and was controlled manually from the PC. 4-[^{18}F]MPPF collected from the HPLC in mobile phase was diluted 1:2 in water and loaded onto a C-18 Sep-Pak light cartridge (Vandecapelle et al., 2004). The cartridge was washed with water (10 mL) and the product eluted in ethanol (0.5 mL).

3.2.7 Radio-TLC

The identity and radio-purity of formulated product was determined by radio thin layer chromatography (TLC). TLC was performed using silica gel plates with aluminium backing (Kieselgel 60F_{254} , 0.2 mm) and CH_3CN:H2O (90:10) mobile phase. Radio-purity was determined using a LabLogic imaging scanner (AR-2000 with Laura software version 4.0.1.5.0, LabLogic, UK) and the identity was confirmed by comparison of a standard Rf value for 4-MPPF.

3.2.8 4-MPPF UV HPLC calibration curve

To create a UV HPLC standard calibration graph for the UV absorption of 4-MPPF, ten standard solutions of 4-MPPF in DMSO (0.24 - 480 nmol, Pipet-Lite XLS, Rainin Instrument, LLC, USA) were prepared by serial dilution, except for 0.0092 µmol and 0.00483 µmol solutions of 4-MPPF which were prepared separately. The solutions were injected on to the HPLC (20 µL injection, Agilent 1200 HPLC, ACE 5 phenyl column (ACE, UK, 150 x 10 mm), mobile phase: (THF:Methanol 40:60):0.05 M NaOAc $_{(aq)}$ (45:55 isocratic) eluting at 4 mL/min). Each solution was run through the HPLC three times. The area under the UV peak (mAU) was measured and the mean was taken for each data point. The UV absoption was plotted against the number of moles (µmol) and the intercept set to (0,0). Linear regression resulted in the equation; Y = 133852x, R^2 = 0.9999.

.

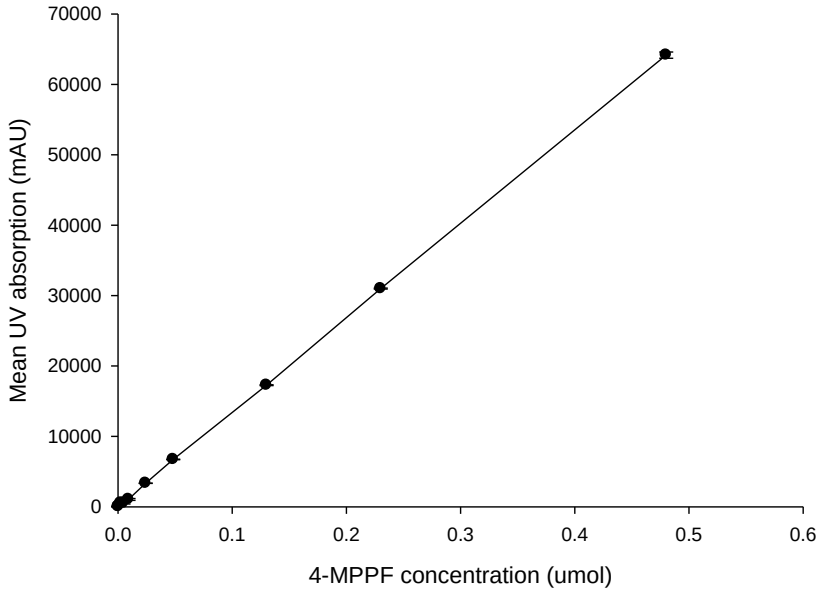

Figure 10: 4-MPPF calibration curve, with linear regression. Values are mean ±sem.

4-MPPF conc. (µmol)	HPLC UV absorption Sample 1 (mAU)	HPLC UV absorption Sample 2 (mAU)	HPLC UV absorption Sample 3 (mAU)	mean	n	Std Dev	sem
0.48	63452.5	64993.2	64014.8	64153.5	3	779.7	450.1
0.23	31116.1	30986.1	30878.1	30993.4	3	119.2	68.8
0.13	17413.5	17215.2	17211.1	17279.9	3	115.7	66.8
0.0483	6664.7	6767.2	6747.6	6726.5	3	54.4	31.4
0.0242	3323.2	3378.5	3364.6	3355.4	3	28.8	16.6
0.0092	1294.6	932.9	919.3	1048.9	3	212.9	122.9
0.0048	256.9	687.1	684.3	542.8	3	247.6	142.9
0.0024	535.8	547.1	545.4	542.8	3	6.1	3.5
0.0004	69.3	70.2	66.5	68.7	3	1.9	1.1
0.0002	42.0	41.7	42.4	42.0	3	0.4	0.2

Table 6: 4-MPPF UV HPLC calibration curve data

3.2.9 Measurement of specific activity of 4-[^{18}F]MPPF

The 4-MPPF calibration graph was used to convert the UV absorption (mAU), as measured from integrating the UV HPLC peak of the collected product, to µmoles of 4-[^{18}F]MPPF. The activity of the product was also taken at time of collection, so in combination with the number of moles, the specific activity (GBq/µmol) of the product was calculated.

3.2.10 Data analysis

Two tailed bivariate Pearson's correlation analysis was performed to determine any relationship between the initial activity of the [^{18}F]fluoride used in the radiosynthesis, on the final activity, RCY and specific activity of the 4-[^{18}F]MPPF produced.

3.3 Results

3.3.1 Advion NanoTek radiosynthesis

Reaction optimisation

In total 120 radiofluoronation reactions were carried out on the Advion NanoTek microfluidic system, of which 94 were isotopic exchange reactions (Scheme 2) and 26 were fluorodenitration reactions (Scheme 1). Factors varied during optimisation were; precursor concentration (mg/mL), reaction temperature (^{0}C), reactor length (m), stoichiometry (precursor: radioisotope) and flow rate (µL/min).

The RCY of 4-[^{18}F]MPPF was calculated from the radio HPLC trace (Figure 11). Mean RCY were calculated only from reactions that produced radiolabelled product and excluded those which did not result in a measurable yield.

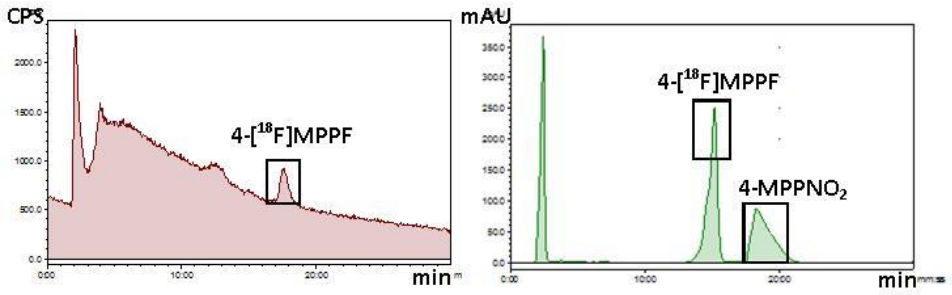

Figure 11: Example of radio (left) and UV (right) HPLC trace from Advion NanoTek radiosynthesis of 4-[^{18}F]MPPF. Separation of product and precursor can be seen on the UV trace. EtOH: water (0.1 % formic acid) 30:70% solvent system with Ace-5 phenyl column (4.6 x 100 mm), RT.

Isotopic exchange reactions:

44 of 94 isotopic exchange reactions produced 4-[^{18}F]MPPF, with a mean RCY of 10.4 ±1.1% (range; 2.1 - 36.8%) (Appendix B).

Effect of precursor concentration

For each reaction condition (Table 7, No. 1 – 4) it was found the precursor concentration had no direct effect on the RCY.

No.	Precursor (mg)	Mean RCY	n	sem	Reactor Length (m)	Flow rate (µL/min)	Stoichiometry	Reactor Temperature (ºC)
1	18	0.0	6	0.0	4	5	1	190
	20	19.2	8	2.9	4	5	1	190
	21	2.5	2	0.4	4	5	1	190
2	18	14.9	5	1.4	8	5	1	190
	25	7.4	3	0.6	8	5	1	190
3	21	5.1	2	0.6	8	10	1	190
	23	4.6	3	0.5	8	10	1	190
4	10	0.0	3	0.0	8	30	1	190
	23	3.8	2	0.2	8	30	1	190
	25	11.3	2	0.9	8	30	1	190

Table 7: Reaction conditions for isotopic exchange reactions in the Advion NenoTek

Effect of reaction temperature

For each reaction condition (Table 8, No. 1 – 2) it was found product was produced at 190 ºC but surprisingly not 200 ºC.

No.	Reactor Temperature (ºC)	Mean RCY	n	sem	Precursor (mg)	Reactor Length (m)	Flow rate (µL/min)	Stoich-iometry
1	190	15.9	10	3.2	18-21	4	5	1
	200	0.0	3	0.0	18-21	4	5	1
2	190	12.1	8	1.6	18-21	8	5	1
	200	0.0	2	0.0	18-22	8	5	1

Table 8: Reaction conditions for isotopic exchange reactions in the Advion NenoTek

Effect of reactor length

At the reaction conditions shown in Table 9 it was found the reactor length had no directional effect on the RCY.

No.	Reactor Length (m)	Mean RCY	n	sem	Precursor (mg)	Flow rate (µL/min)	Stoich-iometry	Reactor Temperature (°C)
1	4	15.9	10	3.18	18-25	5	1	190
	8	12.1	8	1.63	18-25	5	1	190

Table 9: Reaction conditions for isotopic exchange reactions in the Advion NenoTek

Effect of stoichiometry

At the reaction conditions shown in Table 10 it was found the stoichiometry had no directional effect on the RCY.

No.	Stoichiometry	Mean RCY	n	sem	Precursor (mg)	Reactor Length (m)	Flow rate (µL/min)	Reactor Temperature (°C)
1	0.5	11.1	5	1.0	18-25	8	5	190
	1	12.1	8	1.6	18-25	8	5	190

Table 10: Reaction conditions for isotopic exchange reactions in the Advion NenoTek

Effect of flow rate

For each reaction condition (Table 11, No. 1 - 2) it was found a lower flow rate produced the highest RCY (Figure 12).

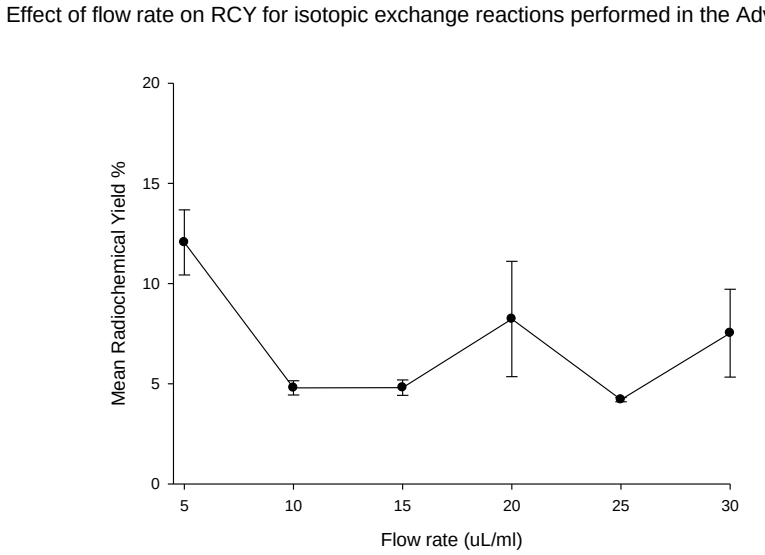

Figure 12: Mean RCY for isotopic exchange reactions performed in the Advion NanoTek at a range of flow rates (µL/min). Values are mean ±sem, n = 8 (5 µL/min), n = 5 (10 µL/min), n = 3 (15 µL/min), n = 4 (20 µL/min), n = 3 (25 µL/min), n = 4 (30 µL/min). Reaction conditions No. 2 from Table 9.

No.	Flow rate (µL/min)	Mean RCY	n	sem	Precursor (mg)	Reactor Length (m)	Stoich iometry	Reactor Temperature (ºC)
1	5	15.9	10	3.2	18-25	4	1	190
	10	21.2	1	NA	18-25	4	1	190
	30	0.0	6	0.0	18-25	4	1	190
2	5	12.1	8	1.6	18-25	8	1	190
	10	4.8	5	0.4	18-25	8	1	190
	15	4.8	3	0.4	18-25	8	1	190
	20	8.2	4	2.9	18-25	8	1	190
	25	4.2	3	0.1	18-25	8	1	190
	30	7.5	4	2.2	18-25	8	1	190

Table 11: Reaction conditions for isotopic exchange reactions in the Advion NanoTek

Fluorodenitration reactions:

9 of 26 fluorodenitration reactions produced 4-[^{18}F]MPPF, with a mean RCY of 14.6 ±3.1% (range; 5.0 – 31.0%) (Appendix C).

Effect of precursor concentration

All reactions were performed using 10 mg/mL 4-MPPNO$_2$ precursor, therefore the effect of precursor concentration could not be examined.

Effect of reaction temperature

At the reaction conditions shown in Table 12 it was found increasing the reaction temperature from 170 to 200 ºC increased the RCY from 8.4 to 25.6% (Figure 13).

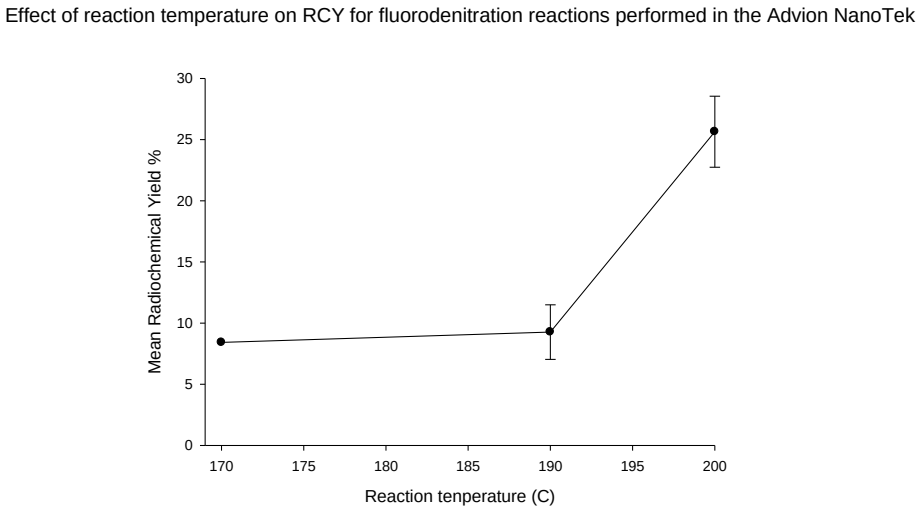

Figure 13: Mean RCY for fluorodenitration reactions performed in the Avion NanoTek at a range of reaction temperatures (ºC). Values are mean ±sem, n = 1 (170 ºC), n = 5 (190 ºC), n = 3 (200 ºC).

No.	Reactor Temperature (°C)	Mean RCY	n	sem	Precursor (mg)	Reactor Length (m)	Flow rate (µL/min)	Stoich-iometry
1	170	8.4	1	0.0	10	8	5	1
	190	9.3	5	2.2	10	8	5	1
	200	25.6	3	2.9	10	8	5	1

Table 12:Reaction conditions for fluorodenitration reactions in the Advion NanoTek

Effect of reactor length

Insufficient data was collected to make a direct comparison of the effect of reactor length on the productions of radiolabeled product. However it should be noted that 4-[^{18}F]MPPF was only produced using a fluorodenitration reaction using an 8 m reactor.

Effect of stoichiometry

Insufficient data was collected to make a direct comparison of the effect of stoichiometry on the production of radiolabeled product.

Effect of flow rate

At the reaction conditions shown in Table 13 it was found only a flow rate of 5 µL/min gave product.

No.	Flow rate (µL/min)	Mean RCY	n	sem	Precursor (mg)	Reactor Length (m)	Stoic-hiometry	Reactor Temperature (°C)
1	5.0	9.3	5	2.2	10.0	8	1	190
	30.0	0.0	5	0.0	10.0	8	1	190

Table 13: Reaction conditions for fluorodenitration reactions in the Advion NanoTek

3.3.2 Eckert and Ziegler ModularLab radiosynthesis

Reaction optimisation

Initially the fluorodenitration reaction using the Eckert and Ziegler ModularLab produced low RCY's, so a number of steps were taken to improve the RCY of the crude product produced by microwave heating in the ModularLab.

Firstly the reaction solvent was changed from DMF to DMSO to allow higher reaction temperatures (DMF b.p. = 153ºC, DMSO b.p. = 189ºC). An Al_2O_3 SPE cartridge was used to remove possible fluoride ion contamination from the precursor (4-MPPNO_2) and reaction solvent (DMSO), which could reduce the specific activity of the product. Lastly the microwave settings (temperature, power, time) were investigated to produce a sufficiently high RCY in the shortest time. In addition, reaction solvent volume was reduced from 1.0 mL to 0.5 mL to reduce HPLC load time.

RCY increased from a mean of 4.7 ±0.2% (3.7 – 5.5%, n=10) under initial conditions to a mean of 33.5 ±3.0% (0.8 - 59.5%, n = 36) under optimised conditions (Appendix D)

Effect of repeating microwave heating

At the reaction conditions shown in Table 14 it was found repetitive microwave heating increased the RCY from 5.9 to 21.3% (Figure 14).

Effect of repeating microwave heating on RCY for fluorodenitration reactions performed on the Eckert and Ziegler Modular Lab

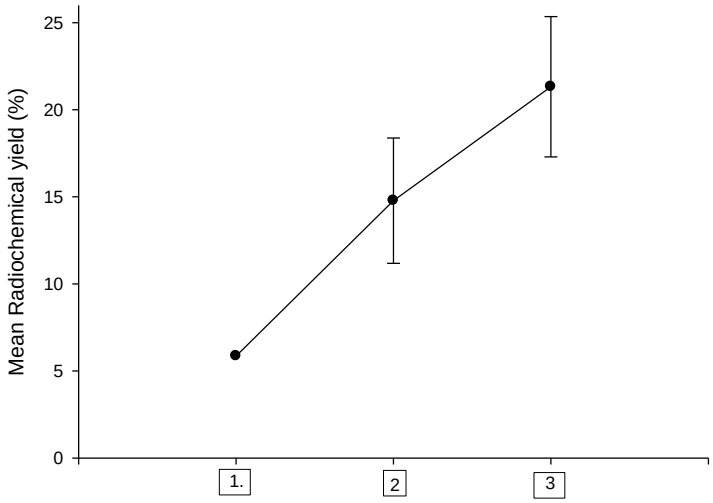

Figure 14: Mean RCY for fluorodenitration reactions performed on the Eckert and Ziegler Modular Lab with repeat microwave heating. Values are mean ±sem, n = 1 (No. 1), n = 3 (No. 2), n = 3 (No. 3).

No.	Mean RCY	n	sem	Solvent Volume (mL)	Microwave settings; Time (s)	Microwave settings; Power (W)	Microwave settings; Temperature (°C)
1	5.9	1	NA	0.5	100	70	165
2	14.8	3	3.6	0.5	100,100	70,100	165, 165
3	21.3	3	4.0	0.5	100, 100, 100, 100, 100, 100	70,70,70,100, 100,100	165, 165, 165, 165, 165, 165

Table 14: Reaction conditions for fluorodenitration reactions on the Eckert and Ziegler ModularLab

Effect of increasing microwave reactor temperature and reducing heating repetition

At the reaction conditions shown in Table 15 it was found increasing the reaction temperature from 165 ºC to 175 ºC and reducing microwave heating repetitions, increased the RCY from 21.3 to 33.5%.

No.	Mean RCY	n	sem	Solvent Volume (mL)	Microwave settings; Time (s)	Microwave settings; Power (W)	Microwave settings; Temperature (ºC)
4	21.3	3	4.0	0.5	100, 100, 100, 100, 100, 100	70, 70, 70, 100, 100, 100	165, 165, 165, 165, 165, 165
5	22.3	3	1.8	0.5	100, 100, 100, 100	100, 100, 70, 70	175, 175, 170, 170
6	33.5	36	3.0	0.5	100, 100, 100, 100	100, 100, 70, 70	175, 175, 175, 175

Table 15: Reaction conditions for fluorodenitration reactions on the Eckert and Ziegler ModularLab

UV HPLC and volume optimisation/C-18 Sep-Pak SPE cartridge formulation

Initially the HPLC mobile phase (EtOH and H_2O (0.1% formic acid)) was chosen so that it was suitable for *in vivo* injection. Working initially at small scale (150 x 4.6 mm analytical column, 20 µL injection crude reaction mixture) this solvent system adequately separated 4-[^{18}F]MPPF from the precursor 4-MPPNO$_2$ (Figure 11). However, to produce sufficient activity for *in vivo* PET scanning and *ex vivo* autoradiography a 500 µL injection volume was necessary, therefore a semi-preparative HPLC column was used (150 x 10 mm column, 500 µL injection volume, 4 mL/min). However, at the larger scale there was poor HPLC separation of the product and precursor (Figure 15). Secondly the product eluted in a large volume of mobile phase (~20 mL), so that the volume to activity ratio was too low to be used *in vivo*.

To address these issues the solvent system, recommended by the published study examining the separation of 4-[^{18}F]MPPF from 4-MPPNO$_2$, greatly improved the separation of the product and precursor (45% THF/MeOH (40:60), 55% 0.05M NaOAC ($_{aq}$)) (Koivula et al., 2010), (Figures 16 and 17), allowing collection of product from the HPLC without precursor contamination. Secondly a protocol for solid phase extraction (SPE) was developed based on a published method (Vandecapelle et al., 2004), to remove the toxic HPLC solvents and elute 4-[^{18}F]MPPF in a small volume of non-toxic solvent. The formulated product was eluted in ethanol giving a final volume of 0.3 mL. The formulated product was further analysed by HPLC and Radio-TLC (Figures 18 and 19).

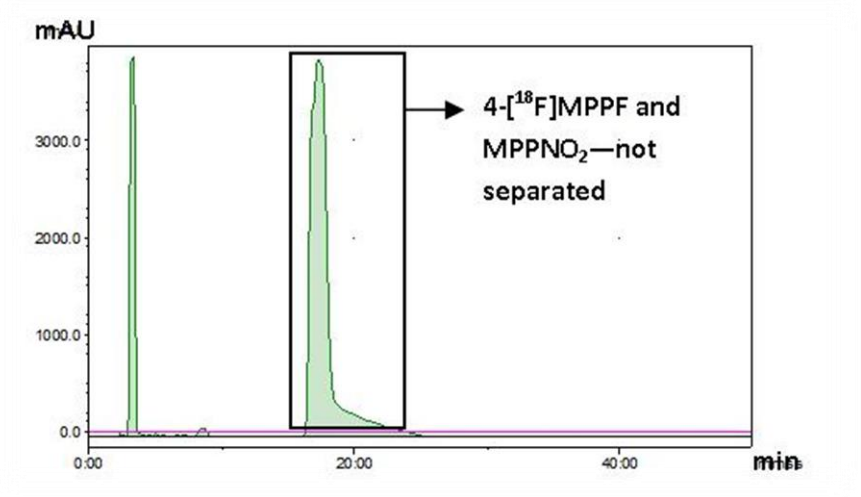

Figure 15: Example UV HPLC trace of 4-[^{18}F]MPPF and 4-MPPNO$_2$ eluting using EtOH: water (0.1 % formic acid) 30:70% solvent system with Ace-5 phenyl column (150 x 10 mm), RT, 500 µL injection volume. No separation between product and precursor can be seen.

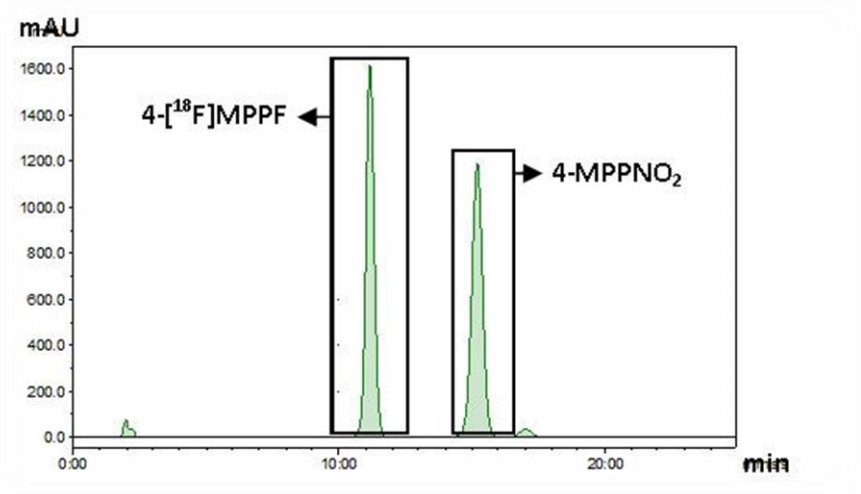

Figure 16: Example UV HPLC trace of 4-[^{18}F]MPPF and 4-MPPNO$_2$ eluting using THF/MeOH (40:60): 0.05M NaOAC ($_{aq}$) 45 : 55), Ace-5 phenyl column (150 x 10 mm), RT, 20 µL injection volume .

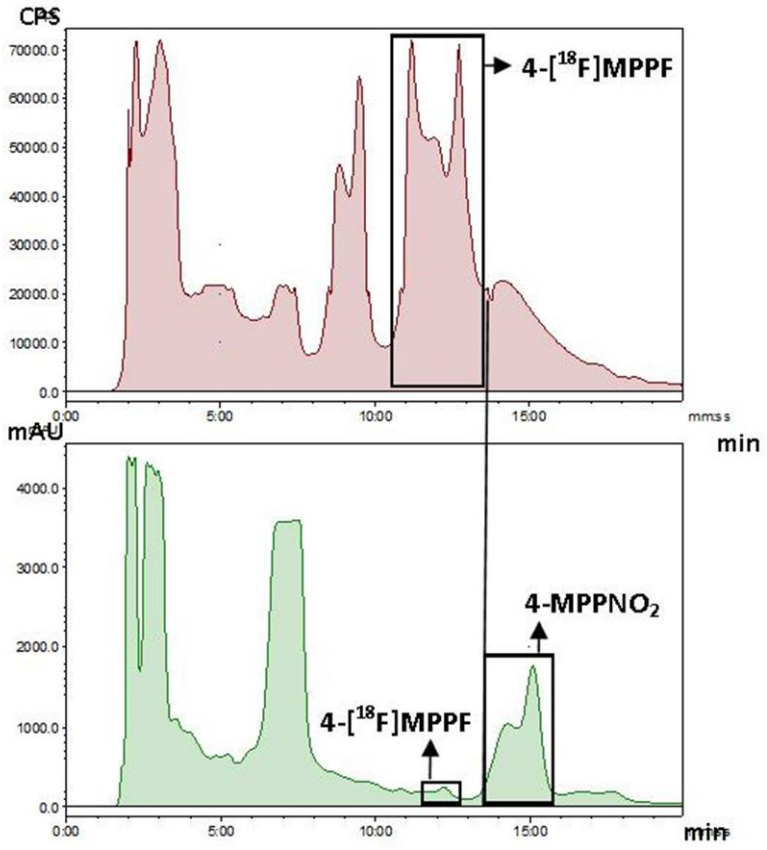

Figure 17: Example radio (top) and UV (bottom) HPLC traces of 4-[^{18}F]MPPF and 4-MPPNO$_2$ in crude reaction mixture eluting using THF/MeOH (40:60): 0.05M NaOAC ($_{aq}$) 45 : 55), Ace-5 phenyl column (150 x 10 mm), RT, 500 µL injection volume . It can be seen that 4-[^{18}F]MPPF has eluted (radiotrace) when 4-MPPNO$_2$ starts to elute (UV trace)

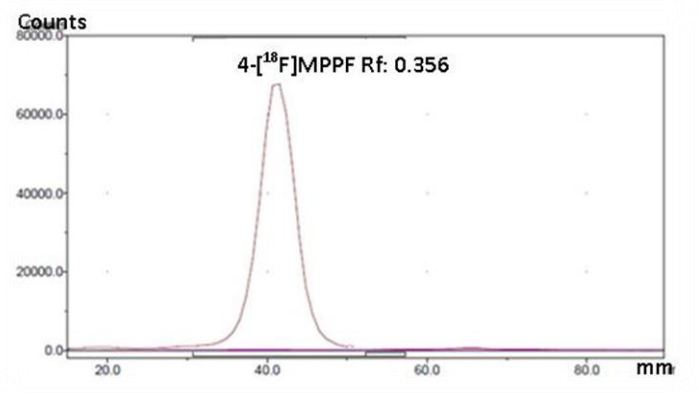

Figure 18: Example of radioTLC for formulated 4-[^{18}F]MPPF showing 100% radiopurity with an Rf of 0.356.

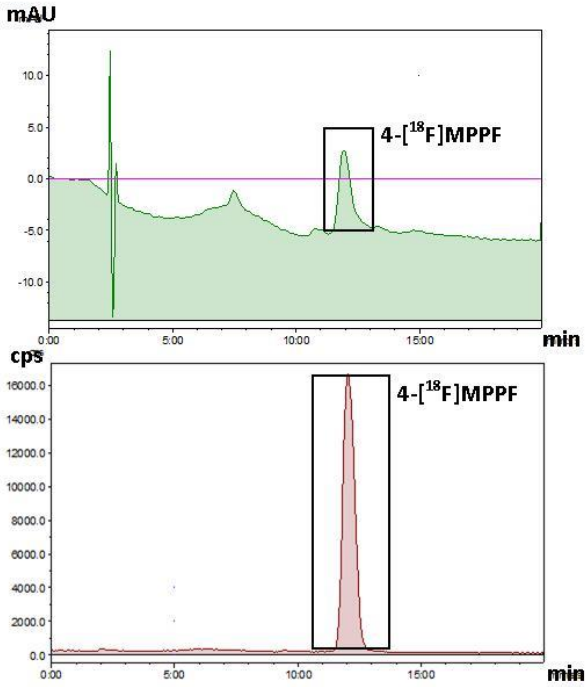

Figure 19: Example of UV and radio HPLC of formulated 4-[^{18}F]MPPF THF/MeOH (40:60): 0.05M NaOAC ($_{aq}$) 45 : 55), Ace-5 phenyl column (150 x 10 mm), RT, 20 µL injection

Production of PET ligand for in vivo PET scanning and ex vivo autoradiography

Radiosynthesis on the Eckert and Ziegler ModularLab produced 4-[^{18}F]MPPF for PET scanning or *ex vivo* autoradiography with a final radioactivity of 5.2 to 251.0 MBq (mean radioactivity 84.5 ±12.1 MBq, n = 36) in ethanol (0.3 mL), with a total synthesis time of 60 min. RCY's were between 0.8 - 59.5% (mean RCY 33.5 ±3.0%, n = 36). Radiopurities were between 72.4 and 100.0%, (mean radiopurity 95.8 ±1.3%, n = 28. One data point (3/7/13) with a radiopurity of 56.2% was excluded from final analysis. Specific activities were between 0.1 – 17.8 GBq/µmol (mean spec. ac. 4.3 ±0.7 GBq/µmol, n = 35). Using the 4-MPPF HPLC calibration curve (section 3.2.8), the following equation was used to calculate the specific activity (GBq/µmol);

4-[^{18}F]MPPF HPLC UV absorption (mAU) = µmol x 133852

Analysis of 4-[^{18}F]MPPF analytical data

Correlation between the initial activity of the fluorine-18 and the specific activity of 4-[^{18}F]MPPF

A Pearson's correlation coefficient was calculated to reveal there was a significant correlation between the initial activity of the fluorine-18 and the specific activity (GBq/µmol) of the 4-[^{18}F]MPPF produced; r =0.51, p =0.002, n=35 (Figure 20).

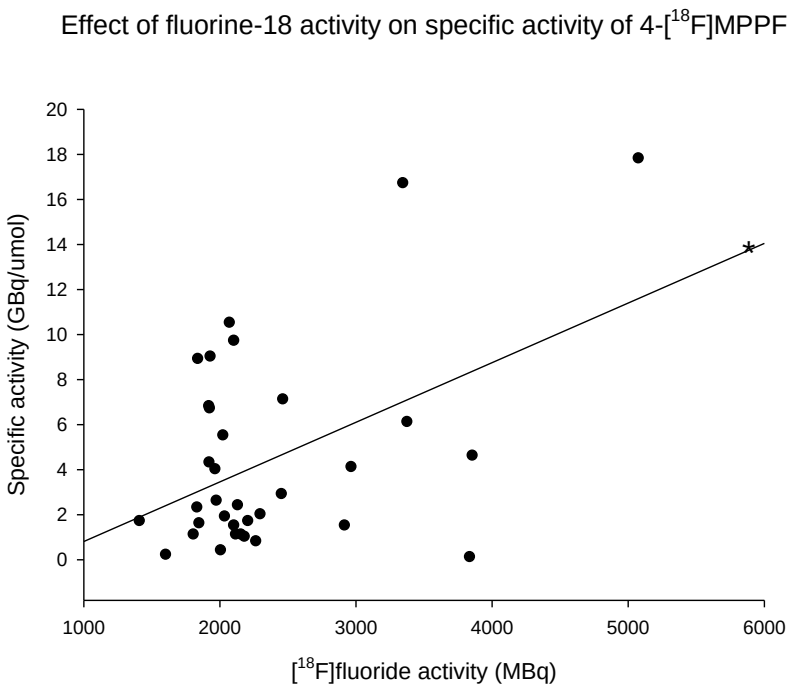

Figure 20: Effect of fluorine-18 activity on 4-[^{18}F]MPPF specific activity (GBq/µmol). Values are plotted with a linear regression best fit curve, n = 35. p < 0.05.*

Correlation between 4-[^{18}F]MPPF radiochemical yield and specific activity

A Pearson's correlation coefficient was calculated to reveal there was a significant correlation between the RCY and specific activity (GBq/µmol) of the 4-[^{18}F]MPPF produced; r = 0.57, p = <0.01, n=35 (Figure 21).

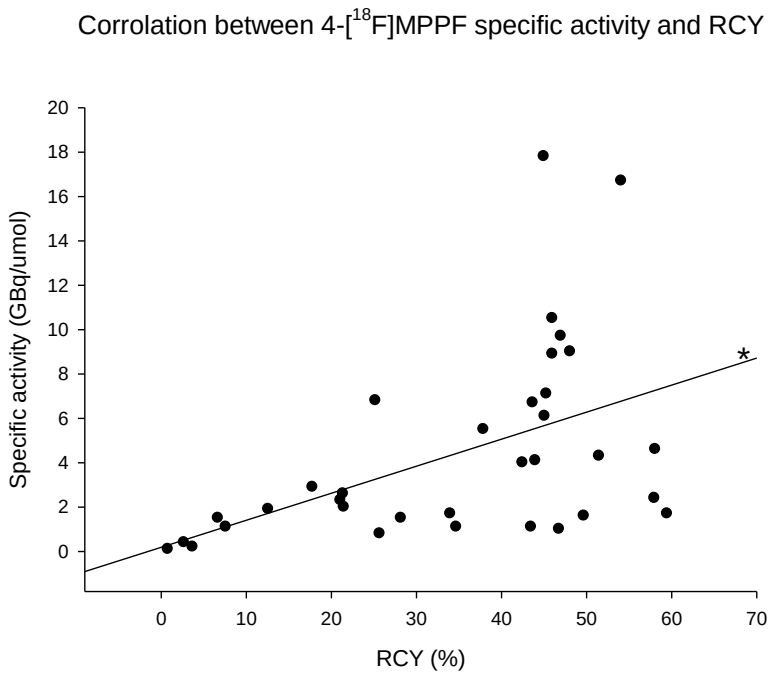

Figure 21: *Correlation between 4-[^{18}F]MPPF RCY and specific activity(GBq/µmol). Values are plotted with a linear regression best fit curve, n = 35.* p < 0.01.*

3.4 Discussion

3.4.1 Advion NanoTek summary

Initial radiosynthesis to produce 4-[^{18}F]MPPF was performed on the Advion NanoTek microfluidic reactor as this provided an advantage over a traditional batch process equipment, such as the Eckert and Ziegler ModularLab. The Advion NanoTek can perform multiple reactions using a single batch of radioisotope and precursor, allowing for rapid reaction assessment and optimisation (Chun et al., 2010). In addition, the Advion NanoTek has an integrated HPLC system allowing radiosynthesis, product identification, determination of RCY and isolation of product to be completed on one piece of kit without handling.

Two reaction routes were available for investigation; ^{19}F/[^{18}F] isotopic exchange (Scheme 2) and NO_2/[^{18}F] nucleophilic aromatic substitution in the form of a fluorodenitration reaction (Scheme 1). As a comprehensive optimisation study

was not performed it was not possible to definitively compare the effect of each variable. However some trends were observed.

Overall, for isotopic exchange reactions, the RCY's were low (maximum mean RCY=19.2%) and the production of 4-[^{18}F]MPPF was inconsistent, often failing to produce any product at conditions that had previously been successful. However, it appeared a lower flow rate (5-10 µL/min) combined with the longer reactor length (8 m), gave the most consistent results. As a precursor concentration of 10 mg/mL did not produce any 4-[^{18}F]MPPF at any condition it may be that this reaction requires a higher concentration. However, there did not appear to be any benefit to concentrations greater than 18 mg/mL. Reaction stoichiometry did not appear to affect the RCY and insufficient data was collected to reveal a trend in the effect of temperature.

Fluorodenitration reactions also produced low RCY's (maximum mean RCY=25.6%). However the production of 4-[^{18}F]MPPF was more consistent than isotopic exchange reactions within a given set of variables, with the reaction favouring a low flow rate (5 µL/min) and high temperature (200 ºC). Insufficient data was collected to comment on the effect of other variables.

Typically nucleophilic aromatic substitution reactions require a high temperature and relatively long reaction time. Due to the design of the NanoTek the maximum reaction time (~13 min) and maximum temperature (200°C) was not sufficient to produce the RCY's required using a fluorodenitration reaction. To make production of 4-[^{18}F]MPPF on the NanoTek viable for use as a PET ligand, it would require one or both of these variables to be exceeded.

3.4.2 Eckert and Ziegler ModularLab summary

The ModularLab is a batch process platform. Therefore, only one radiosynthesis reaction can be performed per batch of radioisotope, so method development required considerable time. Reliable radiosynthesis of 4-[^{18}F]MPPF was quickly achieved using a combination of the ModularLab and microwave heating via a fluorodenitration reaction. However, in order to make 4-[^{18}F]MPPF batches suitable for use *in vivo*, there was a need to increase the activity and reduce the final solvent volume. Therefore preliminary optimisation of the reaction conditions was undertaken, which greatly improved radiochemical yields. In

addition, the HPLC method was altered (Koivula et al., 2010) to accommodate the greater volume of crude reaction mixture injected onto the HPLC in the latter ModularLab experiments. Following this, an SPE cartridge (Vandecapelle et al., 2004) was employed to remove toxic solvents used in HPLC separation and elute the product into a small volume of solvent. This resulted in a reliable method to produce batches of 4-[^{18}F]MPPF suitable for use in pre-clinical PET scanning and autoradiography. The 4-[^{18}F]MPPF produced for PET and autoradiography studies had a mean RCY of 33.5 ± 3.0 %, a mean radioactivity of 84.5 ± 12.1 MBq, a mean radio-purity of 95.8 ±1.3%, with a total synthesis time of 60 minutes. This is an improvement on the standard procedure set out by Bars *et al.*(Bars et al., 1998) which had an RCY of 25% and a synthesis time of 70 minutes. However, the mean specific activity of 4.3 ±0.7 GBq/µmol, is below that reported in the literature for 4-[^{18}F]MPPF PET studies, which report 30 – 185 GBq/µmol (Bars et al., 1998, Aznavour, 2009, Bartmann et al., 2010, Moulin-Sallanon et al., 2009). A significant correlation was found between the initial fluoride activity and 4-[^{18}F]MPPF specific activity. Therefore future productions would benefit from higher [^{18}F]fluoride activity. However, the fluorine-18 activity is limited due to either off site delivery time or the specifications of the on site cyclotron, so to get a higher starting activity would require a higher powered on site cyclotron.

3.5 Conclusion

In summary, it has been shown that, given the constraints of a maximum temperature (200ºC) and available reactor length (8 m) a 4-[^{18}F]MPPF PET ligand cannot be reliably produced on the Advion NanoTek using either an ^{19}F/[^{18}F] isotopic exchange or an NO_2/[^{18}F] nucleophilic aromatic substitution.

It has also been shown for the first time (to my knowledge) that a 4-[^{18}F]MPPF PET ligand, for use in pre-clinical PET and autoradiography, can be reliably produced using a combination of the Eckert and Ziegler ModularLab and a Resonance Instruments microwave reactor *via* a nucleophilic substitution reaction, starting with a low activity.

Chapter 4. Microdialysis

4.1 Introduction

Microdialysis is a technique that can be used to sample extracellular fluid in the brain, giving quantitative data on neurotransmitters. It is performed by inserting a probe into the brain area of interest in order to collect a representative sample of the extracellular fluid. This relies on diffusion of the extracellular fluid across the semi-permeable dialysis membrane, located at the end of the probe, into the perfusion medium (aCSF) passing through the probe's internal void. The perfusion medium, containing the diffused extracellular fluid, passes to a collection vessel for analysis. This is the dialysate sample (Chefer et al., 2009, Sharp and Hjorth, 1990).

Microdialysis has a number of advantages over other methods of measuring 5-HT *in vivo* such as voltammetry, as well as perfusion techniques such as the cortical cup. The advantages include factors such as, the perfusion medium is not directly exposed to the brain tissue, the microdialysis probes are relatively small and the semipermeable membrane is a barrier to substances with large molecular weights, keeping the dialysate relatively 'clean' (Stamford, 1992).

5-HT, as measured by microdialysis, has been shown to originate from functioning neurons rather than other sources such as blood or damaged neurons. For example, 5-HT dialysate levels have been shown to be calcium dependant, sensitive to pharmacological challenges and sensitive to changes in neuronal activity (Stamford, 1992).

This chapter firstly describes the *in vitro* assessment of microdialysis probes and secondly *in vivo* experiments to quantify the concentration of 5-HT in the rat hippocampus, before and after administration of fenfluramine. Fenfluramine is a 5-HT releasing agent which interacts with vesicular monoamine transporters inside the neuron to liberate the 5-HT held within. This is then released into the extracellular space by reversing the serotonin transporter function and exiting the neuron (Jain, 2002).[1]

There is disagreement in the literature as to whether the 4-[^{18}F]MPPF is displaceable by endogenous 5-HT . Furthermore, in the rat 4-[^{18}F]MPPF has

been shown to be a substrate of the p-glycoprotein transporter, so blocking the p-glycoprotein pump (with cyclosporine) increases uptake of 4-[^{18}F]MPPF into the brain (Laćan et al., 2008, Passchier et al., 2000).

Chapter 5 describes 4-[^{18}F]MPPF PET using both cylcosporine and the 5-HT releasing agent fenfluramine in the protocol. Therefore, the aims of the present chapter are to use microdiaysis to determine quantitative data on the amount of endogenous 5-HT released by fenfluramine (with and without a pretreatment of cyclosporine) and ultimately determine an optimum fenfluramine challenge protocol to use in subsequent PET studies.

More specifically the aims of this part of the study are to;

- Determine the percent recovery, precision and temporal resolution of microdialysis probes.
- Characterise the effect of different doses of fenfluramine on the extracellular levels of 5-HT in the rat brain
- Investigate whether the p-glycoprotein pump inhibitor, cyclosporine, has any effect on the fenfluramine induced release of 5-HT

4.2 Methods

4.2.1 Probe construction

Concentric microdialysis probes were constructed with a 5.0 mm dialysing window. Three pieces of stainless steel tubing (Goodfellow, Cambridge, UK; internal diameter 0.38 mm, external diameter 0.5 mm) were cut to size to make the Y-shaped frame. Two lengths of silica glass tubing (SGE Ltd, Milton Keynes, UK; outer diameter 170 µm) were passed through one piece of stainless steel tubing (19 mm) with a length of stainless steel (9 mm) placed on the end of each glass tube. One silica glass tube was retracted (~ 10 mm) into the stainless steel tubing and the three stainless steel tubes were fixed with epoxy resin (Araldite, Simid Ltd., UK) at their intersection. The silica glass tubing still extending from the bottom of the Y-shaped frame was cut (4 mm)

and dialysing membrane (polyacrylonitrile/ sodium methyl sulphonate co-polymer, internal diameter 0.22 mm, external diameter 0.31 mm, 20 kDA molecular weight cut off, AN 69, Hospal, Bologna, Italy) was placed over it and pushed inside the stainless steel tubing. The dialysing membrane was trimmed to extend past the silica glass tube by ~1 mm. Epoxy resin was then introduced to the end of the dialysing membrane and to the intersection with the stainless steel tube producing a dialysing window of 4.5 mm. The probes were made in batches of 4 – 6 and stored in cool, dry area (Figure 22).

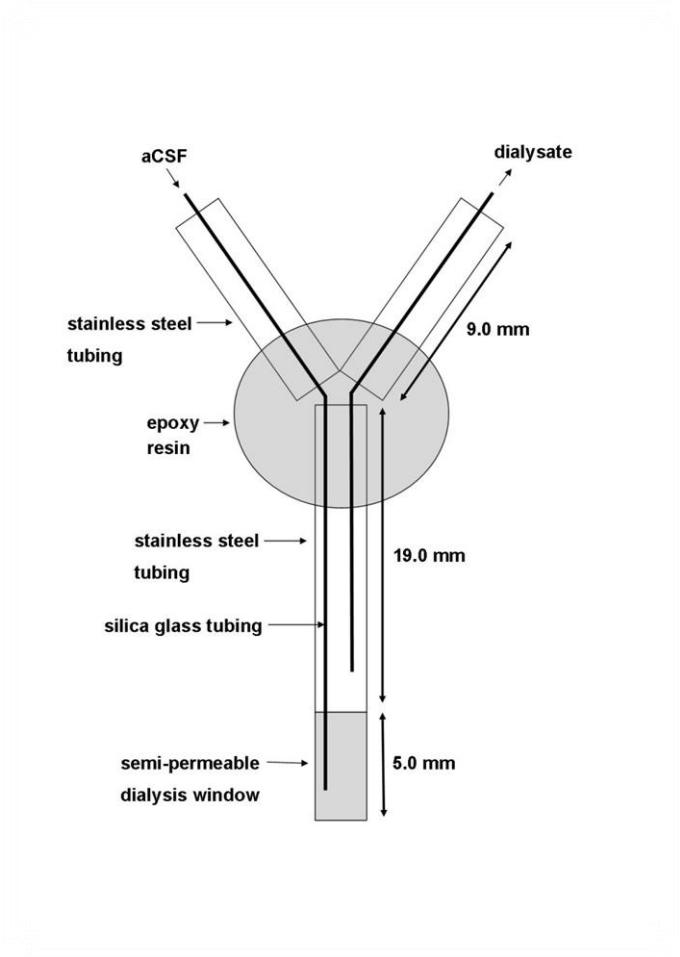

Figure 22: Microdialysis probe construction

4.2.2 Artificial cerebrospinal fluid (aCSF) preparation

aCSF was used as the probe perfusion medium during the microdialysis procedure. A stock solution (minus $CaCl_2$ or glucose) was prepared at the start of the study and refrigerated (4ºC), with $CaCl_2$ and glucose being added to the experimental quantity of aCSF on the day of an experiment.

aCSF composition;

140 mM NaCl

3.0 mM KCl

0.96 mM Na_2HPO_4

0.24 mM NaH_2PO_4

1.0 mM $MgCl_2$

2.4 mM $CaCl_2.6H_20$

7.2 mM $C_6H_{12}O_6$ (D-(+)-glucose)

4.2.3 In vitro microdialysis probe set up

A microcentrifuge tube (0.2 mL, TreffLab, Switzerland) was placed in a heated tube holder (37 ºC, monitored with thermometer in adjacent cell.) and three quarters filled with aCSF. Using a stereotaxic frame, a microdialysis probe was suspended in the centre of the microcentrifuge tube so that the dialysate window was fully submerged in the solution (Figure 23).

aCSF was perfused through the microdialysis probe (2.3 µL/min; Harvard PHD 2000 infusion pump, Harvard Apparatus LtD, UK) for 20 min, then the probe was transferred to an adjacent microdialysis tube containing the lowest standard 5-HT solution concentration, which had been allowed to equilibrate to 37 ºC. Dialysate samples were collected in an inverted polythene tube for HPLC analysis (one per 20 minutes (50 µL dialysate) for 60 min). Once

samples for one concentration of 5-HT were collected, the microdialysis probe was quickly moved to an adjacent tube containing a higher concentration. Once all samples were collected the probe was submerged and rinsed out in distilled water for storage.

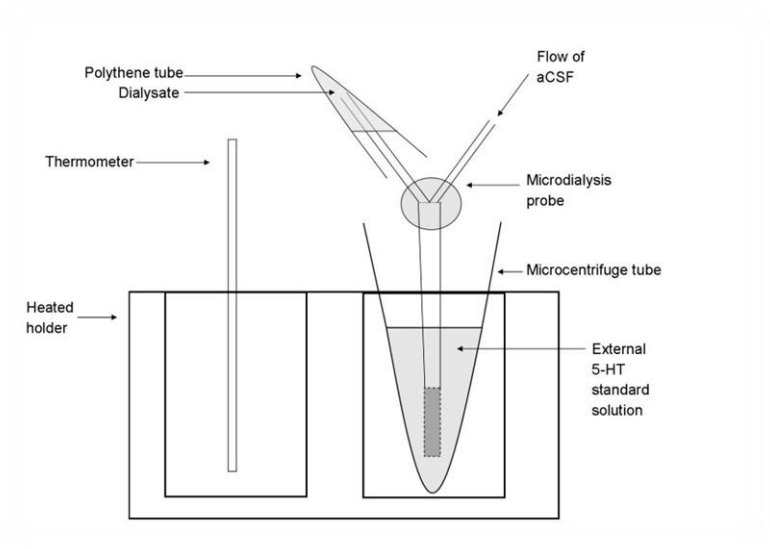

Figure 23: Schematic of in vitro microdialysis set- up

4.2.4 High Performance Liquid Chromatography (HPLC) assay

Dialysate samples were analysed for 5-HT concentration using high performance liquid chromatography (HPLC) with an electrochemical detection cell.

Mobile phase (127 mM $NaH_2PO_4.H_2O$, 1.2 mM, ethylenediamine tetraacetic acid, 74 µM 1-octane sulphonic acid) was prepared in deionised water, vacuum filtered (0.22 µm filter paper, Whatman, UK) and pH adjusted using orthophosphoric acid (pH 3.8). MeOH was added to this solution (85 % NaH_2PO_4 buffer, 15 % MeOH) to complete the mobile phase and degassed for 30 minutes via sonication.

The mobile phase was pumped through the HPLC system (1 mL/min, Gilson 302 HPLC pump/manometric module), being oxidised on a guard cell (ESA model 5020, 350 mV) to remove any electroactive impurities.

Dialysates (50 µL) were loaded using a manual injection system (Rheodyne model 7125, USA with a 50 µL loop, Anachem Ltd, UK), passed through a separating column (4.6 x 100 mm Microsorb 100-3 C18 column, Varian analytical instruments, USA) and oxidised on a coulometric sensor comprising of two electrochemical cells set at 120 mV and 250 mV respectively (ESA, Analytical LtD, UK). Changes in current were detected by an electrochemical detector (Coulochem II 5100A, ESA, Analytical Ltd, UK) and plotted on an integrator (Waters 746 data module).

Dialysate 5-HT concentrations were calculated from peak height compared to a fresh 5-HT standard (1 x 10^{-9} M 5-HT in mobile phase, prepared from a stock solution (10 mM 5-HT in 0.1 M perchloric acid)).

Standards of 5-HIAA and DOPAC (1 x 10^{-9} M 5HIAA or DOPAC in mobile phase, prepared from a stock solution (1 x 10^{-2} mM 5HIAA or DOPAC in 0.1 M perchloric acid)) were prepared to differentiate from the 5-HT peak.

All standard peaks were determined at the start of the day of each experiment.

The linear relationship between peak height and concentration for 5-HT , 5-HIAA and DOPAC was shown using a set of standard concentrations (1 x 10^{-7} M, 1 x 10^{-8} M, 1 x 10^{-9} M).

4.2.5 In vitro microdialysis probe calibration

Measurement of the external solution standard 5-HT content (fmol) vs. microdialysis probe dialysate 5-HT content (fmol) by HPLC assay yielded a calibration graph with the straight line equation Y = 0.0986X + 8.5715, R^2 = 0.5799. However, to obtain a straight line equation to convert measured dialysate 5-HT concentrations to external 5- HT concentrations, the intercept was set to (0,0). This resulted in the straight line equation Y = 0.1233x with R^2 = 0.5224 (Figure 24)

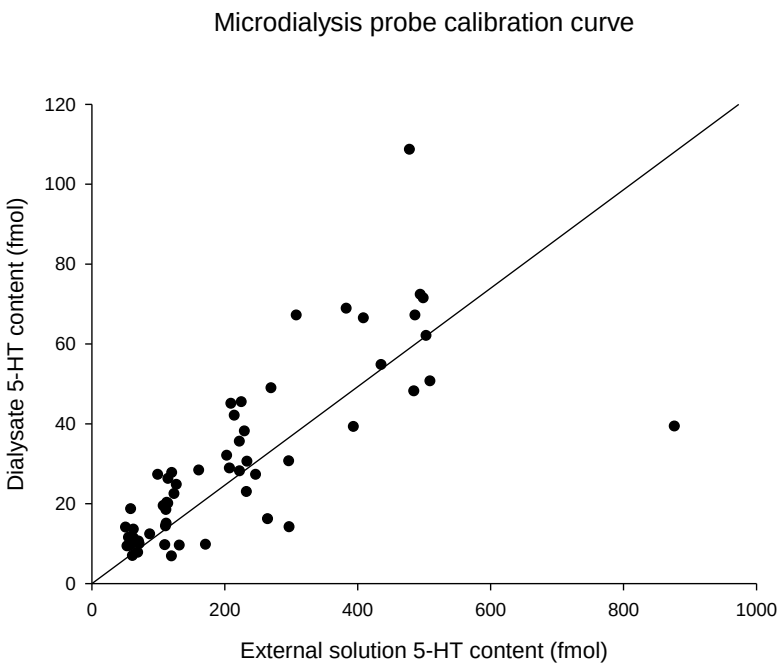

Figure 24: Microdialysis probe calibration curve using linear regression with intercept set to (0,0).

4.2.6 In vivo microdialysis surgery

Untreated male Lister Hooded rats (Charles River UK, 265 – 322 g) were anaesthetised in an induction box (Harvard Apparatus Ltd, UK; 5% isofluorane, 1.5 L/min O_2) then transferred to an anaesthetic mask (3% isofluorane, 1.5 L/min O2) and fitted in to a stereotaxic frame (David Kopf Instruments, USA; incisor bar set 3.3 mm below the interaural line (flat skull position)). A thermostatically controlled heating blanket (Harvard Apparatus Ltd, UK) attached to a rectal probe maintained body temperature at ~36 °C. Isofluorane was adjusted as necessary to achieve a stable breathing pattern then readjusted for surgery (2.5 – 3 % isofluorane, 1.5 L/min O_2).

A longitudinal incision was made in the scalp with bregma exposed and a trephine hole (2 mm diameter) was drilled in the skull (co-ordinates relative to bregma: anterior – posterior -5.2, medial – lateral - 4.8). An indentation was drilled into the skull into which a screw was fixed (Hilco Ltd, UK; 1.2 mm diameter, 2.6 mm length; screw ~3 mm anterior to trephine hole) to aid

purchase of the later applied dental cement. The exposed dura was pierced and a microdialyis probe lowered into the hippocampus using a stereotaxic manipulator (coordinates from bregma; anterior – posterior -5.2 mm, medio – lateral -4.8 mm, dorso – ventral -7.8 mm). Dental cement (Kemdent Simplex Rapid powder) was applied on the skull, around the probe and screw, to fix the probe in place.

aCSF was perfused through the microdialysis probe (2.3 µL/min; Harvard PHD 2000 infusion pump, Harvard Apparatus LtD, UK) and 20 minutes (46 µL) dialysate was collected in an inverted polythene tube for HPLC analysis.

4.2.7 In vivo microdialysis probe location

Animals were given an overdose of sodium pentobarbital i.p. at the end of each experiment. The brain was removed and sectioned through the hippocampal region using a cryostat (30 µM sections, Microm HM500OM, Walldorf, Germany). Sections were mounted on glass slides, stained (see protocol below) and examined under a microscope (Leica MZ6, Image J software) to reveal linear tissue damage caused by probe implantation. Probe placement location was confirmed by comparison to the Paxinos and Watson rat brain atlas (Paxinos and Watson, 1998).

Cresyl violet staining protocol;

- Submerge slides in cresyl violet aqueous solution (3.1 mM cresyl violet ($C_{18}H_{15}N_3O_3$), 43 mM AcOH, 45 mins)
- Wash (70 % EtOH, 30 % H_2O)
- Wash (95% EtOH, 5% H_2O)
- Submerge slides in EtOH (100%, 3 mins)
- Submerge slides in EtOH (100%, 3 mins)
- Submerge slides in Histoclear (Histoclear, National Diagnostics, UK, 100%, 3 mins)
- Submerge slides in Histoclear (Histoclear, National Diagnostics, UK, 100%, 3 mins)
- Coverslip (Eukitt mounting medium, Sigma Aldrich, Germany, #1 coverslips, Ultima)

4.2.8 In vivo microdialysis drug administration

5-HT levels, assessed via HPLC assay of the dialysate, were allowed to stabilise before drug administration.

Drugs were administered via i.p. injection. Cyclosporine (50 mg/kg) or saline vehicle were injected after 5-HT stabilisation. Fenfluramine (1 or 3 mg/kg) was administered one hour later (Figure 26). N.B. Five of nine experiments did not receive a saline vehicle injection one hour before fenfluramine administration (Figure 25). Anaesthesia was maintained throughout the procedure (isofluorane 1.5 – 2%, O_2 1.5 L/min)

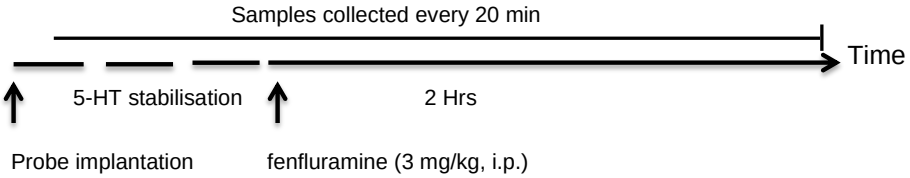

Figure 25: Timeline; Nil saline vehicle 3 mg/kg fenfluramine experiments. (Note; In these experiments no saline vehicle was administered before fenfluramine. These data were combined with saline vehicle pretreatment/3 mg/kg fenfluramine data, as shown in Figure 26, for data analysis)

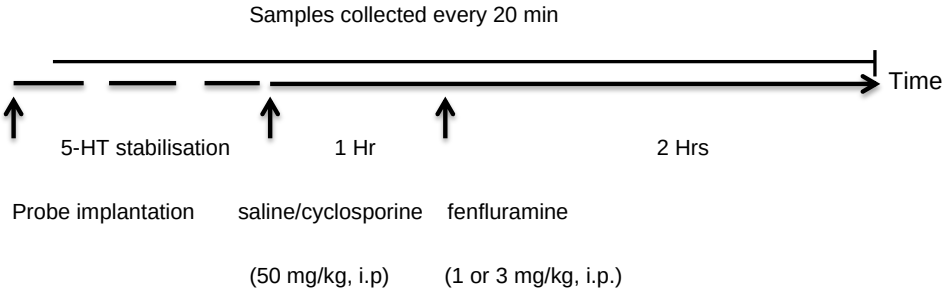

Figure 26: Timeline; Saline vehicle/cyclosporine pretreatment combined with 1 or 3 mg/kg fenfluramine experiments.

4.2.9 In vitro microdialysis data analysis

The percent recovery and variability of microdialysis probes was examined by comparing 5-HT concentration of the standard solutions to the dialysate 5-HT concentration.

To create a calibration graph for microdialysis probes the measured standard 5-HT solution concentration (fmols/50 µL) was plotted against the measured dialysate concentration for every standard solution concentration (fmols/50 µL), probe (A – G) and day. A trend line was plotted through the data and the intercept set to (0,0) to give a straight line equation.

For all other analysis the external 5-HT solution concentrations were corrected so that all data were equal at each concentration (50, 100, 200 or 400 fmol/50 µL). The dialysate concentrations were corrected by the same factor. Only the last of three dialysate sample 5-HT concentrations per experiment was used in data analysis, so that the concentration nearest equilibrium was used.

4.2.10 In vivo microdialysis data analysis

The effect of fenfluramine on 5-HT release in the hippocampus was examined using 5-HT dialysate content, percentage and absolute change in 5-HT content after drug administration.

To examine the effect of cyclosporine on fenfluramine induced 5-HT release in the hippocampus a two-way repeated measures ANOVA was performed. Nil cyclosporine data excluding a vehicle was combined with nil cyclosporine data including the saline vehicle.

The effect of 1mg/kg vs. 3mg/kg fenfluramine induced release of 5-HT in the hippocampus with 50 mg/kg cyclosporine pre-treatment was examined by performing a two-way repeated measures ANOVA.

4.3 Results

4.3.1 Microdialysis probe dialysate 5-HT content vs. external solution 5-HT content for probes at all 5-HT levels

Individual probe dialysates had a mean percentage recovery range of 4.7 to 31.0% of the external 5-HT content. The mean percentage dialysate 5-HT content, for all probes, was 15.7 ± 0.8% the external 5-HT content, (across all 5-HT concentrations)

4.3.2 Variability between microdialysis probe recovery at a range of concentrations

For an external solution 5-HT concentration of 50 fmol/50 µL, the mean dialysate 5-HT concentration was 8.8 ±0.8 fmol/50 µL for probes A – G. At 100 fmols/50 µL external solution 5-HT the mean dialysate 5-HT concentration was 16.9 ±1.5 fmols/50 µL, at 200 fmols/50 µL the mean dialysate 5-HT concentration was 28.9 ±2.7 fmols/50 µL and at 400 fmols/50 µL the mean dialysate 5-HT concentration was 54.1 ±4.9 fmols/50 µL for probes A – G (Figure 27).

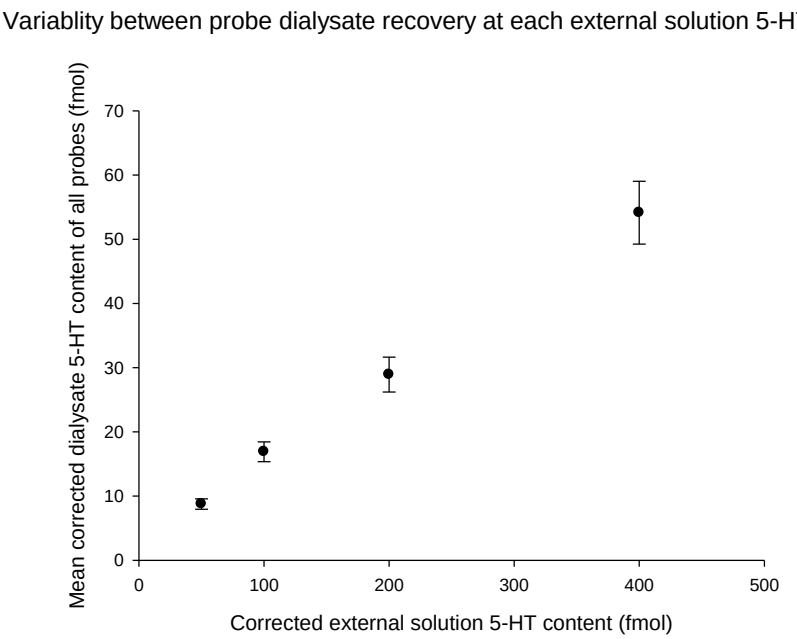

Figure 27: Variability of dialysate 5-HT content recovery for probes A-G at four different external solution 5-HT content. Values are mean ± sem, n = 13.

4.3.3 Probe response time

For an external solution 5-HT concentration of 50 fmols/50 µL the probe dialysate had not stabilised by the third sample (T = 60 min) with the percentage recovery continuing to fall from sample one. There was also large variability in the data with sem ±6.9, 4.2 and 2.9 for samples 1-3 respectively.

For an external solution 5-HT concentration of 100 fmols/50 µL the probe dialysate had not stabilised by the third sample (T = 60 min) with the percentage recovery continuing to rise from sample one. However the variability was not as large as for 50 fmol/50 µL.

For an external solution 5-HT concentration of 200 and 400 fmols/50 µL the probe dialysate had stabilised by the second sample (T = 40 min), with the second and third samples recovery differing by only 0.1% (Figure 28).

Probe response time; time for probe dialysate 5-HT content to stabilise

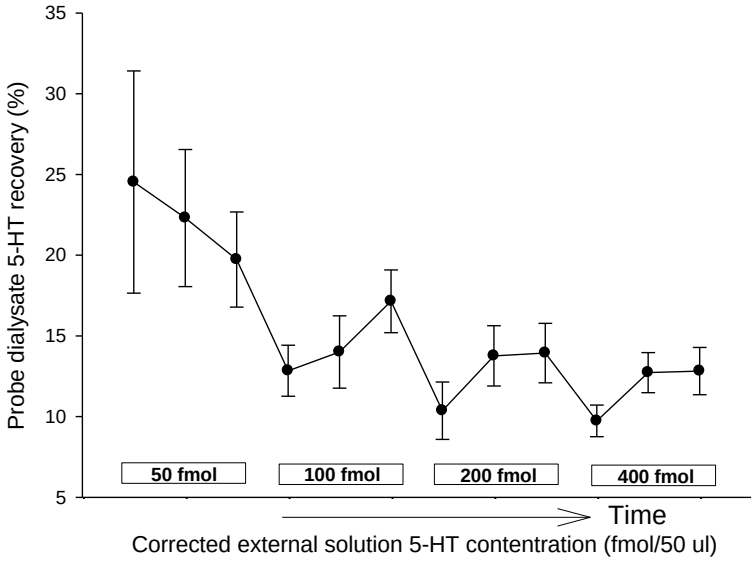

Figure 28: Microdialysis probe response time; time for the dialysate 5-HT content (fmol) to stabilise. Values are mean percent of external solution (% recovery) ±sem, n = 12 (probes A – G).

4.3.4 In vivo microdialysis probe location

The location of each microdialysis probe can be seen by the tissue lesion in the brain slice and were all confirmed to be in the hippocampus (Figure 29) (Paxinos and Watson, 1998).

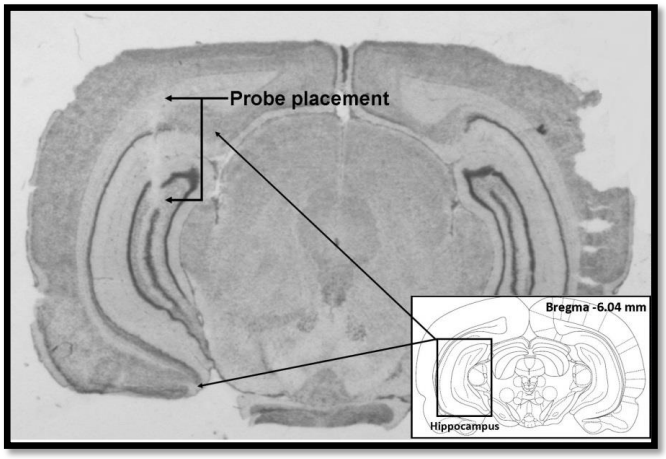

Figure 29: Miocrodialysis probe placement in the hippocampus. Location of probe can be seen by tissues lesion, as indicated by 'probe placement'. Approximate location (Bregma -6.04 mm) indicated by comparison to a rat brain atlas (bottom right).

4.3.5 Effect of cyclosporine on fenfluramine induced release of hippocampal 5-HT

Hippocampal dialysate 5-HT content reached a maximum at 60 minutes after fenfluramine injection (3mg/kg, i.p.) for all experiments.

When fenfluramine 3 mg/kg was administered alone (without cyclosporine pre-treatment) 5-HT dialysates reached a maximum mean of 89.6 ± 16.9 fmols/50 µL, representing a 1480% increase from baseline and an absolute increase of 81.4 ± 15.7 fmols/50 µL (n = 9), (Figure 30).

When fenfluramine 3 mg/kg was administered after pre-treatment with cyclosporine (50 mg/kg, T = -60 min) dialysates reached a maximum mean of 62.5 ± 15.4 fmols/50 µL, representing a 393% increase from baseline and an absolute increase of 46.6 ± 15.3 fmols (n = 7), (Figure 30).

A two-way ANOVA, examining the effect of cyclosporine on the response to fenfluramine 3 mg/kg, revealed a significant main effect of time ($F_{11,154} = 23.7$; $p = < 0.05$), a significant time x group interaction ($F_{11, 154} = 2.0$; $p < 0.05$), but no significant effect of group.

Effect of cyclosporine on fenfluramine induced release of hippocampal 5-HT

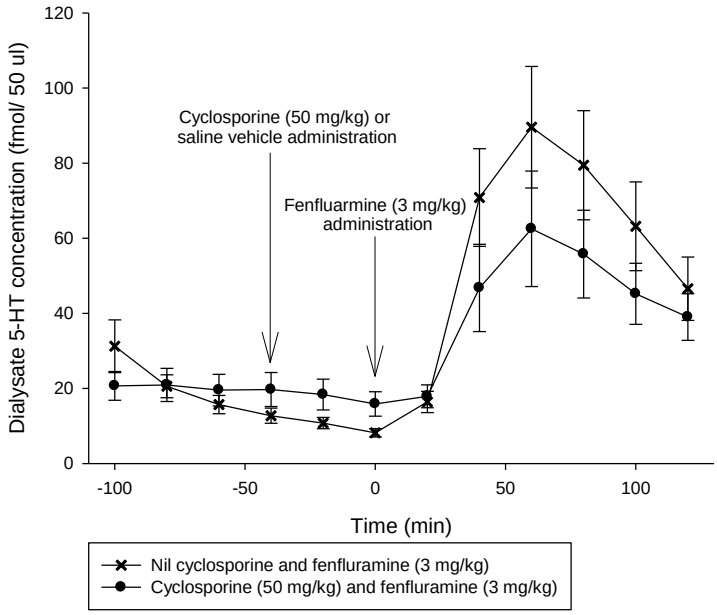

Figure 30: The effect of cyclosporine (50 mg/kg) on fenfluramine (3 mg/kg) induced release of hippocampal 5-HT . Data are mean ± sem, n = 9 (control), n = 7 (cyclosporine).

4.3.6 Effect of fenfluramine dose on hippocampal 5-HT release

Hippocampal dialysate 5-HT concentrations reached a maximum at 80 minutes after a 1 mg/kg fenfluramine injection i.p. and at 60 minutes after a 3 mg/kg fenfluramine injection i.p (both with a 50 mg/kg 60 min pre-treatment with cyclosporine).

After administration of 1 mg/kg fenfluramine 5-HT dialysates reached a maximum mean of 30.9 ± 9.5 fmols/50 µL, representing a 127% increase from baseline and an absolute increase of 17.3 ± 8.8 fmols (n = 4), (Figure 31).

A two-way ANOVA, examining 1 mg/kg vs. 3 mg/kg fenfluramine groups, revealed a significant main effect of time ($F_{12, 108} = 5.9$; $p = < 0.05$) but no significant effect of group or time x group.

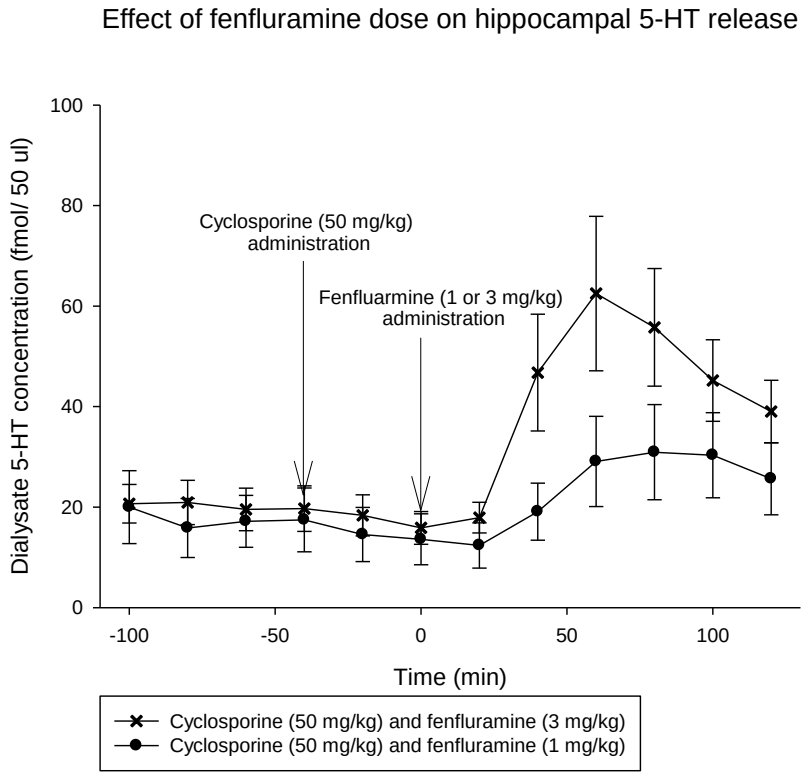

Figure 31: The effect of fenfluramine dose (1 vs.3 mg/kg) on hippocampal 5-HT release. Data are mean ± sem, n = 4 (1 mg/kg fenfluramine), n = 7 (3 mg/kg fenfluramine).

4.3.7 Endogenous 5-HT content in the rat hippocampus after administration of cyclosporine (50 mg/kg) and fenfluramine (3 mg/kg)

The mean dialysate 5-HT concentration after cyclosporine (50 mg/kg) but before fenfluramine injection was 15.9 fmols/50 µL. After fenfluramine (3 mg/kg) injection it reached a maximum of 62.5 fmols/50 µL 60 min post injection.

From the data presented thus far estimates of dialysate hippocampal 5-HT level can be estimated from the dialysate 5-HT concentration taking into account the *in vitro* probe calibration data (section 4.2.5). From these data, it appears that the mean basal (pre-fenfluramine) hippocampal 5-HT level in cyclosporine pre-treated rats was estimated to be 129.0 ± 26.8 fmols/50 µL (approx 2.6 x 10^{-9} M) and that fenfluramine (3 mg/kg) administration, with cyclosporine (50 mg/kg)

pre-treatment, caused a maximum hippocampal 5-HT concentrations of 506.9 ±124.9 fmols/50 µL (approx 1 x 10^{-8} M)

4.4 Discussion

Microdialysis probes were found to have a mean recovery of 15.7 ± 0.8% of the external 5-HT content highlighting the need to produce a calibration curve for probes so that the true value can be calculated. It was also found that the variability between probes increased at higher external 5-HT concentrations. In addition it was shown that the dialysate measurements had stabilised at T = 40 min for external 5-HT concentrations of 200 and 400 fmol/50 µL. However, at lower concentrations of 50 and 100 fmol/50 µL, it appears the dialysate had not stabilised by the last measurement at T = 60 min. It should be noted that there was large variability in these measurements which may be masking the possibility that stability was achieved. It is likely that the greater variability at lower 5-HT concentrations is the product of the contribution of HPLC baseline noise, which will affect smaller measurements of concentration proportionally more than higher concentrations.

As cyclosporine pre-treatment is required to perform PET scans with 4-[^{18}F]MPPF in this project in order to slow down clearance in the brain, it was necessary to ascertain any effect this had on the fenfluramine induced 5-HT release. Cyclosporine pre-treatment did not have a significant effect on fenfluramine induced 5-HT release. However, again there is large variability in the data, and when considering the delta (absolute change) increase in 5-HT after fenfluramine administration, a possible effect of cylcosporine can be seen. Without cyclosporine pre-treatment 5-HT delta increase is 81.4 ± 15.6 fmols, whereas with cyclosporine produces a delta increase of 46.6 ± 15.3. Therefore this could suggest cyclosporine pre-treatment has a small attenuating effect on fenfluramine induced 5-HT release. However, there is still a notable increase in 5-HT levels in the brain with a cyclosporine pre-treatment which is suitable for use in PET ligand binding studies.

No significant difference in 5-HT release was found between 1 mg/kg and 3 mg/kg fenfluramine administration. However again there is a large amount of variability in the data. When considering the delta increase it can be seen that 1

mg/kg fenfluramine produces a delta increase of 17.3 ± 8.8 fmols/50 µL whereas 3 mg/kg results in 46.6 ± 15.3 fmols/50 µL. From the delta increased data it could be suggested that 3 mg/kg fenfluramine causes a greater increase in 5-HT release compared to 1 mg/kg.

Due to the variability in both datasets it could be suggested that the *in vivo* microdialysis studies require higher repetitions to acquire more accurate results.

In the present study our 506.9 ±124.9 fmols/50 µL 5-HT released by fenfluramine 3 mg/kg translates to approximately 400 % increase from baseline in 5-HT levels. Several published studies have conducted microdialysis experiments in tandem with PET or β-probe studies of 4-[^{18}F]MPPF. One study by Zimmer *et al.* (Zimmer et al., 2002a) found a 20% increase in 5-HT in the rat hippocampus for 1 mg/kg fenfluramine and 50% for 2 mg/kg. Another study looking at 5 mg/kg fenfluramine (Udo De Haes et al., 2006) found a 2000% increase in endogenous 5-HT in the monkey frontal cortex. Other studies have been equally inconsistent. Of those that used a higher dose of fenfluramine (10 mg/kg) an increase of 170% was found in the rat DRN (Zimmer et al., 2002b) and 1500 to 3000% increase in the rat hippocampus (Zimmer et al., 2002a, Udo de Haes, 2005). It can be seen that pharmacologically induced 5-HT release is inconsistent between studies, highlighting the importance of microdialysis studies to assess 5-HT concentrations using the same study protocol.

This study has shown the hippocampal brain concentrations of endogenous 5-HT can be approximated to be 506.9 ±124.9 fmols/50 µL (approx 1 x 10^{-8} M) at the time of 4-[^{18}F]MPPF injection for PET scans and *ex vivo* autoradiography studies to be performed in Chapter 5.

4.5 Conclusion

It has been shown that endogenous 5-HT can be increased by a maximum of 400% from baseline in the rat hippocampus by administration of fenfluramine (3 mg/kg) with the addition of cyclosporine pretreatment (50 mg/kg). Using this drug treatment the hippocampal 5-HT concentration of 5-HT at T=60 min has been found to be approximately 1 x 10^{-8} M. The drug treatments (cyclosporine (50 mg/kg)/fenfluramine (3 mg/kg) and timing protocols will be followed in the

PET scans and *ex vivo* autoradiography studies to be performed as described in the following chapter.

Chapter 5. PET and autoradiography

5.1 Introduction

The underlying theory of this thesis is that receptor specific PET ligands can be displaced by endogenous neurotransmitters and this can give a route to examining dysfunction of neurotransmitter systems at the biochemical level.

Previous work, using *in vivo* PET imaging, β microprobes and *ex vivo* autoradiography, has suggested the 5-HT $_{1A}$ receptor PET ligand 4-[^{18}F]MPPF can be displaced from 5-HT $_{1A}$ receptor rich brain areas by endogenous 5-HT , stimulated by pharmacological intervention (Zimmer et al., 2002b, Zimmer et al., 2002a, Aznavour et al., 2006, Riad et al., 2004, Udo de Haes, 2005, Rbah et al., 2003, Zimmer et al., 2003). If 4-[^{18}F]MPPF possesses this characteristic, it would make a valuable tool in the characterisation and diagnosis of disorders involving the 5-HT system, such as depression and anxiety. However, not all studies suggest 4-[^{18}F]MPPF is displaceable (Udo De Haes et al., 2006, Riad, 2008, Moulin-Sallanon et al., 2009, Riad et al., 2004, Ginovart et al., 2000, Plenevaux et al., 2000), so there remains a lack of agreement in the current literature.

Chapter 2 and 3 describe the precursor synthesis and subsequent radiosynthesis of 4-[^{18}F]MPPF which was used for experiments in this chapter. Chapter 4 describes microdialysis studies characterising the release of endogenous 5-HT by the releasing agent fenfluramine, and the effect of the p-glycoprotein transport inhibitor cyclosporine. The protocol used in the *in vivo* microdialysis experiments have been replicated for experiments in this chapter, so that 4-[^{18}F]MPPF is administered at the time of maximum 5-HT release.

Therefore, the aims of this chapter are to:

- Characterise the specific binding of 4-[^{18}F]MPPF, in *ex vivo* autoradiography and 4-[^{3}H]MPPF, *in vitro* autoradiography, in brain areas with a high density of 5-HT $_{1A}$ receptors.
- Determine the concentration of 5-HT which will displace 4-[^{3}H]MPPF from brain areas with a high density of 5-HT $_{1A}$ receptors, using *in vitro* autoradiography.
- Characterise the uptake, washout and distribution of 4-[^{18}F]MPPF in the brain using *ex vivo* autoradiography and PET.
- Determine whether 4-[^{18}F]MPPF can be displaced by endogenous 5-HT using *ex vivo* autoradiography and PET.
- To compare PET and autoradiography as methods for studying 4-[^{18}F]MPPF receptor binding.

As the radioisotope has no effect on the binding profile of the ligand, it is advantageous to choose the one most practical for the proposed experiment. For this reason the present study used a tritiated version of 4-MPPF, 4-[^{3}H]MPPF for *in vitro* autoradiography studies. The advantages of tritium over fluorine-18 are as follows;

- Longer half life (12.3 years for tritium vs 110 min for fluorine-18) allows for longer experimental procedures to be performed such as *in vitro* competition studies, which typically are performed over approx. 6 – 8 hours.
- Can be readily commercially purchased and subsequently stored for use over many years.
- The lower energy of tritium results in better resolution autoradiographs.
- 4-[^{3}H]MPPF can be compared to previously published *in vitro* autoradiography experiments, including those using different ligands, which typically use the tritium isotope.
- Greater ease of safe handling of beta emitting isotopes vs. gamma emitters.

Methods

5.1.1 Animal supply, housing and experimentation

Animal procedures were performed under the UK home office requirements, set out in the Animal (Scientific Procedures) Act 1986.

Male Lister hooded rats were purchased from Charles River (Margate, Kent) and were housed in groups of three or four per cage (56 x 38 x 20 cm) with water and food available *ad libitum*. Animals were left at least three days to acclimatise to the surrounding before use in experimentation, only being disturbed to allow for cage cleaning and food and water replenishment. Animals were kept in controlled conditions consisting of a 12 hr light, 12 hr dark, light cycle (lights on at 7am GMT) at a constant temperature (21 ±2 ºC) and humidity (~40%).

5.1.2 PET ligand

4-[^{18}F]MPPF in ethanol (0.3 mL), was prepared and delivered to the PET scanner room on the morning of use. The ligand was diluted in sterilised water (1.2 mL, Braun Medical Ltd, UK) to give a total volume of 1.5 mL containing 20% ethanol.

5.1.3 General PET protocol

On the day of the experiment, animals were transferred to separate cages (one animal per cage) in the PET scanner room, and treated with cyclosporine (50 mg/ kg, i.p., SANDIMMUN, Novartis Pharmaceuticals Ltd, UK).

5.1.4 Specific binding of 4-[^{18}F]MPPF in different brain regions

As described in Figure 32, animals were anaesthetised (5% isoflurane induction, 1-2% isoflurane maintainance via a facemask, anaesthetic station VTS VetTech Solutions Ltd, UK with active scavenging unit (#6238) and Cardiff absorber (Shirley Aldred & Co. LtD, UK).) and placed on a heated pad). Cold 4-MPPF (10 mg/kg,

i.p, dissolved in a drop of conc. HCl and made up to volume in sterilised water to pH 3 - 4) or acidified water vehicle control was administered to the animal at T-30 minutes before the PET study. A tail vein was cannulated (19 mm I.V. catheters, Abbott Laboratories, China) at approximately T -15 min before the start of the PET study. Post tail cannulation the animal was moved to the PET scanner Minerve tube (Patent PCT/FR2006/001218, Bioscan by Minerve), which maintained anaesthesia for the duration of the scan (0.5 – 1.5 % isofluorane, 1 L/min O_2, scavenger (Halosorb), heating (URT Multipostes 06170030) and pump unit (PCA Multipostes 08220027), Isofluorane tank (NS 07010392), Equipment Veterinaire Minerve, Esternay.), then placed into the PET scanner. The head was positioned using two wedges of oasis foam placed either side of the head and the head and body were fixed in place with tape.

The animal was positioned in the scanner so that the laser positioning cross hairs were approximately over the centre of the brain. At the start of the PET scan (T = 0 min) 4-[^{18}F]MPPF was injected (i.v. tail vein, over approximately 30 seconds). Radioactivity of the syringe containing 4-[^{18}F]MPPF was measured before and after injection so that exact injected activity could be calculated.

Each animal was subjected to a single PET or autoradiography experiment then euthanized by anaesthetic overdose.

5.1.5 Effects of endogenous 5-HT release on 4-[^{18}F]MPPF binding

Essentially the same protocol was used as for the study described above (section 5.2.4). However, as described in Figure 33, fenfluramine (3 mg/kg @ 1mL/kg, i.p) or saline vehicle control (1 mL/kg i.p.) was administered before induction of anaesthesia at T - 60 min.

5.1.6 PET system description

PET studies were performed on a Philips MOSAIC HP preclinical PET system (Phillips Health Care, Netherlands). The scanner uses 14,456 lutetium-yttrium orthosilicate (LYSO) crystals (2 x 2 x 10 mm, Photonic materials Ltd., Scotland)

arranged in 52 rings each containing 278 crystals. The signal from the crystals is read out by a hexagonal array of 288 photomultiplier tubes (19 mm diameter). The detector ring diameter is 19.7 cm and a bore size of 18 cm. The system scans exclusively in 3-D mode, has an axial field of view of 11.9 cm and a spatial resolution of 1.9 mm full width half maximum (FWHM) (Huisman et al., 2007, Surti et al., 2005).

The system quality control checks consisted of system initialization, baseline correction, energy tests and PMT gain tests. This is followed by a short emission QC where a sinogram is generated and observed to see if there are any missing or weak line segments. This was performed at the start of each day with a ^{22}Na point source (2.5 cm disc, 100 µCi, Eckert and Ziegler, California) which was placed in a cradle and centred in the transaxial and axial FOVs.

The scanner is controlled by in-built dedicated Philips Mosaic software running on Sun Microsystems hardware. 30 minute dynamic scans (5 x 1 min, 3 x 5 min and 1 x 10 min) were conducted with the animal weight and an approximate injected radioactivity entered into the software prior to scanning. Raw data from dynamic scans were stored in sinogram format. Each sinogram was corrected for injected activity after scan completion and reconstructed to give images with a voxel size of 1 mm^3. The reconstruction was a 3D RAMLA emission algorithm, which was decay corrected and contains 128 slices. There was no attenuation correction, no scatter correction and no random subtraction.

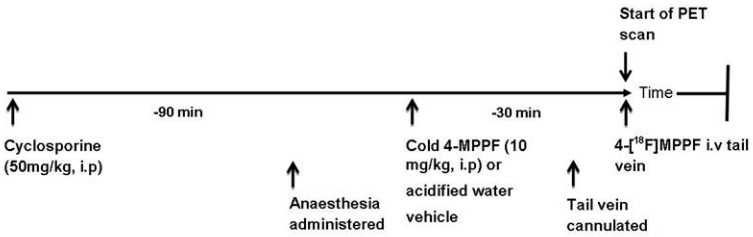

Figure 32: PET imaging experiments timeline; to reveal specific binding of 4-[^{18}F]MPPF by pre-treatment with cold 4-MPPF.

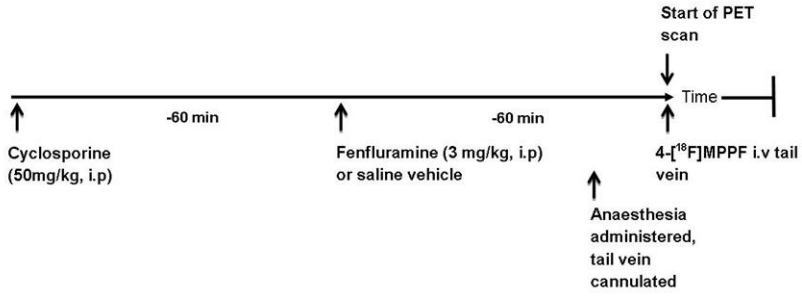

Figure 33: PET imaging experiments timeline; to test effect of pharmacologically induced endogenous 5-HT release (using fenfluramine) on 4-[^{18}F]MPPF binding.

5.1.7 PET data analysis

To create an MRI template, MRI images were taken from 12 untreated male Lister hooded rats. The images were corrected for an artefact and resized to a voxel size of 1 mm^3 using MRIcro (v. 1.40 build 1). The images were co-registered to a single arbitrary MRI image using FSL (v. 5.0), to create a single summed MRI image.

The MRI template was created by Dr. David Cousins, from MRI images produced by Dr. Richard McQuade and Dr. David Cousins.

The MRI template and reconstructed PET image DICOM files were uploaded to Imalytics software (3.0 Rev 3974 (64)) for analysis. Volumes of interest (VOI's) for the prefrontal cortex (PFC), hippocampus, dorsal raphe nucleus (DRN) and the cerebellum were drawn manually on the MRI template, using a rat brain atlas for reference (Paxinos and Watson, 1998). PET images were manually co-registered to the MRI image using the eye socket as an anatomical reference and voxel sizes for each VOI was recorded for each PET image (Figure 34). Time-activity curves (TAC) were calculated for each VOI by the Imalytics software and plotted as mean standard uptake value (SUV) over time (s).

SUV = tissue radioactive concentration (MBq) (t) /

(injected activity (MBq) (t)/ body weight (g))

Non-specific binding was defined as the SUV in the cerebellum and specific binding was calculated by subtracting the cerebellum SUV from that of each brain area. The magnitude of ligand binding was inferred from specific binding at any given time point in each VOI.

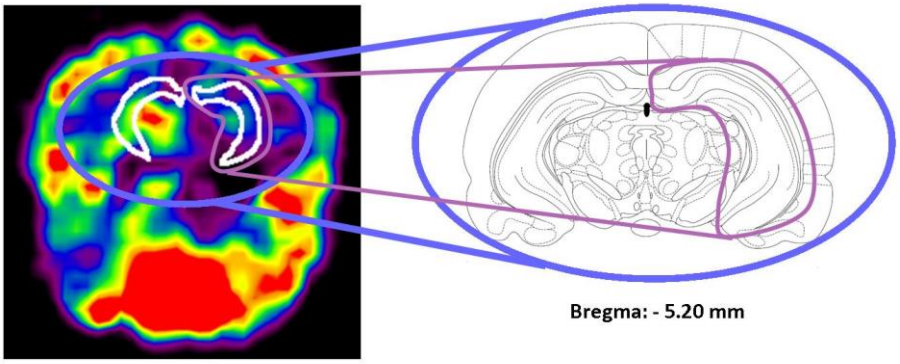

Figure 34: Example of a PET image from a single coronal slice of the whole rat head and neck. Approximate Bregma location (Paxinos and Watson, 1998) for the brain is highlighted in purple and the hippocampal region of interest (ROI) in pink. The region of interest (ROI) in the hippocampus which was used for PET analysis in this slice is outlined in white.

To statistically analyse whether specific binding occurred in the cerebellum, the raw SUV data was used. For all other statistical analysis specific binding data was used and weighted in accordance with the time period it represented. For example, an SUV taken from a 5 minute window was multiplied by five, with comparable treatment given to the 1 and 10 minute window data. The effect of cold 4-MPPF or fenfluramine on the binding profile of 4-[^{18}F]MPPF in the hippocampus, DRN or PFC was examined using a two-way (time and pre-treatment) repeated measures ANOVA followed by a post-hoc independent samples t-test.

5.1.8 Ex vivo 4-[^{18}F]MPPF autoradiography protocol

Here, the protocol was identical to the *in vivo* PET protocol (sections 5.2.3-5). however, the animal was not placed in the PET scanner and was killed by an overdose of anaesthesia 5 min after administration of 4-[^{18}F]MPPF (Figures 35 and 36). After the animal had been killed the brain was rapidly removed and flash

frozen in a bath of iso-pentane (VWR, France) submerged in dry ice. Brain sections were collected (50 µm, hippocampus, DRN, PFC and cerebellum, Microm HM 500 OM cryostat, Germany) and mounted on glass slides before being exposed overnight to autoradiography film (Amersham Hyperfilm M.P, 24 x 30 cm, GE Healthcare Ltd, UK). The individual experiments were designed such that a vehicle and a drug challenge were paired and performed on the same day. Brain sections from each paired experiment were laid down on film after the same interval post 4-[^{18}F]MPPF injection (approx. 1 hr).

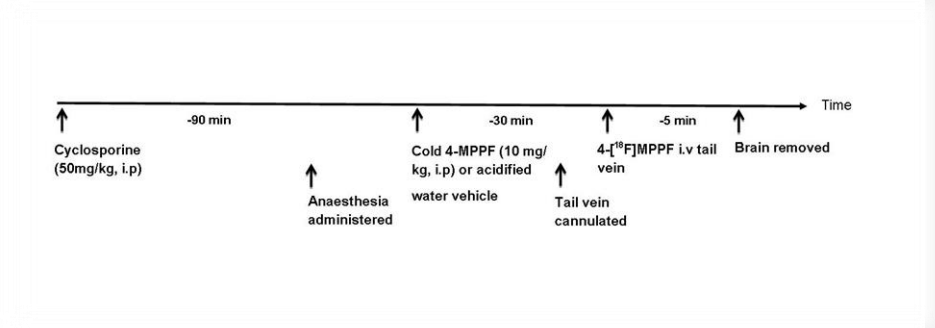

Figure 35: Ex vivo autoradiography experiments timeline; to reveal specific binding of 4-[^{18}F]MPPF by pre-treatment with cold 4-MPPF.

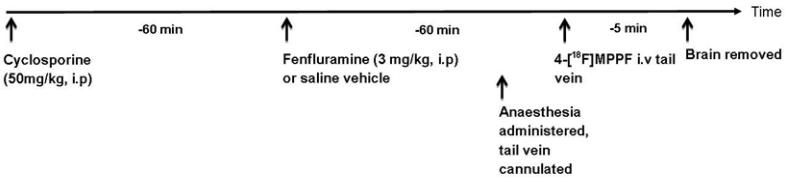

Figure 36: Ex vivo autoradiography experiments timeline; to test effect of pharmacologically induced endogenous 5-HT release (using fenfluramine) on 4-[^{18}F]MPPF binding.

5.1.9 Fluorine-18 autoradiography standards and calibration curve

To create a fluorine-18 autoradiography standard, forebrain tissue from 6 male Lister hooded rats was homogenised using a pestle and mortar then divided into eight 1.0 mL Eppendorfs (0.4g per tube, Kartell Spa, Noviglio (MI)). [^{18}F]FDG (20 µL, 4.8 – 160 Bq) was added to each Eppendorf and vortexed (1 min) to distribute the radioactivity evenly throughout the brain tissue, creating 8 radioactive concentration standards. The activity of each Eppendorf was measured after vortexing. A small amount of tissue (approx. 0.05 – 0.1 mg) from each standard was placed in a well, formed within a block of frozen Tissue-Tek O.C.T compound (Sakura Finetek, USA). The block was mounted in a cryostat (Microm HM 500 OM cryostat, Germany) and sections (50 µm) were taken to be laid on autoradiographic film (24 hr, Amersham Hyperfilm M.P, 24 x 30 cm, GE Healthcare Ltd, UK). All radioactive standards were laid onto film simultaneously. To create a 4-[^{18}F]MPPF standard calibration curve the mean optical density of 14 standard samples, at each of the 8 activities, was measured using ImageJ (v. 1.46 r) and the background subtracted. The mean optical densities were then plotted against the known activity/g (MBq/g) and cubic polynomial regression analysis was performed

to give a correction equation; $Y = 41.882x^3 - 139.89x^2 + 195.3x - 6.4636$, $R^2 = 0.977$ (Figure 37, Table 16).

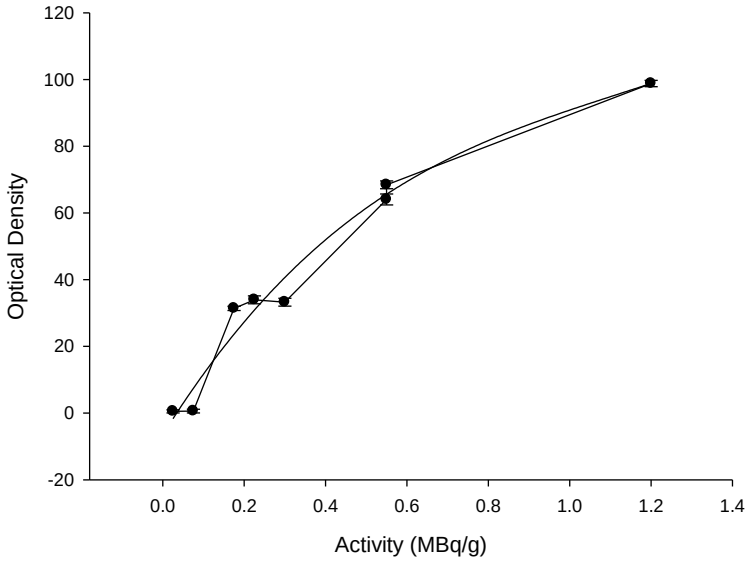

Figure 37: [^{18}F]FDG autoradiography calibration curve, with 3rd order polynomial regression curve. Values are mean ±sem.

MBq/g	Mean optical denisty	n	Standard deviation	sem
1.2	98.8	14	3.5	0.9
0.6	68.4	14	4.4	1.2
0.6	64.0	14	6.2	1.6
0.3	33.2	14	4.4	1.2
0.2	34.0	16	4.7	1.2
0.2	31.4	16	2.6	0.6
0.1	0.6	16	2.2	0.6
0.0	0.5	16	1.9	0.5

Table 16: [^{18}F]FDG autoradiography calibration curve data

5.1.10 In vitro 4-[^{3}H]MPPF autoradiography protocol

For each experiment a solution of 4-[^{3}H]MPPF (0.14, 1.4 or 10 nM) was made up in Tris buffer solution (50mM, Trizma pre-set crystals pH 7.6, Sigma, USA. pH to 7.4 using conc. HCl). Solutions for non-specific binding, using (±) 8-OH-DPAT (0.07 nM (±) 8-hydroxy-2(di-n-propylamino)tetralin hydrobromide, Aldrich, UK) and displacement studies, using 5-HT (1 x 10^{-13} to 2 x 10^{-6} mM 5-hydroxytryptamine hydrochloride, 99%, Alfa Aesar Ltd, UK) were made up in the 4-[^{18}F]MPPF solution.

Four male Lister hooded rats (245 - 373g) were killed by decapitation and the brains removed and flash frozen in a bath of iso-pentane submerged in dry ice. Sections (20 µM) were collected from four brain areas; hippocampus, DRN, PFC and cerebellum and mounted on glass slides. After initial pre-incubated in buffer (30 min, R.T, 50mM Tris HCl (pH 7.4), 2 mM $MgCl_2$), the slides were incubated for 2 hr at room temperature in their respective solutions containing 4-[^{3}H]MPPF and 5-HT or (±) 8-OH-DPAT (Table 17). Following this incubation the sections were rinsed in buffer solution for 15 min. Buffer was washed off by dipping in ice cold distilled water and sections were allowed to dry before being exposed to autoradiographic (Amersham Hyperfilm^{MP}) film for 3 months along with autoradiographic [^{3}H] microscales (Amersham, UK).

Labelling solution	**4-[^{3}H]MPPF concentration**		
	0.14 nM	1.4 nM	10.0 nM
4-[^{3}H]MPPF	✓	✓	✓
8-OH DPAT (0.07 nM)	✓	✓	✓
1 x 10^{-13} mM 5-HT	✓	✓	✓
2 x 10^{-13} mM 5-HT	✓	✓	✓
5 x 10^{-13} mM 5-HT	✓	✓	✓
2 x 10^{-12} mM 5-HT	✓	✓	✓
2 x 10^{-11} mM 5-HT	✓	✓	✓
2 x 10^{-10} mM 5-HT	✓	✓	✓
2 x 10^{-9} mM 5-HT	✓	✓	✓
2 x 10^{-8} mM 5-HT	✓	✓	✓
2 x 10^{-6} mM 5-HT			✓

Table 17: Labelling solutions for 4-[^{3}H]MPPF in vitro autoradiography studies

5.1.11 Autoradiographic film development

After the desired exposure time had elapsed the film was transferred to a dark room and submerged in developer solution (5 min with agitation, RG Universal ready to use X-ray developer, Champion, UK.), washed in water containing wetting agent (20 s, ILFORD wetting agent, Herman Technology Ltd., UK), submerged in fixer (5 min with agitation, Amfix high speed fixer, Champion, UK) then thoroughly washed in water containing wetting agent (3 min, ILFORD wetting agent, Herman Technology Ltd., UK), before hanging to dry.

5.1.12 [^{3}H] autoradiography calibration curve

To create a calibration curve the optical density from a [^{3}H] Amersham microscale standard was measured using ImageJ (v. 1.46 r) and the background subtracted. The optical densities were plotted against the known activity/g (Bq/mg) and cubic polynomial regression analysis was performed to give a correction equation. A calibration curve was constructed for each film. An example calibration curve is shown in Figure 38.

Regression equation; $Y = 0.2314x^3 - 8.9648x^2 + 163.21x + 298.99$, $R^2 = 0.9958$

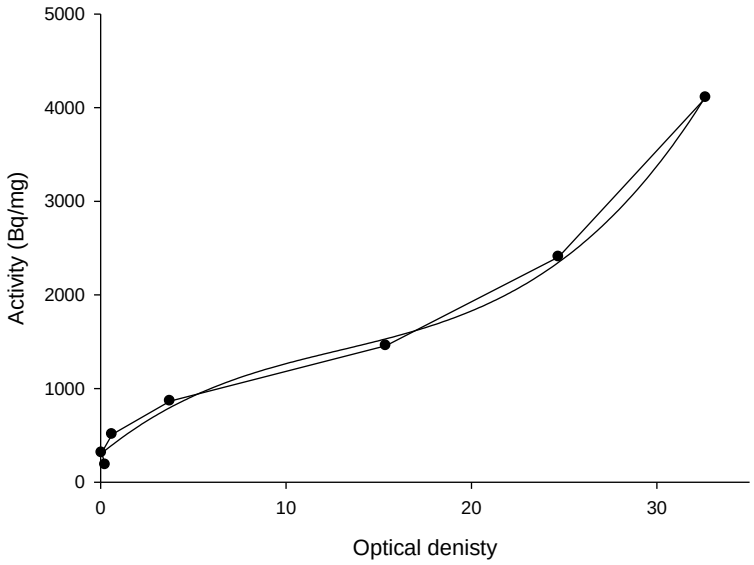

Figure 38. Example of a [^{3}H] autoradiography calibration curve (for film 6/6) with 3rd order polynomial regression.

bq/mg	Optical density
4107.0	32.6
2405.0	24.7
1457.8	15.4
865.8	3.7
510.6	0.6
314.5	0.1
185.0	0.3

Table 18: [^{3}H] autoradiography calibration curve data

5.1.13 Autoradiography data analysis

For both *ex vivo and in vitro* autoradiography brain sections were stained after exposure to the autoradiographic film (Cresyl violet protocol Chapter 4, section 4.2.7) and digital images taken of stained sections as well as the corresponding

autoradiographic brain sections images, (Scion Image software (Beta 4.0.2), Leica M26 microscope with Leica 10445930 1.0 x camera). Microscope manual zoom and focus were kept constant throughout data analysis. Using image J (v. 1.46 r), the brain region of interest (ROI) was manually highlighted on the stained brain section image. ImageJ software was then used to redirect the ROI onto the corresponding autoradiograph image and the optical density of that area was recorded. Measurements were recorded from three brain sections per brain area (hippocampus, DRN, PFC and cerebellum) and the optical density of the background was also recorded to control for any differences in optical density across the film.

The magnitude of ligand binding was calculated from the optical density calibrated to commercial [^{3}H] microscales standards for the 4-[^{3}H]MPPF autoradiography, and in house [^{18}F]FDG standards for the 4-[^{18}F]MPPF autoradiography. Non-specific binding was defined as the mean optical density in the cerebellum and specific binding was calculated by subtracting the mean cerebellum optical density from the mean optical density of each brain area.

The effect of cold 4-MPPF or fenfluramine on the binding profile of 4-[^{18}F]MPPF in the hippocampus, DRN and PFC was examined using two tailed paired t-test.

The effect of 5-HT on 4-[^{3}H]MPPF binding was examined using a one way ANOVA with a post-hoc Dunnetts test.

5.2 Results

5.2.1 4-[^{3}H]MPPF Autoradiography

Distribution of 4-[^{3}H]MPPF in controls

A dense signal was observed in the dorsal and ventral hippocampus (CA1,CA2 & CA3), entorhinal cortex and the dorsal raphe nucleus. A less dense signal was observed in the PFC, dentate gyrus, median raphe nucleus, agranular insular,

parietal, occipital, temporal, perihinal, piriform, cingulate and frontal cortex as well as the entorhinal cortex inferior colliculus and dorsal, lateral and ventral central gray. The cerebellum and caudate putamen showed a very low signal (Figures 39 – 42).

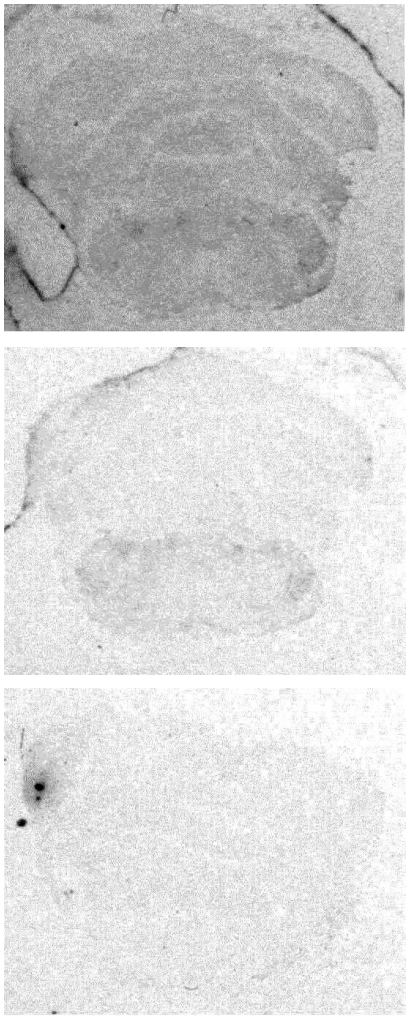

Figure 39: Cerebellum; Top 4-[^{3}H]MPPF only, middle 4-[^{3}H]MPPF + 0.07 nM (±) 8-OH-DPAT, bottom 4-[^{3}H]MPPF + 2 x 10^{-6} M 5-HT

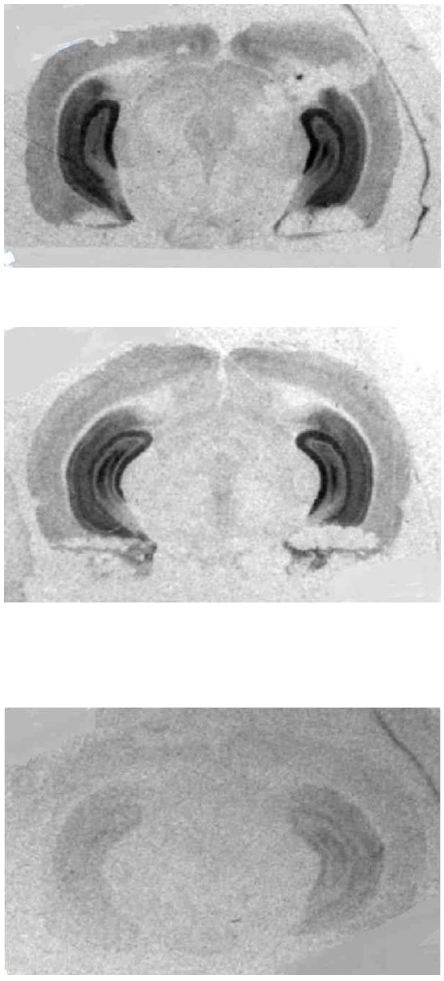

Figure 40: Hippocampus; Top 4-[^{3}H]MPPF only, middle 4-[^{3}H]MPPF + 0.07 nM (±) 8-OH-DPAT, bottom 4-[^{3}H]MPPF + 2 x 10^{-6} M 5-HT

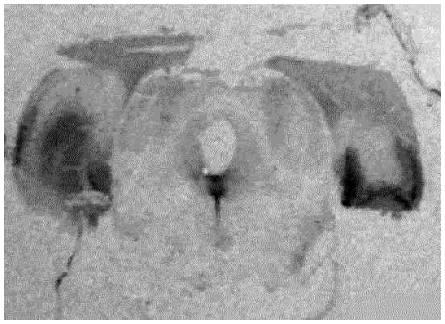

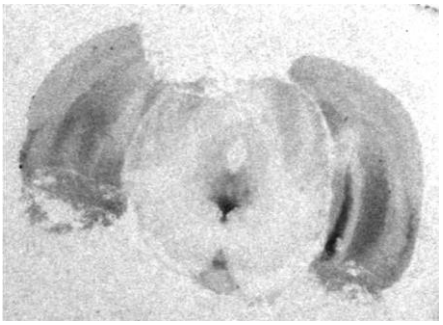

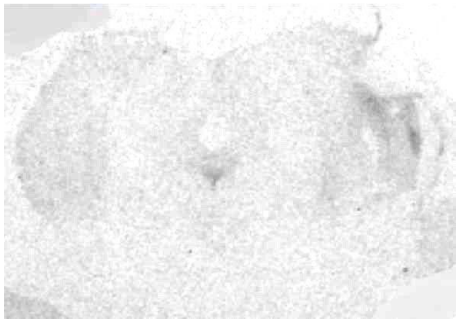

Figure 41: DRN; Top 4-[^{3}H]MPPF only, middle 4-[^{3}H]MPPF + 0.07 nM (±) 8-OH-DPAT, bottom 4-[^{3}H]MPPF + 2 x 10^{-6} M 5-HT

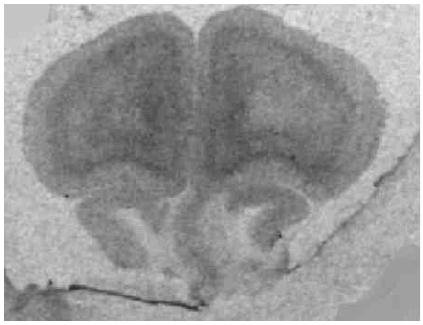

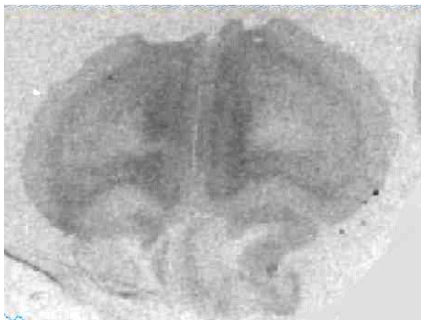

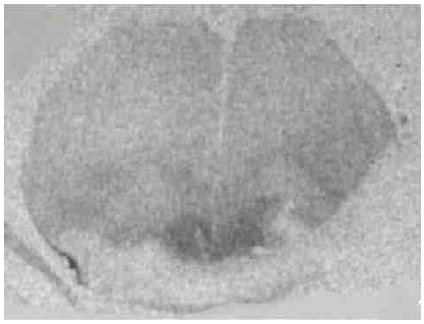

Figure 42: PFC; Top 4-[^{3}H]MPPF only, middle 4-[^{3}H]MPPF + 0.07 nM (±) 8-OH-DPAT, bottom 4-[^{3}H]MPPF + 2 x 10^{-6} M 5-HT

Effect of 0.07 nM (±) 8-OH-DPAT on binding of 4-[^{3}H]MPPF in different brain regions

The 5-HT $_{1A}$ agonist (±) 8-OH-DPAT was used to displace specific 4-[^{3}H]MPPF binding in order to determine of non-specific binding of the ligand. However in this experiment the concentration of (±) 8-OH-DPAT used (0.07 nM) had little or no effect on 4-[^{3}H]MPPF in the hippocampus or DRN in any of the brain areas studied (Table 19). This is discussed further later in this thesis.

10.0 nM 4-[^{3}H]MPPF	**Specific activity (bq/mg)**		
	hippocampus	**DRN**	**PFC**
4-[^{3}H]MPPF	1439.5	1208.2	919.0
4-[^{3}H]MPPF + 0.07nM DPAT	1567.6	1200.1	846.0
	% control binding		
	108.9	99.3	92.1

Table 19: Effect of 0.07 nM (±) 8-OH-DPAT on binding of 4-[^{3}H]MPPF in different brain regions

Effect of 5-HT on specific binding of 4-[^{3}H]MPPF in different brain regions

To determine the concentrations of 5-HT that would cause displacement of 4-[^{3}H]MPPF in the hippocampus, DRN and PFC, brain sections were incubated with 4-[^{3}H]MPPF and increasing concentrations of 5-HT (Table 20).

A one way ANOVA with post-hoc Dunnetts test comparing 4-[^{3}H]MPPF specific binding incubated with 5-HT vs. control (no 5-HT) revealed there was no significant reduction in binding at any 5-HT concentration in the hippocampus. However there was significant reduction in binding vs. control in the DRN and PFC at a 5-HT concentration of 2 x 10^{-6} M 5-HT (DRN and PFC: $p = < 0.05$) (Figures 43 – 45).

10 nM 4-[^{3}H]MPPF	Hippocampus (bq/mg)	% control	DRN (bq/mg)	% control	PFC (bq/mg)	% control
5-HT 0 M	1499.0		1209.1		926.1	
5-HT 2 x 10^{-6} M	480.7	**32.1**	216.0	**17.9**	106.9	**11.5**
5-HT 2 x 10^{-8} M	1173.6	**78.3**	1020.5	**84.4**	790.6	**85.4**
5-HT 2 x 10^{-9} M	1317.5	**87.9**	1225.3	**101.3**	685.6	**74.0**
5-HT 2 x 10^{-10} M	1201.0	**80.1**	1104.8	**91.4**	738.1	**79.7**
5-HT 2 x 10^{-11} M	1438.3	**96.0**	1237.3	**102.3**	657.1	**71.0**
5-HT 2 x 10^{-12} M	1164.6	**77.7**	1117.2	**92.4**	738.6	**79.8**
5-HT 5 x 10^{-13} M	1591.2	**106.1**	1501.3	**124.2**	1187.8	**128.3**
5-HT 2 x 10^{-13} M	1728.0	**115.3**	1585.5	**131.1**	1291.1	**139.4**

Table 20: Effect of 5-HT on specific binding of 4-[^{3}H]MPPF in different brain regions

Effect of 5-HT concentration on 4-[^{3}H]MPPF specific binding in the hippocampus

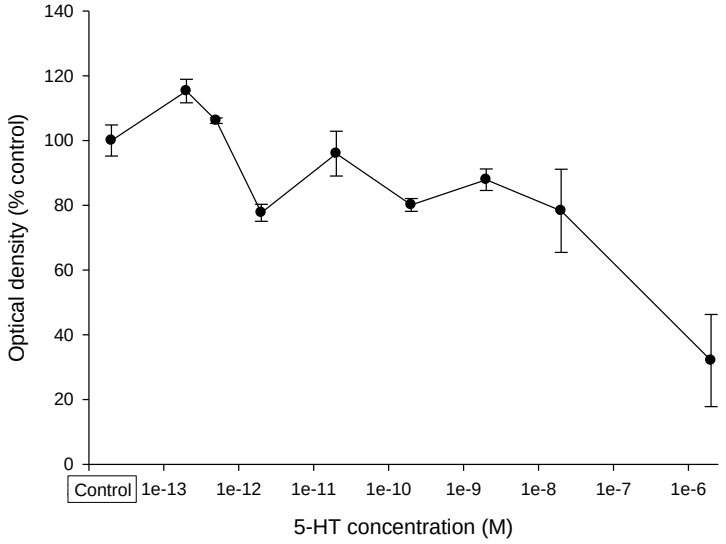

Figure 43: 4-[^{3}H]MPPF (10 nM) specific binding in the hippocampus; effect of 5-HT (2 x 10^{-13} to 2 x 10^{-6} M). Values are optical density of the hippocampus (n=3) with the optical density of the cerebellum (n=3) subtracted.

Effect of 5-HT concentration on 4-[^{3}H]MPPF specific binding in the DRN

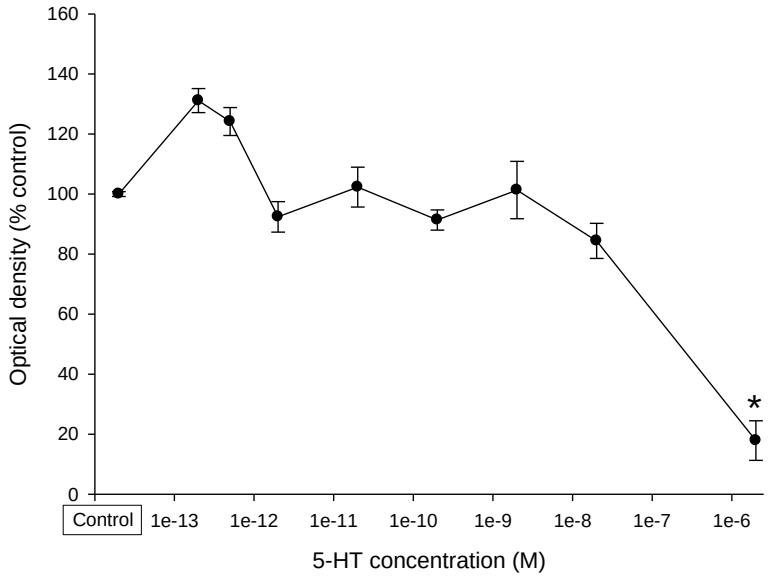

*Figure 44:. 4-[^{3}H]MPPF (10 nM) specific binding in the DRN; effect of 5-HT (2 x 10^{-13} to 2 x 10^{-6} M). Values are mean optical density of the DRN (n=3) with the mean optical density of the cerebellum (n=3) subtracted. * p = < 0.01 relative to control.*

Effect of 5-HT concentration on 4-[^{3}H]MPPF specific binding in the PFC

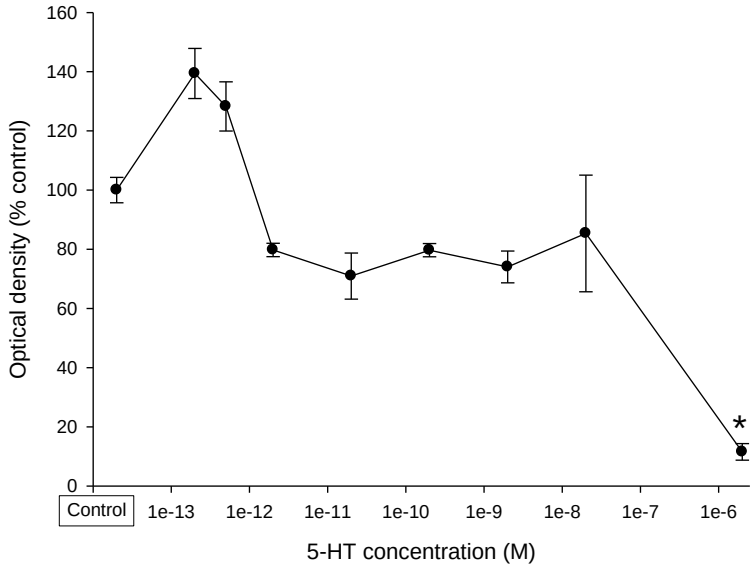

*Figure 45:.4 -[^{3}H]MPPF (10 nM) specific binding in the PFC; effect of 5-HT (2 x 10^{-13} to 2 x 10^{-6} M). Values are mean optical density of the PFC (n=3) with the mean optical density of the cerebellum (n=3) subtracted. * p = <0.01 relative to control.*

5-HT displacement of MPPF at relevant hippocampal 5-HT levels for in vivo 4-[^{18}F]MPPF PET and autoradiography

It was found using *in vivo* microdialysis (Chapter 4) that hippocampal 5-HT increased from 129.0 ± 26.8 fmol/50 µL pre-fenfluramine administration, to 506.9 ±124.9 fmol/50 µL, 1 hour after 3 mg/kg fenfluramine administration. This drug treatment was used to increase endogenous 5-HT in this chapter for *in vivo* autoradiography and PET studies experiments, to examine its effect on 4-[^{18}F]MPPF specific binding. Using the microdialysis probe calibration curve, it could be estimated that actual hippocampal 5-HT concentration before fenfluramine administration was 2.6 x 10^{-9} ± 0.5 x 10^{-9} M and the actual hippocampal 5-HT concentration after fenfluramine administration was 1.0 x 10^{-8} ± 0.3 x 10^{-8} M

From the autoradiography studies described above it appears that there is only partial hippocampal displacement (approx. 78% of control) of 4-[^{3}H]MPPF at 1.0

x 10^{-8} M 5-HT . These are the predicted *in vivo* hippocampal conditions for the PET and autoradiographic examination of the effect of increased endogenous 5-HT on 4-[^{18}F]MPPF specific binding.

0.14 and 1.4 nM 4-[^{3}H]MPPF autoradiography

Experiments using 0.14 nM and 1.4 nM 4-[^{3}H]MPPF concentrations resulted in low optical densities, which resulted in negative calibrated specific activities for two reasons;

- The signal was close to the autoradiographic film background optical density, resulting in high signal to noise ratio
- The range of optical densities making up the calibration curves was above that needed to calibrate this data.

For these reasons these data were excluded from examination.

5.2.2 [^{18}F] Autoradiography Results

Distribution of 4-[^{18}F]MPPF in controls

A dense signal was observed in the dorsal and ventral hippocampus (CA1,CA2 & CA3), the dorsal raphe nucleus, lateral septal nucleus and entorhinal cortex. A less dense signal was observed in the agranular insular, parietal, occipital, temporal, perihinal, cingulate, piriform and prefrontal cortex as well as the median raphe nuclus, dentate gyrus, external cortex inferior colliculus and the pontine reticular nucleus, oral. The cerebellum and caudate putamen showed a very low signal (Figure 46).

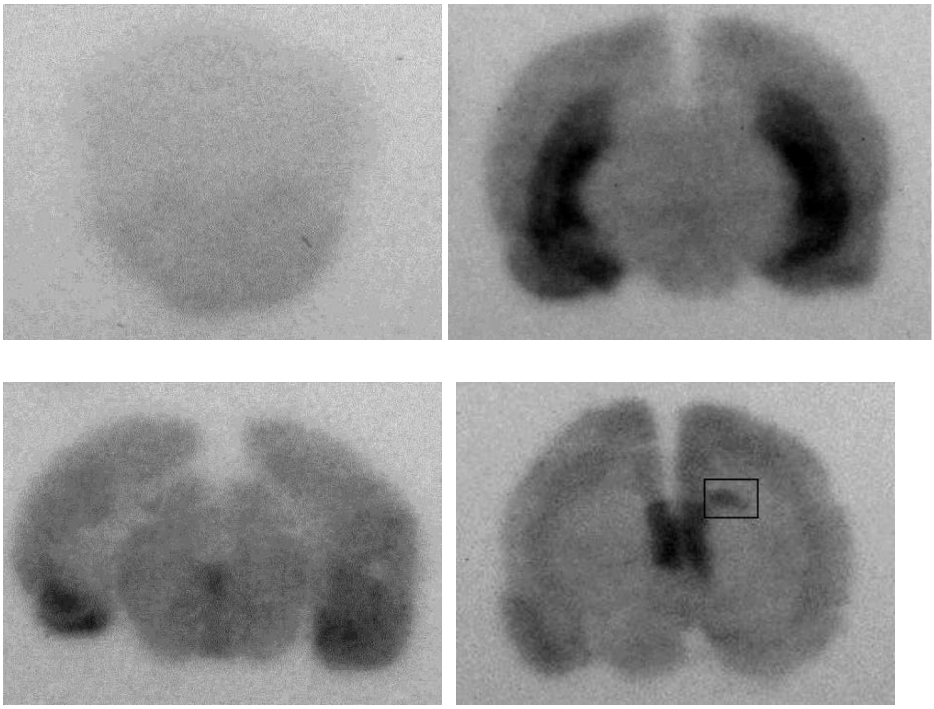

Figure 46: 4-[^{18}F]MPPF binding in the rat brain; Top left cerebellum, top right hippocampus, bottom left DRN, bottom right septal nucleus. An artefact can be seen at the top of the caudate putamen highlighted by the black square.

Specific binding of 4-[^{18}F]MPPF in different brain regions

4-[^{18}F]MPPF binding in the cerebellum (non-specific binding)

Pre-treatment with cold 4-MPPF was used to reveal the non-specific binding of 4-[^{18}F]MPPF. 10 mg/kg 4-MPPF pre-treatment did not affect the binding of 4-[^{18}F]MPPF in the cerebellum, an area reported to be essentially devoid of 5-HT $_{1A}$ receptors. The mean optical density for the cerebellum with cold 4-MPPF pretreatment was 2.65 ±0.06 MBq/g and 2.74 ± 0.06 MBq/g for control. A 2-tailed paired t-test revealed there was no significant difference between vehicle and 4-MPPF pre-treated binding in the cerebellum, ($p = 0.75$, $n = 4$) (Figure 47).

These data indicate that there is minimal specific binding of 4-[^{18}F]MPPF in the cerebellum, and on the basis of these data 4-[^{18}F]MPPF binding (optical

density) in the cerebellum was used as a measure of non-specific binding in the brain.

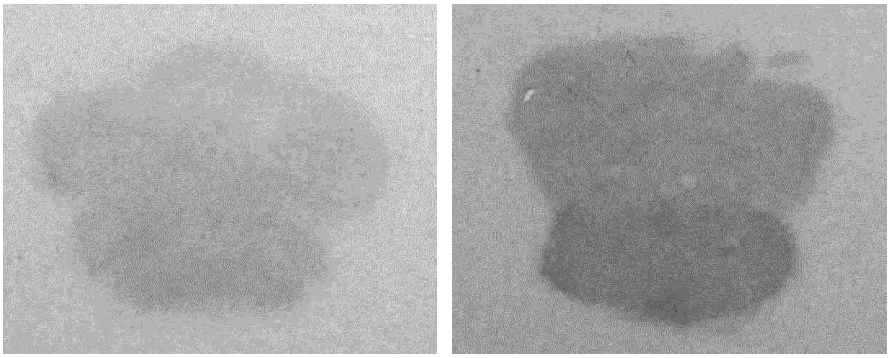

Figure 47: 4-[^{18}F]MPPF binding in the cerebellum; Left control, right cold 4-MPPF (10 mg/kg) pre-treatment

4-[^{18}F]MPPF specific binding in the hippocampus

4-MPPF pre-treatment had no significant effect on the specific binding of 4-[^{18}F]MPPF in the hippocampus. The mean optical density for the hippocampus with cold 4-MPPF pretreatment was 0.067 ±0.002 MBq/g and for control was 0.078 ± 0.008 MBq/g. A two-tailed t-test examining cold 4-MPPF pre-treatment vs. water vehicle found no significance difference in optical density in the hippocampus ($p = 0.17$, $n = 5$) (Figure 48).

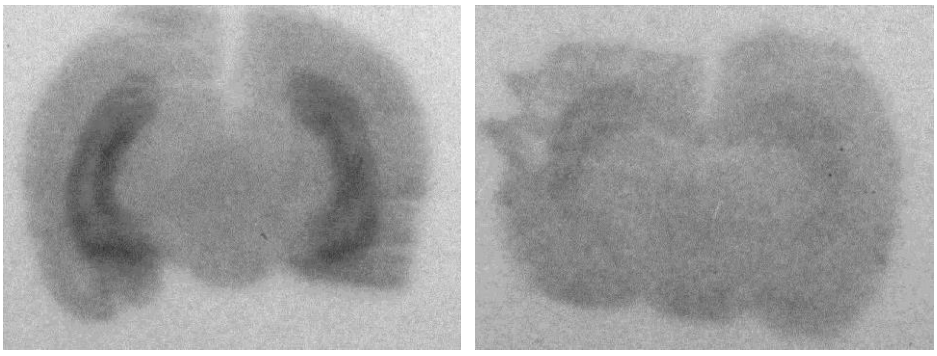

Figure 48: 4-[^{18}F]MPPF binding in the hippocampus; Left control, right cold 4-MPPF (10 mg/kg) pre-treatment

4-[^{18}F]MPPF binding in the DRN

4-MPPF pre-treatment had a possible effect on the specific binding of 4-[^{18}F]MPPF in the DRN. The mean optical density for the DRN with cold 4-MPPF pretreatment was 0.066 ±0.003 MBq/g and for control was 0.076 ± 0.004 MBq/g. A two-tailed t-test examining 10 mg/kg 4-MPPF pre-treatment vs. water vehicle found a strong trend in optical density in the DRN ($p = 0.059$, $n = 4$) (Figure 49).

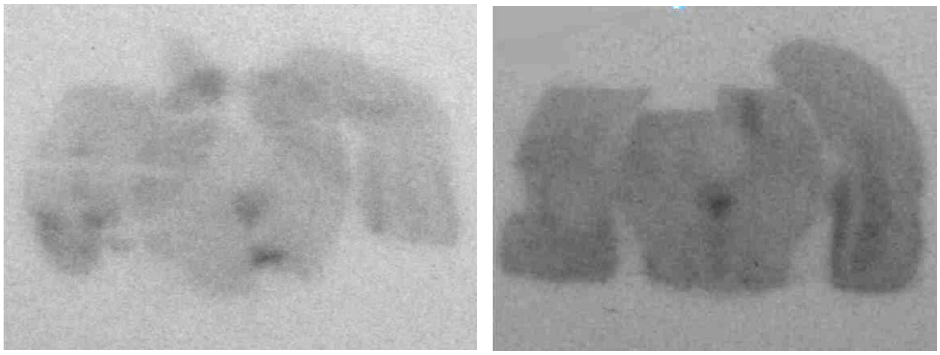

Figure 49: 4-[^{18}F]MPPF binding in the DRN; Left control, right cold 4-MPPF(10 mg/kg) pre-treatment

4-[^{18}F]MPPF specific binding in the PFC

4-MPPF pre-treatment had a significant effect the specific binding of 4-[^{18}F]MPPF in the PFC. The mean optical density for the PFC with cold 4-MPPF pretreatment 0.064 ±0.002 MBq/g was and for control was 0.072 ± 0.002 MBq/g. A two-tailed t-test examining 10 mg/kg 4-MPPF pre-treatment vs. water vehicle found a significance difference in optical density in the PFC ($p = 0.041$, $n = 4$) (Figure 50).

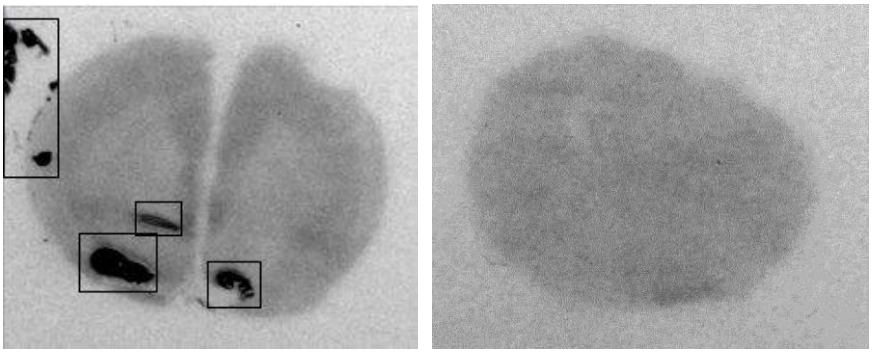

Figure 50: 4-[^{18}F]MPPF binding in the PFC; Left control, right cold 4-MPPF. (10 mg/kg) pre-treatment. Artefacts are highlighted in black squares.

Effects of endogenous 5-HT release on 4-[^{18}F]MPPF specific binding

Here pre-treatment with the 5-HT releasing agent fenfluramine was used to examine the effect of raised levels of endogenous 5-HT on 4-[^{18}F]MPPF specific binding in different brain areas.

Effect of fenfluramine pre-treatment on the specific binding of 4-[^{18}F]MPPF in the hippocampus

Pre-treatment with fenfluramine (3 mg/kg) had no effect on the specific binding of 4-[^{18}F]MPPF in the hippocampus. The mean optical density for the hippocampus with fenfluramine pretreatment was 0.091 ±0.005 MBq/g and for control was 0.15 ± 0.03 MBq/g. A two-tailed t-test examining 3 mg/kg fenfluramine pre-treatment vs. saline vehicle found no significance difference in optical density in the hippocampus ($p = 0.090$, $n = 6$) (Figure 51).

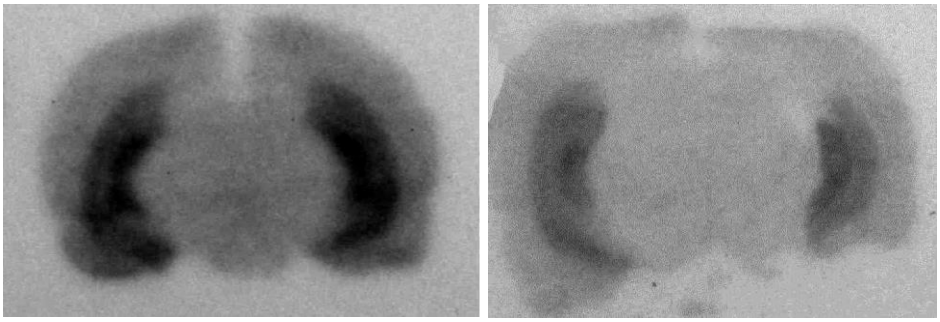

Figure 51: 4-[^{18}F]MPPF binding in the hippocampus; Left control, right fenfluramine (3 mg/kg) pre-treatment

Effect of fenfluramine pre-treatment on the specific binding of 4-[^{18}F]MPPF in the DRN

Pre-treatment with fenfluramine (3 mg/kg) had no effect on the specific binding of 4-[^{18}F]MPPF in the DRN. The mean optical density for the DRN with fenfluramine pretreatment was 0.080 ±0.006 MBq/g and for control was 0.12 ± 0.02 MBq/g. A two-tailed t-test examining 3 mg/kg fenfluramine pre-treatment vs. saline vehicle found no significant difference in optical density in the DRN ($p = 0.065$, $n = 6$) (Figure 52).

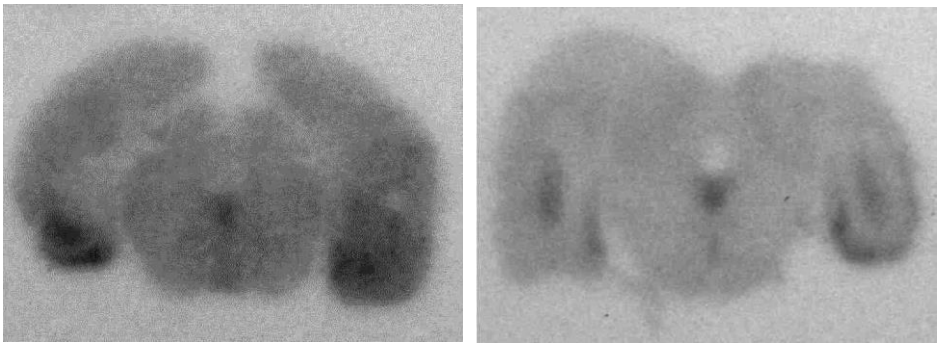

Figure 52: 4-[^{18}F]MPPF binding in the DRN; Left control, right fenfluramine (3 mg/kg) pre-treatment.

Effect of fenfluramine pre-treatment on the specific binding of 4-[^{18}F]MPPF in the PFC/ septal nucleus

Pre-treatment with fenfluramine (3 mg/kg) had no effect on the specific binding of 4-[^{18}F]MPPF in the PFC/ septal nucleus. The mean optical density for the PFC with fenfluramine pretreatment was 0.076 ±0.005 MBq/g and for control was 0.090 ± 0.01 MBq/g. A two-tailed t-test examining 3 mg/kg fenfluramine pre-treatment vs. saline vehicle found no significance difference in ligand binding in the PFC ($p = 0.146$, $n = 5$) (Figure 53).

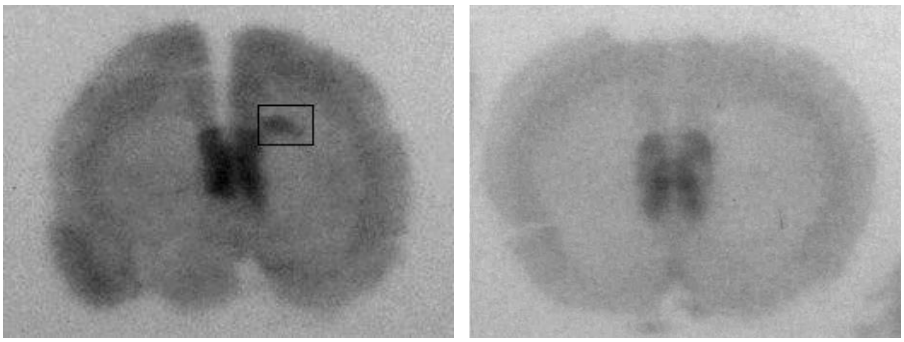

Figure 53: 4-[^{18}F]MPPF binding in the septal nucleus; Left control, right fenfluramine (3 mg/kg) pre-treatment. Artefact highlighted in a black square.

Effect of 4-[^{18}F]MPPF quantity injected and radio-purity on ligand kinetics (specific binding)

Pearson's correlation coefficients were calculated to determine any relationship between both the quantity (µmol/kg) and radio-purity (%) of 4-[^{18}F]MPPF injected and the specific binding (optical density (MBq/g)). 2-tailed bivariate correlation analysis was performed, with water and saline vehicles combined. 10mg/ kg 4-MPPF and 3 mg/kg fenfluramine pre-treatments were examined separately.

Correlation of quantity injected and specific binding

As shown in Table 21 there was no significant correlation between quantity of 4-[^{18}F]MPPF injected and the specific binding in any brain area, for any of the treatment groups.

	Hippocampus			DRN			PFC		
	Pearson correlation	p (2-tailed)	n	Pearson correlation	p (2-tailed)	n	Pearson correlation	p (2-tailed)	n
Vehicle	0.32	0.92	12	-0.091	0.80	11	-0.027	0.94	10
4-MPPF	-0.65	0.16	6	-0.36	0.56	5	-0.56	0.44	4
Fenfluramine	-0.53	0.29	6	-0.45	0.37	6	0.24	0.70	5

Table 21: Correlation between specific binding (optical density (MBq/g)) and quantity of 4-[^{18}F]MPPF injected (µmol/Kg). Data based on specific activity obtained from crude HPLC measurement.

Correlation of radio-purity and specific binding

As shown in Table 22 there was no significant correlation between radiopurity of the 4-[^{18}F]MPPF injected and the specific binding in the vehicle group (all brain areas). Whilst there did appear to be a significant correlation between radiopurity and specific binding in the 4-MPPF treatment group (PFC) there was an insufficient range to provide a reliable correlation, as both data points were almost the same value.

	Hippocampus			DRN			PFC		
	Pearson correlatio	p (2-tailed)	n	Pearson correlation	p (2-tailed)	n	Pearson correlation	p (2-tailed)	n
Vehicle	0.32	0.44	8	0.32	0.44	8	0.46	0.26	8
4-MPPF	0.20	0.82	4	-0.51	0.50	4	1*	-	2
Fenfluramine	**	**	**	**	**	**	**	**	**

*Table 22: Correlation between specific binding (optical density (MBq/g)) and radio-purity (%) of 4-[^{18}F]MPPF injected (µmol/Kg) * Insufficient range of data points to provide correlation (both data points almost same values).** Cannot be calculated as radio-purity was constant (100%) for all fenfluramine pre-treatment experiments.*

5.2.3 PET results

Uptake and distribution of 4-[^{18}F]MPPF in controls

4-[^{18}F]MPPF rapidly accumulated in the brain after i.v. injection, with the greatest uptake in the second minute. This was followed by fast washout, with a mean of 48.7% (range of 27.3 – 58.4%) of the maximum SUV remaining after 5 mins across all brain areas. The washout rate was fastest in the DRN, with all other brain areas having an approximately equal washout rate (Figure 54).

The maximum ratio of hippocampus/DRN/PFC:cerebellum SUV uptake occurred at 3 min; 1.7 for the hippocampus and DRN and 1.8 for the PFC. In agreement with previous PET studies using 4-[^{18}F]MPPF to study 5-HT $_{1A}$ receptor density in the rat brain, the uptake was lowest in the cerebellum and greatest in the 5-HT $_{1A}$ receptor rich areas; the hippocampus, DRN and PFC for all experiments (Udo De Haes et al., 2006, Kung et al., 1995, Sijbesma et al., 1991, Khawaja, 1995).

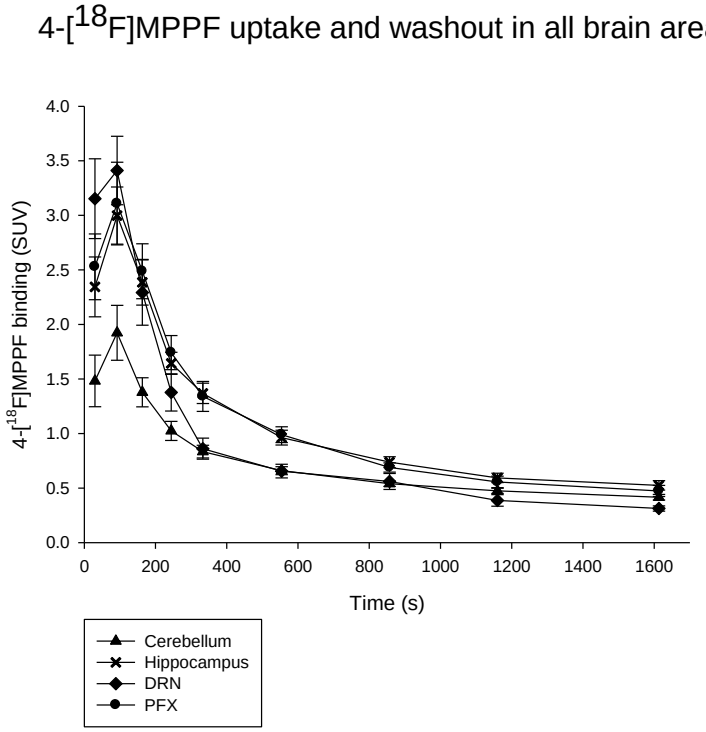

Figure 54: Mean 4-[^{18}F]MPPF uptake and washout in four brain regions; the cerebellum, hippocampus, DRN and PFC. Values are mean ±sem, n = 12.

PET image resolution (voxel/region of interest)

The mean number of voxels within the different regions of interest were as follows: cerebellum- 87.7 voxels (78 – 91 voxels)), hippocampus- 98.5 voxels (86 – 99 voxels), DRN- 2.5 voxels (1-5 voxels), PFC- 13.9 voxels (10-15 voxels)

Specific binding of 4-[^{18}F]MPPF in different brain regions

4-[^{18}F]MPPF binding in the cerebellum (non-specific binding)

Pre-treatment with cold 4-MPPF was used to reveal the non-specific binding of 4-[^{18}F]MPPF. 10 mg/kg 4-MPPF pre-treatment did not affect the binding of 4-[^{18}F]MPPF in the cerebellum, an area reported to be essentially devoid of 5-HT

$_{1A}$ receptors. Thus a two-way ANOVA, examining water vehicle vs. 10 mg/kg 4-MPPF pre-treatment, revealed a significant main effect of time (F 8, 80 = 27.4; p = < 0.001), but no significant time x pre-treatment interaction (F 8, 80 = 0.3; p = 0.973), and no significant effect of pre-treatment (F1,10 = 0.4; p = 0.521). These data indicate that there is minimal specific binding of 4-[^{18}F]MPPF in the cerebellum, and on the basis of these data 4-[^{18}F]MPPF binding (SUV) in the cerebellum was used as a measure of non-specific binding in the brain (Figure 55).

Effect of cold 4-MPPF (10 mg/kg) pre-treatment on 4-[^{18}F]MPPF binding in the cerebellum

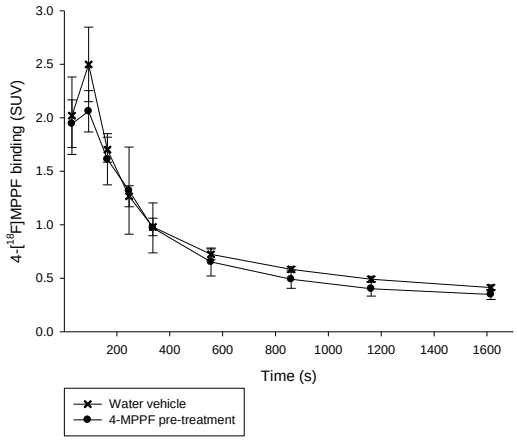

Figure 55: Mean 4-[^{18}F]MPPF uptake and washout in the cerebellum; effect of cold 4-MPPF (10 mg/kg) pre-treatment. Values are mean ±sem, n = 5 (water) and n = 7 (4-MPPF).

4-[^{18}F]MPPF binding in the hippocampus

4-[^{18}F]MPPF accumulated rapidly in the hippocampus within the first minute followed by a fast washout, nearing equilibrium within 10 minutes. 4-MPPF pre-treatment decreased the specific binding of 4-[^{18}F]MPPF in the hippocampus by 83.4% at 5 min. Thus, a two-way ANOVA, examining the effect of 10 mg/kg 4-MPPF pre-treatment revealed a significant main effect of time (F 8, 80 = 3.9; p = 0.001), a significant time x pre-treatment interaction (F 8, 80 = 6.1; p = < 0.001), and a significant effect of pre-treatment (F1,10 = 15.6; p = 0.003). A post-hoc t-

test revealed a significant effect of 4-MPPF pre-treatment at time points between t = 3 – 30 min (p = 0.002 – 0.038) (Figure 56).

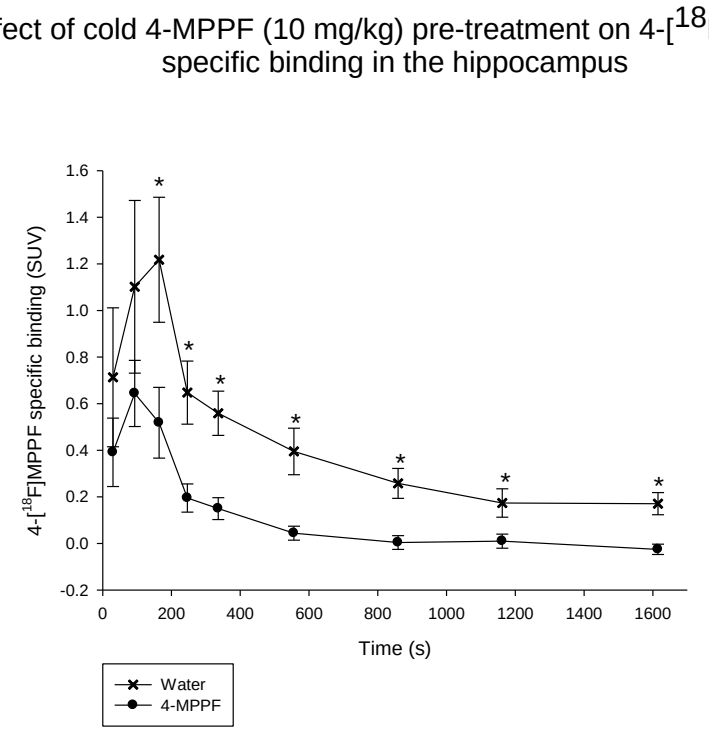

*Figure 56: Mean 4-[^{18}F]MPPF specific binding in the hippocampus; effect of cold 4-MPPF (10 mg/kg) pre-treatment. Values are mean ±sem, n = 5 (water) and n = 7 (4-MPPF). * p < 0.05 (post-hoc t-test.).*

4-[^{18}F]MPPF binding in the DRN

4-[^{18}F]MPPF accumulated rapidly in the DRN within the first minute followed by a fast washout, nearing equilibrium within 5 minutes. 4-MPPF pre-treatment increased the specific binding of 4-[^{18}F]MPPF in the DRN by 300% at 5 min. However, a two-way ANOVA, examining 10 mg/kg 4-MPPF pre-treatment *vs*. water vehicle, revealed a significant main effect of time (F 8, 80 = 5.4; p = < 0.001), but no significant effect of time x pre-treatment (F 8, 80 = 4.7; p =

0.875), and no significant effect of pre-treatment (F1,10 = 0.1; p = 0.263) (Figure 57).

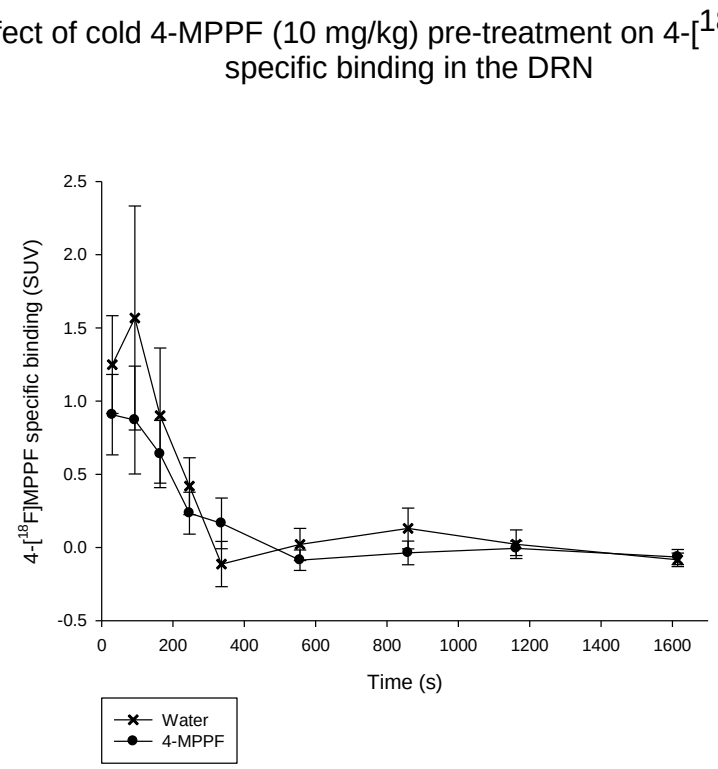

Figure 57: Mean 4-[^{18}F]MPPF specific binding in the DRN; effect of cold 4-MPPF (10 mg/kg) pre-treatment. Values are mean ±sem, n = 5 (water) and n = 7 (4-MPPF).

4-[^{18}F]MPPF binding in the PFC

4-[^{18}F]MPPF accumulated rapidly in the PFC within the first minute followed by a fast washout, nearing equilibrium within 10 minutes. 4-MPPF pre-treatment decreased the specific binding of 4-[^{18}F]MPPF in the PFC by 71.4% at 5 min. Thus, A two-way ANOVA, examining 10 mg/kg 4-MPPF pre-treatment *vs*. water vehicle, revealed a significant main effect of time (F 8, 80 = 4.0; p = 0.001), a significant time x pre-treatment interaction (F 8, 80 = 5.1; p = < 0.001), and a significant effect of pre-treatment (F1,10 = 7.0; p = 0.024). A post-hoc t-test

revealed a significant difference of 4-MPPF pre-treatment at time points between t = 6 – 30 min (p = 0.01 – 0.02) (Figure 58).

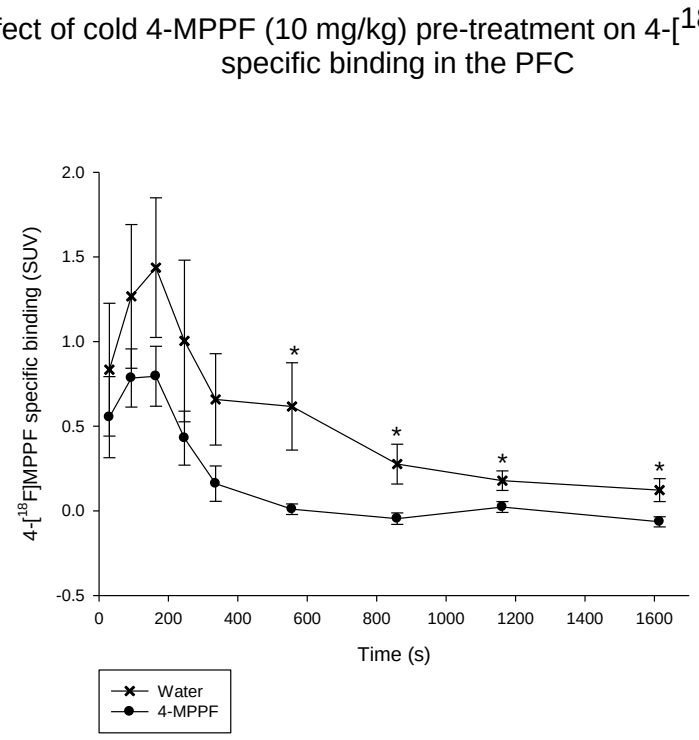

*Figure 58: Mean 4-[^{18}F]MPPF specific binding in the PFC; effect of cold 4-MPPF (10 mg/kg) pre-treatment. Values are mean ±sem, n = 5 (water) and n = 7 (4-MPPF). * p < 0.05 (post-hoc t-test.).*

Effects of endogenous 5-HT release on 4-[^{18}F]MPPF binding

Here pre-treatment with the 5-HT releasing agent fenfluramine was used to examine the effect of raised levels of endogenous 5-HT on 4-[^{18}F]MPPF specific binding in different brain areas.

Effect of fenfluramine pre-treatment on the binding of 4-[^{18}F]MPPF in the hippocampus

Pre-treatment with fenfluramine (3 mg/kg) had no effect on the specific binding of 4-[^{18}F]MPPF in the hippocampus. Thus, a two-way ANOVA, examining effects of 3 mg/kg fenfluramine pre-treatment *vs*. saline vehicle, revealed a significant main effect of time (F 8, 80 = 5.1; p = < 0.001), but no significant time x fenfluramine interaction (F 8, 80 = 0.7; p = 0.658), and no significant effect of fenfluramine (F1,10 = 0.1; p = 0.741) (Figure 59).

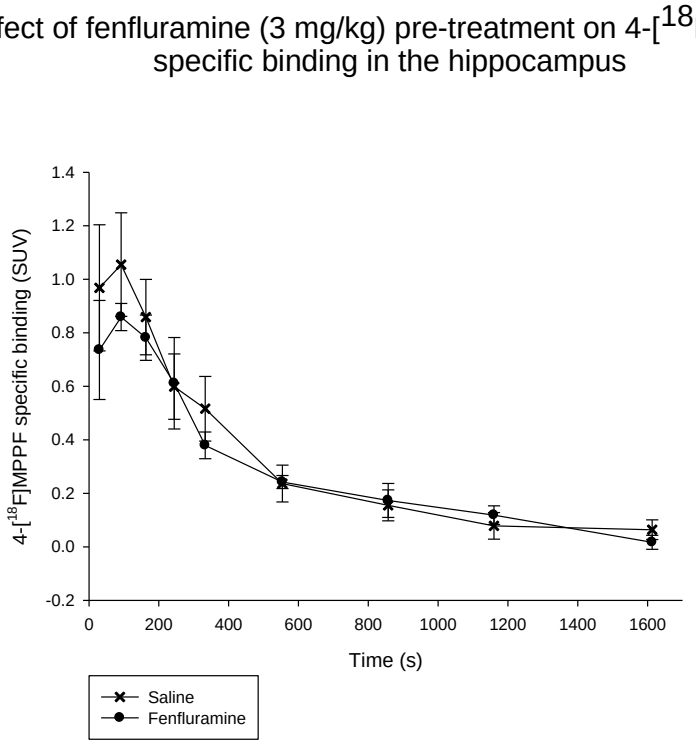

Figure 59: Mean 4-[^{18}F]MPPF specific binding in the hippocampus; effect of fenfluramine (3 mg/kg) pre-treatment. Values are mean ±sem, n = 7 (saline) and n = 5 (fenfluramine).

Effect of fenfluramine pre-treatment on the binding of 4-[^{18}F]MPPF in the DRN.

Pre-treatment with fenfluramine (3 mg/kg) had no effect on the specific binding of 4-[^{18}F]MPPF in the DRN. Thus, a two-way ANOVA, examining 3 mg/kg fenfluramine pre-treatment *vs*. saline vehicle, revealed a significant main effect of time ($F_{8, 80} = 12.1$; $p = < 0.001$), but no significant time x fenfluramine interaction ($F_{8, 80} = 1.3$; $p = 0.246$) and no significant effect of fenfluramine ($F_{1,10} = 0.2$; $p = 0.653$) (Figure 60).

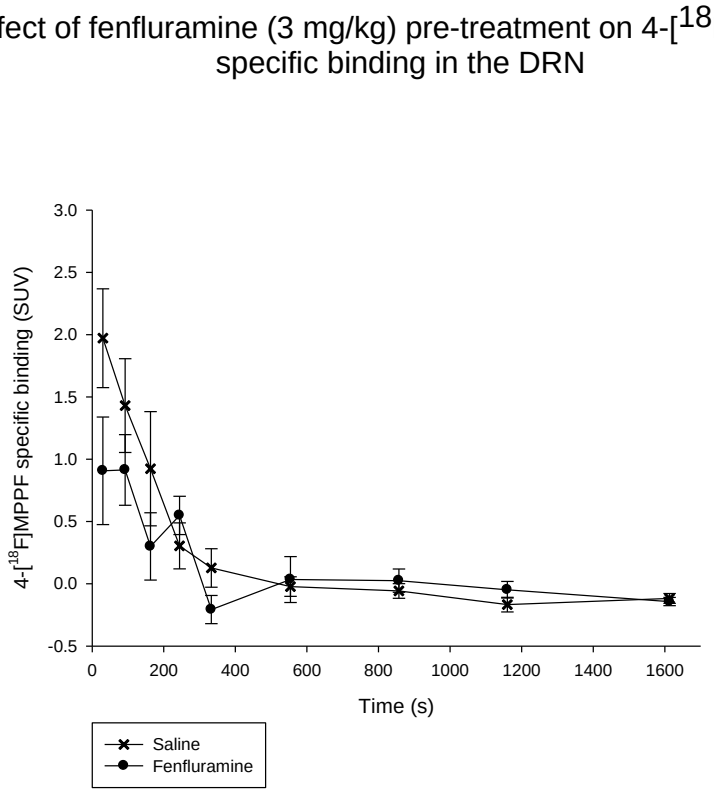

Figure 60: Mean 4-[^{18}F]MPPF specific binding in the DRN; effect of fenfluramine (3 mg/kg) pre-treatment. Values are mean ±sem, n = 7 (saline) and n = 5 (fenfluramine).

Effect of fenfluramine pre-treatment on the binding of 4-[^{18}F]MPPF in the PFC

Pre-treatment with fenfluramine (3 mg/kg) had no effect on the specific binding of 4-[^{18}F]MPPF in the PFC. Thus, a two-way ANOVA, examining 3 mg/kg fenfluramine pre-treatment *vs*. saline vehicle, revealed a significant main effect of time ($F_{8, 80} = 3.4$; $p = 0.002$), but no significant time x fenfluramine interaction ($F_{8, 80} = 0.3$; $p = 0.952$), and no significant effect of fenfluramine ($F_{1,10} = 0.5$; $p = 0.486$) (Figure 61).

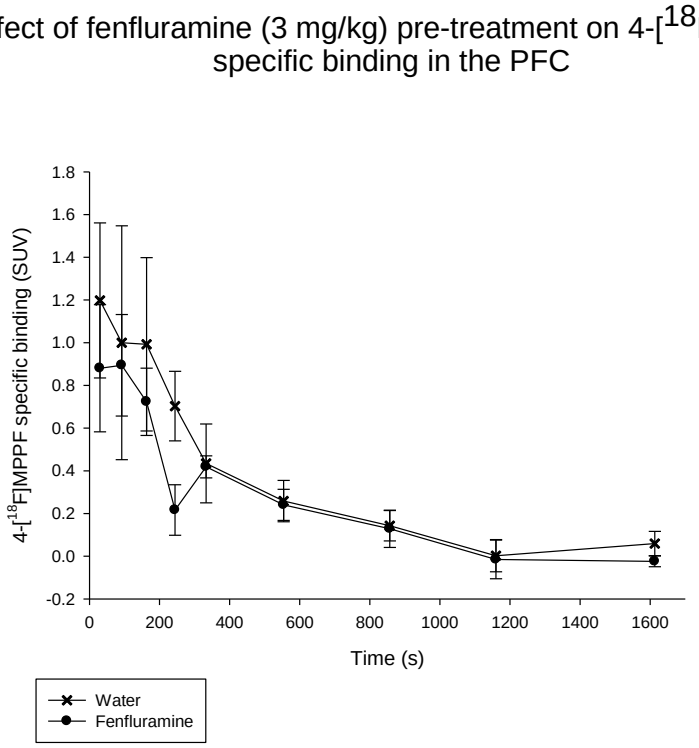

Figure 61: Mean 4-[^{18}F]MPPF specific binding in the PFC; effect of fenfluramine (3 mg/kg) pre-treatment. Values are mean ±sem, n = 7 (saline) and n = 5 (fenfluramine).

Effect of 4-[^{18}F]MPPF quantity injected and radio-purity on ligand kinetics (specific binding and washout)

Pearson's correlation coefficients were calculated to determine any relationship between both the quantity (µmol/kg) and radio-purity (%) of 4-[^{18}F]MPPF injected and the maximum specific binding (SUV) and washout in each brain area.

Correlation of quantity injected and maximum specific binding

As shown in Table 23 there was no significant correlation between quantity of 4-[^{18}F]MPPF injected and the maximal specific binding in any brain area, for any of the treatment groups.

	Hippocampus			DRN			PFC		
	Pearson correlati	p (2-tailed)	n	Pearson correlation	p (2-tailed))	n	Pearson correlation	p (2-tailed)	n
Vehicle	-0.263	0.410	12	-0.021	0.949	12	-0.303	0.338	12
4-MPPF	-0.389	0.388	7	-0.391	0.386	7	-0.274	0.552	7
Fenfluramine	0.790	0.112	5	-0.714	0.176	5	0.817	0.091	5

Table 23: Correlation between maximum specific binding (SUV) and quantity of 4-[^{18}F]MPPF injected (µmol/Kg). Data based on specific activity obtained from crude HPLC measurement.

Correlation of radiopurity and maximum specific binding

As shown in Table 24 there was no significant correlation between radiopurity of the 4-[^{18}F]MPPF injected and the maximal specific binding in the vehicle group (all brain areas). Whilst there did appear to be a significant correlation between radiopurity and maximal specific binding in fenfluramine treatment group (hippocampus and PFC), all data points had a radio-purity of 100% except for one, which was 93.1%. As only one data point differed it may have resulted in a skewed significance.

	Hippocampus			DRN			PFC		
	Pearson correlati	p (2-tailed)	n	Pearson correlati	p (2-tailed)	n	Pearson correlation	p (2-tailed)	**n**
Vehicle	0.129	0.761	8	-0.245	0.559	8	0.080	0.851	8
4-MPPF	**	**	**	**	**	**	**	**	**
Fenfluramine	**-0.959**	**0.010**	**5**	0.421	0.480	5	**-0.932**	**0.021**	**5**

*Table 24: Correlation between maximum specific binding (SUV) and radio-purity (%) of 4-[^{18}F]MPPF injected (µmol/Kg). ** insufficient data for analysis.*

Correlation of quantity injected on washout

As shown in Table 25 there was no significant correlation between quantity of 4-[^{18}F]MPPF injected and the washout rate in any brain area, for any of the treatment groups.

	Hippocampus			DRN			PFC		
	Pearson correlation	p (2-tailed)	n	Pearson correlation	p (2-tailed)	n	Pearson correlation	p (2-tailed)	n
Vehicle	0.042	0.897	12	0.021	0.949	12	-0.104	0.749	12
4-MPPF	-0.336	0.461	7	-0.210	0.651	7	0.119	0.8	7
Fenfluramine	0.614	0.271	5	-0.721	0.169	5	0.727	0.164	5

Table 25: Correlation between brain area ligand washout (SUV) and 4-[^{18}F]MPPF injected (µmol/Kg). Data based on specific activity obtained from crude HPLC measurement

Correlation of radiopurity on washout

As shown in Table 26 there was no significant correlation between radiopurity of the 4-[^{18}F]MPPF injected and the washout rate in the vehicle group (all brain areas). Whilst there did appear to be a significant correlation between radiopurity and washout rate in fenfluramine treatment group (hippocampus and PFC), all data points had a radiopurity of 100% except for one, which was 93.1%. As only one data point differed it may have resulted in a skewed significance.

	Hippocampus			DRN			PFC		
	Pearson correlation	p (2-tailed)	n	Pearson correlation	p (2-tailed)	n	Pearson correlation	p (2-tailed)	n
Vehicle	-0.256	0.541	8	-0.307	0.459	8	-0.136	0.748	8
4-MPPF	**	**	**	**	**	**	**	**	**
Fenfluramine	**-0.910**	**0.032**	**5**	0.624	0.261	5	**-0.939**	**0.018**	**5**

*Table 26: Correlation between ligand washout (SUV) and radio-purity (%) of 4-[^{18}F]MPPF injected (µmol/Kg). ** insufficient data for analysis.*

5.3 Discussion

4-[^{13}H]MPPF in vitro autoradiography

Brain distribution of 4-[^{3}H]MPPF

The brain distribution of 4-[^{3}H]MPPF binding was similar to areas shown to be high in 5-HT $_{1A}$ receptor sites in studies labelling with the selective 5-HT $_{1A}$ receptor agonist (±)-8-OH-DPAT and selective antagonist WAY100635 (Sijbesma et al., 1991, Khawaja, 1995, Plenevaux et al., 2000). The distribution is also in agreement with previous studies examining the autoradiographic profile of 4-[^{18}F]MPPF (Plenevaux et al., 2000, Moulin-Sallanon et al., 2009, Riad et al., 2004, Udo de Haes, 2005, Zimmer et al., 2002b, Desbree et al., 2008). The cerebellum showed a very low level of labelling in agreement with that seen in tissue incubated in the presence of 10µM (±)-8-OH-DPAT or WAY100635 (Kung et al., 1995, Riad et al., 2004, Duncan and Hensler, 2002) which is generally taken to indicate non-specific binding in the literature.

Effect of (±)-8-OH-DPAT on the binding of 4-[^{3}H]MPPF in different brain areas

This study found 0.07 nM (±)-8-OH-DPAT had negligible effect on the binding of 4-[^{3}H]MPPF, with only the PFC showing a reduction in binding to 92.1% vs. control. It had been intended to use this as a measure of non-specific binding, as (±)-8-OH-DPAT is a 5-HT $_{1A}$ receptor agonist and therefore competes with 4-MPPF binding at the 5-HT $_{1A}$ receptor. However, to obtain a measure of non-specific binding the 4-[^{3}H]MPPF must be fully displaced. However, it appears a

concentration of 0.07 nM is not sufficient to fully displace 4-[^{3}H]MPPF. Other studies have used 10 µM (±)-8-OH-DPAT or WAY100635-HT to fully displace 4-[^{18}F]MPPF (Duncan and Hensler, 2002, Kung et al., 1995, Riad et al., 2004) which appears to be a more suitable concentration.

Effect of 5-HT on specific binding of 4-[^{3}H]MPPF in different brain regions

In chapter 4 the microdialysis study found that fenfluramine (3 mg/kg) administration increased the hippocampal 5-HT concentration to 1 x 10^{-8} M. Therefore, it is of interest to examine the reduction in binding of 4-[^{3}H]MPPF *in vitro* to assess the impact of 1 x 10^{-8} M 5-HT on specific binding, as this will be the predicted hippocampal 5-HT concentration in the PET and *ex vivo* autoradiography studies in this thesis.

In this study 4-[^{3}H]MPPF specific binding was reduced to 78.3 – 85.4% of control in the hippocampus, DRN and PFC when incubated with 5-HT at a concentration of 2 x 10^{-8} M. This is in conflict with one report, examining 4-[^{125}I]MPPF in the rat hippocampus, which reports a reduction in binding to 25% control at this 5-HT concentration (Kung et al., 1995).

In this study a significant reduction in binding was found when 4-[^{3}H]MPPF was incubated with the higher concentration of 5-HT of 2 x 10^{-6} M in the DRN and PFC. Binding was reduced to 11.5% control for the PFC, 17.9% for the DRN but only 32.1% for the hippocampus. Other studies have reported binding reduced to 10% or 60% control in the hippocampus at the same 5-HT concentration (Kung et al., 1995, Moulin-Sallanon et al., 2009). Therefore it appears there is considerable variability in the reports. In fact our present study adds to the variability.

Displacement curves, as those shown in Figures 43 – 45, should fit a sigmoidal curve with a slope of 1 if binding to only one site. However, insufficient data at the high 5-HT concentrations precluded the fitting of such a curve to the present data, so evidence of the number of binding sites could not be shown.

0.14 and 1.4 nM 4-[^{3}H]MPPF autoradiography

In contrast to the 10nM concentration, it was found that 0.14 nM and 1.4 nM concentrations of 4-[^{3}H]MPPF gave a very weak signal compared to the background optical density of the autoradiographic film. Due to this, a high signal to noise ratio was observed. In addition, the scale of the calibration curves was above the range required to calibrate the low optical density values from these experiments resulting in many of the calibrated measurements having negative activities.

One study examining the autoradiographic profile of 4-[^{3}H]MPPF in the rat hippocampus and PFC used a concentration of 2 nM 4-[^{3}H]MPPF (Landry and Di Paolo, 2003) and found this to provide adequate images. This study used the same autoradiographic film and had a similar ligand specific activity (66.2 Ci/µmol vs. 75 Ci/µmol in this study), and used a shorter exposure time than this study (6 weeks vs.3 months used in this study).

4-[^{18}F]MPPF ex vivo autoradiography

Brain distribution of 4-[^{18}F]MPPF

As with the 4-[^{3}H]MPPF binding, the brain distribution of 4-[^{18}F]MPPF binding was similar to areas shown to be high in 5-HT $_{1A}$ receptor sites in studies labelling with the selective 5-HT $_{1A}$ receptor agonist (±)-8-OH-DPAT and selective antagonist WAY100635 (Sijbesma et al., 1991, Khawaja, 1995, Plenevaux et al., 2000). The distribution is also in agreement with previous studies examining the autoradiographic profile of 4-[^{18}F]MPPF (Plenevaux et al., 2000, Moulin-Sallanon et al., 2009, Riad et al., 2004, Udo de Haes, 2005, Zimmer et al., 2002b, Desbree et al., 2008). The cerebellum showed a very low level of labelling in agreement with that seen in tissue incubated in the presence of 10µM (±)-8-OH-DPAT or WAY100635 (Kung et al., 1995, Riad et al., 2004, Duncan and Hensler, 2002) which is generally taken to indicate non-specific binding in the literature.

Specific binding of 4-[^{18}F]MPPF in different brain regions

In this study a pre-treatment with cold 4-MPPF was used to block the binding of 4-[^{18}F]MPPF with a view to differentiating regions of specific and non-specific binding. The specific binding of 4-[^{18}F]MPPF was examined in four brain regions, three 5-HT $_{1A}$ receptor rich areas; hippocampus, DRN and PFC, and one where 5-HT $_{1A}$ receptors are sparse; the cerebellum.

Pre-treatment with 4-MPPF did not affect the binding in the cerebellum, suggesting there was no specific binding of 4-[^{18}F]MPPF in this region. This conclusion supports the use of the cerebellum as a region of non-specific binding in this study, which is in line with the protocol used in previous 4-[^{18}F]MPPF *ex vivo* autoradiographic studies (Moulin-Sallanon et al., 2009, Udo de Haes, 2005).

In this study, 4-MPPF (10 mg/kg) pre-treatment had no significant effect on the specific binding 4-[^{18}F]MPPF in the hippocampus ($p = 0.17$). However there was a possible effect seen in the DRN ($p = 0.059$) and the specific binding was significantly reduced in the PFC ($p = 0.041$). This suggests 4-[^{18}F]MPPF was specifically bound in the PFC and strongly indicates this was also the case in the DRN. Unexpectedly no effect was seen in the hippocampus.

Using a YAP-(S)PET scanner, a scanner which combines the PET and SPECT techniques (YAP-(S)PET), one study demonstrated that a dose of 0.5 mg/kg 4-MPPF caused complete displacement of 4-[^{18}F]MPPF in the hippocampus, raphe nucleus and frontal cortex of the rat (Millet et al., 2008), suggesting the dose used in this study (10 mg/kg) is sufficient to cause complete displacement of 4-[^{18}F]MPPF. The present findings are in agreement with the reported study when considering the PFC and are strongly suggestive that this is also the case in the DRN. However this is not the case in the hippocampus in this study. This may be due to experimental error resulting from intra-hippocampal differences in 5-HT $_{1A}$ receptor density. Sub-regions of the hippocampus do have differences in 5-HT $_{1A}$ receptor density whilst the DRN and the PFC appear to have a more homogenous distribution of 5-HT $_{1A}$ receptors. Given only three

random samples were examined from each area, the large variance in the hippocampal measurements may explain the lack of statistical significance.

Effects of endogenous 5-HT release on 4-[^{18}F]MPPF binding in the Hippocampus, DRN and PFC

This study found pre-treatment with the 5-HT releasing agent fenfluramine (3 mg/kg) did not have a significant effect on the binding of 4- [^{18}F]MPPF in any brain region. This is in conflict with one study examining the effect of fenfluramine (10 mg/kg) on 4-[^{18}F]MPPF using *ex vivo* autoradiography, which found a significant reduction in binding in the frontal cortex, hippocampus and DRN of the rat in the fenfluramine treated group (Udo de Haes, 2005). The difference could be explained by the higher dose of fenfluramine used in the study. Two further studies examined the effect of fluoxetine (2 or 10 mg/kg) (Plenevaux et al., 2000, Riad et al., 2004) on 4-[^{18}F]MPPF binding in the rat brain. In agreement with this study no significant effect on binding was observed in the hippocampus, DRN or frontal cortex. Other studies have examined the effects of citalopram (0.5 mg/kg) or combined citalopram/ketanserin (10 µmol/kg / 100 nmol/kg) using *ex vivo* autoradiography in the rat brain (Moulin-Sallanon et al., 2009, Udo de Haes, 2005). Significant decrease in binding was only found in one study in the DRN after citalopram/ketanserin (10 µmol/kg / 100 nmol/kg) treatment (Udo de Haes, 2005). However it is difficult to interpret the results of some of these earlier studies as it is unclear what the consequences of acute SSRI's were on extracellular 5-HT levels, and furthermore any changes in extracellular 5-HT were not quantified.

Effect of 4-[^{18}F]MPPF quantity injected and radio-purity on ligand kinetics (specific binding and washout)

This study found no correlation between the maximum specific binding or washout of 4-[^{18}F]MPPF and the quantity administered or radiopurity. This will be further discussed and compared to the PET results in the PET discussion

PET imaging

Uptake kinetics and brain distribution of 4-[^{18}F]MPPF in the rat (controls)

In accordance with the literature, uptake of 4-[^{18}F]MPPF (in control groups) was highest in the 5-HT $_{1A}$ receptor rich areas of the hippocampus, DRN and PFC and lowest in the 5-HT $_{1A}$ receptor poor cerebellum (Sijbesma et al., 1991, Khawaja, 1995, Passchier et al., 2000, Plenevaux et al., 2000, Aznavour and Zimmer, 2007).

Whilst the literature to date reports that uptake is highest in areas known to be rich in 5-HT $_{1A}$ receptors, it also reports that washout is slowest in these areas (Bars et al., 1998, Shiue et al., 1997, Aznavour and Zimmer, 2007, Plenevaux et al., 2000, Kung et al., 1996b, Passchier et al., 2000, Sijbesma et al., 1991, Khawaja, 1995, Millet et al., 2008). However, in contrast to published data, in this study we found that the washout rate was fastest in the DRN, an area rich in 5-HT $_{1A}$ receptors, and the hippocampus, PFC and cerebellum had approximately equal washout rates.

Previous *in vivo* PET and β-microprobe studies have demonstrated a rapid initial uptake of [^{18}F]4-MPPF in the rat brain within the first 10 – 15 minutes, with the maximum uptake (hippocampal to cerebellum ratio) occurring at around 20 - 30 mins, followed by a fast washout up to around 60 - 70 min (Plenevaux et al., 2000, Shiue et al., 1997, Zimmer et al., 2003, Wu et al., 2004) with one study showing only 0.03% activity remaining at 60 min (Shiue et al., 1997). However other studies using a β-microprobe have shown activity remaining up to 3 hours post injection (Zimmer et al., 2002a, Zimmer et al., 2002b).
In the present study it was found the washout rate of 4-[^{18}F]MPPF was considerably faster than reported in the literature, with maximum hippocampus/DRN/PFC:cerebellum ratio occurring at 3 minutes, in contrast with 20 minutes in the literature (Shiue et al., 1997, Plenevaux et al., 2000, Zimmer et al., 2003, Wu et al., 2004). In addition, a cerebellum to brain area ratio of 1.7 – 1.8 was obtained in these experiments, in contrast with 5.6 at 30 minutes in one study (Shiue et al., 1997). This could indicate there was less specific binding in our experiments compared to the literature. This would be consistent

with the lower specific activity used, being between 0.1 – 17.8 GBq/µmol in comparison to between 30 – 185 GBq/µmol in the literature, as specific activity has an effect on radioligand specific binding and washout profiles (Bars et al., 1998, Aznavour, 2009, Bartmann et al., 2010, Moulin-Sallanon et al., 2009).

In the present study, in order to increase the uptake and reduce the washout time of the 4-[^{18}F]MPPF, animals were pre-treated with cyclosporine (50 mg/kg). Cyclosporine (50 mg/kg) pre-treatment has been shown increase in 4-[^{18}F]MPPF uptake by 200 -1000% (Passchier et al., 2000, Elsinga et al., 2005 , Laćan et al., 2008). In addition cyclosporine has been shown not to have an effect on the brain distribution of 4-[^{18}F]MPPF, correlating to the binding of methoxy-[^{3}H]WAY100635 (Passchier et al., 2000). Therefore, cyclosporine pre-treatment should provide the positive effect of slowing the washout time, without affecting actual 4-[^{18}F]MPPF binding.

Specific binding of 4-[^{18}F]MPPF in different brain regions

In this study pre-treatment with cold 4-MPPF was used to block the binding of 4-[^{18}F]MPPF with a view to identifying regions of specific binding. A dose of 10 mg/kg was chosen in line with previous studies (Thielen and Frazer, 1995, Thielen, 1996). In a later YAP-(S)PET study it was shown a dose of 0.5 mg/kg 4-MPPF caused complete displacement of 4-[^{18}F]MPPF in the hippocampus, raphe and frontal cortex of the rat (Millet et al., 2008), confirming that the dose used in this study is sufficient to cause complete displacement.

The specific binding of 4-[^{18}F]MPPF was examined in four brain regions, three 5-HT $_{1A}$ receptor rich areas; hippocampus, DRN and PFC, and one where 5-HT $_{1A}$ receptors are sparse; the cerebellum.

Pre-treatment with 4-MPPF did not affect the binding in the cerebellum, suggesting there was no specific binding of 4-[^{18}F]MPPF in this region. This conclusion supports the use of the cerebellum as a region of non-specific binding in this study, which is in line with the protocol in previous 4-[^{18}F]MPPF PET studies (Aznavour et al., 2006, Udo De Haes et al., 2006, Ginovart et al., 2000).

In this study, the binding of 4-[^{18}F]MPPF was significantly reduced in the hippocampus and PFC with a pre-treatment of 4-MPPF. This suggests 4-[^{18}F]MPPF was specifically bound in these areas.

However, in this study pre-treatment with 4-MPPF did not significantly affect the binding of 4-[^{18}F]MPPF in the DRN. This is in conflict with the literature which reports a significant decrease in binding using a lower dose of 1 mg /kg 4-MPPF post treatment (Zimmer et al., 2002b) and a total displacement using 0.5 mg/kg post treatment in the raphe of the rat (Millet et al., 2008).

However there are issues related to the spatial resolution for the Phillips Mosaic PET scanner which is reported to be between 1.9 – 2.7 mm (FWHM) (Surti et al., 2005, Huisman et al., 2007, Yao et al., 2012). The hippocampus, cerebellum and PFC are relatively large brain areas, so the volume of interest for each area contained a sufficient number of voxels to assume it was above the level of the scanner resolution. However, the DRN is a comparatively small brain area, (2 mm anterior – posterior, 1 – 2.6 mm medo-lateral, 1 – 5.1 mm dorsal – ventral) with the VOI containing a mean of 2.5 voxels (1- 5 voxels). Although it is difficult to make a general comment on the impact of the size of the VOI with regards to the PET scanner spatial resolution, especially as the shape of the VOI and the number of voxels it contains will change for each image due to the co-registration process, it can be assumed that a VOI containing only a few voxels will be near the limit of the detector resolution. This fact, coupled with the low sample numbers (n = 5 – 7), it can be concluded that the SUV data from the DRN will be less accurate than those from the larger brain areas. Therefore, the inconsistency in this study could be explained by the small size of the DRN and subsequent potential for variability in the results.

Effects of endogenous 5-HT release on 4-[^{18}F]MPPF binding in the **hippocampus, DRN and PFC**

The classic receptor occupancy model suggests a correlation between the levels of endogenous neurotransmitters and the amount of *in vivo* binding of competing radiolabelled ligands (Aznavour and Zimmer, 2007). In the case of 4-[^{18}F]MPPF an increase of endogenous 5-HT could therefore compete for

binding sites at the 5-HT $_{1A}$ receptor resulting in reduced binding of 4-[^{18}F]MPPF. Inversely a reduction in endogenous 5-HT could leave more binding sites free for 4- [^{18}F]MPPF therefore increasing its overall binding. Drug challenges have been used in many studies to examine the relationship between endogenous 5-HT levels and 4-[^{18}F]MPPF binding in the brain, but there are inconsistencies in the reported characteristics of 4-[^{18}F]MPPF in the presence of a drug induced increase of endogenous 5-HT . Some studies report 4-[^{18}F]MPPF binding is reduced by an increased level of 5-HT , indicating it is displaceable by 5-HT and consistent with the occupancy model (Aznavour et al., 2006, Rbah et al., 2003, Riad et al., 2004, Zimmer et al., 2002b, Zimmer et al., 2002a, Zimmer et al., 2003). However, other studies report no such change in binding during the drug challenge (Aznavour et al., 2006, Ginovart et al., 2000, Moulin-Sallanon et al., 2009, Riad et al., 2004, Riad, 2008, Udo De Haes et al., 2006).

The present study found pre-treatment with the 5-HT releasing agent fenfluramine (3 mg/kg) did not have a significant effect on the binding of 4-[^{18}F]MPPF in any brain region. As the microdialysis study performed in chapter 3 revealed the 5-HT concentration at the time of 4-[^{18}F]MPPF injection would be 1 x 10^{-8} M, the PET result would suggest 4- [^{18}F]MPPF is not displaceable by 1 x 10^{-8} M endogenous 5-HT. This is consistent with the *in vitro* 4-[^{3}H]MPPF study performed in this chapter, which showed no significant reduction in binding in any brain area when incubated with 2 x 10^{-8} M 5-HT . However in the *in vitro* study, 2 x 10^{-6} M 5-HT caused significant displacement in all brain areas. Therefore it would be of interest to repeat our PET study at a higher dose of fenfluramine which replicated an endogenous 5-HT concentration of 2 x 10^{-6} M or above, to assess whether this would displace 4- [^{18}F]MPPF *in vivo*.

However, one issue that needs to be raised is that part of the aim of the present study was not only to use a characterised (w.r.t. 5-HT release) dose of fenfluramine, but also attempt to use the dose of fenfluramine that could be translated in human studies. Whilst it is not easy to compare rodent and human doses, the fenfluramine dose used here (3 mg/kg) was still double that of the maximum daily dose of 1.7 mg /kg of fenfluramine used in published human studies (Lewis et al., 1971). Therefore increasing to higher dosages in this pre-clinical studies may not represent conditions possible for clinical studies.

In conflict with the present study, five PET or β microprobe studies have reported significantly decreased 4-[^{18}F]MPPF binding in the hippocampus, DRN or frontal cortex of the rat (Rbah et al., 2003, Riad et al., 2004, Zimmer et al., 2002b, Zimmer et al., 2002a, Zimmer et al., 2003), and in the cat (Aznavour et al., 2006) with pharmacologically induced increased endogenous 5-HT . Furthermore, one has shown significantly increased binding in the hippocampus of the rat with decreased 5-HT. These results suggest 4-[^{18}F]MPPF is sensitive and to changes in endogenous 5-HT and displaceable. In contrast, six studies performed in monkey, cat and rat have not shown any effect of increased endogenous 5-HT on the binding of 4-[^{18}F]MPPF in the same areas (Aznavour et al., 2006, Ginovart et al., 2000, Moulin-Sallanon et al., 2009, Riad et al., 2004, Riad, 2008, Udo De Haes et al., 2006).

The different reports can possibly be explained by several factors which are not consistent between the experimental protocols.

Firstly there are variable reports as to the concentration of endogenous 5-HT examined in the displacement experiments. In this study a pre-treatment of fenfluramine (3 mg/kg) (in combination with cyclosporine) was found by microdialysis study in chapter 3 to produce a maximum 400% increase in endogenous 5-HT in the hippocampus. As the PET protocol was under the same conditions as the microdialysis experiment, it can be predicted that the endogenous 5-HT in the hippocampus of the rat at the time of 4-[^{18}F]MPPF administration was at this maximum value of 1 x 10^{-8} M. However other studies have used doses of fenfuramine ranging from 1-10 mg/kg in a range of different species (e.g cat, monkey, rat) and using different time courses.

There is also the state of the 5-HT $_{1A}$ receptor to take into consideration, which can exist in a high or low affinity state (Gozlan et al., 1995, Khawaja, 1995, Nenonene et al., 1994, Udo De Haes et al., 2006, Watson et al., 2000). Receptor antagonists, such as 4-[^{18}F]MPPF bind equally to both affinity states, whereas agonists, such as 5-HT , will bind preferentially to the high affinity state (Gozlan et al., 1995, Khawaja, 1995, Nenonene et al., 1994, Udo De Haes et al., 2006, Watson et al., 2000). Therefore it is possible that changes in 5-HT will only effect the 4-[^{18}F]MPPF that is bound to high affinity state receptors. If

the proportion of high to low affinity state 5-HT $_{1A}$ receptors is different between studies this could affect the resultant binding profiles.
Lastly the brain area examined differs between studies and it could be concluded that binding characteristics for a particular PET ligand will not be consistent in different areas (Udo De Haes et al., 2006).
In this thesis the experimental protocol was designed such that variables such as anaesthesia, 4-[^{18}F]MPPF administration vs. max 5-HT concentrations, brain areas examined and animal type were all kept constant. It is clear that any future PET studies with 4-[^{18}F]MPPF will need to take into account the many variables discussed above and design the experimental protocol to minimise such differences.

Clinical studies

4-[^{18}F]MPPF has been used in a number of clinical PET studies. The binding, distribution and test to test variability have been characterised in several studies and found to be suitable for clinical PET studies of the 5-HT system (Costes et al., 2005, Costes, 2007, Passchier, 2000, Sanabria-Bohórquez et al., 2002). In addition 4-[^{18}F]MPPF has been examined in variety of CNS diseases and disorders including; temporal lobe epilepsy, depression, narcolepsy, Alzheimer's, dementia, anorexia nervosa, migraine, Parkinsons and schizophrenia (Ballanger et al., 2012, Demarquay et al., 2011, Derry et al., 2006, Didelot et al., 2008, Galusca et al., 2008, Kepe et al., 2006, Lerond et al., 2013, Lothe et al., 2008a, Lothe et al., 2008b, Lothe et al., 2012, Merlet et al., 2004, Merlet, 2004, Truchot et al., 2008, Truchot et al., 2007). In addition 4-[^{18}F]MPPF has been used in combination with drug challenges in the humans, (Lerond et al., 2013, Lothe et al., 2012, Passchier, 2000, Udo De Haes et al., 2002a, Passchier et al., 2001, Sibon et al., 2008). Two of these studies are of particular interest to the present study. In the first study a reduction in binding of 4-[^{18}F]MPPF was found in the DRN after administration with fluoxetine (20 mg, 0.3 mg/kg). This suggests 4-[^{18}F]MPPF is sensitive to increases in endogenous 5-HT in the human brain. This is of interest to compare to pre-clinical studies with fluoxetine (10 mg/kg) where two studies found reduced binding in the DRN (Aznavour et al., 2006, Riad et al., 2004) but a further four studies found no change in binding in the cortex, hippocampus and DRN

(Aznavour et al., 2006, Ginovart et al., 2000, Riad et al., 2004, Riad, 2008). This suggests that pre-clinical studies, at present, do not always predict the clinical outcome. In a second study there was no change in binding of 4-[^{18}F]MPPF in the cortex and raphe nucleus after tryptophan depletion suggesting it is not sensitive to a reduction in endogenous 5-HT (Udo De Haes et al., 2002b). It is clear that further work is needed to find accurate and reproducible methods.

Effect of 4-[^{18}F]MPPF quantity injected and radio-purity on ligand kinetics (specific binding and washout)

The quantity of 4-[^{18}F]MPPF injected into each animal was based on radioactivity, therefore the molar quantity of hot vs. cold 4-MPPF injected varied across experiments, as the specific activity of each batch varied. In addition the radiopurity was not the same between experiments, so that the amount of 4-[^{18}F]MPPF vs. a radioactive side product varied.

Therefore, it was hypothesized that these variations may have an effect on the maximum uptake and washout rate of 4-[^{18}F]MPPF. However, this study found no correlation between the maximum specific binding or washout of 4-[^{18}F]MPPF and the quantity administered or radiopurity.

This may be due to the small range of values examined, as quantity injected ranged from 0.003 -0.02 µmol/kg and the radiopurity ranged from 83.9 – 100%, with only 4 of 14 not being 100%. If larger ranges or datasets were examined a correlation may be seen. There were two apparent correlations for radiopurity, but in these instances only one data point differed from the group, so these were assumed to have skewed the correlation.

Comparison of PET and *ex vivo* autoradiography methods for examination of 4-[^{18}F]MPPF ligand binding

Autoradiography typically has a spatial resolution approximately an order of magnitude higher than that of PET, being in the range of a few hundreds microns compared to around 1-2 mm with PET (Schmidt and Smith, 2005).

Therefore it would be expected autoradiography would be more accurate when looking for change in ligand binding in small structures, such as are found in the rat brain. However, PET has the advantage that ligand binding can be assessed over time in an entire brain region, whereas autoradiography may only study a few sections in each brain area at one time point.

In this study the distribution and changes in 4-[^{18}F]MPPF specific binding, revealed by PET and *ex vivo* autroradiographic studies following the same protocols, were generally in agreement. However, in one instance a significant reduction in binding was found in PET where no significance was found in autoradiography, which was with a 4-MPPF pre-treatment in the hippocampus.

Several studies have compared PET and autoradiography methods, for a variety of PET ligands, and found good consensus in the results (Toyama et al., 2004, Strome et al., 2006, Mizuma et al., 2010). One study compared PET and autoradiography for the PET ligand [^{18}F]FDG (Prieto et al., 2011). The study employed the same Philips MOSAIC PET scanner as the present study but, in difference to this study, performed 3-D autoradiography where complete brain regions were sectioned as usual then stacked into 3-D volumes and co-registered with an MRI image for analysis. This study concluded that PET and autoradiography are generally in good agreement in detecting changes in the rodent brain though admit PET may have difficultly detecting changes in small brain areas which are detectable by autoradiography (Toyama et al., 2004, Strome et al., 2006, Mizuma et al., 2010).

One last consideration when comparing PET to autoradiography is the difference between the resolutions on autoradiographic film resulting from different isotopes. A low energy β emitter such as tritium (max. 18.5 KeV) produces sharper images on autoradiographic film than a high energy positron emitter (511 KeV) such as fluorine-18 (Rogers, 1979). Therefore comparisons between PET and autoradiography in small brain areas may also be affected by the radioisotope used. Although examination of the absolute differences was beyond the scope of this study, a visual comparison can be seen in Figure 62 and is in agreement with radioisotope image comparisons seen in the literature (Plenevaux et al., 2000).

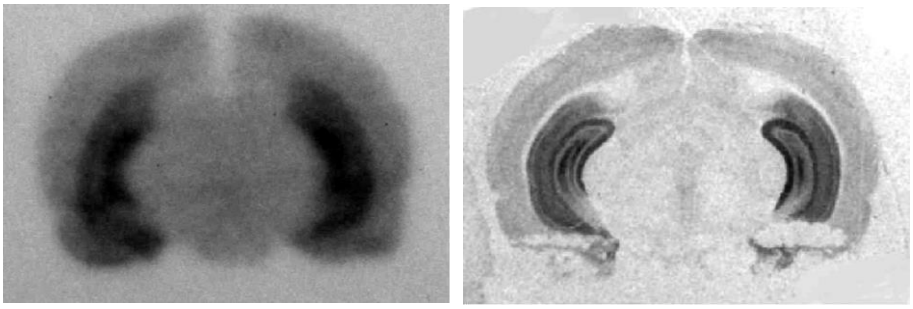

Figure 62: Comparison of the autoradiographic resolution given by fluorine-18 (left) and tritium (right) with an 4-MPPF ligand in the hippocampus of the rat brain.

Chapter 6. General Discussion

There is evidence that dysfunction of the 5-HT $_{1A}$ receptor plays a role in affective disorders such as anxiety and depression (Didelot et al., 2008, Drevets et al., 2000, Hirvonen et al., 2008, Sargent et al., 2000, Shively et al., 2006, Savitz et al., 2009, Arango et al., 1995, Detke et al., 1995, Haddjeri et al., 1998, Matsubara et al., 1991, Neff et al., 2009, Stockmeier et al., 1998, Szewczyk et al., 2009, Zhang et al., 2009) and it has been proposed that altered 5-HT levels in the brain are also associated with these disorders (Ruhé et al., 2007, Asberg et al., 1976, Traskman-Bendz et al., 1984). Therefore it is of interest to study both changes in receptor density and distribution as well as pre-synaptic neurotransmitter release.

The underlying hypothesis of this thesis is that 5-HT receptor specific PET ligands can be displaced by endogenous neurotransmitters and this can give a route to examining dysfunction of neurotransmitter systems at the biochemical level. However, although there are currently 5-HT $_{1A}$ ligands suitable to examine receptor density and distribution, the challenge taken on by this study was to find a 5-HT $_{1A}$ ligand sensitive to changes in synaptic levels of 5-HT . Thus, the present study aimed to chemically synthesise and biologically characterise 4-[^{18}F]MPPF to determine its suitability to examine pre-synaptic changes in the 5-HT system using PET and autoradiography.

In chapter two alternative precursors to 4-[^{18}F]MPPF, 4-MPPF and 4-MPPNO$_2$ were successfully synthesised *via* the published route and fully characterised. In chapter three the development of a routine radiosynthesis of 4-[^{18}F]MPPF was achieved using a combination of the Eckert and Zielgler ModularLab and a microwave reactor *via* a fluorodenitration reaction of 4-MPPNO$_2$ with fluorine-18. 4-[^{18}F]MPPF with a radiochemical yield of 33.5%, mean specific activity of. 4.3 ±0.7 GBq/µmol, mean radioactivity of 84.5 ± 12.1 MBq and a mean radiopurity of 95.8 ± 1.3% was produced with a total synthesis time of 60 minutes. The 4-[^{18}F]MPPF synthesised was then used in the following PET *and ex vivo* autoradiographic studies (chapter five).

In chapter four and five PET and *ex vivo/in vitro* autoradiography studies in rats revealed that 4-[^{18}F]MPPF specifically bound in areas rich in 5-HT $_{1A}$ receptors and binding could be blocked by pre-treatment with cold 4-MPPF. The 5-HT releasing agent fenfluramine was used to increase the concentration of endogenous 5-HT in the brain in parallel PET, autoradiography, and microdialysis studies. The microdialysis studies revealed that fenfluramine 3 mg/kg increased 5-HT levels to approximately 400% of basal levels, reaching a maximum concentration of 1 x 10^{-8} M 5-HT in the rat hippocampus. However, the present PET and autoradiography studies indicated that 4-[^{18}F]MPPF was not displaced by fenfluramine induced 5-HT release at this dose.

6.1 Strengths of the study

There are a number of strengths to the present study. Firstly, this study successfully performed chemical synthesis of two precursors, 4-MPPF and 4-MPPNO$_{2.}$ This was followed by the development of a routine production method for 4-[^{18}F]MPPF starting with low levels of activity. The final activity and high radiopurity of the 4-[^{18}F]MPPF produced made it suitable for *in vivo* PET imaging.

Secondly this study performed parallel microdialysis, PET and autoradiographic studies, maintaining the same protocol throughout. Unlike 4-[^{18}F]MPPF PET studies in the literature, the present study determined the endogenous 5-HT concentration in the hippocampus at the time of ligand administration in PET and *ex vivo* autoradiography studies. Therefore we were able to directly compare ligand binding with a specific 5-HT concentration. It was also shown that 3 mg/kg fenfluramine does not produce sufficient 5-HT release to displace 4-[^{18}F]MPPF in the rat brain.

Thirdly a direct comparison of PET and autoradiography methods was performed to characterise the distribution and displacement of 4-[^{18}F]MPPF. Although here, the results of the two experimental methods were not always consistent with each other.

Lastly, the present study was the first PET neuroimaging performed at Newcastle University. Therefore a protocol for the development of radioligand synthesis starting with a low fluorine-18 activity, followed by PET imaging has

now been laid down for future studies. In addition, software for PET data analysis was adapted for neuroimaging specifically for this project, and now includes a co-registration function. This is now available for future studies.

6.2 Limitations of the study

A number of limitations were found in the present study. Firstly, due to the low starting activity of the fluorine-18, the specific activity of the 4-[^{18}F]MPPF produced was lower than commonly reported in the literature, which is likely to affect the binding and washout profile. However, It should be noted that no correlation between quantity 4-[^{18}F]MPPF injected (a factor dependent on specific activity and radioactivity) and specific binding was found. This is likely due to the limited range of specific activity and radioactivities examined. In relation to the limitation above, in the present study we administered lower activities (11 ±1 MBq) compared to published 4-[^{18}F]MPPF PET studies (37 - 510 MBq) which may have affected the accuracy of detection by the PET scanner (Aznavour et al., 2006, Ginovart et al., 2000, Moulin-Sallanon et al., 2009, Rbah et al., 2003, Riad, 2008, Udo De Haes et al., 2006, Zimmer et al., 2002b, Zimmer et al., 2002a, Zimmer et al., 2003).

In addition the present study had low group sizes which had an effect on the data for two reasons; due to the small volume of interest (VOI) being examined, particularly in the DRN, it was found that the area being examined was close to the PET scanner resolution. To improve the accuracy of these results would require performing additional experiments to increase the group size. The small group size may also have affected the comparison of PET and *ex vivo* autoradiography methods. In general these two methods were in agreement, but significant change in binding was found in PET in one experiment where it was not in *ex vivo* autoradiography.

6.3 Translation of this study to human studies

When considering translating the present study to clinical studies, a number of factors should be considered. Firstly, due to the larger size of the human brain, the spatial resolution will be less of an issue, even when differences in

resolution of human and small animal PET scanners are taken into consideration (Yao et al., 2012).

Secondly, small animal PET studies must be performed under anaesthesia, which is likely to have an effect on 5-HT function. Clinical studies can be performed without the use of anaesthesia so this complication is avoided.

Finally, even though fenfluramine induced release of endogenous 5-HT was directly measured in the present study, it is difficult to predict how much release this would produce in humans.

This said, the finding that 4-[^{18}F]MPPF was not displaced by endogenous 5-HT could be exploited to some degree. For example, should a clinical study reveal a change in 4-[^{18}F]MPPF binding, it could be concluded that this change is due to a difference in receptor number/binding capacity and not a difference in endogenous 5-HT levels. Thus, 4-[^{18}F]MPPF could still be added to the research armamentarium of biological psychiatrist.

6.4 Future directions

To date only the 4- regioisomer of MPPF has been radiolabelled for PET imaging because a method for radiolabelling the 2- and 3- regioisomers has not been available until recently. A limitation of the direct aromatic nucleophilic substitution reaction used in the present study is its inability to label electron rich arenes. In addition, obtaining adequate yields from nucleophilic substitution reactions are limited to the *2*- or 4- position. However, novel diaryliodonium salt or copper mediated nucleophilic fluorination reactions can now be used for the fluorine-18 labelling of both electron rich and electron deficient arenes at any position on the aryl ring (Carroll and Wood, 2007, Tredwell et al., 2014). Therefore, these novel reactions could be used to label sites which are not favoured by nucleophilic substitution (Cai et al., 2008, Chun et al., 2010).

It is hypothesised that the 3- regioisomer, and possibly to a lesser extent the *2*-regioisomer, will be less susceptible to metabolism of the fluoride atom *in vivo* and therefore provide improved PET imaging resolution compared to 4-MPPF. It could also be speculated that 2- and 3- regioisomers may also demonstrate other properties conducive to 5-HT $_{1A}$ PET imaging which are not available

using 4-MPPF. Therefore future studies following from the present study will examine the regioisomers of [^{18}F]MPPF with respects to PET characteristics. In addition, future PET neuroimaging studies at Newcastle University now have a routine protocol for radiosynthesis and PET imaging in place.

As the majority of PET ligands under study are antagonists, another vital avenue for future PET imaging research is to find suitable agonist ligands in order to exploit their particular characteristics.

This is of particular interest in the search for a ligand that can be displaced by 5-HT, as an agonist may be more sensitive to changes in endogenous 5-HT. It is known that 5-HT agonists preferentially bind to receptors that are coupled to G-proteins (i.e. in the high affinity state) and therefore endogenous 5-HT could fully displace this ligand which is competing for binding at the same population of receptors (Zimmer and Le Bars, 2013, Billard et al., 2014). 5-HT antagonists bind to both high and low affinity state receptors, so endogenous 5-HT would not in theory displace the antagonist ligand bound to low affinity state receptors, resulting in a less sensitive measurement.

In addition there is recent evidence that the state of the G-protein receptor coupling is linked with the pathogenesis of mood disorders (Schreiber and Avissar, 2007, Thathiah and De Strooper, 2011), making new agonist ligands, in combination with current antagonist ligands, a vital tool to differentiate between high and low affinity state receptors.

6.5 Conclusion

These studies demonstrate that a combination of the Eckert and Zielgler ModularLab with a microwave reactor is an effective production method, when starting with low activity, for the synthesis of 4-[^{18}F]MPPF for use in PET. This study has also shown that 4-[^{18}F]MPPF is a suitable PET ligand for the examination of the distribution of 5-HT $_{1A}$ receptors in the rat brain. However, this study suggests that 4-[^{18}F]MPPF may not be suitable for use in examining possible changes in 5-HT in the brain in affective disorders.

Appendix

Appendix: A X-ray crystal structure data for 4-MPPF

Table 1. Crystal data and structure refinement for mac104.

Identification code	mac104
Chemical formula (moiety)	$C_{25}H_{27}FN_4O_2$
Chemical formula (total)	$C_{25}H_{27}FN_4O_2$
Formula weight	434.51
Temperature	150(2) K
Radiation, wavelength	MoK□, 0.71073 Å
Crystal system, space group	triclinic, $P\bar{1}$
Unit cell parameters	a = 13.7504(9) Å □ = 96.878(6)°
	b = 14.5099(10) Å □ = 91.371(6)°
	c = 16.8016(12) Å □ = 90.222(5)°
Cell volume	3327.0(4) $Å^3$
Z	6
Calculated density	1.301 g/cm^3
Absorption coefficient □	0.090 mm^{-1}
F(000)	1380
Reflections for cell refinement	5948 (□ range 2.8 to 28.6°)
Data collection method	Xcalibur, Atlas, Gemini ultra thick-slice □ scans
□ range for data collection	2.8 to 25.0°
Index ranges	h –16 to 16, k –17 to 16, l –19 to 19
Completeness to □ = 25.0°	99.9 %
Reflections collected	39547
Independent reflections	11694 (R_{int} = 0.0479)
Reflections with F^2>2□	3301
Absorption correction	semi-empirical from equivalents
Min. and max. transmission	0.84833 and 1.00000
Structure solution	direct methods
Refinement method	Full-matrix least-squares on F^2
Weighting parameters a, b	0.0816, 0.0000
Data / restraints / parameters	11694 / 0 / 869
Final R indices [F^2>2□]	R1 = 0.0551, wR2 = 0.1529
R indices (all data)	R1 = 0.1529, wR2 = 0.2238
Goodness-of-fit on F^2	0.984
Extinction coefficient	0.0009(3)
Largest and mean shift/su	0.397 and 0.076
Largest diff. peak and hole	0.27 and –0.20 e $Å^{-3}$

Table 2. Atomic coordinates and equivalent isotropic displacement parameters ($Å^2$)
for mac104. U_{eq} is defined as one third of the trace of the orthogonalized U^{ij} tensor.

	x	y	z	U_{eq}
O(1)	0.4841(2)	0.7217(2)	0.47322(18)	0.0323(8)
O(2)	0.0303(3)	0.6880(2)	0.79602(19)	0.0347(9)
N(1)	0.3344(3)	0.6176(3)	0.5132(2)	0.0221(9)
N(2)	0.2803(3)	0.5879(3)	0.6711(2)	0.0260(9)
N(3)	0.1396(3)	0.6058(3)	0.8605(2)	0.0263(9)
N(4)	0.2046(3)	0.4969(3)	0.9360(2)	0.0297(10)
C(1)	0.5508(3)	0.7887(4)	0.4511(3)	0.0369(13)
C(2)	0.4412(3)	0.6641(3)	0.4120(3)	0.0273(12)
C(3)	0.4675(4)	0.6587(4)	0.3317(3)	0.0348(13)
C(4)	0.4176(4)	0.6030(4)	0.2728(3)	0.0393(14)
C(5)	0.3396(4)	0.5519(4)	0.2926(3)	0.0444(15)
C(6)	0.3136(4)	0.5544(4)	0.3714(3)	0.0372(13)
C(7)	0.3619(4)	0.6101(3)	0.4320(3)	0.0264(11)
C(8)	0.2367(3)	0.5869(3)	0.5281(3)	0.0302(12)
C(9)	0.2125(3)	0.6224(3)	0.6134(3)	0.0228(11)
C(10)	0.3792(3)	0.6156(3)	0.6538(3)	0.0284(12)
C(11)	0.4041(3)	0.5813(3)	0.5686(3)	0.0274(11)
C(12)	0.2556(3)	0.6235(3)	0.7531(3)	0.0300(12)
C(13)	0.1766(4)	0.5646(3)	0.7834(3)	0.0285(12)
C(14)	0.0622(3)	0.6642(3)	0.8590(3)	0.0256(11)
C(15)	0.0150(3)	0.6994(3)	0.9360(3)	0.0205(10)
C(16)	−0.0081(3)	0.6423(3)	0.9932(3)	0.0276(12)
C(17)	−0.0527(4)	0.6785(4)	1.0631(3)	0.0373(13)
C(18)	−0.0707(4)	0.7712(4)	1.0736(3)	0.0398(15)
C(19)	−0.0503(4)	0.8298(4)	1.0185(3)	0.0376(14)
C(20)	−0.0086(3)	0.7925(3)	0.9487(3)	0.0278(12)
C(21)	0.1900(3)	0.5873(3)	0.9314(3)	0.0234(11)
C(22)	0.2230(3)	0.6569(4)	0.9891(3)	0.0302(12)
C(23)	0.2694(3)	0.6310(4)	1.0568(3)	0.0377(14)
C(24)	0.2838(4)	0.5381(4)	1.0628(3)	0.0353(13)
C(25)	0.2511(4)	0.4735(4)	1.0014(3)	0.0347(13)
F(1)	−0.1104(2)	0.8082(2)	1.14503(19)	0.0601(10)
F(2)	−0.1107(2)	0.4750(2)	0.81126(19)	0.0608(10)
F(3)	1.1109(2)	0.8579(2)	−0.47831(19)	0.0628(10)
O(3)	0.4837(2)	0.3884(2)	0.13914(19)	0.0332(8)
O(4)	0.0307(3)	0.3551(2)	0.46235(19)	0.0352(9)
N(5)	0.3353(3)	0.2841(3)	0.1799(2)	0.0237(9)
N(6)	0.2800(3)	0.2535(3)	0.3377(2)	0.0242(9)
N(7)	0.1392(3)	0.2728(3)	0.5267(2)	0.0247(9)
N(8)	0.2054(3)	0.1627(3)	0.6025(2)	0.0264(9)
C(26)	0.5500(4)	0.4559(4)	0.1175(3)	0.0385(13)

C(27)	0.4403(3)	0.3303(3)	0.0774(3)	0.0278(12)
C(28)	0.4683(4)	0.3259(3)	–0.0001(3)	0.0328(13)
C(29)	0.4176(4)	0.2685(4)	–0.0595(3)	0.0399(14)
C(30)	0.3400(4)	0.2180(4)	–0.0412(3)	0.0427(14)
C(31)	0.3132(4)	0.2215(3)	0.0386(3)	0.0366(13)
C(32)	0.3626(3)	0.2764(3)	0.0996(3)	0.0260(11)
C(33)	0.2362(3)	0.2526(3)	0.1961(3)	0.0274(11)
C(34)	0.2125(3)	0.2894(3)	0.2802(3)	0.0304(12)
C(35)	0.4050(3)	0.2476(4)	0.2351(3)	0.0313(12)
C(36)	0.3794(3)	0.2818(4)	0.3204(3)	0.0313(12)
C(37)	0.2545(3)	0.2898(4)	0.4197(3)	0.0288(12)
C(38)	0.1756(3)	0.2304(3)	0.4498(3)	0.0245(11)
C(39)	0.0612(3)	0.3315(3)	0.5257(3)	0.0241(11)
C(40)	0.0157(3)	0.3658(3)	0.6021(3)	0.0241(11)
C(41)	–0.0086(4)	0.3091(4)	0.6612(3)	0.0353(13)
C(42)	–0.0531(4)	0.3448(4)	0.7296(3)	0.0406(14)
C(43)	–0.0711(3)	0.4384(4)	0.7414(3)	0.0387(14)
C(44)	–0.0495(4)	0.4976(4)	0.6849(3)	0.0364(13)
C(45)	–0.0079(3)	0.4598(3)	0.6152(3)	0.0259(11)
C(46)	0.1898(3)	0.2530(3)	0.5970(3)	0.0234(11)
C(47)	0.2235(3)	0.3227(3)	0.6551(3)	0.0301(12)
C(48)	0.2700(4)	0.2976(4)	0.7228(3)	0.0418(14)
C(49)	0.2835(4)	0.2048(4)	0.7286(3)	0.0396(14)
C(50)	0.2524(4)	0.1409(4)	0.6677(3)	0.0355(13)
O(5)	0.5163(2)	0.9449(2)	0.19395(19)	0.0351(9)
O(6)	0.9688(2)	0.9789(2)	–0.12901(19)	0.0340(8)
N(9)	0.6659(3)	1.0490(3)	0.1537(2)	0.0256(9)
N(10)	0.7195(3)	1.0791(3)	–0.0044(2)	0.0264(9)
N(11)	0.8606(3)	1.0613(2)	–0.1942(2)	0.0224(9)
N(12)	0.7952(3)	1.1703(3)	–0.2689(2)	0.0295(10)
C(51)	0.4495(3)	0.8777(4)	0.2152(3)	0.0368(13)
C(52)	0.5587(3)	1.0025(3)	0.2559(3)	0.0269(11)
C(53)	0.5312(4)	1.0065(4)	0.3331(3)	0.0337(13)
C(54)	0.5819(4)	1.0630(4)	0.3932(3)	0.0427(15)
C(55)	0.6599(4)	1.1151(4)	0.3741(3)	0.0419(14)
C(56)	0.6874(4)	1.1114(3)	0.2955(3)	0.0328(12)
C(57)	0.6373(3)	1.0566(3)	0.2339(3)	0.0239(11)
C(58)	0.7641(3)	1.0792(3)	0.1384(3)	0.0256(11)
C(59)	0.7873(3)	1.0451(3)	0.0524(3)	0.0258(11)
C(60)	0.6196(3)	1.0516(4)	0.0129(3)	0.0304(12)
C(61)	0.5965(3)	1.0862(3)	0.0981(3)	0.0276(12)
C(62)	0.7454(3)	1.0431(3)	–0.0855(3)	0.0308(12)
C(63)	0.8241(4)	1.1030(3)	–0.1166(3)	0.0300(12)
C(64)	0.9376(4)	1.0020(3)	–0.1930(3)	0.0254(11)
C(65)	0.9839(3)	0.9673(3)	–0.2708(3)	0.0259(11)
C(66)	1.0087(3)	0.8750(3)	–0.2818(3)	0.0286(12)
C(67)	1.0511(3)	0.8380(3)	–0.3518(3)	0.0308(12)

C(68)	1.0703(3)	0.8956(4)	–0.4081(3)	0.0360(13)
C(69)	1.0515(4)	0.9876(4)	–0.3964(3)	0.0398(14)
C(70)	1.0080(4)	1.0244(4)	–0.3266(3)	0.0333(12)
C(71)	0.8093(3)	1.0809(3)	–0.2648(3)	0.0222(11)
C(72)	0.7768(3)	1.0114(3)	–0.3218(3)	0.0288(12)
C(73)	0.7307(4)	1.0370(4)	–0.3898(3)	0.0358(13)
C(74)	0.7159(4)	1.1292(4)	–0.3972(3)	0.0372(13)
C(75)	0.7481(4)	1.1930(4)	–0.3346(3)	0.0370(14)

Table 3. Bond lengths [Å] and angles [°] for mac104.

O(1)–C(1)	1.421(6)	O(1)–C(2)	1.366(6)
O(2)–C(14)	1.224(5)	N(1)–C(7)	1.416(5)
N(1)–C(8)	1.451(5)	N(1)–C(11)	1.463(6)
N(2)–C(9)	1.462(6)	N(2)–C(10)	1.462(6)
N(2)–C(12)	1.461(5)	N(3)–C(13)	1.464(5)
N(3)–C(14)	1.365(6)	N(3)–C(21)	1.419(6)
N(4)–C(21)	1.339(6)	N(4)–C(25)	1.337(6)
C(1)–H(1A)	0.980	C(1)–H(1B)	0.980
C(1)–H(1C)	0.980	C(2)–C(3)	1.399(6)
C(2)–C(7)	1.410(6)	C(3)–H(3A)	0.950
C(3)–C(4)	1.370(7)	C(4)–H(4A)	0.950
C(4)–C(5)	1.372(7)	C(5)–H(5A)	0.950
C(5)–C(6)	1.374(7)	C(6)–H(6A)	0.950
C(6)–C(7)	1.378(7)	C(8)–H(8A)	0.990
C(8)–H(8B)	0.990	C(8)–C(9)	1.509(6)
C(9)–H(9A)	0.990	C(9)–H(9B)	0.990
C(10)–H(10A)	0.990	C(10)–H(10B)	0.990
C(10)–C(11)	1.505(6)	C(11)–H(11A)	0.990
C(11)–H(11B)	0.990	C(12)–H(12A)	0.990
C(12)–H(12B)	0.990	C(12)–C(13)	1.514(6)
C(13)–H(13A)	0.990	C(13)–H(13B)	0.990
C(14)–C(15)	1.496(6)	C(15)–C(16)	1.384(6)
C(15)–C(20)	1.383(6)	C(16)–H(16A)	0.950
C(16)–C(17)	1.385(6)	C(17)–H(17A)	0.950
C(17)–C(18)	1.359(7)	C(18)–C(19)	1.364(7)
C(18)–F(1)	1.381(5)	C(19)–H(19A)	0.950
C(19)–C(20)	1.370(6)	C(20)–H(20A)	0.950
C(21)–C(22)	1.380(7)	C(22)–H(22A)	0.950
C(22)–C(23)	1.382(7)	C(23)–H(23A)	0.950
C(23)–C(24)	1.379(7)	C(24)–H(24A)	0.950
C(24)–C(25)	1.374(7)	C(25)–H(25A)	0.950
F(2)–C(43)	1.356(5)	F(3)–C(68)	1.372(6)
O(3)–C(26)	1.421(5)	O(3)–C(27)	1.378(6)
O(4)–C(39)	1.222(5)	N(5)–C(32)	1.400(5)
N(5)–C(33)	1.477(5)	N(5)–C(35)	1.462(6)
N(6)–C(34)	1.465(6)	N(6)–C(36)	1.472(6)
N(6)–C(37)	1.465(5)	N(7)–C(38)	1.464(5)
N(7)–C(39)	1.374(6)	N(7)–C(46)	1.416(6)
N(8)–C(46)	1.343(6)	N(8)–C(50)	1.330(6)
C(26)–H(26A)	0.980	C(26)–H(26B)	0.980
C(26)–H(26C)	0.980	C(27)–C(28)	1.362(6)
C(27)–C(32)	1.406(6)	C(28)–H(28A)	0.950
C(28)–C(29)	1.391(7)	C(29)–H(29A)	0.950
C(29)–C(30)	1.354(7)	C(30)–H(30A)	0.950
C(30)–C(31)	1.395(6)	C(31)–H(31A)	0.950
C(31)–C(32)	1.384(7)	C(33)–H(33A)	0.990

C(33)–H(33B)	0.990	C(33)–C(34)	1.493(6)
C(34)–H(34A)	0.990	C(34)–H(34B)	0.990
C(35)–H(35A)	0.990	C(35)–H(35B)	0.990
C(35)–C(36)	1.509(6)	C(36)–H(36A)	0.990
C(36)–H(36B)	0.990	C(37)–H(37A)	0.990
C(37)–H(37B)	0.990	C(37)–C(38)	1.517(6)
C(38)–H(38A)	0.990	C(38)–H(38B)	0.990
C(39)–C(40)	1.476(6)	C(40)–C(41)	1.408(6)
C(40)–C(45)	1.396(6)	C(41)–H(41A)	0.950
C(41)–C(42)	1.363(7)	C(42)–H(42A)	0.950
C(42)–C(43)	1.373(7)	C(43)–C(44)	1.390(7)
C(44)–H(44A)	0.950	C(44)–C(45)	1.371(6)
C(45)–H(45A)	0.950	C(46)–C(47)	1.388(7)
C(47)–H(47A)	0.950	C(47)–C(48)	1.379(7)
C(48)–H(48A)	0.950	C(48)–C(49)	1.375(7)
C(49)–H(49A)	0.950	C(49)–C(50)	1.356(7)
C(50)–H(50A)	0.950	O(5)–C(51)	1.420(5)
O(5)–C(52)	1.370(6)	O(6)–C(64)	1.232(5)
N(9)–C(57)	1.405(5)	N(9)–C(58)	1.456(5)
N(9)–C(61)	1.469(6)	N(10)–C(59)	1.449(6)
N(10)–C(60)	1.475(5)	N(10)–C(62)	1.454(5)
N(11)–C(63)	1.471(5)	N(11)–C(64)	1.368(6)
N(11)–C(71)	1.424(6)	N(12)–C(71)	1.322(6)
N(12)–C(75)	1.342(6)	C(51)–H(51A)	0.980
C(51)–H(51B)	0.980	C(51)–H(51C)	0.980
C(52)–C(53)	1.354(6)	C(52)–C(57)	1.416(6)
C(53)–H(53A)	0.950	C(53)–C(54)	1.394(7)
C(54)–H(54A)	0.950	C(54)–C(55)	1.377(7)
C(55)–H(55A)	0.950	C(55)–C(56)	1.377(6)
C(56)–H(56A)	0.950	C(56)–C(57)	1.394(6)
C(58)–H(58A)	0.990	C(58)–H(58B)	0.990
C(58)–C(59)	1.511(6)	C(59)–H(59A)	0.990
C(59)–H(59B)	0.990	C(60)–H(60A)	0.990
C(60)–H(60B)	0.990	C(60)–C(61)	1.501(6)
C(61)–H(61A)	0.990	C(61)–H(61B)	0.990
C(62)–H(62A)	0.990	C(62)–H(62B)	0.990
C(62)–C(63)	1.526(7)	C(63)–H(63A)	0.990
C(63)–H(63B)	0.990	C(64)–C(65)	1.501(6)
C(65)–C(66)	1.375(6)	C(65)–C(70)	1.369(6)
C(66)–H(66A)	0.950	C(66)–C(67)	1.378(6)
C(67)–H(67A)	0.950	C(67)–C(68)	1.364(7)
C(68)–C(69)	1.352(7)	C(69)–H(69A)	0.950
C(69)–C(70)	1.381(6)	C(70)–H(70A)	0.950
C(71)–C(72)	1.370(6)	C(72)–H(72A)	0.950
C(72)–C(73)	1.383(7)	C(73)–H(73A)	0.950
C(73)–C(74)	1.374(7)	C(74)–H(74A)	0.950
C(74)–C(75)	1.378(7)	C(75)–H(75A)	0.950

C(1)–O(1)–C(2)	116.5(4)	C(7)–N(1)–C(8)	116.5(4)
C(7)–N(1)–C(11)	115.8(3)	C(8)–N(1)–C(11)	110.1(4)
C(9)–N(2)–C(10)	109.0(3)	C(9)–N(2)–C(12)	110.7(3)
C(10)–N(2)–C(12)	110.6(4)	C(13)–N(3)–C(14)	117.6(4)
C(13)–N(3)–C(21)	118.0(4)	C(14)–N(3)–C(21)	124.3(4)
C(21)–N(4)–C(25)	117.7(4)	O(1)–C(1)–H(1A)	109.5
O(1)–C(1)–H(1B)	109.5	O(1)–C(1)–H(1C)	109.4
H(1A)–C(1)–H(1B)	109.5	H(1A)–C(1)–H(1C)	109.5
H(1B)–C(1)–H(1C)	109.5	O(1)–C(2)–C(3)	124.6(4)
O(1)–C(2)–C(7)	116.6(4)	C(3)–C(2)–C(7)	118.7(4)
C(2)–C(3)–H(3A)	119.3	C(2)–C(3)–C(4)	121.4(5)
H(3A)–C(3)–C(4)	119.3	C(3)–C(4)–H(4A)	120.3
C(3)–C(4)–C(5)	119.5(5)	H(4A)–C(4)–C(5)	120.3
C(4)–C(5)–H(5A)	119.9	C(4)–C(5)–C(6)	120.2(5)
H(5A)–C(5)–C(6)	119.9	C(5)–C(6)–H(6A)	119.1
C(5)–C(6)–C(7)	121.8(5)	H(6A)–C(6)–C(7)	119.1
N(1)–C(7)–C(2)	118.3(4)	N(1)–C(7)–C(6)	123.2(4)
C(2)–C(7)–C(6)	118.4(4)	N(1)–C(8)–H(8A)	110.0
N(1)–C(8)–H(8B)	110.1	N(1)–C(8)–C(9)	108.3(4)
H(8A)–C(8)–H(8B)	108.4	H(8A)–C(8)–C(9)	110.0
H(8B)–C(8)–C(9)	110.1	N(2)–C(9)–C(8)	111.8(4)
N(2)–C(9)–H(9A)	109.2	N(2)–C(9)–H(9B)	109.3
C(8)–C(9)–H(9A)	109.2	C(8)–C(9)–H(9B)	109.3
H(9A)–C(9)–H(9B)	107.9	N(2)–C(10)–H(10A)	109.5
N(2)–C(10)–H(10B)	109.5	N(2)–C(10)–C(11)	110.8(4)
H(10A)–C(10)–H(10B)	108.1	H(10A)–C(10)–C(11)	109.5
H(10B)–C(10)–C(11)	109.5	N(1)–C(11)–C(10)	110.0(4)
N(1)–C(11)–H(11A)	109.7	N(1)–C(11)–H(11B)	109.6
C(10)–C(11)–H(11A)	109.7	C(10)–C(11)–H(11B)	109.6
H(11A)–C(11)–H(11B)	108.2	N(2)–C(12)–H(12A)	109.5
N(2)–C(12)–H(12B)	109.5	N(2)–C(12)–C(13)	110.6(4)
H(12A)–C(12)–H(12B)	108.1	H(12A)–C(12)–C(13)	109.5
H(12B)–C(12)–C(13)	109.5	N(3)–C(13)–C(12)	112.2(4)
N(3)–C(13)–H(13A)	109.2	N(3)–C(13)–H(13B)	109.2
C(12)–C(13)–H(13A)	109.1	C(12)–C(13)–H(13B)	109.2
H(13A)–C(13)–H(13B)	107.9	O(2)–C(14)–N(3)	121.4(4)
O(2)–C(14)–C(15)	119.4(4)	N(3)–C(14)–C(15)	119.3(4)
C(14)–C(15)–C(16)	122.8(4)	C(14)–C(15)–C(20)	118.0(4)
C(16)–C(15)–C(20)	119.2(4)	C(15)–C(16)–H(16A)	119.9
C(15)–C(16)–C(17)	120.3(4)	H(16A)–C(16)–C(17)	119.9
C(16)–C(17)–H(17A)	121.1	C(16)–C(17)–C(18)	117.8(5)
H(17A)–C(17)–C(18)	121.1	C(17)–C(18)–C(19)	123.9(5)
C(17)–C(18)–F(1)	117.9(5)	C(19)–C(18)–F(1)	118.2(5)
C(18)–C(19)–H(19A)	121.2	C(18)–C(19)–C(20)	117.5(5)
H(19A)–C(19)–C(20)	121.2	C(15)–C(20)–C(19)	121.2(5)
C(15)–C(20)–H(20A)	119.4	C(19)–C(20)–H(20A)	119.4
N(3)–C(21)–N(4)	113.9(4)	N(3)–C(21)–C(22)	122.6(4)
N(4)–C(21)–C(22)	123.4(4)	C(21)–C(22)–H(22A)	121.1

C(21)–C(22)–C(23)	117.8(5)	H(22A)–C(22)–C(23)	121.1
C(22)–C(23)–H(23A)	120.3	C(22)–C(23)–C(24)	119.3(5)
H(23A)–C(23)–C(24)	120.4	C(23)–C(24)–H(24A)	120.5
C(23)–C(24)–C(25)	119.0(5)	H(24A)–C(24)–C(25)	120.5
N(4)–C(25)–C(24)	122.7(5)	N(4)–C(25)–H(25A)	118.7
C(24)–C(25)–H(25A)	118.6	C(26)–O(3)–C(27)	116.9(4)
C(32)–N(5)–C(33)	117.1(4)	C(32)–N(5)–C(35)	115.5(3)
C(33)–N(5)–C(35)	109.5(3)	C(34)–N(6)–C(36)	108.5(4)
C(34)–N(6)–C(37)	109.9(3)	C(36)–N(6)–C(37)	110.7(4)
C(38)–N(7)–C(39)	118.0(4)	C(38)–N(7)–C(46)	117.3(4)
C(39)–N(7)–C(46)	124.6(4)	C(46)–N(8)–C(50)	117.6(4)
O(3)–C(26)–H(26A)	109.5	O(3)–C(26)–H(26B)	109.5
O(3)–C(26)–H(26C)	109.5	H(26A)–C(26)–H(26B)	109.5
H(26A)–C(26)–H(26C)	109.5	H(26B)–C(26)–H(26C)	109.5
O(3)–C(27)–C(28)	123.2(4)	O(3)–C(27)–C(32)	115.2(4)
C(28)–C(27)–C(32)	121.6(5)	C(27)–C(28)–H(28A)	120.2
C(27)–C(28)–C(29)	119.6(5)	H(28A)–C(28)–C(29)	120.2
C(28)–C(29)–H(29A)	119.6	C(28)–C(29)–C(30)	120.8(5)
H(29A)–C(29)–C(30)	119.6	C(29)–C(30)–H(30A)	120.4
C(29)–C(30)–C(31)	119.1(5)	H(30A)–C(30)–C(31)	120.5
C(30)–C(31)–H(31A)	119.0	C(30)–C(31)–C(32)	121.9(5)
H(31A)–C(31)–C(32)	119.1	N(5)–C(32)–C(27)	119.7(4)
N(5)–C(32)–C(31)	123.3(4)	C(27)–C(32)–C(31)	116.9(4)
N(5)–C(33)–H(33A)	110.1	N(5)–C(33)–H(33B)	110.0
N(5)–C(33)–C(34)	108.4(4)	H(33A)–C(33)–H(33B)	108.4
H(33A)–C(33)–C(34)	110.0	H(33B)–C(33)–C(34)	110.0
N(6)–C(34)–C(33)	111.1(4)	N(6)–C(34)–H(34A)	109.5
N(6)–C(34)–H(34B)	109.4	C(33)–C(34)–H(34A)	109.4
C(33)–C(34)–H(34B)	109.4	H(34A)–C(34)–H(34B)	108.0
N(5)–C(35)–H(35A)	109.7	N(5)–C(35)–H(35B)	109.8
N(5)–C(35)–C(36)	109.5(4)	H(35A)–C(35)–H(35B)	108.2
H(35A)–C(35)–C(36)	109.7	H(35B)–C(35)–C(36)	109.8
N(6)–C(36)–C(35)	111.1(4)	N(6)–C(36)–H(36A)	109.4
N(6)–C(36)–H(36B)	109.4	C(35)–C(36)–H(36A)	109.4
C(35)–C(36)–H(36B)	109.5	H(36A)–C(36)–H(36B)	108.0
N(6)–C(37)–H(37A)	109.6	N(6)–C(37)–H(37B)	109.6
N(6)–C(37)–C(38)	110.3(4)	H(37A)–C(37)–H(37B)	108.1
H(37A)–C(37)–C(38)	109.6	H(37B)–C(37)–C(38)	109.6
N(7)–C(38)–C(37)	111.2(4)	N(7)–C(38)–H(38A)	109.4
N(7)–C(38)–H(38B)	109.4	C(37)–C(38)–H(38A)	109.4
C(37)–C(38)–H(38B)	109.4	H(38A)–C(38)–H(38B)	108.0
O(4)–C(39)–N(7)	120.3(4)	O(4)–C(39)–C(40)	120.8(4)
N(7)–C(39)–C(40)	118.9(4)	C(39)–C(40)–C(41)	124.2(4)
C(39)–C(40)–C(45)	117.7(4)	C(41)–C(40)–C(45)	118.1(4)
C(40)–C(41)–H(41A)	119.4	C(40)–C(41)–C(42)	121.2(5)
H(41A)–C(41)–C(42)	119.4	C(41)–C(42)–H(42A)	120.7
C(41)–C(42)–C(43)	118.6(5)	H(42A)–C(42)–C(43)	120.7
F(2)–C(43)–C(42)	118.8(5)	F(2)–C(43)–C(44)	118.5(5)

C(42)–C(43)–C(44)	122.7(5)	C(43)–C(44)–H(44A)	121.1
C(43)–C(44)–C(45)	117.8(5)	H(44A)–C(44)–C(45)	121.1
C(40)–C(45)–C(44)	121.6(5)	C(40)–C(45)–H(45A)	119.2
C(44)–C(45)–H(45A)	119.2	N(7)–C(46)–N(8)	115.5(4)
N(7)–C(46)–C(47)	122.1(4)	N(8)–C(46)–C(47)	122.3(4)
C(46)–C(47)–H(47A)	120.7	C(46)–C(47)–C(48)	118.6(5)
H(47A)–C(47)–C(48)	120.7	C(47)–C(48)–H(48A)	120.7
C(47)–C(48)–C(49)	118.5(5)	H(48A)–C(48)–C(49)	120.8
C(48)–C(49)–H(49A)	120.2	C(48)–C(49)–C(50)	119.6(5)
H(49A)–C(49)–C(50)	120.2	N(8)–C(50)–C(49)	123.4(5)
N(8)–C(50)–H(50A)	118.3	C(49)–C(50)–H(50A)	118.3
C(51)–O(5)–C(52)	116.6(4)	C(57)–N(9)–C(58)	117.4(4)
C(57)–N(9)–C(61)	115.1(3)	C(58)–N(9)–C(61)	109.7(4)
C(59)–N(10)–C(60)	109.7(3)	C(59)–N(10)–C(62)	109.6(3)
C(60)–N(10)–C(62)	111.1(4)	C(63)–N(11)–C(64)	117.5(4)
C(63)–N(11)–C(71)	117.6(3)	C(64)–N(11)–C(71)	124.8(4)
C(71)–N(12)–C(75)	116.7(4)	O(5)–C(51)–H(51A)	109.5
O(5)–C(51)–H(51B)	109.5	O(5)–C(51)–H(51C)	109.5
H(51A)–C(51)–H(51B)	109.5	H(51A)–C(51)–H(51C)	109.5
H(51B)–C(51)–H(51C)	109.5	O(5)–C(52)–C(53)	123.8(5)
O(5)–C(52)–C(57)	114.8(4)	C(53)–C(52)–C(57)	121.3(5)
C(52)–C(53)–H(53A)	119.9	C(52)–C(53)–C(54)	120.2(5)
H(53A)–C(53)–C(54)	119.9	C(53)–C(54)–H(54A)	120.0
C(53)–C(54)–C(55)	120.0(5)	H(54A)–C(54)–C(55)	120.0
C(54)–C(55)–H(55A)	120.2	C(54)–C(55)–C(56)	119.7(5)
H(55A)–C(55)–C(56)	120.1	C(55)–C(56)–H(56A)	119.2
C(55)–C(56)–C(57)	121.6(5)	H(56A)–C(56)–C(57)	119.1
N(9)–C(57)–C(52)	120.0(4)	N(9)–C(57)–C(56)	122.7(4)
C(52)–C(57)–C(56)	117.1(4)	N(9)–C(58)–H(58A)	110.0
N(9)–C(58)–H(58B)	110.0	N(9)–C(58)–C(59)	108.5(4)
H(58A)–C(58)–H(58B)	108.4	H(58A)–C(58)–C(59)	110.0
H(58B)–C(58)–C(59)	110.0	N(10)–C(59)–C(58)	112.4(4)
N(10)–C(59)–H(59A)	109.1	N(10)–C(59)–H(59B)	109.1
C(58)–C(59)–H(59A)	109.1	C(58)–C(59)–H(59B)	109.2
H(59A)–C(59)–H(59B)	107.9	N(10)–C(60)–H(60A)	109.6
N(10)–C(60)–H(60B)	109.7	N(10)–C(60)–C(61)	109.9(4)
H(60A)–C(60)–H(60B)	108.2	H(60A)–C(60)–C(61)	109.7
H(60B)–C(60)–C(61)	109.7	N(9)–C(61)–C(60)	110.5(4)
N(9)–C(61)–H(61A)	109.6	N(9)–C(61)–H(61B)	109.6
C(60)–C(61)–H(61A)	109.5	C(60)–C(61)–H(61B)	109.6
H(61A)–C(61)–H(61B)	108.1	N(10)–C(62)–H(62A)	109.5
N(10)–C(62)–H(62B)	109.4	N(10)–C(62)–C(63)	110.9(4)
H(62A)–C(62)–H(62B)	108.0	H(62A)–C(62)–C(63)	109.5
H(62B)–C(62)–C(63)	109.5	N(11)–C(63)–C(62)	111.9(4)
N(11)–C(63)–H(63A)	109.2	N(11)–C(63)–H(63B)	109.2
C(62)–C(63)–H(63A)	109.2	C(62)–C(63)–H(63B)	109.2
H(63A)–C(63)–H(63B)	107.9	O(6)–C(64)–N(11)	120.3(4)
O(6)–C(64)–C(65)	121.0(4)	N(11)–C(64)–C(65)	118.7(4)

C(64)–C(65)–C(66)	116.8(4)	C(64)–C(65)–C(70)	122.8(4)
C(66)–C(65)–C(70)	120.2(4)	C(65)–C(66)–H(66A)	119.9
C(65)–C(66)–C(67)	120.1(5)	H(66A)–C(66)–C(67)	120.0
C(66)–C(67)–H(67A)	120.8	C(66)–C(67)–C(68)	118.4(5)
H(67A)–C(67)–C(68)	120.8	F(3)–C(68)–C(67)	118.1(5)
F(3)–C(68)–C(69)	119.7(5)	C(67)–C(68)–C(69)	122.3(5)
C(68)–C(69)–H(69A)	120.4	C(68)–C(69)–C(70)	119.3(5)
H(69A)–C(69)–C(70)	120.3	C(65)–C(70)–C(69)	119.5(5)
C(65)–C(70)–H(70A)	120.2	C(69)–C(70)–H(70A)	120.3
N(11)–C(71)–N(12)	114.1(4)	N(11)–C(71)–C(72)	121.6(4)
N(12)–C(71)–C(72)	124.2(4)	C(71)–C(72)–H(72A)	121.2
C(71)–C(72)–C(73)	117.6(5)	H(72A)–C(72)–C(73)	121.2
C(72)–C(73)–H(73A)	120.0	C(72)–C(73)–C(74)	120.0(5)
H(73A)–C(73)–C(74)	120.0	C(73)–C(74)–H(74A)	121.4
C(73)–C(74)–C(75)	117.3(5)	H(74A)–C(74)–C(75)	121.4
N(12)–C(75)–C(74)	124.0(5)	N(12)–C(75)–H(75A)	118.0
C(74)–C(75)–H(75A)	118.0		

Table 4. Anisotropic displacement parameters ($Å^2$) for mac104. The anisotropic displacement factor exponent takes the form: $-2\pi^2[h^2a^{*2}U^{11} + ...+ 2hka^*b^*U^{12}]$

	U^{11}	U^{22}	U^{33}	U^{23}	U^{13}	U^{12}
O(1)	0.0285(19)	0.043(2)	0.0249(19)	0.0046(16)	−0.0030(15)	−0.0104(16)
O(2)	0.051(2)	0.028(2)	0.027(2)	0.0100(16)	−0.0005(17)	0.0095(17)
N(1)	0.022(2)	0.026(2)	0.018(2)	0.0034(17)	0.0018(17)	0.0007(17)
N(2)	0.023(2)	0.033(2)	0.022(2)	0.0066(18)	0.0032(18)	0.0033(18)
N(3)	0.030(2)	0.027(2)	0.023(2)	0.0070(18)	0.0029(18)	0.0003(18)
N(4)	0.026(2)	0.032(3)	0.033(2)	0.0109(19)	0.0025(19)	−0.0043(18)
C(1)	0.021(3)	0.037(3)	0.054(4)	0.012(3)	0.003(2)	−0.003(2)
C(2)	0.027(3)	0.029(3)	0.026(3)	0.005(2)	−0.001(2)	0.005(2)
C(3)	0.034(3)	0.048(4)	0.026(3)	0.016(3)	0.009(2)	0.008(3)
C(4)	0.053(4)	0.047(4)	0.017(3)	0.000(2)	0.004(3)	0.004(3)
C(5)	0.060(4)	0.046(4)	0.027(3)	0.004(3)	−0.002(3)	−0.016(3)
C(6)	0.051(3)	0.038(3)	0.024(3)	0.008(2)	0.001(3)	−0.014(3)
C(7)	0.032(3)	0.028(3)	0.020(3)	0.007(2)	0.003(2)	0.006(2)
C(8)	0.029(3)	0.038(3)	0.025(3)	0.008(2)	0.003(2)	−0.004(2)
C(9)	0.019(2)	0.028(3)	0.023(3)	0.010(2)	−0.001(2)	−0.005(2)
C(10)	0.028(3)	0.037(3)	0.020(3)	0.006(2)	−0.006(2)	0.000(2)
C(11)	0.024(3)	0.037(3)	0.023(3)	0.010(2)	0.003(2)	0.005(2)
C(12)	0.031(3)	0.037(3)	0.022(3)	0.002(2)	0.001(2)	0.000(2)
C(13)	0.041(3)	0.023(3)	0.020(3)	−0.003(2)	0.005(2)	−0.002(2)
C(14)	0.028(3)	0.019(3)	0.031(3)	0.009(2)	0.005(2)	0.002(2)
C(15)	0.015(2)	0.021(3)	0.026(3)	0.005(2)	0.000(2)	−0.0002(19)
C(16)	0.026(3)	0.022(3)	0.036(3)	0.006(2)	0.009(2)	−0.003(2)
C(17)	0.033(3)	0.040(4)	0.040(3)	0.009(3)	0.011(3)	−0.006(3)
C(18)	0.027(3)	0.054(4)	0.035(3)	−0.008(3)	0.016(2)	−0.005(3)
C(19)	0.035(3)	0.032(3)	0.041(3)	−0.013(3)	−0.003(3)	0.006(2)
C(20)	0.024(3)	0.023(3)	0.036(3)	0.005(2)	−0.010(2)	0.004(2)
C(21)	0.027(3)	0.027(3)	0.018(3)	0.009(2)	0.012(2)	0.002(2)
C(22)	0.028(3)	0.033(3)	0.028(3)	−0.004(2)	0.000(2)	0.001(2)
C(23)	0.025(3)	0.054(4)	0.033(3)	−0.002(3)	−0.001(2)	0.009(3)
C(24)	0.027(3)	0.055(4)	0.026(3)	0.015(3)	0.003(2)	0.008(3)
C(25)	0.029(3)	0.043(3)	0.035(3)	0.016(3)	0.005(3)	0.006(3)
F(1)	0.051(2)	0.075(3)	0.051(2)	−0.0074(18)	0.0236(18)	0.0000(18)
F(2)	0.051(2)	0.076(3)	0.052(2)	−0.0110(18)	0.0251(18)	0.0011(19)
F(3)	0.051(2)	0.080(3)	0.053(2)	−0.0152(18)	0.0264(18)	

	0.0018(19)					
O(3)	0.0294(19)	0.040(2)	0.031(2)	0.0062(17)	0.0033(16)	
–0.0108(16)						
O(4)	0.047(2)	0.032(2)	0.028(2)	0.0108(16)	–0.0055(17)	
	0.0062(17)					
N(5)	0.020(2)	0.031(2)	0.020(2)	0.0052(18)	–0.0003(17)	
–0.0012(17)						
N(6)	0.022(2)	0.033(2)	0.018(2)	0.0020(18)	0.0006(17)	
	0.0004(18)					
N(7)	0.028(2)	0.027(2)	0.019(2)	0.0050(18)	0.0008(18)	
–0.0003(18)						
N(8)	0.024(2)	0.027(3)	0.030(2)	0.0107(19)	–0.0032(18)	
	0.0037(18)					
C(26)	0.034(3)	0.038(3)	0.045(3)	0.012(3)	0.005(3)	–0.009(3)
C(27)	0.027(3)	0.028(3)	0.029(3)	0.004(2)	0.005(2)	0.003(2)
C(28)	0.028(3)	0.035(3)	0.038(3)	0.013(3)	0.008(2)	0.001(2)
C(29)	0.058(4)	0.039(3)	0.023(3)	0.000(2)	0.009(3)	–0.001(3)
C(30)	0.060(4)	0.043(4)	0.023(3)	0.000(3)	–0.001(3)	–0.006(3)
C(31)	0.050(3)	0.026(3)	0.033(3)	0.003(2)	0.007(3)	–0.011(3)
C(32)	0.028(3)	0.025(3)	0.026(3)	0.006(2)	0.007(2)	0.004(2)
C(33)	0.027(3)	0.032(3)	0.023(3)	0.006(2)	–0.012(2)	–0.006(2)
C(34)	0.020(3)	0.036(3)	0.035(3)	0.001(2)	–0.003(2)	0.005(2)
C(35)	0.026(3)	0.043(3)	0.027(3)	0.014(2)	0.000(2)	0.006(2)
C(36)	0.021(3)	0.046(3)	0.028(3)	0.010(2)	0.000(2)	0.009(2)
C(37)	0.027(3)	0.041(3)	0.017(3)	–0.003(2)	0.007(2)	–0.002(2)
C(38)	0.034(3)	0.021(3)	0.020(2)	0.002(2)	0.007(2)	0.001(2)
C(39)	0.027(3)	0.019(3)	0.027(3)	0.003(2)	–0.004(2)	–0.001(2)
C(40)	0.026(3)	0.020(3)	0.027(3)	0.006(2)	–0.008(2)	–0.006(2)
C(41)	0.032(3)	0.029(3)	0.046(3)	0.005(3)	0.009(3)	–0.004(2)
C(42)	0.032(3)	0.054(4)	0.037(3)	0.008(3)	0.019(3)	–0.006(3)
C(43)	0.021(3)	0.051(4)	0.040(3)	–0.014(3)	0.011(2)	0.002(3)
C(44)	0.027(3)	0.030(3)	0.050(4)	–0.002(3)	0.001(3)	0.006(2)
C(45)	0.021(3)	0.024(3)	0.033(3)	0.004(2)	–0.003(2)	0.005(2)
C(46)	0.019(2)	0.025(3)	0.026(3)	0.006(2)	0.005(2)	0.000(2)
C(47)	0.034(3)	0.028(3)	0.029(3)	0.004(2)	0.005(2)	0.006(2)
C(48)	0.037(3)	0.055(4)	0.032(3)	–0.003(3)	0.004(3)	0.007(3)
C(49)	0.031(3)	0.061(4)	0.030(3)	0.019(3)	–0.001(2)	0.002(3)
C(50)	0.038(3)	0.030(3)	0.040(3)	0.011(3)	–0.004(3)	0.005(2)
O(5)	0.031(2)	0.047(2)	0.0276(19)	0.0057(17)	0.0045(16)	
–0.0107(17)						
O(6)	0.045(2)	0.030(2)	0.028(2)	0.0089(16)	–0.0068(17)	
	0.0013(16)					
N(9)	0.022(2)	0.035(3)	0.021(2)	0.0073(18)	–0.0027(17)	
	0.0010(18)					
N(10)	0.027(2)	0.036(3)	0.017(2)	0.0040(18)	–0.0017(17)	
	0.0048(19)					

N(11)	0.026(2)	0.020(2)	0.021(2)	0.0027(17)	0.0077(18)	0.0060(17)
N(12)	0.031(2)	0.027(3)	0.032(2)	0.0093(19)	0.000(2)	0.0012(19)
C(51)	0.028(3)	0.051(4)	0.032(3)	0.008(3)	0.005(2)	–0.005(3)
C(52)	0.024(3)	0.034(3)	0.024(3)	0.010(2)	–0.004(2)	0.005(2)
C(53)	0.034(3)	0.042(3)	0.026(3)	0.006(2)	0.005(2)	0.000(3)
C(54)	0.051(4)	0.050(4)	0.030(3)	0.013(3)	0.014(3)	0.011(3)
C(55)	0.067(4)	0.036(3)	0.021(3)	–0.004(2)	0.008(3)	–0.005(3)
C(56)	0.042(3)	0.030(3)	0.027(3)	0.005(2)	–0.005(2)	–0.004(2)
C(57)	0.028(3)	0.025(3)	0.020(3)	0.007(2)	–0.002(2)	0.004(2)
C(58)	0.017(2)	0.035(3)	0.025(3)	0.006(2)	–0.002(2)	–0.006(2)
C(59)	0.022(3)	0.031(3)	0.026(3)	0.007(2)	0.004(2)	–0.004(2)
C(60)	0.013(2)	0.055(4)	0.024(3)	0.011(2)	–0.002(2)	–0.001(2)
C(61)	0.024(3)	0.033(3)	0.027(3)	0.010(2)	0.003(2)	0.007(2)
C(62)	0.029(3)	0.039(3)	0.025(3)	0.008(2)	–0.006(2)	–0.003(2)
C(63)	0.034(3)	0.034(3)	0.023(3)	0.007(2)	0.004(2)	0.009(2)
C(64)	0.037(3)	0.013(3)	0.026(3)	0.008(2)	–0.004(2)	–0.006(2)
C(65)	0.021(3)	0.032(3)	0.025(3)	0.005(2)	0.002(2)	0.006(2)
C(66)	0.021(3)	0.036(3)	0.030(3)	0.006(2)	–0.006(2)	–0.002(2)
C(67)	0.015(2)	0.029(3)	0.047(3)	0.001(3)	–0.002(2)	0.007(2)
C(68)	0.021(3)	0.046(4)	0.041(3)	0.001(3)	0.006(2)	0.002(2)
C(69)	0.039(3)	0.049(4)	0.033(3)	0.010(3)	0.002(3)	–0.011(3)
C(70)	0.040(3)	0.029(3)	0.033(3)	0.008(2)	0.006(2)	0.000(2)
C(71)	0.017(2)	0.028(3)	0.022(3)	0.008(2)	0.003(2)	0.002(2)
C(72)	0.025(3)	0.031(3)	0.030(3)	0.003(2)	0.003(2)	0.007(2)
C(73)	0.034(3)	0.049(4)	0.022(3)	–0.005(3)	0.001(2)	0.001(3)
C(74)	0.026(3)	0.060(4)	0.026(3)	0.007(3)	–0.003(2)	0.012(3)
C(75)	0.030(3)	0.044(4)	0.043(3)	0.028(3)	0.002(3)	0.000(3)

Table 5. Hydrogen coordinates and isotropic displacement parameters ($Å^2$) for mac104.

	x	y	z	U
H(1A)	0.5750	0.8274	0.4993	0.055
H(1B)	0.5179	0.8278	0.4152	0.055
H(1C)	0.6054	0.7569	0.4235	0.055
H(3A)	0.5212	0.6945	0.3177	0.042
H(4A)	0.4368	0.5998	0.2186	0.047
H(5A)	0.3034	0.5146	0.2519	0.053
H(6A)	0.2610	0.5168	0.3843	0.045
H(8A)	0.2329	0.5183	0.5200	0.036
H(8B)	0.1896	0.6114	0.4905	0.036
H(9A)	0.2145	0.6911	0.6203	0.027
H(9B)	0.1456	0.6026	0.6242	0.027
H(10A)	0.4259	0.5898	0.6909	0.034
H(10B)	0.3850	0.6841	0.6625	0.034
H(11A)	0.4706	0.6019	0.5577	0.033
H(11B)	0.4023	0.5126	0.5607	0.033
H(12A)	0.2329	0.6884	0.7546	0.036
H(12B)	0.3142	0.6234	0.7884	0.036
H(13A)	0.1223	0.5567	0.7434	0.034
H(13B)	0.2029	0.5023	0.7894	0.034
H(16A)	0.0067	0.5781	0.9846	0.033
H(17A)	−0.0701	0.6399	1.1024	0.045
H(19A)	−0.0644	0.8942	1.0280	0.045
H(20A)	0.0042	0.8312	0.9084	0.033
H(22A)	0.2141	0.7204	0.9825	0.036
H(23A)	0.2911	0.6768	1.0987	0.045
H(24A)	0.3159	0.5191	1.1088	0.042
H(25A)	0.2620	0.4096	1.0056	0.042
H(26A)	0.5692	0.4983	0.1652	0.058
H(26B)	0.5188	0.4912	0.0778	0.058
H(26C)	0.6078	0.4248	0.0944	0.058
H(28A)	0.5220	0.3618	−0.0136	0.039
H(29A)	0.4377	0.2648	−0.1135	0.048
H(30A)	0.3043	0.1806	−0.0823	0.051
H(31A)	0.2595	0.1851	0.0514	0.044
H(33A)	0.2330	0.1839	0.1891	0.033
H(33B)	0.1887	0.2758	0.1581	0.033
H(34A)	0.2162	0.3580	0.2866	0.036
H(34B)	0.1452	0.2712	0.2913	0.036
H(35A)	0.4716	0.2685	0.2244	0.038
H(35B)	0.4035	0.1789	0.2270	0.038
H(36A)	0.4261	0.2563	0.3577	0.038
H(36B)	0.3848	0.3503	0.3290	0.038
H(37A)	0.2313	0.3545	0.4207	0.035

H(37B)	0.3129	0.2903	0.4553	0.035
H(38A)	0.1213	0.2223	0.4098	0.029
H(38B)	0.2021	0.1682	0.4560	0.029
H(41A)	0.0064	0.2449	0.6533	0.042
H(42A)	–0.0714	0.3057	0.7683	0.049
H(44A)	–0.0632	0.5620	0.6943	0.044
H(45A)	0.0052	0.4985	0.5749	0.031
H(47A)	0.2148	0.3862	0.6483	0.036
H(48A)	0.2923	0.3435	0.7644	0.050
H(49A)	0.3143	0.1856	0.7750	0.048
H(50A)	0.2648	0.0772	0.6719	0.043
H(51A)	0.4272	0.8381	0.1668	0.055
H(51B)	0.3936	0.9091	0.2412	0.055
H(51C)	0.4816	0.8395	0.2522	0.055
H(53A)	0.4773	0.9706	0.3463	0.040
H(54A)	0.5626	1.0655	0.4473	0.051
H(55A)	0.6947	1.1536	0.4151	0.050
H(56A)	0.7418	1.1471	0.2830	0.039
H(58A)	0.8112	1.0536	0.1753	0.031
H(58B)	0.7685	1.1478	0.1474	0.031
H(59A)	0.8539	1.0655	0.0414	0.031
H(59B)	0.7860	0.9763	0.0450	0.031
H(60A)	0.6133	0.9831	0.0042	0.036
H(60B)	0.5729	1.0779	–0.0240	0.036
H(61A)	0.5994	1.1549	0.1059	0.033
H(61B)	0.5296	1.0668	0.1095	0.033
H(62A)	0.6870	1.0418	–0.1213	0.037
H(62B)	0.7692	0.9787	–0.0862	0.037
H(63A)	0.7972	1.1651	–0.1225	0.036
H(63B)	0.8788	1.1113	–0.0769	0.036
H(66A)	0.9966	0.8367	–0.2410	0.034
H(67A)	1.0666	0.7739	–0.3608	0.037
H(69A)	1.0681	1.0264	–0.4358	0.048
H(70A)	0.9948	1.0890	–0.3173	0.040
H(72A)	0.7857	0.9479	–0.3149	0.035
H(73A)	0.7092	0.9908	–0.4315	0.043
H(74A)	0.6847	1.1483	–0.4435	0.045
H(75A)	0.7363	1.2568	–0.3382	0.044

Table 6. Torsion angles [°] for mac104.

C(1)–O(1)–C(2)–C(3)	8.6(7)	C(1)–O(1)–C(2)–C(7)	–168.2(4)
O(1)–C(2)–C(3)–C(4)	–176.2(5)	C(7)–C(2)–C(3)–C(4)	0.5(7)
C(2)–C(3)–C(4)–C(5)	0.5(8)	C(3)–C(4)–C(5)–C(6)	–2.0(8)
C(4)–C(5)–C(6)–C(7)	2.4(8)	C(5)–C(6)–C(7)–N(1)	177.0(5)
C(5)–C(6)–C(7)–C(2)	–1.3(8)	O(1)–C(2)–C(7)–N(1)	–1.5(6)
O(1)–C(2)–C(7)–C(6)	176.9(4)	C(3)–C(2)–C(7)–N(1)	–178.5(4)
C(3)–C(2)–C(7)–C(6)	–0.1(7)	C(8)–N(1)–C(7)–C(2)	160.3(4)
C(8)–N(1)–C(7)–C(6)	–18.0(7)	C(11)–N(1)–C(7)–C(2)	–67.8(5)
C(11)–N(1)–C(7)–C(6)	113.9(5)	C(7)–N(1)–C(8)–C(9)	–165.7(4)
C(11)–N(1)–C(8)–C(9)	59.8(5)	C(10)–N(2)–C(9)–C(8)	57.8(5)
C(12)–N(2)–C(9)–C(8)	179.7(4)	N(1)–C(8)–C(9)–N(2)	–59.7(5)
C(9)–N(2)–C(10)–C(11)	–56.4(5)	C(12)–N(2)–C(10)–C(11)	–178.4(4)
C(7)–N(1)–C(11)–C(10)	165.2(4)	C(8)–N(1)–C(11)–C(10)	–60.0(5)
N(2)–C(10)–C(11)–N(1)	58.1(5)	C(9)–N(2)–C(12)–C(13)	83.4(5)
C(10)–N(2)–C(12)–C(13)	–155.6(4)	C(14)–N(3)–C(13)–C(12)	90.5(5)
C(21)–N(3)–C(13)–C(12)	–85.6(5)	N(2)–C(12)–C(13)–N(3)	–171.4(4)
C(13)–N(3)–C(14)–O(2)	–6.5(7)	C(13)–N(3)–C(14)–C(15)	173.1(4)
C(21)–N(3)–C(14)–O(2)	169.4(4)	C(21)–N(3)–C(14)–C(15)	–11.0(7)
O(2)–C(14)–C(15)–C(16)	133.8(5)	O(2)–C(14)–C(15)–C(20)	–44.4(6)
N(3)–C(14)–C(15)–C(16)	–45.8(7)	N(3)–C(14)–C(15)–C(20)	136.0(5)
C(14)–C(15)–C(16)–C(17)	–179.3(4)	C(20)–C(15)–C(16)–C(17)	–1.2(7)
C(15)–C(16)–C(17)–C(18)	–1.3(7)	C(16)–C(17)–C(18)–C(19)	2.2(8)
C(16)–C(17)–C(18)–F(1)	–176.7(4)	C(17)–C(18)–C(19)–C(20)	–0.4(8)
F(1)–C(18)–C(19)–C(20)	178.4(4)	C(18)–C(19)–C(20)–C(15)	–2.2(7)
C(14)–C(15)–C(20)–C(19)	–178.7(4)	C(16)–C(15)–C(20)–C(19)	3.0(7)
C(25)–N(4)–C(21)–N(3)	–179.5(4)	C(25)–N(4)–C(21)–C(22)	2.1(7)
C(13)–N(3)–C(21)–N(4)	–52.1(5)	C(13)–N(3)–C(21)–C(22)	126.3(5)
C(14)–N(3)–C(21)–N(4)	132.1(5)	C(14)–N(3)–C(21)–C(22)	–49.5(7)
N(3)–C(21)–C(22)–C(23)	178.6(4)	N(4)–C(21)–C(22)–C(23)	–3.2(7)
C(21)–C(22)–C(23)–C(24)	2.2(7)	C(22)–C(23)–C(24)–C(25)	–0.3(7)
C(21)–N(4)–C(25)–C(24)	–0.1(7)	C(23)–C(24)–C(25)–N(4)	–0.8(8)
C(26)–O(3)–C(27)–C(28)	9.8(7)	C(26)–O(3)–C(27)–C(32)	–168.8(4)
O(3)–C(27)–C(28)–C(29)	–176.9(5)	C(32)–C(27)–C(28)–C(29)	1.6(7)
C(27)–C(28)–C(29)–C(30)	0.9(8)	C(28)–C(29)–C(30)–C(31)	–2.2(8)
C(29)–C(30)–C(31)–C(32)	1.1(8)	C(30)–C(31)–C(32)–N(5)	177.6(5)
C(30)–C(31)–C(32)–C(27)	1.2(8)	C(33)–N(5)–C(32)–C(27)	159.6(4)
C(33)–N(5)–C(32)–C(31)	–16.6(7)	C(35)–N(5)–C(32)–C(27)	–69.0(6)
C(35)–N(5)–C(32)–C(31)	114.7(5)	O(3)–C(27)–C(32)–N(5)	–0.4(6)
O(3)–C(27)–C(32)–C(31)	176.0(4)	C(28)–C(27)–C(32)–N(5)	–179.1(4)
C(28)–C(27)–C(32)–C(31)	–2.6(7)	C(32)–N(5)–C(33)–C(34)	

−165.0(4)

C(35)–N(5)–C(33)–C(34)	61.0(5)	C(36)–N(6)–C(34)–C(33)	59.4(5)
C(37)–N(6)–C(34)–C(33)	−179.4(4)	N(5)–C(33)–C(34)–N(6)	−61.5(5)
C(32)–N(5)–C(35)–C(36)	165.6(4)	C(33)–N(5)–C(35)–C(36)	−59.5(5)
C(34)–N(6)–C(36)–C(35)	−57.2(5)	C(37)–N(6)–C(36)–C(35)	

−177.9(4)

N(5)–C(35)–C(36)–N(6)	58.3(5)	C(34)–N(6)–C(37)–C(38)	84.6(5)
C(36)–N(6)–C(37)–C(38)	−155.6(4)	C(39)–N(7)–C(38)–C(37)	90.8(5)
C(46)–N(7)–C(38)–C(37)	−86.7(5)	N(6)–C(37)–C(38)–N(7)	−171.8(4)
C(38)–N(7)–C(39)–O(4)	−7.9(6)	C(38)–N(7)–C(39)–C(40)	172.5(4)
C(46)–N(7)–C(39)–O(4)	169.4(4)	C(46)–N(7)–C(39)–C(40)	−10.3(7)
O(4)–C(39)–C(40)–C(41)	133.9(5)	O(4)–C(39)–C(40)–C(45)	

−43.7(6)

N(7)–C(39)–C(40)–C(41)	−46.4(7)	N(7)–C(39)–C(40)–C(45)	135.9(4)
C(39)–C(40)–C(41)–C(42)	−178.1(5)	C(45)–C(40)–C(41)–C(42)	−0.5(7)
C(40)–C(41)–C(42)–C(43)	−2.3(8)	C(41)–C(42)–C(43)–F(2)	

−176.5(5)

C(41)–C(42)–C(43)–C(44)	2.8(8)	F(2)–C(43)–C(44)–C(45)	178.8(4)
C(42)–C(43)–C(44)–C(45)	−0.5(8)	C(43)–C(44)–C(45)–C(40)	−2.4(7)
C(39)–C(40)–C(45)–C(44)	−179.4(4)	C(41)–C(40)–C(45)–C(44)	2.9(7)
C(50)–N(8)–C(46)–N(7)	−179.8(4)	C(50)–N(8)–C(46)–C(47)	2.1(7)
C(38)–N(7)–C(46)–N(8)	−50.9(5)	C(38)–N(7)–C(46)–C(47)	127.2(5)
C(39)–N(7)–C(46)–N(8)	131.8(4)	C(39)–N(7)–C(46)–C(47)	−50.1(7)
N(7)–C(46)–C(47)–C(48)	178.4(4)	N(8)–C(46)–C(47)–C(48)	−3.6(7)
C(46)–C(47)–C(48)–C(49)	1.9(7)	C(47)–C(48)–C(49)–C(50)	1.1(8)
C(46)–N(8)–C(50)–C(49)	1.1(7)	C(48)–C(49)–C(50)–N(8)	−2.7(8)
C(51)–O(5)–C(52)–C(53)	−8.8(7)	C(51)–O(5)–C(52)–C(57)	168.9(4)
O(5)–C(52)–C(53)–C(54)	176.2(5)	C(57)–C(52)–C(53)–C(54)	−1.4(7)
C(52)–C(53)–C(54)–C(55)	0.2(8)	C(53)–C(54)–C(55)–C(56)	0.2(8)
C(54)–C(55)–C(56)–C(57)	0.7(8)	C(55)–C(56)–C(57)–N(9)	

−177.6(4)

C(55)–C(56)–C(57)–C(52)	−1.9(7)	C(58)–N(9)–C(57)–C(52)	

−159.2(4)

C(58)–N(9)–C(57)–C(56)	16.5(6)	C(61)–N(9)–C(57)–C(52)	69.2(6)
C(61)–N(9)–C(57)–C(56)	−115.1(5)	O(5)–C(52)–C(57)–N(9)	0.3(6)
O(5)–C(52)–C(57)–C(56)	−175.5(4)	C(53)–C(52)–C(57)–N(9)	178.1(4)
C(53)–C(52)–C(57)–C(56)	2.3(7)	C(57)–N(9)–C(58)–C(59)	167.1(4)
C(61)–N(9)–C(58)–C(59)	−58.9(5)	C(60)–N(10)–C(59)–C(58)	

−57.1(5)

C(62)–N(10)–C(59)–C(58)	−179.4(4)	N(9)–C(58)–C(59)–N(10)	58.6(5)
C(59)–N(10)–C(60)–C(61)	56.1(5)	C(62)–N(10)–C(60)–C(61)	
	177.6(4)		
C(57)–N(9)–C(61)–C(60)	−164.2(4)	C(58)–N(9)–C(61)–C(60)	60.6(5)
N(10)–C(60)–C(61)–N(9)	−58.5(5)	C(59)–N(10)–C(62)–C(63)	

−84.0(5)

C(60)–N(10)–C(62)–C(63)	154.5(4)	C(64)–N(11)–C(63)–C(62)	

–89.4(5)			
C(71)–N(11)–C(63)–C(62)	86.6(5)	N(10)–C(62)–C(63)–N(11)	172.5(4)
C(63)–N(11)–C(64)–O(6)	6.1(6)	C(63)–N(11)–C(64)–C(65)	–172.9(4)
C(71)–N(11)–C(64)–O(6)	–169.6(4)	C(71)–N(11)–C(64)–C(65)	11.4(7)
O(6)–C(64)–C(65)–C(66)	42.8(6)	O(6)–C(64)–C(65)–C(70)	–132.2(5)
N(11)–C(64)–C(65)–C(66)	–138.2(4)	N(11)–C(64)–C(65)–C(70)	46.7(7)
C(64)–C(65)–C(66)–C(67)	179.7(4)	C(70)–C(65)–C(66)–C(67)	–5.1(7)
C(65)–C(66)–C(67)–C(68)	2.1(7)	C(66)–C(67)–C(68)–F(3)	–178.8(4)
C(66)–C(67)–C(68)–C(69)	1.7(8)	F(3)–C(68)–C(69)–C(70)	178.1(4)
C(67)–C(68)–C(69)–C(70)	–2.5(8)	C(64)–C(65)–C(70)–C(69)	179.2(4)
C(66)–C(65)–C(70)–C(69)	4.3(7)	C(68)–C(69)–C(70)–C(65)	–0.6(8)
C(75)–N(12)–C(71)–N(11)	179.3(4)	C(75)–N(12)–C(71)–C(72)	–1.8(7)
C(63)–N(11)–C(71)–N(12)	51.8(5)	C(63)–N(11)–C(71)–C(72)	–127.0(5)
C(64)–N(11)–C(71)–N(12)	–132.5(5)	C(64)–N(11)–C(71)–C(72)	48.6(6)
N(11)–C(71)–C(72)–C(73)	–177.8(4)	N(12)–C(71)–C(72)–C(73)	3.5(7)
C(71)–C(72)–C(73)–C(74)	–2.2(7)	C(72)–C(73)–C(74)–C(75)	–0.4(7)
C(71)–N(12)–C(75)–C(74)	–1.1(7)	C(73)–C(74)–C(75)–N(12)	2.2(8)

Appendix: B Advion NanoTek reaction optimisation; isotopic exchange reactions

Target precursor concentration in DMSO mg/mL	Reaction Temperature (ºC)	Stoichiometry (Precursor: [^{18}F]fluoride)	Flow rate (µL/min)	Reactor length (m)	Radiochemical yield (%)
18	190	1	5	4	0
18	190	1	5	4	0
18	190	1	5	4	0
18	190	1	5	4	0
18	190	1	5	4	0
18	190	1	5	4	0
20	190	1	5	4	12.46
20	190	1	5	4	17.61
20	190	1	5	4	19.98
20	190	1	5	4	0
20	190	1	5	4	0
20	190	1	5	4	21.52
20	190	1	5	4	10.15
20	190	1	5	4	36.76
20	190	1	5	4	14.69
20	190	1	5	4	20.6
20	190	1	5	4	0
20	190	1	5	4	0
20	190	1	5	4	0
20	190	1	5	4	0
20	190	1	5	4	0
20	190	1	5	4	0
20	190	1	5	4	0
21	190	1	5	4	2.14
21	190	1	5	4	2.94
21	190	1	5	4	0
20	200	1	5	4	0
20	200	1	5	4	0
20	190	1	10	4	21.18
20	190	1	10	4	0
20	200	1	10	4	0
18	190	1	30	4	0
20	190	1	30	4	0
20	190	1	30	4	0
20	190	1	30	4	0
21	190	1	30	4	0
21	190	1	30	4	0
10	100	0.1	50	8	0
10	110	0.5	10	8	0

Target precursor concentration in DMSO mg/mL	Reaction Temperature (ºC)	Stoichiometry (Precursor: [^{18}F]fluoride)	Flow rate (µL/min)	Reactor length (m)	Radiochemical yield (%)
10	110	1	10	8	0
18	190	0.5	5	8	12.74
18	190	0.5	5	8	12.92
18	190	0.5	5	8	12.27
25	190	0.5	5	8	7.85
25	190	0.5	5	8	9.66
25	190	0.5	5	8	0
				8	
10	190	1	5	8	0
18	190	1	5	8	11.37
18	190	1	5	8	19.35
18	190	1	5	8	15.32
18	190	1	5	8	16.07
18	190	1	5	8	12.17
25	190	1	5	8	8.38
25	190	1	5	8	7.47
25	190	1	5	8	6.31
10	190	0.5	10	8	0
10	190	0.5	10	8	0
10	190	1	10	8	0
21	190	1	10	8	4.52
21	190	1	10	8	0
21	190	1	10	8	0
21	190	1	10	8	5.67
21	190	1	10	8	0
23	190	1	10	8	0
23	190	1	10	8	4.45
23	190	1	10	8	5.54
23	190	1	10	8	3.79
23	190	1	15	8	5.15
23	190	1	15	8	5.23
23	190	1	15	8	4.04
23	190	1	20	8	5.84
23	190	1	20	8	5.88
23	190	1	20	8	4.41
25	190	1	20	8	16.81
25	190	1	20	8	0
23	190	1	25	8	4.15
23	190	1	25	8	4.41
23	190	1	25	8	4.06
10	190	1	30	8	0

Target precursor concentration in DMSO mg/mL	Reaction Temperature (ºC)	Stoichiometry (Precursor: [^{18}F]fluoride)	Flow rate (µL/min)	Reactor length (m)	Radiochemical yield (%)
10	190	1	30		0
10	190	1	30	8	0
18	190	1	30	8	0
21	190	1	30	8	0
23	190	1	30	8	3.59
23	190	1	30	8	3.98
23	190	1	30	8	0
23	190	1	30	8	0
25	190	1	30	8	0
25	190	1	30	8	10.36
25	190	1	30	8	12.17
10	190	2	10	8	0
18	190	2	5	8	13.52
10	200	0.1	50	8	0
10	200	1	5	8	0

Appendix: C Advion NanoTek reaction optimisation; Fluorodenitration reactions

Target precursor concentration in DMSO	Reaction Temperature (ºC)	Stoichiometry (Precursor: [^{18}F]fluoride)	Flow rate (µL/min)	Reactor length (m)	Radiochemical yield (%)
10	190	0.1	10	4	0
10	190	0.1	35	4	0
10	190	0.2	10	4	0
10	190	0.5	10	4	0
10	190	1	30	4	0
10	190	1	30	4	0
10	190	1	30	4	0
10	190	1	30	4	0
10	170	1	5	8	8.42
10	190	0.1	10	8	0
10	190	0.5	10	8	0
10	190	1	10	8	0
10	190	1	5	8	6.61
10	190	1	5	8	5.01
10	190	1	5	8	5.57
10	190	1	5	8	13.07
10	190	1	5	8	16.07
10	190	1	5	8	0
10	190	1	30	8	0
10	190	1	30	8	0
10	190	1	30	8	0
10	190	1	30	8	0
10	190	1	30	8	0
10	200	1	5	8	21.00
10	200	1	5	8	24.95
10	200	1	5	8	30.99

Appendix: D Eckert and Ziegler ModularLab reaction optimisation;

Fluorodenitration reactions

No.	Precursor	Reaction solvent	Solvent Volume (mL)	Microwave settings; Time (s)	Microwave settings; Power (W)	Microwave settings; Temperature (^{0}C)	Radio-chemical yield (%)
1	4-MPPNO$_2$	DMF	1.0	150	50	120	4.88
	4-MPPNO$_2$	DMF	1.0	150	50	120	3.74
	4-MPPNO$_2$	DMF	1.0	150	50	120	5.50
	4-MPPNO$_2$	DMF	1.0	150	50	120	4.50
	4-MPPNO$_2$	DMF	1.0	150	50	120	4.50
	4-MPPNO$_2$	DMF	1.0	150	50	120	3.97
	4-MPPNO$_2$	DMF	1.0	150	50	120	4.86
	4-MPPNO$_2$	DMF	1.0	150	50	120	5.46
	4-MPPNO$_2$	DMF	1.0	150	50	120	4.67
	4-MPPNO$_2$	DMF	1.0	150	50	120	4.54
	4-MPPNO$_2$	DMF	1.0	150	50	120	0.00
	Mean RCY:						**4.66**
2	4-MPPNO$_2$	DMF	1.0	150	70	120	4.20
3	4-MPPNO$_2$	DMF	1.0	150 ,150	50, 50	120, 120	3.58
	4-MPPNO$_2$	DMF	1.0	150 ,150	50, 50	120, 120	4.27
	Mean RCY:						**3.93**
4	4-MPPNO$_2$	DMF	0.5	150	100	140	4.89
	4-MPPNO$_2$	DMF	0.5	150	100	140	8.50
	Mean RCY:						**6.70**
5	4-MPPNO$_2$	DMSO	1.0	200	100	180	5.67
6	4-MPPNO$_2$	DMSO	0.5	100	70	165	5.86
7	4-MPPNO$_2$	DMSO	0.5	100,100	70,100	165,165	20.62
	4-MPPNO$_2$	DMSO	0.5	100,100	70,100	165,165	15.50
	4-MPPNO$_2$	DMSO	0.5	100,100	70,100	165,165	8.22
	Mean RCY:						**14.78**
8	4-MPPNO$_2$	DMSO (Al_2O_3)	0.5	100,100,100, 100,100,100	70,70,70,100 100,100	165,165,165, 165,165, 165	24.67
	4-MPPNO$_2$	DMSO (Al_2O_3)	0.5	100,100,100, 100,100,100	70,70,70,100 100,100	165,165,165, 165,165, 165	25.99
	4-MPPNO$_2$	DMSO (Al_2O_3)	0.5	100,100,100, 100,100,100	70,70,70,100 100,100	165,165,165, 165,165, 165	13.30
	Mean RCY:						**21.32**
9	4-MPPNO$_2$	DMSO (Al_2O_3)	0.5	100,100,100, 100	100,100,70, 70	175,175,170, 170	18.78
	4-MPPNO$_2$	DMSO (Al_2O_3)	0.5	100,100,100, 100	100,100,70, 70	175,175,170, 170	23.67
	4-MPPNO$_2$	DMSO (Al_2O_3)	0.5	100,100,100, 100	100,100,70, 70	175,175,170, 170	24.48
	Mean RCY:						**22.31**
	Final conditions						**Mean**
10	4-MPPNO$_2$	DMSO (Al_2O_3)	0.5	100,100,100, 100	100,100,70, 70	175,175,175, 175	33.48 (n = 36)

References

Advion Biosciences Ltd, Ithaca, New York. http://www.advion.com/products/nanotek/.

ALSTRUP, A., K., & SMITH, D., F. 2013. Anaesthesia for positron emission tomography scanning of animal brains. *Laboratory Animals,* 47**,** 12.

ARANGO, V., UNDERWOOD, M. D., GUBBI, A. V. & MANN, J. J. 1995. Localized alterations in pre- and postsynaptic serotonin binding sistes in the ventrolateral prefrontal cortex of suicide victims. *Brain Research,* 688**,** 121-133.

ASBERG, M., THOREN, P., TRASKMAN, L., BERTILSSON, L. & RINGBERGER, V. 1976. 'Serotonin depression' A biochemical subgroup within the affective disorders? *Science,* 191**,** 478-480.

AZNAVOUR, N., BENKELFAT, C., GRAVEL, P., ALIAGA, A., ROSA-NETO, P., BEDELL, B., ZIMMER, L., DESCARRIES, L., 2009. MicroPET imaging of 5-HT_{1A} receptors in rat brain: a test-retest [^{18}F]MPPF study. *European Journal of Nuclear Medicine and Molecular Imaging,* 36**,** 53-62.

AZNAVOUR, N., RBAH, L., RIAD, M., REILHAC, A., COSTES, N., DESCARRIES, L. & ZIMMER, L. 2006. A PET imaging study of 5-HT1A receptors in cat brain after acute and chronic fluoxetine treatment. *NeuroImage,* 33**,** 834-842.

AZNAVOUR, N. & ZIMMER, L. 2007. [18F]MPPF as a tool for the in vivo imaging of 5-HT1A receptors in animal and human brain. *Neuropharmacology,* 52**,** 695-707.

BALLANGER, B., KLINGER, H., ECHE, J., LEROND, J., VALLET, A. E., LE BARS, D., TREMBLAY, L., SGAMBATO-FAURE, V., BROUSSOLLE, E. & THOBOIS, S. 2012. Role of serotonergic 1A receptor dysfunction in depression associated with Parkinson's disease. *Movement Disorders,* 27**,** 84-89.

BARS, D. L., LEMAIRE, C., GINOVART, N., PLENEVAUX, A., AERTS, J., BRIHAYE, C., HASSOUN, W., LEVIEL, V., MEKHSIAN, P., WEISSMAN, D., PUJOL, J. F., LUXEN, A. & COMAR, D. 1998. High-Yield Radiosynthesis and Preliminary In Vivo Evaluation of p-[18F]MPPF, a Fluoro Analog of WAY-100635. *Nuclear Medicine & Biology,* 25**,** 343-350.

BARTMANN, H., FUEST, C., LA FOUGERE, C., XIONG, G., JUST, T., SCHLICHTIGER, J., WINTER, P., BONING, G., WANGLER, B., PEKCEC, A., SOERENSEN, J., BARTENSTEIN, P., CUMMING, P. & POTSCHKA, H. 2010. Imaging of P-glycoprotein–mediated pharmacoresistance in the hippocampus: Proof-of-concept in a chronic rat model of temporal lobe epilepsy. *Epilepsia,* 51**,** 1780-1790.

BILLARD, T., LE BARS, D. & ZIMMER, L. 2014. PET radiotracers for molecular imaging of serotonin 5-HT1A receptors. *Current Medicinal Chemistry,* 21**,** 70-81.

BLOM, E., KARIMI, F. & LÅNGSTRÖM, B. 2009. [18F]/19F exchange in fluorine containing compounds for potential use in 18F-labelling strategies. *Journal of Labelled Compounds and Radiopharmaceuticals* 52**,** 504-511.

BOLDRINI, M., UNDERWOOD, M. D., MANN, J. J. & ARANGO, V. 2008. Serotonin-1A autoreceptor binding in the dorsal raphe nucleus of depressed suicides. *Journal of Psychiatric Research,* 42**,** 433-442.

BREIER, A., SU, T., P., , SAUNDERS, R., CARSON, R., E., , KOLACHANA, B., S., , DE BARTOLOMEIS, A., WEINBERGER, D., R.,, WEISENFELD, N., MALHOTRA, A., K., , ECKELMAN, W., C., & PICKAR, D. 1997. Schizophrenia is associated with elevated amphetamine-induced synaptic dopamine concentrations: evidence from a novel positron emission tomography method. *Proceedings of the National Academy of Sciences.,* 94**,** 2569-74.

CAI, L., LU, S. & PIKE, V. W. 2008. Chemistry with [18F]fluoride ion *European Journal of Organic Chemistry,* 17**,** 2853-2873.

CARROLL, M. A. & WOOD, R. A. 2007. Arylation of anilines: formation of diarylamines using diaryliodonium salts. *Tetrahedron,* 63**,** 11349-11354.

CHEFER, V. I., THOMPSON, A. C., ZAPATA, A. & SHIPPENBERG, T. S. 2009. Overview of Brain Microdialysis. *Current Protocols in Neuroscience,* 47**,** 7.1.1–7.1.28.

CHUN, J.-H., LU, S., LEE, Y.-S. & PIKE, V. W. 2010. Fast and high-yield microreactor syntheses of ortho -substituted [^{18}F]Fluoroarenes from reactions of [^{18}F]Fluoride ion with diaryliodonium salts. *Journal of Organic Chemistry,* 75**,** 3332-3338.

CLIFFE, I. A. 2000. A retrospect on the discovery of WAY-100635 and the prospect for improved 5-HT(1A) receptor PET radioligands *Nuclear Medicine and Biology* 27**,** 441-447.

COSTES, N., MERLET, I., OSTROWSKY, K., FAILLENOT, I., LAVENNE, F., ZIMMER, L., RYVLIN, P. & LE BARS, D. 2005. A 18F-MPPF PET Normative Database of 5-HT1A Receptor Binding in Men and Women Over Aging. *Journal of Nuclear Medicine,* 46**,** 1980-1989.

COSTES, N., ZIMMER, L., REILHAC, A., LAVENNE, F., RYVLIN, P., LE BARS, D. 2007. Test–Retest Reproducibility of 18F-MPPF PET in Healthy Humans: A Reliability Study. *Journal of Nuclear Medicine,* 48**,** 1279-1288.

DEMARQUAY, G., LOTHE, A., ROYET, J. P., COSTES, N., MICK, G., MAUGUIÈRE, F. & RYVLIN, P. 2011. Brainstem changes in 5-HT 1A receptor availability during migraine attack. *Cephalalgia,* 31**,** 84-94.

DERRY, C., BENJAMIN, C., BLADIN, P., LE BARS, D., TOCHON-DANGUY, H., BERKOVIC, S., ZIMMER, L., COSTES, N., MULLIGAN, R. & REUTENS, D. 2006. Increased serotonin receptor availability in human sleep: Evidence from an [18F]MPPF PET study in narcolepsy. *NeuroImage,* 30**,** 341-348.

DESBREE, A., VERDURAND, M., GODART, J., DUBOIS, A., MASTRIPPOLITO, R., PAIN, F., PINOT, L., DELZESCAUX, T., GURDEN, H., ZIMMER, L. & LANI`ECE, P. 2008. The Potential of a Radiosensitive Intracerebral Probe to Monitor 18F-MPPF Binding in Mouse Hippocampus In Vivo. *Journal of Nuclear Medicine,* 49**,** 1155-1161.

DETKE, M. J., WIELAND, S. & LUCKI, I. 1995. Blockade of the antidepressant-like effects of 8-OH-DPAT, buspirone and desipramine in the rat forced swim test by 5HT1A receptor antagonists. *Psychopharmacology,* 119**,** 47-54.

DIDELOT, A., RYVLIN, P., LOTHE, A., MERLET, I., HAMMERS, A. & MAUGUIÈRE, F. 2008. PET imaging of brain 5-HT1A receptors in the preoperative evaluation of temporal lobe epilepsy. *Brain,* 131**,** 2751-2764.

DREVETS, W. C., FRANK, E., PRICE, J. C., KUPFER, D. J., GREER, P. J. & MATHIS, C. 2000. Serotonin type-1A receptor imaging in depression. *Nuclear Medicine and Biology,* 27**,** 499-507.

DUNCAN, M. J. & HENSLER, J. G. 2002. Aging alters in a region-specific manner serotonin transporter sites and 5-HT1A receptor-G protein interactions in hamster brain. *Neuropharmacology,* 43**,** 36-44.

ELSINGA, P. H., HENDRIKSE, N. H., BART, J., VAN WAARDE, A. & VAALBURG, W. 2005 Positron Emission Tomography Studies on Binding of Central Nervous System Drugs and P-Glycoprotein Function in the Rodent Brain. *Academy of Molecular Imaging* 7**,** 37-44.

ERSPAMER, V. 1986. Historical introduction: the Italian contribution to the discovery of 5-hydroxytryptamine (enteramine, serotonin). *Journal of hypertension. Supplement : official journal of the International Society of Hypertension,* 4**,** S3-5.

FUMITA, M. & INNIS, R. B. 2002. *In vivo Molecular Imaging: Ligand Development and Research Applications*, American College of Neuropsychopharmacology.

GÁL, E. M., ROGGEVEEN, A. E. & MILLARD, S. A. 1970. DL-[2-14C]p-chlorophenylalanine as an inhibitor of tryptophan 5-hydroxylase. *Journal of Neurochemistry,* 17**,** 1221-1235.

GALUSCA, B., COSTES, N., ZITO, N. G., PEYRON, R., BOSSU, C., LANG, F., LE BARS, D. & ESTOUR, B. 2008. Organic Background of Restrictive-Type Anorexia Nervosa Suggested by Increased Serotonin1A Receptor Binding in Right Frontotemporal Cortex of Both Lean and Recovered Patients: [18F]MPPF PET Scan Study. *Biological Psychiatry,* 64**,** 1009-1013.

GARCIA-ALLOZA, M. & BACSKAI, B. J. 2004. Techniques for brain imaging *in vivo. NeuroMolecular Medicine,* 6**,** 65-78.

GINOVART, N., HASSOUN, W., LE BARS, D., WEISSMANN, D. & LEVIEL, V. 2000. *In Vivo* Characterization of p-[^{18}F]MPPF, a Fluoro Analog of WAY-100635 forVisualization of 5-HT1A Receptors. *Synapse,* 35**,** 192-200.

GOZLAN, H., THIBAULT, S., LAPORTE, A. M., LIMA, L. & HAMON, M. 1995. The selective 5-HT1A antagonist radioligand [3H]WAY 100635 labels both G-protein-coupled and free 5-HT1A receptors in rat brain membranes. *European Journal of Pharmacology - Molecular Pharmacology Section,* 288**,** 173-86.

GREEN, A., R. 2006. Neuropharmacology of 5-hydroxytryptamine. *British Journal of Pharmacology,* 147**,** Suppl 1:S145-52.

HADDJERI, N., BLIER, P. & DE MONTIGNY, C. 1998. Long-term antidepressant treatments result in a tonic activation of forebrain 5-HT(1A) receptors. *Journal of Neuroscience,* 18**,** 10150-10156.

HAYASHI, K., FURUTSUKA, K., ITO, T., MUTO, M., AKI, H., FUKUMURA, T. & SUZUKI, K. 2012. Fully automated synthesis and purification of 4-(2'-methoxyphenyl)-1-[2'-(N-2"-pyridinyl)-p-[18F]fluorobenzamido]ethylpiperazine. *Journal of Labelled Compounds and Radiopharmaceuticals,* 55**,** 120-124.

HEISLER, L., K. , CHU, H. & TECOTT, L., H. 1998. Elevated anxiety and antidepressant-like responses in serotonin 5-HT1A receptor mutant mice. *Proceedings of the National Academy of Sciences,* 95**,** 15049–15054.

HIRVONEN, J., KARLSSON, H., KAJANDER, J., LEPOLA, A., MARKKULA, J., RASI-HAKALA, H., NÅGREN, K., SALMINEN, J. K. & HIETALA, J. 2008. Decreased brain serotonin 5-HT1A receptor availability in medication-naive patients with major depressive disorder: An in-vivo imaging study using PET and [carbonyl-11C]WAY-100635. *International Journal of Neuropsychopharmacology,* 11**,** 465-476.

HUISMAN, M. C., REDER, S., WEBER, A. W., ZIEGLER, S. I. & SCHWAIGER, M. 2007. Performance evaluation of the Philips MOSAIC small animal PET scanner. *Eur J Nucl Med Mol Imaging,* 34**,** 532–540

JAGODA, E. M., LANG, L., TOKUGAWA, J., SIMMONS, A., MA, Y., CONTOREGGI, C., KIESEWETTER, D. & ECKELMAN, W. C. 2006. Development of 5-HT1A receptor radioligands to determine receptor density and changes in endogenous 5-HT *Synapse,* 59**,** 330-341.

JAIN, K. K. 2002. Neuropharmacology: Molecular Neuropharmacology: A foundation for clinical neuroscience. *Trends in Pharmacological Sciences,* 23**,** 99.

JONES, B., J., & BLACKBURN, T., P. 2002. The medical benefit of 5-HT research. *Pharmacology Biochemistry & Behavior,* 71**,** 555-68.

KEPE, V., BARRIO, J. R., HUANG, S. C., ERCOLI, L., SIDDARTH, P., SHOGHI-JADID, K., COLE, G. M., SATYAMURTHY, N., CUMMINGS, J. L., SMALL, G. W. & PHELPS, M. E. 2006. Serotonin 1A receptors in the living brain of Alzheimer's disease patients. *Proceedings of the National Academy of Sciences of the United States of America,* 103**,** 702-707.

KHAWAJA, X. 1995. Quantitative autoradiographic characterisation of the binding of [^{3}H]WAY-100635, a selective 5-HT1A receptor antagonist. *Brain Research,* 673**,** 217-225.

KOIVULA, T., LAINE, J., LIPPONEN, T., PERHOLA, O., KAMARAINEN, E., BERGSTROM, K. & SOLIN, O. 2010. Assessment of labelled products with different radioanalytical methods: study on ^{18}F-fluorination reaction of 4-[^{18}F]fluoro-N-[2-[1-(2-methoxyphenyl)-1-piperazinyl]ethyl-N-2-pyridinyl-benzamide (*p*-[^{18}F]MPPF) *Journal of Radioanalytical and Nuclear Chemistry,* 286**,** 841-846.

KUMAR, J. S. D. & MANN, J. J. 2007. PET tracers for 5-HT1A receptors and uses thereof *Drug Discovery Today* 12**,** 748-756.

KUNG, H. F., FREDERICK, D., KIM, H.-J., MCELGIN, W., KUNG, M.-P., MU, M., MOZLEY, P. D., VESSOTSKIE, J. M. B., STEVENSON, D. A. A., KUSHNER, S. A. A. & ZHUANG, Z.-P. 1996a. In vivo SPECT imaging of 5-HT_{1A} receptors with [123I]p-MPPI in nonhuman primates. *Synapse* 24**,** 273-281.

KUNG, H. F., STEVENSON, D. A., ZHUANG, Z.-P., KUNG, M.-P., FREDERICK, D. & HURT, S. D. 1996b. New 5-HT(1A) receptor antagonist: [^{3}H]p-MPPF. ! *Synapse,* 23**,** 344-346.

KUNG, H. F., STEVENSON, D. A., ZHUANG, Z. P., KUNG, M. P., FREDERICK, D. & HURT, S. D. 1996c. New 5-HT(1A) receptor antagonist: [3H]p-MPPF. *Synapse,* 23**,** 344-346.

KUNG, M. P., FREDERICK, D., MU, M., ZHUANG, Z. P. & KUNG, H. F. 1995. 4-(2'-Methoxy-phenyl)-1-[2'-(n-2"-pyridinyl)-p-iodobenzamido]-ethyl- piperazine ([^{125}I]p-MPPI) as a new selective radioligand of serotonin-$_{1A}$ sites in rat brain: in vitro binding and autoradiographic studies. . *The Journal of Pharmacology and Experimental Therapeutics* 272 429-437

KUSSEROW, H., DAVIE, S. B., HÖRTNAGL, H., VOIGT, I., STROH, T., , BERT, B., DENG, D., R., , FINK, H., VEH, R., W., & THEURING, F. 2004. Reduced anxiety-related behaviour in transgenic mice overexpressing serotonin 1A receptors. *Molecular Brain Research,* 129**,** 104-116.

LAĆAN, G., PLENEVAUX, A., RUBINS, D. J., WAY, B. M., DEFRAITEUR, C., LEMAIRE, C., AERTS, J., LUXEN, A., CHERRY, S. R. & MELEGA, W. P. 2008. Cyclosporine, a P-glycoprotein modulator, increases [^{18}F]MPPF uptake in rat brain and peripheral tissues: microPET and ex vivo studies. *Eur J Nucl Med Mol Imaging,* 35.

LANDRY, M. & DI PAOLO, T. 2003. Effect of chronic estradiol, tamoxifen or raloxifene treatment on serotonin 5-HT receptor 1A. *Molecular Brain Research,* 112**,** 82-89.

LANG, L., JAGODA, E., SCHMALL, B., VUONG, B.-K., ADAMS, H. R., NELSON, D. L., CARSON, R. E. & ECKELMAN, W. C. 1999. Development of fluorine-18-labeled 5-HT(1A) antagonists *Journal of Medicinal Chemistry* 42**,** 1576-1586.

LARUELLE, M. 2000. Imaging synaptic neurotransmission with in vivo binding competition techniques: a critical review. *Journal of Cerebral Blood Flow & Metabolism,* 20**,** 423-451.

LARUELLE, M., ABI-DARGHAM, A., GIL, R., KEGELES, L. & INNIS, R. 1999. Increased dopamine transmission in schizophrenia: relationship to illness phases. *Biological Psychiatry,* 46**,** 56-72.

LEMOINE, L., VERDURAND, M., VACHER, B., BLANC, E., LE BARS, D., NEWMAN-TANCREDI, A. & ZIMMER, L. 2010. F15599, a novel 5-HT1A receptor agonist, as a radioligand for PET neuroimaging *European Journal of Nuclear Medicine and Molecular Imaging* 37**,** 594-605.

LEROND, J., LOTHE, A., RYVLIN, P., BOUVARD, S., D'AMATO, T., CIUMAS, C., DALÉRY, J., POULET, E. & SAOUD, M. 2013. Effects of aripiprazole, risperidone, and olanzapine on 5-HT1A receptors in patients with schizophrenia. *Journal of Clinical Psychopharmacology,* 33**,** 84-89.

LESCH, K., P. & GUTKNECHT, L. 2004. Focus on The 5-HT^{1A} receptor: emerging role of a gene regulatory variant in psychopathology and pharmacogenetics. *The International Journal of Neuropsychopharmacology,* 7**,** 381-385.

LEVIN, C., S. & ZAIDI, H. 2007. Current Trends in Preclinical PET System Design. *PET Clinics,* 2**,** 125-160.

LEWIS, S. A., OSWALD, I. & DUNLEAVY, D. L. 1971. Chronic fenfluramine administration: some cerebral effects. *British Medical Journal,* 3**,** 67-70.

LOTHE, A., DIDELOT, A., HAMMERS, A., COSTES, N., SAOUD, M., GILLIAM, F. & RYVLIN, P. 2008a. Comorbidity between temporal lobe epilepsy and depression: A [18F]MPPF PET study. *Brain,* 131**,** 2765-2782.

LOTHE, A., MERLET, I., DEMARQUAY, G., COSTES, N., RYVLIN, P. & MAUGUIÈRE, F. 2008b. Interictal brain 5-HT1A receptors binding in migraine without aura: A 18F-MPPF-PET study. *Cephalalgia,* 28**,** 1282-1291.

LOTHE, A., SAOUD, M., BOUVARD, S., REDOUTÉ, J., LEROND, J. & RYVLIN, P. 2012. 5-HT1A receptor binding changes in patients with major depressive disorder before and after antidepressant treatment: A pilot [18F]MPPF positron emission tomography study. *Psychiatry Research - Neuroimaging,* 203**,** 103-104.

MATSUBARA, S., ARORA, R. C. & MELTZER, H. Y. 1991. Serotonergic measures in suicide brain: 5-HT1A binding sites in frontal cortex of suicide victims. *Journal of Neural Transmission,* 85**,** 181-194.

MCCARDLE, C., E. & GARTSIDE, S., E. 2012. Effects of general anaesthetics on 5-HT neuronal activity in the dorsal raphe nucleus. *Neuropharmacology* 62**,** 1787-1796.

MCCARRON, J. A., PIKE, V. W., HALLDIN, C., SANDELL, J., SÓVÁGÓ, J., GULYAS, B., CSELÉNYI, Z., WIKSTROM., H. V., MARCHAIS-OBERWINKLER, S. C., NOWICKI, B. C., DOLLÉ, F. & FARDE, L. 2004. The Pyridinyl-6 position of WAY-100635 as a site for radiofluorination - Effect on 5-HT1A receptor radioligand behavior in vivo *Molecular Imaging and Biology,* 6**,** 17-26.

MEDISO. Available: http://www.medisousa.com/preclinical/nanoscan/pet-ct.

MERLET, I., OSTROWSKY, K., COSTES, N., RYVLIN, P., ISNARD, J., FAILLENOT, I., LAVENNE, F., DUFOURNEL, D., LE BARS, D., MAUGUIE, F. 2004. 5-HT1A receptor binding and intracerebral activity in temporal lobe epilepsy: an [18F]MPPF-PET study. *Brain,* 127**,** 900-913.

MERLET, I., RYVLIN, P., COSTES, N., DUFOURNEL, D., ISNARD, J., FAILLENOT, I., OSTROWSKY, K., LAVENNE, F., LE BARS, D. & MAUGUIEREA, F. 2004. Statistical parametric mapping of 5-HT1A receptor binding in temporal lobe epilepsy with hippocampal ictal onset onintracranial EEG. *NeuroImage* 22**,** 886-896.

MILLER, P. W., LONG, N. J., VILAR, R. & GEE, A. D. 2008. Synthesis of11C, 18F, 15O, and 13N radiolabels for positron emission tomography *Angewandte Chemie - International Edition* 47**,** 8998-9033.

MILLET, P., MOULIN, M., BARTOLI, A., DEL GUERRA, A., GINOVART, N., LEMOUCHEUX, L., BUONO, S., FAGRET, D., CHARNAY, Y. & IBÁÑEZA, V. 2008. In vivo quantification of 5-HT1A–[^{18}F]MPPF interactions in rats using the YAP-(S)PET scanner and a β-microprobe. *NeuroImage,* 41**,** 823-834.

MIZUMA, H., SHUKURI, M., HAYASHI, T., WATANABE, Y. & ONOE, H. 2010. Establishment of in vivo brain imaging method in conscious mice. *Journal of Nuclear Medicine,* 51**,** 1068-75.

MOULIN-SALLANON, M., CHARNAY, Y., GINOVART, N., PERRET, P., LANFUMEY, L., HAMON, M., RENÉ, H., FAGRET, D., IBANEZ, V. & MILLET, P. 2009. Acute and chronic effects of citalopram on 5-HT1Areceptor- labeling by [18F]MPPF and-coupling to receptors-G proteins *Synapse* 63**,** 106-116.

MYERS, R. & HUME, S. 2002. Small animal PET. *European Neuropsychopharmacology,* 12**,** 545-555.

NEFF, C. D., ABKEVICH, V., PACKER, J. C. L., CHEN, Y., POTTER, J., RILEY, R., DAVENPORT, C., DEGRADO WARREN, J., JAMMULAPATI, S., BHATHENA, A., CHOI, W. S., KROEGER, P. E., METZGER, R. E., GUTIN, A., SKOLNICK, M. H., SHATTUCK, D. & KATZ, D. A. 2009. Evidence for HTR1A and LHPP as interacting genetic risk factors in major depression. *Molecular Psychiatry,* 14**,** 621-630.

NENONENE, E. K., RADJA, F., CARLI, M., GRONDIN, L. & READER, T. A. 1994. Heterogeneity of Cortical and Hippocampal 5-HT$_{1A}$ Receptors - A reappraisal of Homogenate Binding with 8-[^{3}H]Hydroxydiprolaminotetralin. *Journal of Neurochemistry,* 62**,** 1822-1834.

OHNO, Y. 2011. Therapeutic role of 5-HT1A receptors in the treatment of schizophrenia and Parkinson's disease. *CNS Neuroscience & Therapeutics,* 17**,** 58-65.

PARK, S., H., GWON, H., J., LEE, H., S. & PARK, K., B. 2005. Microwave-assisted rapid synthesis of arylpiperazine derivatives for imaging 5-HT1A receptors. *Bulletin of the Korean Chemical Society,* 26**,** 1701-1705.

PARKS, C., L., ROBINSON, P., S., , SIBILLE, E., SHENK, T. & TOTH, M. 1998. Increased anxiety of mice lacking the serotonin$_{1A}$ receptor. *Proceedings of the National Academy of Sciences.,* 95**,** 10734-9.

PASCALIA, G., MAZZONE, G., SACCOMANNIC, G., MANERAC, C. & SALVADORIA, P. A. 2010. Microfluidic approach for fast labeling optimization and dose-on-demand implementation. *Nuclear Medicine and Biology,* 37**,** 547-555.

PASSCHIER, J., VAN WAARDE, A., PIETERMAN, R. M., WILLEMSEN, A. T. M. & VAALBURG, W. 2001. Quantifying drug-related 5-HT1A receptor occupancy with [18F]MPPF. *Psychopharmacology,* 155**,** 193-197.

PASSCHIER, J., VAN WAARDEA, A., DOZEA, P., ELSINGAA, P. H. & VAALBURGA, W. 2000. Influence of P-glycoprotein on brain uptake of [^{18}F]MPPF in rats. *European Journal of Pharmacology - Molecular Pharmacology Section,* 407**,** 273-280.

PASSCHIER, J., VANWAARDE, A., PIETERMAN, R., ELSINGA, P., PRUIM, J., HENDRIKSE, H., WILLEMSEN, A., VAALBURG, W. 2000. In Vivo Delineation of 5-HT1A Receptors in Human Brain with [18F]MPPF. *Journal of Nuclear Medicine,* 41**,** 1830-1835.

PATERSON, L. M., KORNUM, B. R., NUTT, D. J., PIKE, V. W. & KNUDSEN, G. M. 2013. 5-HT radioligands for human brain imaging with PET and SPECT. *Medicinal Research Reviews,* 33**,** 54-111.

PAXINOS, G. & WATSON, C. 1998. The Rat Brain in Stereotaxtic Coordinates. *Academic Press, Ltd.,* Fourth Edition.

PAZOS, A., PROBST, A. & PALACIOS, J. M. 1987. Serotonin receptors in the human brain - III. Autoradiographic mapping of serotonin-1 receptors. *Neuroscience* 21**,** 97-122.

PLENEVAUX, A., WEISSMANN, D., AERTS, J., LEMAIRE, C., BRIHAYE, C., DEGUELDRE, C., LE BARS, D., CORNAR, D., PUJOL, J. F. & LUXEN, A. 2000. Tissue distribution, autoradiography, and metabolism of 4-(2'- methoxyphenyl)-1-[2'-[N-(2''-pyridinyl)-p-[18F]fluorobenzamido]ethyl]piperazine (p-[^{18}F]MPPF), a new serotonin 5- HT_{1A} antagonist for positron emission tomography: An in vivo study in rats. *Journal of Neurochemistry* 75**,** 803-811.

PRIETO, E., COLLANTES, M., DELGADO, M., JURI, C., GARCÍA-GARCÍA, L., MOLINET, F., FERNÁNDEZ-VALLE, M. E., POZO, M. A., GAGO, B., MARTÍ-CLIMENT, J. M., OBESO, J. A. & PEÑUELAS, I. 2011. Statistical parametric maps of 18F-FDG PET and 3-D autoradiography in the rat brain: a cross-validation study. *European Journal of Nuclear Medicine and Molecular Imaging* 38**,** 2228-2237

RAMBOZ, S., OOSTING, R., AMARA, D., A., , KUNG, H., F., , BLIER, P., MENDELSOHN, M., MANN, J., J., , BRUNNER, D. & HEN, R. 1998. Serotonin receptor 1A knockout: an animal model of anxiety-related disorder. *Proceedings of the National Academy of Sciences,* 95**,** 14476-81.

RAPPORT, M., M. 1949. Serum vasoconstrictor (serotonin) the presence of creatinine in the complex; a proposed structure of the vasoconstrictor principle. *Journal of Biological Chemistry,* 180**,** 961-969.

RBAH, L., VINCENT, L. & ZIMMER, L. 2003. Displacement of the PET Ligand ^{18}F-MPPF by the Electrically Evoked Serotonin Release in the Rat Hippocampus. *Synapse,* 49**,** 239-245.

REED, C. D., LAUNAY, G. G. & CARROLL, M. A. 2012. Evaluation of tetraethylammonium bicarbonate as a phase-transfer agent in the formation of [^{18}F]fluoroarenes. *Journal of Fluorine Chemistry* 143**,** 231-237.

RESONANCE INSTRUMENTS INC. 2011. *Instruments for Microwave Accelerated Chemistry* [Online]. Available: http://resonanceinstruments.com/htr1.html.

RIAD, M., RBAH, L., VERDURAND, M., AZNAVOUR, N., ZIMMER, L., DESCARRIES, L. 2008. Unchanged density of 5-HT1A autoreceptors on the plasma membrane of nucleus raphe dorsalis neurons in rats chronically treated with fluoxetine *Neuroscience* 151**,** 692-700.

RIAD, M., ZIMMER, L., RBAH, L., WATKINS, K., C., , HAMON, M. & DESCARRIES, L. 2004. Acute Treatment with the Antidepressant Fluoxetine Internalizes 5-HT_{1A} Autoreceptors and Reduces the *In Vivo* Binding of the PET Radioligand [^{18}F]MPPF in the Nucleus Raphe Dorsalis of Rat. *The Journal of Neuroscience,* 24**,** 5420 –5426.

RITMAN, E. L. 2002. Molecular imaging in small animals - Roles for micro-CT *Journal of Cellular Biochemistry* (SUPPL. 39)**,** 116-124.
ROGERS, A. W. 1979. *Techniques in Autoradiography*, Elsevier.
ROWLAND, D. J., LEWIS, J. S. & WELCH, M. J. 2002. Molecular imaging: The application of small animal positron emission tomography. *Journal of Cellular Biochemistry,* SUPPL. 39**,** 110-115.
RUHÉ, H. G., MASON, N. S. & SCHENE, A. H. 2007. Mood is indirectly related to serotonin, norepinephrine and dopamine levels in humans: A meta-analysis of monoamine depletion studies. *Molecular Psychiatry,* 12**,** 331-359.
SAHA, G., B. 2010. *Basics of PET imaging; Physics, Chemistry and Regulations; Performance Characteristics of PET Scanners.*, Springer.
SANABRIA-BOHÓRQUEZ, S. M., BIVER, F., DAMHAUT, P., WIKLER, D. & VERAART, C., GOLDMAN, S. 2002. Quantification of 5-HT1A receptors in human brain using p-MPPF kinetic modelling and PET. *European Journal of Nuclear Medicine,* 29**,** 76-81.
SARGENT, P. A., HUSTED KJAER, K., BENCH, C. J., RABINER, E. A., MESSA, C., MEYER, J., GUNN, R. N., GRASBY, P. M. & COWEN, P. J. 2000. Brain serotonin(1A) receptor binding measured by positron emission tomography with [11C]WAY-100635: Effects of depression and antidepressant treatment. *Archives of General Psychiatry,* 57**,** 174-180.
SAVITZ, J., LUCKI, I. & DREVETS, W., C. 2009. 5-HT(1A) receptor function in major depressive disorder. *Progress in Neurobiology,* 88**,** 17-31.
SCHMIDT, K. C. & SMITH, C. B. 2005. Resolution, sensitivity and precision with autoradiography and small animal positron emission tomography: implications for functional brain imaging in animal research. *Nuclear Medicine and Biology,* 32**,** 719-725.
SCHREIBER, G. & AVISSAR, S. 2007. Regulators of G-protein-coupled receptor-G-protein coupling: Antidepressants mechanism of action. *Expert Review of Neurotherapeutics,* 7**,** 75-84.
SHAO, X., HOAREAU, R., HOCKLEY, B. G., TLUCZEK, L. J. M., HENDERSON, B. D., PADGETT, H. & SCOTT, P. J. H. 2011. Highlighting the versatility of the tracerlab synthesis modules. Part 1: fully automated production of [F-18]labelled radiopharmaceuticals using a Tracerlab FX_{FN} *JOURNAL OF LABELLED COMPOUNDS & RADIOPHARMACEUTICALS* 54**,** 292-307.
SHARP, T., BOOTHMAN, L., RALEY, J. & QUÉRÉE, P. 2007. Important messages in the 'post': recent discoveries in 5-HT neurone feedback control. *Trends in Pharmacological Sciences,* 28**,** 629-636.
SHARP, T. & HJORTH, S. 1990. Application of brain microdialysis to study the pharmacology of the 5-HT1A autoreceptor. *Journal of Neuroscience Methods,* 34**,** 83-90.
SHIUE, C.-Y., SHIUE, G. G., MOZLEY, P. D., KUNG, M.-P., ZHUANG, Z.-P., KIM, H.-J. & KUNG, H. F. 1997. p-[^{18}F]-MPPF: A potential radioligand for PET studies of 5-HT_{1A} receptors in humans. *Synapse,* 25**,** 147-154.
SHIVELY, C. A., FRIEDMAN, D. P., GAGE, H. D., BOUNDS, M. C., BROWN-PROCTOR, C., BLAIR, J. B., HENDERSON, J. A., SMITH, M. A. & BUCHHEIMER, N. 2006. Behavioral depression and positron emission tomography-determined serotonin 1A receptor binding potential in cynomolgus monkeys. *Archives of General Psychiatry,* 63**,** 396-403.
SIBON, I., BENKELFAT, C., GRAVEL, P., AZNAVOUR, N., COSTES, N., MZENGEZA, S., BOOIJ, L., BAKER, G., SOUCY, J. P., ZIMMER, L. & DESCARRIES, L. 2008. Decreased [18F]MPPF Binding Potential in the Dorsal Raphe Nucleus After a Single Oral Dose of Fluoxetine: A Positron-Emission Tomography Study in Healthy Volunteers. *Biological Psychiatry,* 63**,** 1135-1140.
SIJBESMA, H., SCHIPPER, J., CORNELISSEN, J. C. H. M. & DE KLOET, E. R. 1991. Species differences in the distribution of central 5-HT1 binding sites: a comparative autoradiographic study between rat and guinea pig. *Brain Research,* 555**,** 295-304.
SLIFSTEIN, M., KEGELES, L., S., , XU, X., THOMPSON, J., L., , URBAN, N., CASTRILLON, J., HACKETT, E., BAE, S., A., , LARUELLE, M. & ABI-DARGHAM, A. 2010. Striatal and

extrastriatal dopamine release measured with PET and [^{18}F] fallypride. *Synapse,* 64**,** 350-62.
SOFIEBIOSCIENCES. Available: http://sofiebio.com/products/imaging/.
STALEY, J. K., VAN DYCK, C. H., TAN, P. Z., AL TIKRITI, M., RAMSBY, Q., KLUMP, H., NG, C., GARG, P., SOUFER, R., BALDWIN, R. M. & INNIS, R. B. 2001. Comparison of [18F]altanserin and [18F]deuteroaltanserin for PET imaging of serotonin2A receptors in baboon brain: Pharmacological studies. *Nuclear Medicine and Biology,* 28**,** 271-279.
STAMFORD, J., A 1992. *Monitoring Neuronal Activity: A Practical Approach*, IRL Press.
STOCKMEIER, C. A., SHAPIRO, L. A., DILLEY, G. E., KOLLI, T. N., FRIEDMAN, L. & RAJKOWSKA, G. 1998. Increase in serotonin-1A autoreceptors in the midbrain of suicide victims with major depression - Postmortem evidence for decreased serotonin activity. *Journal of Neuroscience,* 18**,** 7394-7401.
STOKES, A., H. , XU, Y., DAUNAIS, J., A., , TAMIR. H., GERSHON, M., D., , BUTKERAIT, P., KAYSER, B., ALTMAN, J., BECK, W. & VRANA, K., E. 2000. p-ethynylphenylalanine: a potent inhibitor of tryptophan hydroxylase. *Journal of Neurochemistry,* 74**,** 2067-73.
STONE-ELANDER, S. & ELANDER, N. 2002. Microwave applications in radiolabelling with short-lived positron-emitting radionuclides *Journal of Labelled Compounds and Radiopharmaceuticals* 45**,** 715-746.
STROME, E. M., CEPEDA, I. L., SOSSI, V. & DOUDET, D. J. 2006. Evaluation of the integrity of the dopamine system in a rodent model of Parkinson's disease: small animal positron emission tomography compared to behavioral assessment and autoradiography. *Molecular Imaging and Biology,* 8**,** 292-9.
SURTI, S., KARP, J. S., PERKINS, A., MEMBER, C., C. A., , DAUBE-WITHERSPOON, M. E., KUHN, A. & MUEHLLEHNER, G. 2005. Imaging Performance of A-PET: A Small Animal PET Camera. *IEEE Transaction on Medical Imaging,* 24**,** 844-852.
SZEWCZYK, B., ALBERT, P. R., BURNS, A. M., CZESAK, M., OVERHOLSER, J. C., JURJUS, G. J., MELTZER, H. Y., KONICK, L. C., DIETER, L., HERBST, N., MAY, W., RAJKOWSKA, G., STOCKMEIER, C. A. & AUSTIN, M. C. 2009. Gender-specific decrease in NUDR and 5-HT1A receptor proteins in the prefrontal cortex of subjects with major depressive disorder. *International Journal of Neuropsychopharmacology,* 12**,** 155-168.
THATHIAH, A. & DE STROOPER, B. 2011. The role of G protein-coupled receptors in the pathology of Alzheimer's disease. *Nature Reviews Neuroscience,* 12**,** 73-87.
THIELEN, R. J., FANGON, N.B., FRAZER, A. 1996. 4-(2′-methoxyphenyl)-1-[2′-[N-(2″-pyridinyl)-p-iodobenzamido]ethyl]piperazine and 4-(2′-methoxyphenyl)-1-[2′-[N-(2″-pyridinyl)-p-fluorobenzamido]ethyl]piperazine, two new antagonists at pre- and postsynaptic serotonin-1A receptors. *Journal of Pharmacology and Experimental Therapeutics* 277**,** 661-670.
THIELEN, R. J. & FRAZER, A. 1995. Effects of novel 5-HT(1A) receptor antagonists on measures of post-synaptic 5-HT(1A) receptor activation in vivo. *Life Sciences* 56**,** PL 163-PL 168.
TOYAMA, H., ICHISE, M., LIOW, J. S., MODELL, K. J., VINES. D. C., ESAKI, T., COOK, M., SEIDEL, J., SOKOLOFF, L., GREEN, M. V. & INNIS, R. B. 2004. Absolute quantification of regional cerebral glucose utilization in mice by 18F-FDG small animal PET scanning and 2-14C-DG autoradiography. *Journal of Nuclear Medicine,* 45**,** 1398-405.
TRASKMAN-BENDZ, L., ASBERG, M., BERTILSSON, L. & THOREN, P. 1984. CSF monoamine metabolites of depressed patients during illness and after recovery. *Acta Psychiatrica Scandinavica,* 69**,** 333-342.
TREDWELL, M., PRESHLOCK, S. M., TAYLOR, N. J., GRUBER, S., HUIBAN, M., PASSCHIER, J., MERCIER, J., GÉNICOT, C. & GOUVERNEUR, V. 2014. A general copper-mediated nucleophilic 18F fluorination of arenes. *Angewandte Chemie - International Edition*.
TRUCHOT, L., COSTES, N., ZIMMER, L., LAURENT, B., LE BARS, D., THOMAS-ANTÉRION, C., MERCIER, B., HERMIER, M., VIGHETTO, A. & KROLAK-SALMON, P. 2008. A distinct [18F]MPPF PET profile in amnestic mild cognitive impairment compared to mild Alzheimer's disease. *NeuroImage,* 40**,** 1251-1256.

TRUCHOT, L., COSTES, S. N., ZIMMER, L., LAURENT, B., LE BARS, D., THOMAS-ANTÉRION, C., CROISILE, B., MERCIER, B., HERMIER, M., VIGHETTO, A. & KROLAK-SALMON, P. 2007. Up-regulation of hippocampal serotonin metabolism in mild cognitive impairment. *Neurology,* 69**,** 1012-1017.

UDO DE HAES, J., CREMERS, T., BOSKER, F., J., POSTEMA, F., TIEMERSMA-WEGMAN, T., D., BOER, J., A. 2005. Effect of Increased Serotonin Levels on [^{18}F]MPPF Binding in Rat Brain: Fenfluramine vs the Combination of Citalopram and Ketanserin. *Neuropsychopharmacology,* 30**,** 1624-1631.

UDO DE HAES, J., I. , BOSKER, F., J., , VAN WAARDE, A., PRUIM, J., WILLEMSEN, A., T., M., , VAALBURG, W. & DEN BOER, J., A. 2002a. 5-HT$_{1A}$ Receptor Imaging in the Human Brain: Effect of Tryptophan Depletion and Infusion on [^{18}F]MPPF Binding. *Synapse,* 46**,** 108-115.

UDO DE HAES, J. I., BOSKER, F. J., VAN WAARDE, A., PRUIM, J., WILLEMSEN, A. T. M., VAALBURG, W. & DEN BOER, J. A. 2002b. 5-HT1A receptor imaging in the human brain: Effect of tryptophan depletion and infusion on [18F]MPPF binding. *Synapse,* 46**,** 108-115.

UDO DE HAES, J. I., HARADA, N., ELSINGA, P. H., MAGUIRE, R. P. & TSUKADA, H. 2006. Effect of fenfluramine-induced increases in serotonin release on [18F]MPPF binding: A continuous infusion PET study in conscious monkeys *Synapse* 59**,** 18-26.

VAN WIJNGAARDEN, I., TULP, M. T. M. & SOUDIJN, W. 1990. The concept of selectivity in 5-HT receptor research. *European Journal of Pharmacology - Molecular Pharmacology Section* 188**,** 301-312.

VANDECAPELLE, M., DUMONT, F., DE VOS, F., STRIJCKMANS, K., LEYSEN, D., AUDENAERT, K., DIERCKX, R. A. & SLEGERS, G. 2004. Synthesis and preliminary in vivo evaluation of 4-[^{18}F]fluoro-N-{2-[4-(6-trifluoromethylpyridin-2-yl)piperazin-1-yl]ethyl}benzamide, a potential PET radioligand for the 5-HT$_{1A}$ receptor. *Journal of Labelled Compounds and Radiopharmaceuticals,* 47**,** 531-542.

WADSAK, W. & MITTERHAUSER, M. 2010. Basics and principles of radiopharmaceuticals for PET/CT. *European Journal of Radiology,* 73 461-469.

WATSON, J., COLLIN, L., HO, M., RILEY, G., SCOTT, C., SELKIRK, J. & PRICE, G. 2000. 5-HT$_{1A}$ receptor agonist-antagonist binding affinity difference as a measure of intrinsic activity in recombinant and native tissue systems. *British Journal of Pharmacology,* 130**,** 1108–1114.

WHITAKER-AZMITIA, P., M., DRUSE, M., WALKER, P. & LAUDER, J., M. 1996. Serotonin as a developmental signal. *Behavioural Brain Research,* 73**,** 19-29.

WU, C., LIN, X., LU, C., ZOU, M., ZHANG, Z., LIU, P., XUE, F., CHEN, Z., JIANG, Q., FU, R., WANG, S., ZHANG, T., LI, X. & ZHU, J. 2004. Preparation and biological evaluation of 18F-MPPF as a 5-HT$_{1A}$ imaging agent. *Chinese Journal of Nuclear Medicine and Molecular Imaging,* 24**,** 121-123.

YAO, R., LECOMTE, R. & CRAWFORD, E., S. 2012. Small-Animal PET: What Is It, and Why Do We Need It? *Journal of Nuclear Medicine Technology,* 40**,** 157-165.

YAP-(S)PET. Available: http://www.df.unipi.it/~fiig/research_yapspet.htm.

ZHANG, K., XU, Q., XU, Y., YANG, H., LUO, J., SUN, Y., SUN, N., WANG, S. & SHEN, Y. 2009. The combined effects of the 5-HTTLPR and 5-HTR1A genes modulates the relationship between negative life events and major depressive disorder in a Chinese population. *Journal of Affective Disorders,* 114**,** 224-231.

ZHUANG, Z.-P., KUNG, M.-P. & KUNG, H. F. 1994. Synthesis and evaluation of 4-(2'-methoxyphenyl)-1-[2'-[N-(2''-pyridinyl)-p-iodobenzamido] ethyl]piperazine (p-MPPI): A new iodinated 5-HT1A ligand. *Journal of Medicinal Chemistry* 37 1406-1407.

ZIMMER, L. & LE BARS, D. 2013. Current status of positron emission tomography radiotracers for serotonin receptors in humans. *Journal of Labelled Compounds and Radiopharmaceuticals,* 56**,** 105-113.

ZIMMER, L., MAUGER, G., LE BARS, D., BONMARCHAND, G., LUXEN, A. & PUJOL, J. F. 2002a. Effect of endogenous serotonin on the binding of the 5-HT1A PET ligand 18F-MPPF in the rat hippocampus: Kinetic β measurements combined with microdialysis. *Journal of Neurochemistry,* 80**,** 278-286.

ZIMMER, L., PAIN, F., MAUGER, G., PLENEVAUX, A., LE BARS, D., MASTRIPPOLITO, R., PUJOL, J., RENAUD, B. & LANIÈCE, P. 2002b. The potential of the β-Microprobe, an intracerebral radiosensitive probe, to monitor the [18F]MPPF binding in the rat dorsal raphe nucleus. *European Journal of Nuclear Medicine* 29**,** 1237-1247.

ZIMMER, L., RBAH, L., GIACOMELLI, F., LE BARS, D. & RENAUD, B. 2003. A reduced extracellular serotonin level increases the 5-HT1A PET ligand 18F-MPPF binding in the rat hippocampus. *Journal of Nuclear Medicine* 44**,** 1495-1501.